The Adaptation of a Rapid Screening Test to Rank the Corrosion Behaviour of Stainless Steel Reinforcing Bars in Concrete

by

Peter Gordon Houston Loudfoot

A thesis
presented to the University of Waterloo
in fulfillment of the
thesis requirement for the degree of
Master of Applied Science
in
Civil Engineering

Waterloo, Ontario, Canada, 2018

AUTHOR'S DECLARATION

I hereby declare that I am the sole author of this thesis. This is a true copy of the thesis, including any required final revisions, as accepted by my examiners.

I understand that my thesis may be made electronically available to the public.

Abstract

The costs associated with aging reinforced concrete infrastructure in Ontario continue to rise as highway infrastructure, such as bridges, continuously deteriorate. The use of de-icing salts on these bridges in the winter often leads to the corrosion of the reinforcing steel, cracking the concrete and reducing the service life of the structure. To meet a minimum required service life of 75 years for bridge infrastructure, the Ministry of Transportation of Ontario uses stainless steel grades UNS S31653 (316LN) and UNS S31803 (2205) for corrosion resistance [1], [2]. However, with the wide variety of existing stainless steel grades and the continuous development of new grades, the selection of the most appropriate grade of stainless steel for current projects is limited by the time necessary to determine their corrosion resistance under realistic conditions.

An experimental project was undertaken to determine, through a rapid screening test, if less costly grades of stainless steel would be competitive with 2205 or 316LN in their corrosion resistance. The relative corrosion resistance of three grades of stainless steel were compared: UNS S24100 (XM-28) and S32304 (2304) with S31803 (2205) as the "control". The main objectives for this project were as follows: 1) to experimentally assess and evaluate the parameters of the Rapid Screening Test such that recommended parameters can be used to compare the relative corrosion resistance of new and existing grades of stainless steel, and 2) to assess the impact of the parameters on the probability of corrosion for each tested stainless steel grade using statistical analyses.

The experimental procedure involved casting stainless steel specimens into concrete with admixed chloride concentrations of 4, 6, or 7.5% by mass of cementitious materials, measuring the open circuit potentials (E_{corr}) of the specimens from 24 hours to 48 after casting, and immediately applying an anodic polarization potential of +100, +200, +300, or +400 mV to the specimens for 96 hours after the E_{corr} monitoring period. During the applied polarization potential period, corrosion current density (i_{corr}) values were monitored. Corrosion initiation was considered to have occurred if the i_{corr} of a specimen surpassed the proposed pass/fail limit of 0.025 A/m^2 for more than 2 hours. All specimens were autopsied at the end of the test and visually examined for any signs of corrosion. The results of the electrochemical testing and the observations made during and after autopsying the bars were found to differ. The detection of corrosion initiation in the electrochemical testing was then changed

to reflect the results of the autopsied bars. If any bar had an increase in i_{corr} by at least one order of magnitude, it is considered to have corroded.

Logistic regression models were created to model the probability of corrosion in each of the tested grades of stainless steel based on the electrochemical testing and autopsy results. It was determined that increasing the admixed chloride concentration of the concrete has a far more significant impact on the corrosion initiation of the bars than the applied polarization potential. Theoretical critical chloride thresholds of the XM-28, 2304, and 2205 bars directly exposed to admixed chlorides in concrete were estimated to be 7.1%, 7.1%, and 9.4% by mass of cementitious materials, respectively. However, based on the limited pitting corrosion damage observed in the photomicrographs, it is believed that 2304 has a higher chloride threshold than XM-28. The threshold values of the 2304 and 2205 specimens may not be accurately estimated due to the imbalanced number of corroded versus non-corroded specimens for each of these grades.

Based on the experimental and analytical results, 7.5% admixed chlorides by mass of cementitious and an applied polarization potential of +300 mV are the recommended parameters for the Rapid Screening Test. The proposed relative ranking of stainless steel specimens is based on the number of corroded specimens, the order of magnitude of the corrosion rates experienced by the specimens, and the severity of the pitting corrosion observed on the specimens. The ranking of the relative corrosion performance of the stainless steel grades tested in the Rapid Screening Test is as follows, in order of the most to least resistant: 2205, 2304, and XM-28. Based on the results of this test, it is recommended that 2304 would be a suitable alternative to 2205 as corrosion resistant reinforcing bars in concrete highway structures. It should be noted that chloride concentrations in excess of 5% by mass of cementitious material in concrete highway structures have not been reported in the available literature to date.

Acknowledgements

I would like to sincerely thank Dr. Carolyn Hansson, for her continuous encouragement, guidance, and support of my graduate studies. The advice she has given me and the critical thinking skills she has helped to foster are invaluable and I will be forever grateful to her. It has been an honor to be her M.A.Sc. student. I would also like to thank our research group: Colin Van Niejenhuis, Michael Benoit, Ibrahim Ogunsanya, Leah Kristufek, Marc Johnson, and Adam Felinczak, as well as the structural and materials lab technicians: Richard Morrison, Douglas Hirst, and Mark Griffett for the help and support that they have each provided along the way.

Without the financial support of the Ministry of Transportation of Ontario and the materials supplied by Vector Corrosion Technologies, Salit Specialty Steels, Commercial Metals Company, and Harris Rebar, this project would not have been possible.

To my friends, Graeme Milligan, James St. Onge, Adam Felinczak, Marc Johnson, Nicholas Charron, Colin Van Niejenhuis, and Leah Kristufek, I sincerely thank, as they have made my time at the University far too short. I would like to especially thank my roommates Graeme Milligan and James St. Onge, for putting up with my antics and for being some of the finest gentlemen I have ever had the pleasure of calling friends. I would also like to thank my dear friends Jarod Witvoet and Spencer Baron for their endless encouragement and support of my academic career since elementary school. These two gentlemen have challenged me to grow as an individual, and I look forward to having a beer with them once this thesis is done.

Finally, I would like to thank my parents and family: Mom, Dad, Grandad, Meg, Adam, John, and Thomas for standing behind me throughout my academic career and pushing me to excel in everything that I do.

Table of Contents

List of Figures

List of Tables

List of Equations

List of Variables

Variable	Units	Definition
A	mV	The applied overpotential (polarization potential)
AB	-	The interaction term between the applied overpotential and the admixed chloride concentrations
AIC	-	Akaike's Information Criterion
AIC_c	-	The corrected Akaike's Information Criterion
B	Weight % by mass of cementitious materials	The admixed chloride concentration
Cr	-	The element chromium
D	-	The deviance of a model
df	-	The number of degrees of freedom for a given statistical model
D_{null}	-	The null deviance of a model given a set of data
$D_{residual}$	-	The residual deviance of model given a set of data
$E(Y \mid \theta)$	-	The conditional mean of the predictor Y given the set of independent variables denoted by θ for a logistic regression model
E_{SCE}	mV	Electrochemical potential with respect to the saturated calomel electrode
E_{SHE}	mV	Electrochemical potential with respect to the standard hydrogen electrode
FNR	-	The false negative rate of a model
FPR	-	The false positive rate of a model
G	-	A test statistic to compare the residual and null deviances of a model for a given set of data
g(x)	-	The logit transformation of the conditional mean
k	-	The number of independent variables in a given logistic regression model
k*	-	The number of independent variables plus the intercept for a given statistical model
$L(\hat{\theta}\|y)$	-	The likelihood function of the parameter vector θ
Mo	-	The element molybdenum
N	-	The element nitrogen
n	-	The number of observations
PRE_{16N}	-	The pitting resistance equivalent number, typically used for austenitic stainless steels
PRE_{30N}	-	The pitting resistance equivalent number, typically used for duplex stainless steels
$r_{x_i x_j}$	-	The coefficient of correlation between predictors xi and xj
TNR	-	The true negative rate of a model

TPR	-	The true positive rate of a model
x_i	-	Independent variable (i) used in the standardized determinant
Y	-	The expected value Y for a regression model
y_i	-	The predicted value for the ith observed value
Z	-	The Z-test statistic
$\hat{\beta}$	-	The standardized regression coefficient for a given parameter
β_i	-	The estimated parameter coefficient i for a logistic regression model
Δ_i	-	The AICc differences between a model and the model with the lowest AICc
ε	-	The error term associated with a logistic regression model
θ	-	The set of independent variables for a logistic regression model
$\hat{\pi}_i(x_i)$	-	The maximum likelihood estimate of the conditional mean
$\pi(x)$	-	The conditional mean for a logistic regression model
$\hat{\sigma}_{\hat{\beta}}$	-	The standardized error associated with $\hat{\beta}$
χ^2	-	Chi-square test statistic

Chapter 1 – Introduction

1.1 Background

Concrete has been used as a predominant structural material since the Roman Empire because of its durability and ease of construction [3]. Even to this day, concrete is widely used in structural applications, such as buildings, marine construction, and highway infrastructure. The durability of concrete stems from its low permeability, its non-reactive nature in most environments, and its inherent compressive strength. However, the low tensile strength of concrete can lead to significant cracking and failure of concrete structural members if reinforcing bars (sometimes referred to as rebar) are not present within the concrete. Reinforcing bars are typically made of materials with high tensile strength, such as steel, to compliment the high compressive capacity of concrete. The resulting highly durable composite material is used in most structural applications in a variety of loading conditions, but it is highly susceptible to another form of deterioration – corrosion of the reinforcing bars [4].

Typically, carbon steel (also known as black steel) is used as the reinforcing material in reinforced concrete. Under normal conditions, the high pH of the concrete allows for the formation of a stable passive film on the steel rebar. However, this passive layer can deteriorate in the presence of chloride ions or through a reduction in the alkalinity of the concrete from carbonation. Either deterioration mechanism can lead to the corrosion of the reinforcing bars, resulting in a reduction in the cross-sectional area of the rebar and cracking of the concrete via the expansive corrosion products [5].

Reinforced concrete infrastructure in Ontario is particularly susceptible to chloride-induced corrosion. The use of de-icing salts on concrete bridges and their substructure has been found to lead to extensive corrosion damage of their reinforcing bars. A report written in 2002 by the US Department of Transportation Federal Highway Administration [6] found that approximately 15% of all bridges in the United States are structurally deficient because of corroded steel and steel reinforcement. The annual direct cost estimate to repair and maintain these bridges was $8.3 billion, while the indirect costs, such as traffic delays and lost productivity, could be as much as 10 times more than the direct cost [6], [7].

Corrosion of the reinforcing steel leads to the deterioration of the reinforced concrete, and as a result, reduces the service life of the structure [8], [9]. This is very concerning when one considers the current age of infrastructure in both the United States and Canada. Of the 614,387 bridges in the United States,

39% of the bridges are 50 years or older, and another 15% of the bridges are between 40 and 49 years old [10], as shown in Figure 1.1. The designed service life for these bridges was approximately 50 years old, meaning that most of these bridges will either need to be rehabilitated or decommissioned in the near future [10].

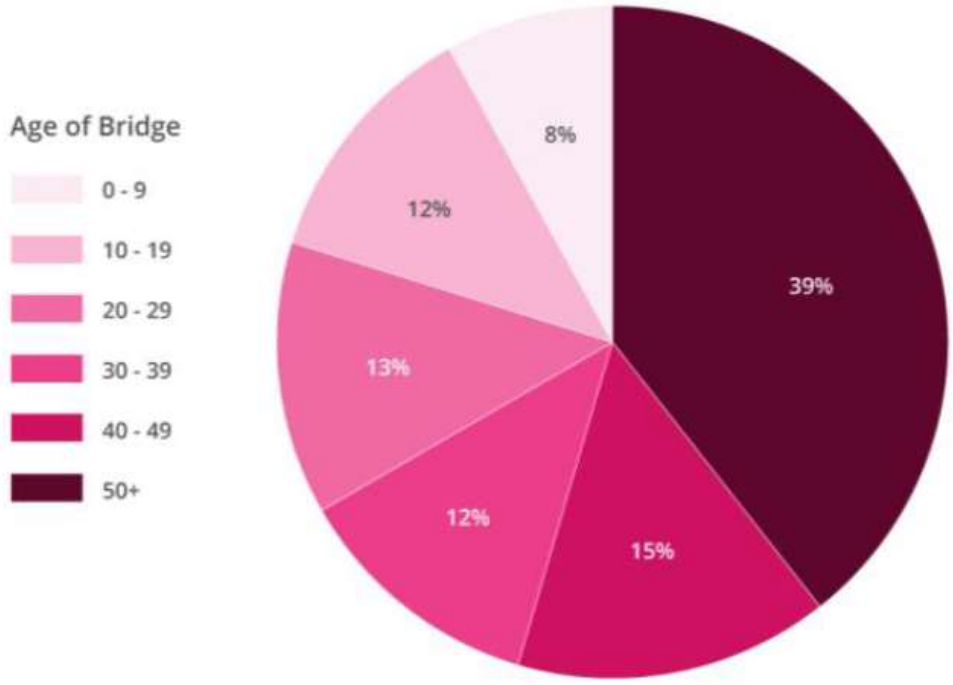

Figure 1.1: Age of Bridges in the United States' [10]

When compared to Ontario's infrastructure, a 2015 report by the Association of Municipalities of Ontario [11] found that in 93 municipalities across Ontario, 34.9% of the bridges were found to be between 51-100 years old, and that 1% of the bridges were over 100 years old. Furthermore, 26% of all bridges in Ontario were found to have a poor condition rating based on the Ministry of Ontario's (MTO) Bridge Condition Index (BCI). The 2013 replacement cost for these bridges was estimated to be $1 billion.

1.2 Research Objectives

In accordance with the Canadian Highway Bridge Design Code [12], the Ministry of Transportation of Ontario (MTO) endeavors to provide bridge infrastructure that meets a minimum service life of 75 years [4]. To meet this constraint in environments exposed to de-icing salts and anti-icing agents, one option to

increase the service life of bridge infrastructure is to use steel reinforcing bars with improved corrosion resistance.

The MTO currently uses stainless steel grades UNS 31653 (316 LN) and UNS 31803 (2205) for corrosion resistant reinforcing bars [1], [2]. However, there is a wide variety of stainless steel grades used for concrete reinforcement**.** In order to procure corrosion performance information of the newer steels to allow the most appropriate grade(s) of stainless steel in current projects, the MTO currently requires compliance with ASTM A955M, which involves between 5 and 22 months of testing. In the meantime, the European Union is proposing an adaptation of EN-480-14:2006 rapid screening test [13] to rapidly compare the relative corrosion resistance of different stainless steel rebar grades. This test is now included in the British Standard BS 6744-16 and is the basis of the current research project.

The objectives of this project are as follows:

1. To assess and evaluate the parameters of the adapted Rapid Screening Test (RST) such that the recommended parameters can be used to compare other new and existing grades of stainless steel;

2. To investigate the impact of passivating the stainless steels in synthetic pore solution on the response of the steels in the adapted RST,

3. To evaluate and rank the relative corrosion resistance of stainless steel rebar grades UNS 32205, UNS 32304, and UNS 24100 using the recommended parameters of the Rapid Screening Test, and

4. To develop statistical models to assess the impact of various RST parameters on the probability of corrosion for each of the tested stainless steel grades.

1.3 Scope

The scope of this thesis is limited as follows:

- Due to the nature of the modified rapid screening test, the results are not representative of a service life of at least 75 years. The purpose of this test is to provide a basis for a relative comparison between different stainless steel grades in terms of their corrosion behaviour in a concrete environment.

- The experimental procedure involved using electrochemical test methods to determine the corrosion rates of the stainless steels in a concrete environment. As such, the measured corrosion currents were averaged over the exposed area of each stainless steel specimen to determine the corrosion current density. However, localized corrosion is more likely, and thus, the corrosion rates do not fully capture the effects of localized corrosion pits and crevices.
- By curing the concrete in a sealed environment for 24 hours before subjecting the test specimens to electrochemical testing, the concrete is considered to be unrepresentative of field concrete. Therefore, the results for corrosion initiation time, open circuit potential, and corrosion current density for each stainless steel grade are unrepresentative and should only be used on a relative comparative basis.
- The stainless steels that were used in this study do not fully encompass all commercially available grades. Stainless steel grade UNS S32205 was used as a control specimen as it is known to be highly durable, while stainless steel grades UNS S32304 and UNS S24100 were used because of their significantly lower cost, their lower nickel concentrations, and their relatively low to no molybdenum content.

Chapter 2 – Literature Review

2.1 Corrosion Resistant Reinforcement in Concrete

In aggressive environments that are highly prone to cause carbonation- or chloride-induced corrosion of concrete reinforcing steel, the reinforcing steel in a bridge deck often dictates the operational life of the structure. Spalling of the concrete, induced by reinforcement corrosion can lead to the deterioration of the deck surface, and eventually structural insufficiency [14]. As a result, corrosion resistant reinforcement have been increasingly used in aggressive environments for the last 40 to 50 years due to their material longevity and lower life cycle cost compared to traditional carbon steel reinforcement [14], [15]. Various studies suggest that even though corrosion resistant reinforcement can initially cost up to four times that of carbon steel, the savings incurred from increased service life, reduced concrete deck thickness, and indirect user costs outweigh the initial costs [14]–[16]. Stainless steel reinforcement in particular has been shown to provide superior performance compared to traditional reinforcing bars [4], [17]–[20]**.** However, the wide variety of stainless steel grades and their differing chemical compositions and microstructures makes it difficult to determine an optimal grade for a particular service life and price range.

2.2 Stainless Steel Reinforcement

The use of stainless steel reinforcement in reinforced concrete for improved corrosion resistance is by no means a new concept. A concrete pier in Puerto Progresso, Mexico was constructed sometime between 1937 and 1941 with stainless steel grade 304 reinforcing bars. At the time of the Arminox inspection of the dock in 1999 [21], the inspectors stated that no significant corrosion was observed on the stainless steel reinforcement, and that the estimated remaining service life of the structure was another 20 to 30 years, equating to an 80 to 90 year service life. A similar pier had been constructed with carbon steel reinforcing bars approximately 30 years prior to the Arminox inspection, and severe corrosion of the reinforcing bars had essentially disintegrated the pier's reinforcing steel.

Over the last 20 years, the long-term cost savings, reduced liability, and aesthetic benefits of stainless steel have been recognized, particularly for bridge construction. For example, EN grade 14362 (UNS S32304) was used in the construction of the Padre Arrupe Bridge (completed in 2003) in Bilbao, Spain and for the Celtic Gateway footbridge (completed in 2006) in Holyhead, UK. The new Champlain Bridge in Montreal, currently under construction, is also being reinforced with UNS 32304 stainless rebar [22].

The material's durability, aesthetics, and low maintenance requirements were key factors for the selection as main structural elements in the bridges [23].

2.2.1 The Chemical Composition of Stainless Steel

Stainless steel reinforcement has been found to provide at least 3-4 times the service life of traditional carbon steel in aggressive environments [21], [23]–[25]. This increase in service life has primarily been attributed to the high corrosion resistance provided by chromium, nickel, molybdenum, and other alloying elements [26], [27]. Stainless steels are iron-based alloys containing at least 10.5% chromium [26], and are classified into one of five categories: ferritic, austenitic, martensitic, duplex, and precipitation-hardening. Austenitic, duplex, and ferritic grades are typically commercially available to today's construction industry. As such, these three grades are the focus of this literature review. The chemical compositions of some commonly used austenitic, duplex, and ferritic grades of stainless steel are shown in Table 2.1.

The addition of chromium in a stainless steel alloy has been shown to provide relatively uniform corrosion resistance [28], largely in part due to the high concentration of chromium at a stainless steel's passive film (oxide)-electrolyte boundary [29]. Additional elements are added into different stainless steel alloys for a variety of reasons, such as improved corrosion resistance, strength, machinability, formability, and toughness [30], Table 2.2.

The exceptional corrosion resistance inherent to austenitic stainless steels has been attributed to their relatively high nickel content, typically containing 8% nickel [23], [31]. On the other hand, the duplex and ferritic grades typically have nickel contents that are at most half of that of austenitic grades; containing 1-8% and 0% nickel, respectively [23], [31]. However, duplex S32205 (2205) has been shown to have better overall corrosion resistance than austenitic grades 304 and 316 due to its higher chromium content [32].

Table 2.1: Comparison of the composition and the mechanical properties of austenitic, duplex, and ferritic stainless steel – Adapted from [23]

Stainless Steel Type	Grade		Composition (EN 10088)		
	EN	ASTM (UNS)	Cr	Ni	Mo
Austenitic	1.4301	S30400	17.5 - 19.5	8.0 - 10.5	-
	1.4401	S31600	16.5 - 18.5	10.0 - 13.0	2.0 - 2.5
Duplex	1.4162	S32101	21.0	1.5	0.3
	1.4362	S32304	22.0 - 24.0	3.5 - 5.5	0.1 - 0.5
	1.4462	S32205/S31803	21.0 - 23.0	4.5 - 6.5	2.5 - 3.5
Ferritic	1.4510	S43036	16.0 - 18.0	-	-
	1.4509	AISI 441*	17.5 - 18.5	-	-
	1.4521	S44400	17.0 - 20.0	-	1.8 - 2.5

*No UNS equivalent

Table 2.2: Typical effects of various elements in stainless steel alloys – Adapted from [30]

Material Properties	Elements
Corrosion Resistance	Nickel, Molybdenum, Nitrogen
Strength	Carbon, Molybdenum, Titanium, Aluminum, Copper, Nitrogen
Formability	Nickel
Toughness	Nickel

The Pitting Resistance Equivalent Number (PREN) has been used to compare the corrosion resistance of stainless steels based on their chemical composition, where Equation 2.1 is typically used for austenitic stainless steels, and Equation 2.2 is typically used for duplex steels [33].

$$PRE_{16N} = (\%Cr) + 3.3\ (\%Mo) + 16(\%N) \quad \text{Equation 2.1}$$

$$PRE_{30N} = (\%Cr) + 3.3\ (\%Mo) + 30(\%N) \quad \text{Equation 2.2}$$

However, the PREN equations were derived for the critical pitting temperatures of alloys in neutral or acidic solutions, [33], [34] and as such, they are not applicable to stainless steels in ambient temperatures in concrete with its high alkaline nature. It has been suggested [35], [36] that the contribution of nickel and manganese, among other elements, could significantly affect the accuracy of the PREN numbers in

alkaline media. Short of experimental testing, there are no quantitative metrics used to definitively compare the corrosion resistance of various stainless steel grades.

2.2.2 The Cost of Stainless Steels and their Alloying Elements

One of the major barriers associated with specifying stainless steel alloys versus traditional carbon steel for concrete reinforcement is the high cost. A cost analysis of three Oregon coastal bridges built between 1999 and 2003 [25] found that the use of stainless steel reinforcement resulted in a 10% premium compared to using carbon steel reinforcement. However, the use of stainless steel for concrete reinforcement is expected to yield over 100-year design life, substantially reducing inspection costs, maintenance and repair costs, and eliminating the costs associated with bridge deck replacement [15], [37].

When selecting an optimal grade of stainless steel, one must not only consider the corrosion-resistance of the steel, but its associated cost. The variation in alloy component costs over the last 15 years, courtesy of ASW Inc., are plotted in Figure 2.1. It was found that when comparing different grades of stainless steels, the per unit price of molybdenum and nickel are as much as 8 to 30 times that of chromium and manganese [4].

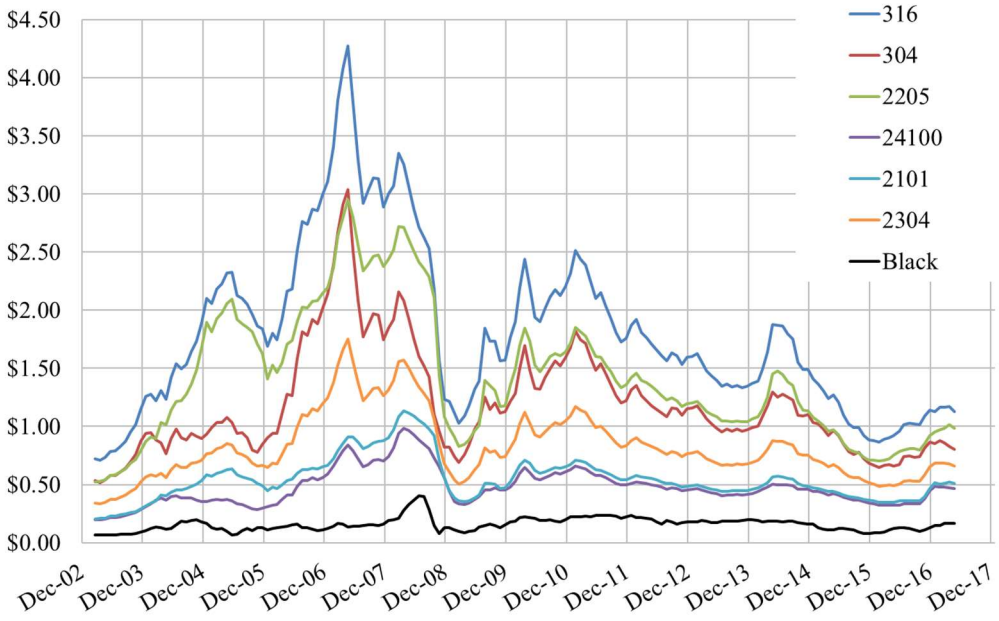

Figure 2.1: Raw material cost (US $/lb) comparison of various stainless steel grades

2.3 Corrosion Testing

Standard corrosion resistance testing of stainless steel reinforcing bars in concrete can take several years. Testing of these bars that are embedded in concrete can resemble realistic conditions. It can be advantageous if the goal is to simulate the chloride diffusion into the concrete, as is the case with real structures. However, since the rebar is expected to resist corrosion for decades, the testing times for corrosion initiation and propagation are unrealistic without some form of acceleration [38]. Furthermore, corrosion initiation of stainless steel reinforcing bars can be difficult to determine because of the difficulties associated with detecting localized pitting of the alloys [39].

Two ASTM standards are currently used to evaluate the corrosion performance of reinforcing steel in concrete: ASTM G109 for black steel [26] and ASTM A955 specifically for stainless steels [27]. The ASTM G109 method evaluates the corrosion of the rebar in concrete using half-cell and macro-cell measurements, while the ASTM A955 specifies two procedures. Procedure 2 is very similar to the G109 test but the concrete contains a simulated crack to accelerate the ingress of chlorides into the concrete. Procedure 1 is the same in principle, but the steel is immersed in a synthetic concrete pore solution, rather than embedded in concrete. All three tests measure the corrosion current between an anode and a cathode, calculated from the voltage drop across an external standard resistor.

One of the major concerns with the ASTM A955 Procedure 2 test is that the long testing duration (75-96 weeks) makes it difficult for highway jurisdictions to evaluate and select new corrosion protection methods offered by industry [40]. The test uses 280 mm x 150 mm x 115 mm concrete specimens with two layers of reinforcement, Figure 2.2. The two layers of reinforcement are electrically connected with a 100 Ω resistor, and the concrete specimen is subjected to alternating wet-dry ponding cycles containing a sodium chloride solution. The typical test duration for the G109 test requires a minimum of 6 months of monitoring the concrete specimens [40].

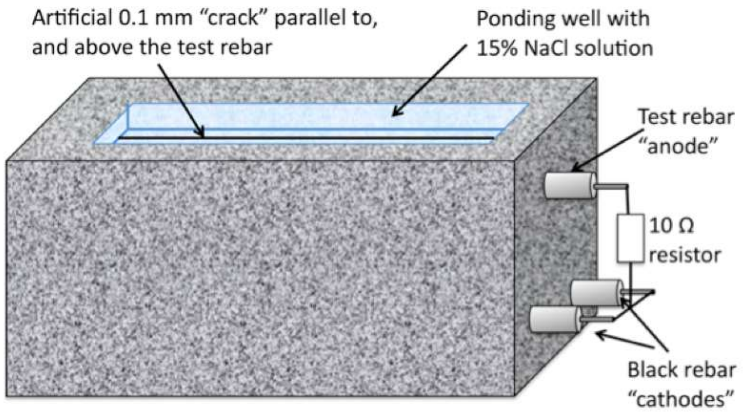

Figure 2.2: ASTM A955 Concrete Test Specimen. Adapted from [41]

Annex 2 Procedure 1 of ASTM A955 describes a "rapid macrocell test" used to measure the corrosion rate and corrosion potential of stainless steel reinforcing bars in separate cathodic and anodic cells, illustrated in Figure 2.3. The anodic cell contains one bar in synthetic concrete pore solution with 15% by weight (wt.%) of solution sodium chloride (NaCl), while the cathodic cell contains two reinforcing bars of the same grade of steel in chloride-free synthetic concrete pore solution, Figure 2.3. A 10 Ω resistor is used to electrically connect the two cells, and a salt bridge provides an ionic path between the solutions in the two cells. The typical test duration for the A955 test requires a minimum of 15 weeks of monitoring.

Other forms of testing of the steel embedded in concrete involve measuring the corrosion performance of stainless steel reinforcement using macrocell current measurements in simulated deck slab tests [24] or in concrete prisms with chlorides added to the mixing water [42]. Active corrosion was not observed for any stainless steel specimens for either the 4 or 2 year durations of either test, respectively.

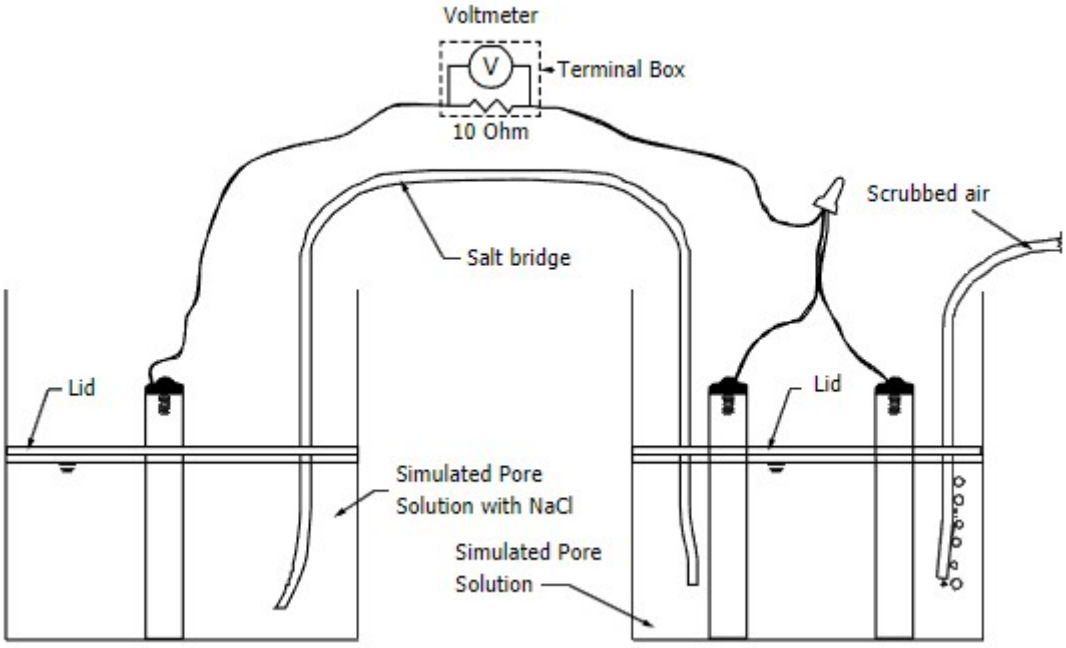

Figure 2.3: ASTM A955 Rapid Macrocell Test Setup [41]

2.3.1 Accelerated Corrosion Testing

In an attempt to reduce the time required for determining corrosion performance of reinforcing steels, many researchers accelerate corrosion testing using a variety of testing methods that utilize different corrosion monitoring methods. A brief review of various corrosion monitoring techniques for determining the extent of rebar corrosion was summarized by Song and Saraswathy [33] is shown in Figure 2.4. Some of these test methods include the application of an electric field to accelerate the rate of chloride penetration into the concrete [43], [44] or using different wetting and drying techniques to utilize various transport mechanisms [45].

However, these accelerated test methods need to be evaluated based on their required testing duration, their complexity, and the degree to which their results correlate with standard corrosion testing techniques currently employed by highway jurisdictions [40]. Soleymani and Ismail (2004) performed four common corrosion techniques on over 100 concrete specimens to estimate the corrosion behaviour of their respective reinforcing steels. It was found that the four different tests were able to accurately correlate the corrosion activity of only 24% of the specimens [46].

Characteristics	Potential Mapping	Concrete Resistivity	Linear Polarization Method	Guard Ring Method	Coulastic Method	Electrochemical Noise	EIS	Harmonics	Gravimetric Test	Visual Observation
Speed for Measurement	●	●	●	●	●	◊	◊	◊	○	○
Speed of Response to Changes	●	●	●	●	●	●	●	●	○	○
Quantitative Information	○	◊	●	●	●	◊	◊	●	●	●
Non-destructive	●	●	●	●	●	●	●	●	○	○
Non-disturbing	●	○	○	○	◊	●	◊	○	○	○
Measurement Parameter	Probability of Corrosion	Probability of Corrosion	i_{corr}	i_{corr}	i_{corr}	i_{corr}	i_{corr} mechanism	i_{corr}	Mean i_{corr}	Geometric failure of attack

● Method possesses the listed characteristic in an optimal degree.

◊ Method possesses the listed characteristic in a less than fully-satisfactory degree.

○ Method does not possess the listed characteristic.

Figure 2.4: Features of Widely Used Methods of Corrosion Monitoring – Adapted from [40], [47]

2.3.1.1 Accelerated Chloride Threshold Tests in Concrete

Developed by Trejo and Pillai (2003), the accelerated chloride threshold (ACT) test is used to determine the critical chloride threshold of reinforcing steels in cementitious materials [48], Figure 2.5. By applying a potential gradient of up to 20V across two electrodes (one within the specimen, and one in the ponding well), chloride ions migrate to the reinforcing steel's surface instead of slowly diffusing into the concrete via concentration gradients. The use of varying applied potentials for the electrical field were evaluated, and it was determined that the chloride profile in mortar specimens did not change significantly up to 10 V. The electrical field was applied in intervals of 6 hours, and after a 42 hour wait period the polarization resistance of the reinforcement was measured. The chloride concentration at the steel reinforcement at the time of corrosion initiation was used to determine the chloride threshold value of the reinforcement [48].

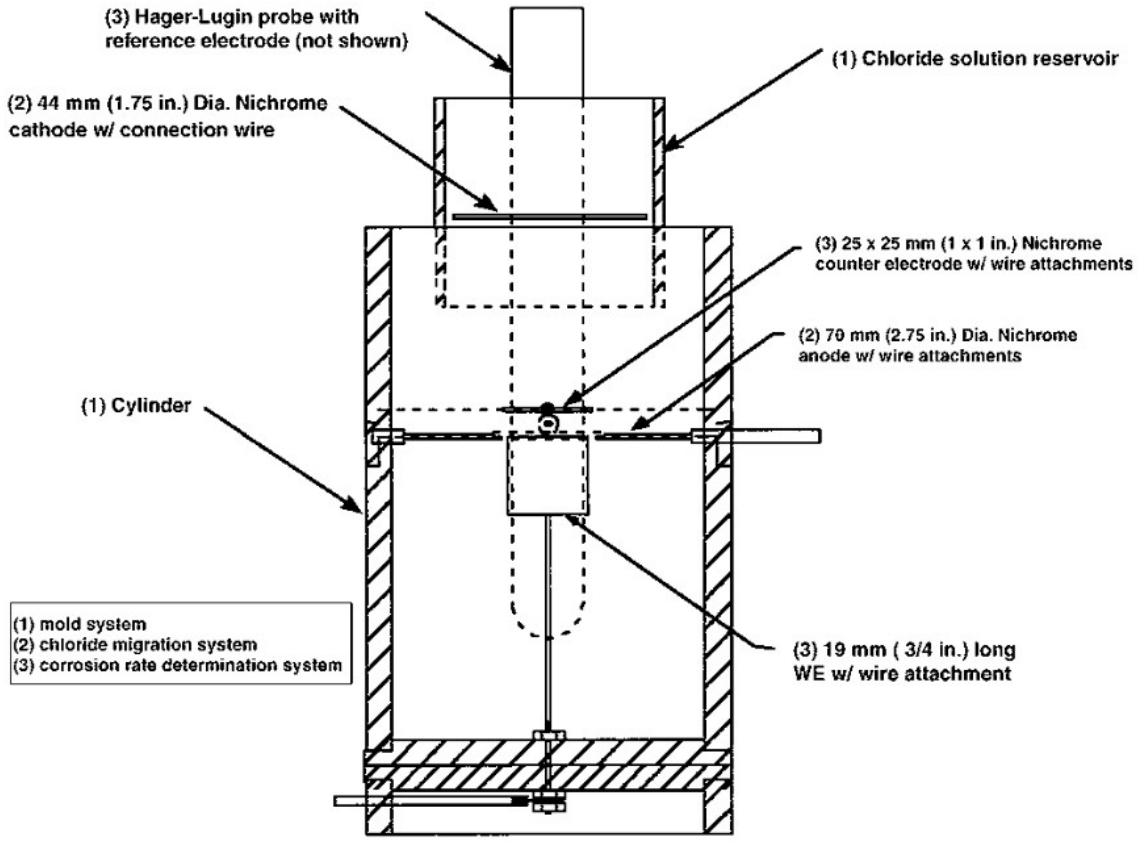

Figure 2.5: Accelerated Chloride Threshold (ACT) test setup [48]**.** Authorized reprint from ACI Materials Journal Nov-Dec 2003, Volume 100 No. 6. "Accelerated Chloride Threshold Testing: Part I-ASTM A 615 and A 706 Reinforcement".

Castellote et al. (2002) developed a similar test method that also used an electrical field to accelerate the transfer of chloride ions. Using mortar specimens, the corrosion initiation of the specimens was monitored using polarization resistance techniques. However, the two electrodes were not embedded in the specimen, but placed on the underside of the concrete specimen (anode) and in the ponding well (cathode). Castellote et al. (2002) recommended an applied potential difference of 10 to 13 V to successfully achieve an adequate chloride profile using a 1 M sodium chloride solution [44].

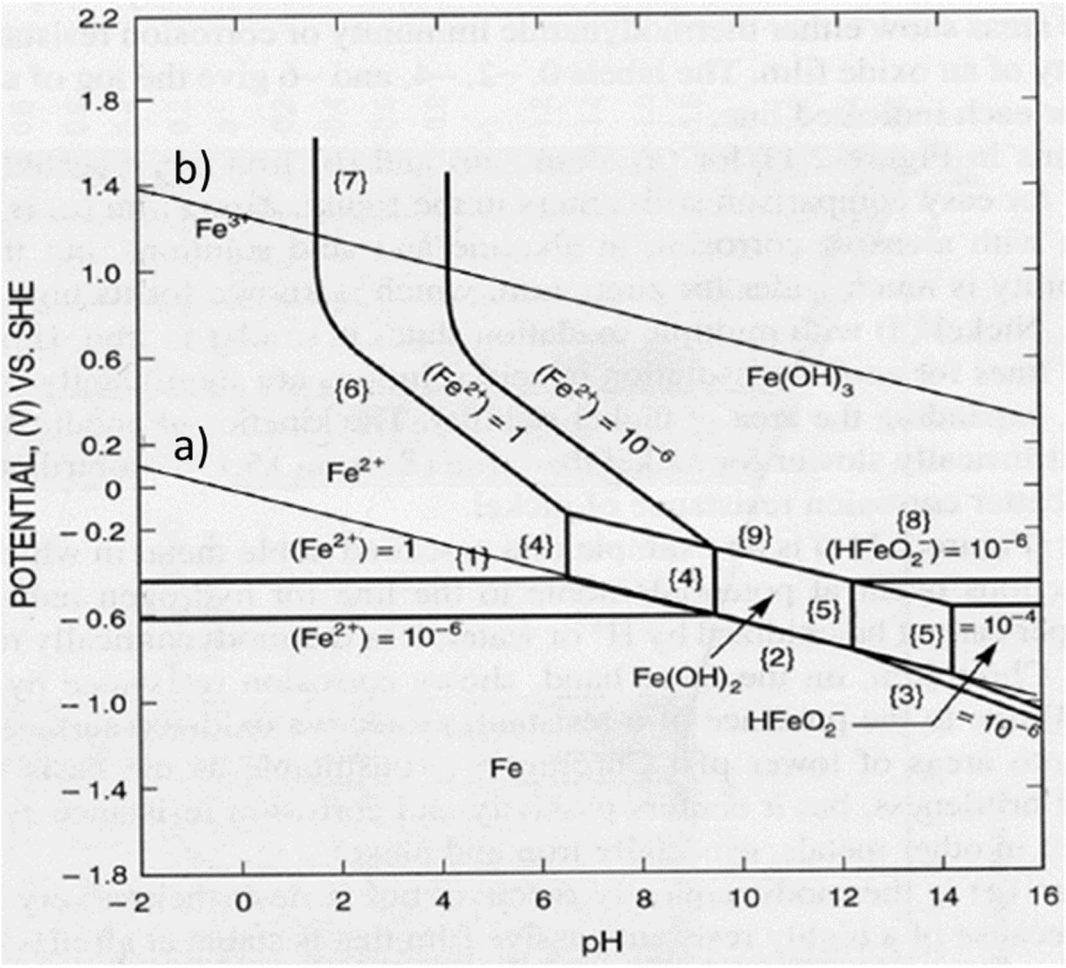

Figure 2.6: Equilibrium E/pH diagram for Iron (Fe) [49]**.** The a and b lines represent H^+/H_2 equilibrium and OH^-/O_2 equilibrium, respectively.

One of the primary concerns with this accelerated test method is that while accelerating the transport of chlorides into the cementitious material, the reinforcing steel is also being polarized. It has been found that the chloride thresholds for reinforcing steels are independent of potentials more anodic than -200 $\pm$ 50 mV_{SCE} [50] and that they linearly increase with electrochemical potentials more negative than -200 $\pm$ 50 mV_{SCE} [51].

$$E_{SCE} = E_{SHE} + 241\ mV \qquad \text{Equation 2.3}$$

Furthermore, by applying potentials in excess of +200 mV_{SCE}, which is approximately to the equilibrium potential for the oxygen/hydroxyl ion reaction in concrete media [52], Figure 2.6, the steel/mortar

interface may be altered, affecting the corrosion products that may form and the rate of the reaction [53]. The conversion between potentials measured using a saturated calomel electrode (SCE) and a saturated hydrogen electrode (SHE) is calculated using Equation 2.3. Finally, the use of an electrical field has been found to affect the pH of the mortar environment [48].

2.3.1.2 Corrosion Tests in Pore Solution

Corrosion testing of reinforcing steels in synthetic pore solution have often been used to obtain more rapid results compared to testing steel in concrete. Even though testing in synthetic pore solutions do not account for the solid concrete matrix or the interface effects with the concrete [54], these tests have been shown to predict the corrosion resistance and the chloride tolerance of a reinforcing bar in a fast and efficient manner [38].These solutions have been simulated using saturated calcium hydroxide ($Ca(OH)_2$) solutions with a pH of 12.6 [55]–[57] or in synthetic pore solutions which are more representative of "realistic" concrete, containing potassium hydroxide (KOH) and sodium hydroxide (NaOH) in addition to $Ca(OH)_2$ [27], [56], [58], [59]. The pH of these "realistic" simulations of concrete pore solutions have been found to range between 13 and 13.9. Chlorides can be incrementally added into these solutions in an attempt to capture the chloride threshold at which corrosion initiation occurs. Corrosion testing using synthetic pore solution can last up to 15 weeks [59]–[61].

2.3.2 Precursors to the Rapid Screening Test

The test evaluated in this thesis is a modification of the EN 480-14:2006 test, which uses an applied anodic potential and monitors the resultant anodic current from a given metallic reinforcing bar. This experimental procedure was originally applied by Hansson and Sørensen [62] to determine the influence of several variables on the critical chloride concentration and corrosion initiation of carbon steel. Carbon steel reinforcing bars were cast in mortar prisms, which were immersed in sodium chloride (NaCl) or calcium chloride ($CaCl_2$) solutions containing $Ca(OH)_2$. The specimens were then held at a constant applied potential of +100 mV_{SCE} and the corrosion current densities of the bars were measured daily. It is important to note that the reinforcing steel specimens developed passive films in the mortar before the chlorides reached the steel surfaces. Once the chlorides reached the steel surface, the corrosion current density of each specimen was found to increase by three orders of magnitude over several days. The minimum and maximum average times required to initiate corrosion was observed to be 27 and 389 days,

respectively. The mortar specimens were then autopsied to analyze the chloride content in the mortar directly adjacent to where active corrosion of reinforcing bars was occurring.

Sørensen et al. [63] slightly modified this test method for stainless steel grades UNS S30400 and S31600. Chlorides were admixed into the mortar specimens via the mixing water, ranging from 0-8% Cl^- by weight of cement. The stainless steel specimens were also potentiostatically polarized at 0 mV_{SCE} for 5 days, at +150 mV_{SCE} for 1.5 days, and at +200 mV_{SCE} for 2.5 days. The corrosion current density of the specimens was recorded twice per day during the potentiostatic polarization of the bars. Corrosion initiation was observed only on a few of the stainless steel specimens, making a quantitative evaluation of the test method impossible. This was attributed to the existence of a dense and uniform passive film formed on the surface of the steel in the atmosphere prior to interaction with the chlorides [63].

Modifications of this potentiostatic test have recently been used to determine the chloride levels and relative corrosion resistance ranking of stainless steel reinforcing bars in synthetic pore solution with incremental additions of chlorides [18], [38], [56], [59], and in concrete with admixed chlorides [33]. This potentiostatic method has been found to be extremely useful in determining the chloride tolerance of reinforcing bars because localized corrosion initiation is immediately detected by an increase in current [56].

2.3.3 The Rapid Screening Test and its Adaptions

EN 480-14:2006 outlines a test method for determining the influence of a given admixture on the corrosion behaviour of a steel reinforcing bar in concrete, mortar, or grout. The effect of the admixture on the corrosion behavior of the steel was evaluated by comparing specimens with and without the admixture. This test method combines the shorter testing duration of an accelerated potentiostatic tests with steel embedded in concrete, which more accurately simulate “realistic” conditions than simulated pore solutions.

Schönning and Randström [13] proposed an adapted form of the EN 480-14:2006 test as a screening test to evaluate the relative corrosion resistance of stainless steel reinforcing bars. Admixed chlorides were considered as the admixture and minor modifications were made to the test such as using an applied potential of +200 mV_{SCE} and increasing the testing duration from 1 to 4 days [13]. The procedure for the adapted test is as follows:

1. Ten stainless steel rebar specimens, Figure 2.7, were cast into individual cylindrical mortar specimens with a water-to-cementitious material (w/cm) ratio of 0.5 with 4 wt. % admixed NaCl by mass of cementitious material added to the mixing water.
2. The mortar specimens were cured for 24 hours within their molds, and then demolded and cured for another 24 hours in a saturated $Ca(OH)_2$ solution at room temperature.
3. While in the saturated $Ca(OH)_2$ solution, the open circuit potential (OCP) of the specimens was monitored for 24 hours.
4. A potentiostatic potential of +200 mV_{SCE} was applied and held for at least 87 hours, during which time the corrosion current density was continuously monitored.
5. If the corrosion current density was observed to exceed 0.025 mA/cm^2 for more than 2 hours, corrosion was considered to have initiated and the monitoring was stopped. If at least 9 of the 10 specimens did not surpass the proposed pass/fail limit for more than 2 hours, then the tested stainless steel rebar grade was said to have passed the test.

Van Niejenhuis et al. [52] evaluated the test described above on the basis of whether similar rankings of stainless steels from the test would correspond with long term tests of the same stainless steels embedded in concrete. The test was evaluated based on the following four questions:

i. Is an applied potential of +200 mV_{SCE} appropriate?
ii. Is 4 wt.% NaCl by mass of cementitious material an appropriate concentration?
iii. Is the proposed pass/fall criterion of 0.025 mA/cm^2 (0.250 A/m^2) appropriate?
iv. Does the concrete/mortar mixture design influence the results?

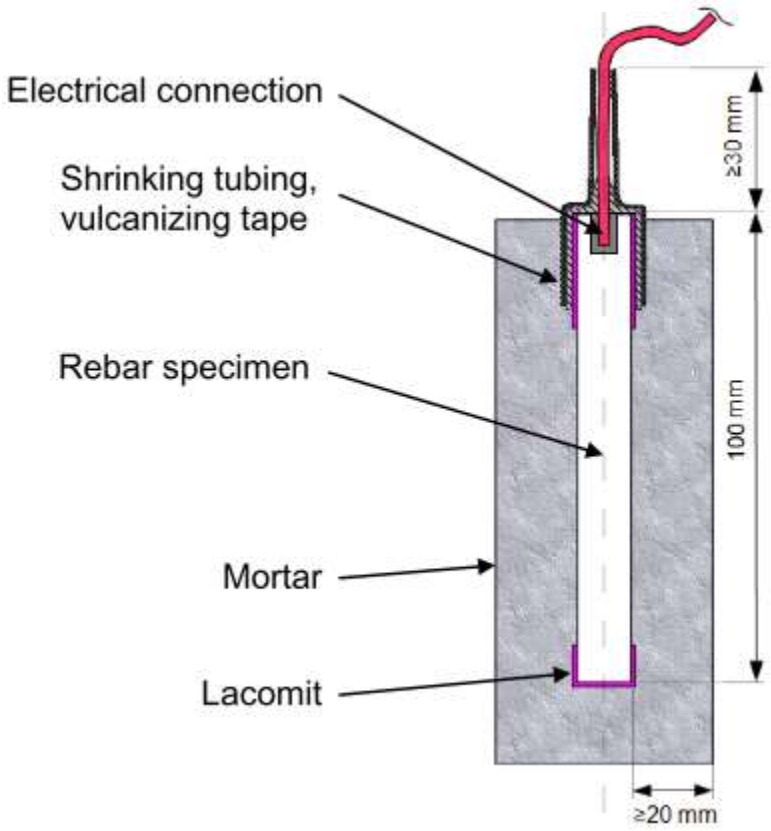

Figure 2.7: Cross-sectional view of a cast-in solution test specimen [13]

Regarding the first question, as previously mentioned in Section 2.3.1.1, an applied potential of +200 mV_{SCE} corresponds to the equilibrium potential of the oxygen/hydroxyl ion reaction, Equation 2.4, occurs given the pH of concrete pore solution. At more anodic (positive) potentials, the half-cell reaction is anodic and results in oxidation of $(OH)^-$ and the formation of O_2. At more cathodic (negative) potentials, the cathodic half-cell reaction would reduce the dissolved oxygen [52]. Consequently, the authors opted to test the reinforcing bars at +100 mV_{SCE} and +200 mV_{SCE}.

$$O_2 + H_2O + 2e^- = 4(OH)^- \qquad \text{Equation 2.4}$$

For the second question, the authors stated that the highest level of Cl^- by weight of cement reported in the field was 5%. In order to provide a realistic comparison with the long term tests, [64], the same concrete mixture design was selected to allow a direct comparison of the ranking of the stainless steels.

2.3.3.1 Modifications by Van Niejenhuis et al. [38]

The stainless steels and their respective alloys that were tested are shown in Table 2.3. A typical concrete mixture for Ontario highway bridges was used, which contained 25% blast furnace slag and 75% Portland cement, a w/cm ratio of 0.4, but the maximum aggregate size was 12.5 mm to because of the 20 mm cover on the bars. Some tests were also conducted on an ordinary Portland cement mix. Chlorides were dissolved into the mixing water as NaCl.

Table 2.3: Compositions of Alloys Tested (% by mass) by Van Niejenhuis et al. (2006) – Adapted from [52]. Reproduced with permission from NACE International, Houston, TX. All rights reserved. VanNiejenhuis, Bandura, and Hansson, Evaluation of the Proposed European Test Procedure for Ranking Stainless Steel Rebar, Corrosion Journal, Volume 72, Issue 6, 2016. © NACE International 2016.

Steel Type	C	N	Cr	Ni	Mo	Mn
S31653	0.025	0.140	18.000	10.540	2.030	1.170
S24100	0.050	0.310	17.200	0.700	0.200	12.120
S32205	0.023	0.140	22.710	4.950	3.030	1.460
S32304	0.018	0.136	22.440	4.050	0.190	1.610
S32101	0.022	0.211	21.430	1.510	0.180	4.810

The electrochemical testing procedure used by the authors was similar to that of Schönning and Randström (2011). The only notable modification to the electrochemical testing was that the applied potentials of +100 mV_{SCE} and +200 mV_{SCE} were held for 95 hours instead of 87 hrs.

A comparison of the ranking of the stainless steel bars, based on these modifications to the Rapid Screening Test versus long-term testing results in concrete, is shown in Table 2.4. The results of the Modified EN: 480-14 were not found to exactly match the results of the long-term testing.

Table 2.4: Comparative Ranking of Corrosion Resistance of Stainless Steel Between the Current Test and Long-Term Testing in Concrete [52]**.** Reproduced with permission from NACE International, Houston, TX. All rights reserved. VanNiejenhuis, Bandura, and Hansson, Evaluation of the Proposed European Test Procedure for Ranking Stainless Steel Rebar, Corrosion Journal, Volume 72, Issue 6, 2016. © NACE International 2016.

Stainless Steel Grade	Modified EN: 480-14	Longitudinally Cracked Concrete	Transversely Cracked Concrete
S32205	1	1	1
S32101	2	2	3
S31653	3	5	5
S24100	4	4	4
S32304	5	3	2

The authors found that the some of the metrics of the tests may have skewed the results. A summary of their recommendations are as follows:

- The wide variation of half-cell potentials of the different grades of bars, coupled with the applied potentials of +100 mV_{SCE} and +200 mV_{SCE} resulted in different levels of anodic polarization. As a result, some bars were subjected to more aggressive conditions than others.
- The influence of the air-formed passive films on each stainless steel grade are undetermined. The authors concluded that the specimens should be immersed in a synthetic pore solution to allow for the development of a passive film in a highly alkaline environment prior to being cast in concrete.
- The proposed pass-fail limit should be lowered such that it correlates with visual observations of corrosion initiation. This was also recommended by Schönning and Randström (2011).

Chapter 3 – Experimental Procedure

The experimental procedure for the experiments was based on the work of Schönning and Randström [13] and the recommendations of Van Niejenhuis, Bandura, and Hansson [52] on the EN 480-14:2006 test. Schönning & Randström [13] adapted the EN 480-14:2006 to evaluate the relative corrosion resistance of stainless steel reinforcing bars, and further modifications were made to the test based on the recommendations of Van Niejenhuis et al. [52] to simulate real world conditions, as explained below. For the purpose of this report, the adapted EN 480-14:2006 test is abbreviated to the Rapid Screening Test (RST).

3.1 Specimen Design

The RST specimens consisted of concrete cylinders with a centrally placed length of rebar. The cylinders were approximately 65 mm in diameter by 140 mm tall, allowing for a minimum of 25 mm of concrete cover on all sides, except for the top of the specimen with a protruding electrical wire, shown in Figure 3.1.

The experiments for the RST were designed to compare the relative corrosion resistance of three grades of stainless reinforcing steels under similar conditions. As previously stated in Section 1.3, three stainless steel grades were selected, shown in Table 3.1. Each of the stainless steels were 15M (US #5) bars in 1220 mm (4 ft.) lengths.

Table 3.1: Stainless Steel Rebar Grades

UNS Designation	Rebar Type
S24100	XM28
S32304	2304
S32205	2205

The American Society for Testing and Materials specifies that each stainless steel grade must comply with certain chemical requirements according to A276 [65], as shown in Table 3.2. The values listed in Table 3.2 for the first five elements are the maximum composition requirements. The chemical composition of each of the stainless steel grades reported by the respective manufacturers are shown in

Table 3.3. Both the 2205 and 2304 grades provided were found to be in compliance with ASTM A276, but the XM-28 grade was found to be non-compliant with respect to its carbon and silicon content.

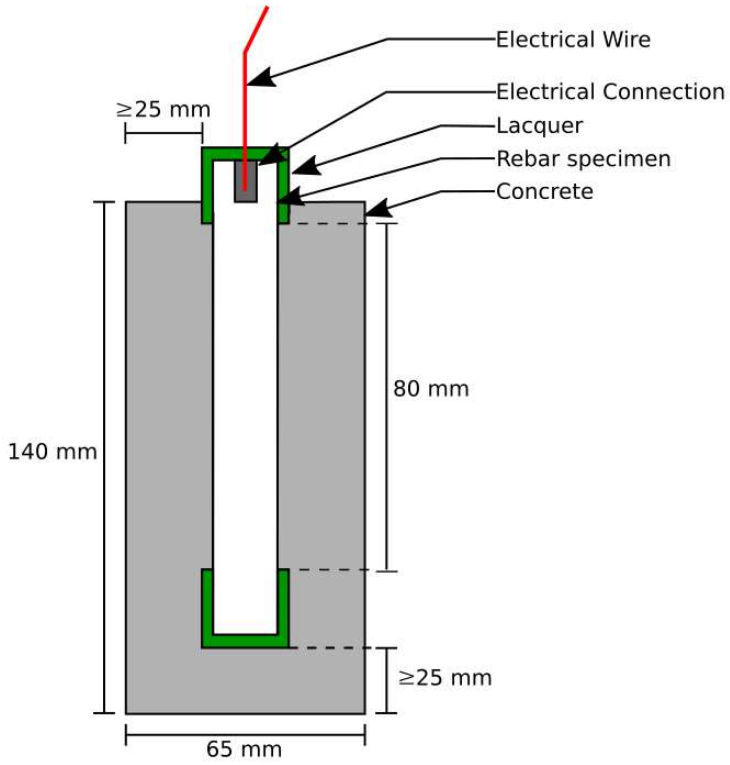

Figure 3.1: Cross-section of a Rapid Screening Test Specimen (Not to Scale)

Table 3.2: ASTM A276/A276M - 17 Chemical composition (wt.%) requirements [65]

UNS Designation	Type	Element								
		C	Mn	P	S	Si	Cr	Ni	Mo	N
S32205	2205	≤0.03	≤2.0	≤0.03	≤0.02	≤1.0	≤22.0 - 23.0	≤4.5 - 6.5	≤3.0 - 3.5	≤0.14 - 0.20
S32304	2304	≤0.03	≤2.5	≤0.04	≤0.03	≤1.0	≤21.5 - 24.5	≤3.0 - 5.5	≤0.05 - 0.60	≤0.05 - 0.2
S24100	XM-28	≤0.15	≤11.0 -14.0	≤0.045	≤0.03	≤1.0	≤16.5 - 19.0	≤0.5 - 2.5	-	≤0.20 - 0.45

Table 3.3: Chemical compositions (%) reported by manufacturers

UNS Designation	Type	Element								
		C	Mn	P	S	Si	Cr	Ni	Mo	N
S32205	2205	0.024	1.46	0.028	0.001	0.37	22.18	4.68	3.14	0.178
S32304	2304	0.02	1.74	0.02	0.001	0.38	22.86	3.55	0.31	0.16
S24100	XM-28	0.063	12.86	0.032	0.0036	0.73	18.06	0.92	-	0.326

3.1.1 Rebar Preparation

The bars were cut into 127 mm (5 in) lengths using a horizontal band saw and deburred using a belt grinder. A 5.3 mm diameter hole was then drilled 10 mm deep on one face and a 20-gauge copper wire was soldered into the hole to create an electrical connection. Once an electrical connection was established, the bars were weighed and labelled. Each stainless steel grade was designated its own wire colour to differentiate the different grades when the bars were embedded in concrete. Each grade of stainless steel and its designated wire colour are shown in Table 3.4. The bars ends were then covered and sealed with a Enplate Stop-off No. 1 (lacquer) such that a length of 80 mm of rebar was exposed to the environment, shown in Figure 3.2. Unless otherwise noted, bars were tested in the as-received surface condition subsequent to acetone cleaning.

Table 3.4: Wire colour for each grade of stainless steel

UNS Designation	Wire Colour
S32205	Red
S32304	Green
S24100	Orange

3.2 Pore Solution

A simulated concrete pore solution, Table 3.5, based on the composition of pore solution expressed from a 75% General Use (GU) and 25% blast furnace slag (BFS) cement mix with a water to cement (w/cm) ratio of 0.4 by Van Niejenhuis, Ogunsanya, and Hansson [66], was used to passivate some of the rebar prior to exposing the bars to chloride-contaminated concrete.

Figure 3.2: Rapid Screening Test Specimens with Lacquered Ends. From top to bottom, a) S24100 (XM-28), b) S32304, and c) S32205

Table 3.5: 75% GU/ 25% BFS Simulated Pore Solution Mix per Litre

Chemical Compound	Weight per L of Distilled Water (g)
KOH	26.8
$CaSO_4 \cdot 2H_2O$	0.3
NaOH	5
$Ca(OH)_2$	0.1

It was assumed that the passive film developed on the stainless steel embedded for some time in concrete will be different from that formed in the atmosphere and, therefore, steels immediately exposed to chlorides in the NaCl-containing concrete might behave very differently from those exposed to the salt after a period of time embedded in salt-free concrete. Consequently, five specimens in total for each grade of stainless-steel were passivated in the synthetic pore solution in a sealed container for 24 hours prior to placing the bars in concrete. Open circuit potentials were measured periodically with respect to a saturated calomel electrode (SCE) and observed to become stable within the 24 hr. period.

3.3 Concrete

3.3.1 Concrete Mix Design

The concrete mix design, shown in Table 3.6, complies with Ontario Provincial Standard Specifications (OPSS) 1002 and 1350 [67], [68], with the exception of the curing time and the aggregate size.

Table 3.6: Ontario bridge mix design

Concrete Mix Design		
Constituent	Amount (per m^3)	
Gravel (9mm)	1045	kg
Sand	705	kg
GU Cement	297	kg
Slag or Fly ash	98	kg
Euclid Air Extra	237	mL
Superplasticizer	900	mL
Water	158	L + abs
w/cm ratio	0.40	ratio

The coarse aggregate in the concrete was limited to 9 mm, instead of the 19 mm aggregate specified by OPSS 1002 [67] to ensure a relatively uniform distribution throughout the small specimens and 25 mm cover.

Chlorides were introduced to the concrete by admixing sodium chloride (NaCl) into the mixing water. Chloride concentrations of 4, 6, and 7.5% by mass of cementitious material were applied in different iterations of the RST. As shown by Van Niejenhuis, Ogunsanya, and Hansson [66], 4, 6, and 7.5% admixed chlorides by mass of cementitious material correspond to approximately 14, 18, and 19% of chlorides in the pore solution of the concrete.

To ensure compaction of the concrete, the concrete was cast in two lifts and thoroughly compacted by hand using a tamping rod. Once each mould was filled, Figure 3.3, the moulds were vibrated on a vibrating table to release any air bubbles trapped in the concrete.

Figure 3.3: Concrete Moulds for the Rapid Screening Test Specimens

OPSS 904 [69] states that the minimum curing time for this concrete should be a minimum of 4 days when the curing temperature is above 0˚C, and that burlap should be applied 24 hours immediately after the concrete has been placed. Due to the nature of the RST, the concrete specimens containing the stainless steel bars were removed from their moulds 24 hours after the concrete was placed.

The RST specimens were initially cured in a humidity room at 100% relative humidity (RH) at room temperature for 24 hours. However, in the early stages of the testing, it was determined that curing the relatively small specimens of concrete in 100% RH had a significant impact on the open circuit potential (OCP) and corrosion current density of the embedded stainless-steel grades. This could be attributed to the change in the w/cm ratio of the specimens over the 24 hours. This is further discussed in Chapter 4. After observing this phenomenon, the RST specimens were instead cured in a sealed environment for 24 hours to minimize any changes in the w/cm ratios.

3.4 Electrochemical Testing

After curing for 24 hours, the RST specimens were removed from their respective moulds and placed in sealed containers containing distilled water saturated with $Ca(OH)_2$, a titanium mesh acting as a counter electrode, and a Mg/MgO_2 reference electrode. The Mg/MgO_2 reference electrodes were calibrated against SCE electrodes every week. The specimens were completely immersed in the saturated $Ca(OH)_2$ water. The counter electrode, the reference electrode, and the wires protruding from the RST specimens were then attached to a potentiostat, as shown in Figure 3.4.

Prior to measuring the open circuit potential (OCP) of each stainless steel specimen, the manganese dioxide reference electrodes used to monitor the OCP of each specimen were measured against a

calibrated saturated calomel electrode to ensure that the manganese dioxide reference electrodes were properly calibrated. The average difference in potential between the manganese dioxide electrodes and the saturated calomel electrodes was found to be +150 mV, which was found to agree with literature for a saturated $Ca(OH)_2$ solution [70].

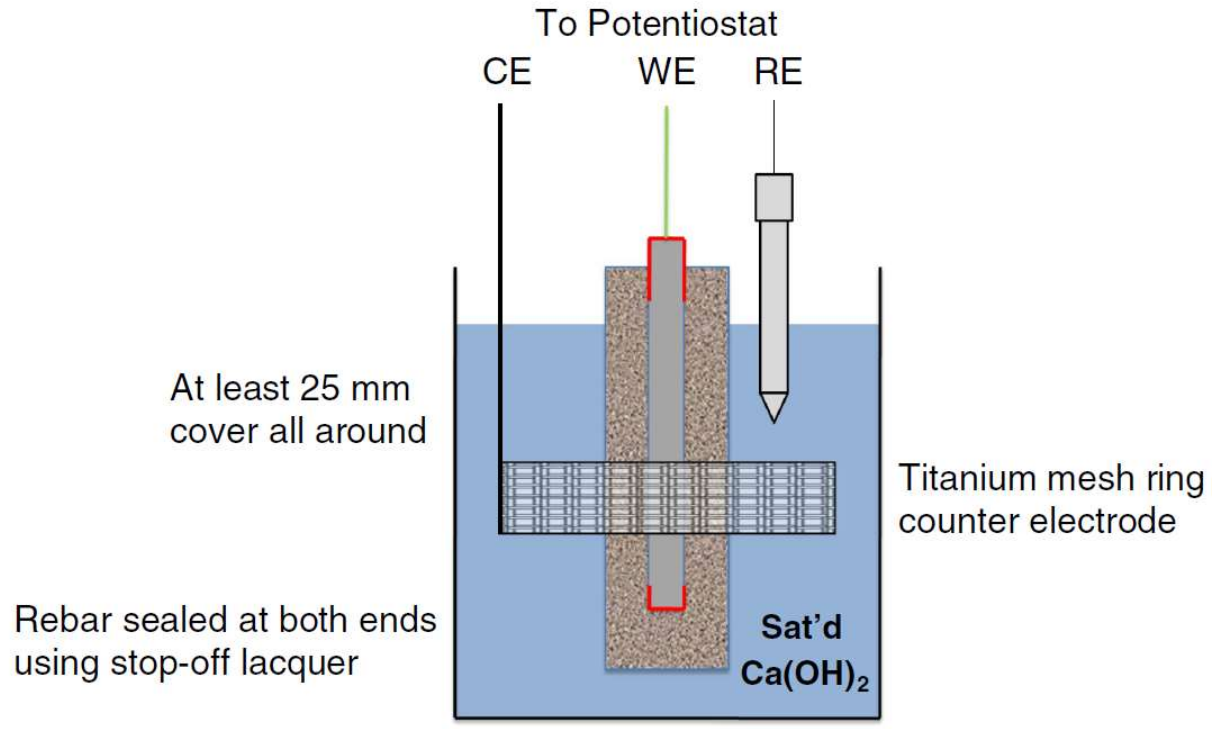

Figure 3.4: Schematic diagram of experimental test cell [52]**.** Reproduced with permission from NACE International, Houston, TX. All rights reserved. VanNiejenhuis, Bandura, and Hansson, *Evaluation of the Proposed European Test Procedure for Ranking Stainless Steel Rebar*, Corrosion Journal, Volume 72, Issue 6, 2016. © NACE International 2016.

Six specimens of each stainless steel grade were tested for each chloride/potential combination with two specimens of each steel being tested on a weekly basis.

First, the open circuit potential (OCP) of each specimen was monitored for 24 hours and was recorded every 5 minutes. Immediately after the 24 hour period, each specimen was subjected to an anodic potentiostatic polarization (also referred to as an applied overpotential) of 100, 200, 300, or 400 mV with respect to its OCP for 96 hours, as shown in Figure 3.5, and the resultant corrosion current flowing between the specimen and the counter electrode was recorded every 15 min for the 96 hr period. The steel

was considered to have "passed the test" if the corrosion current density did not exceed a critical level of 0.025 A/m^2 for a 2 hour period. Specific considerations were made such that the applied overpotentials would not exceed the equilibrium potential of +200 mV_{SCE} for the oxygen/hydroxyl ion reaction in concrete media [52].

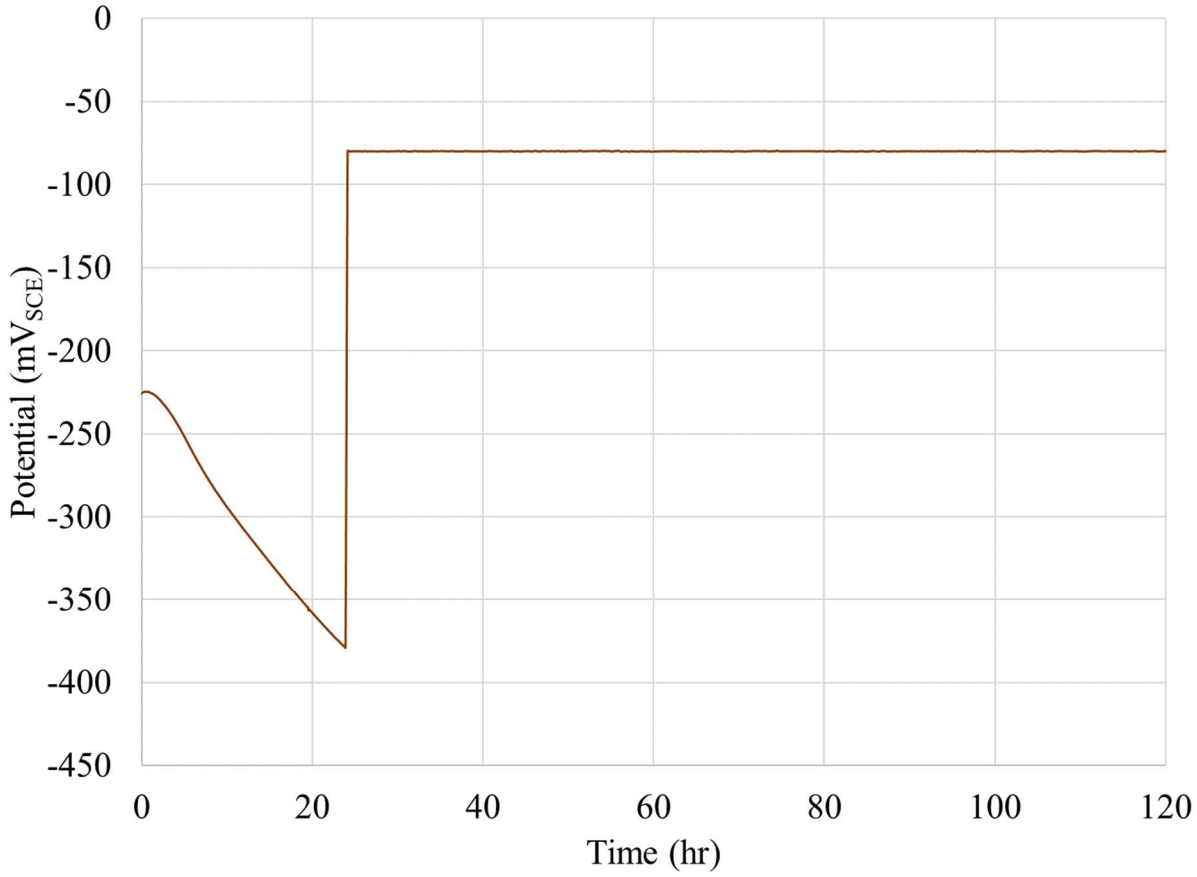

Figure 3.5: RST potential measurements for a 2304 specimen. The data for the first 24 hours represents the OCP measurements, while the data after 24 hours represents the applied potential during the potentiostatic polarization. Test parameters: 300 mV applied polarization potential and 6% admixed chloride

3.5 Autopsying of RST specimens after testing

At the end of the test, the cylinders were visually examined for any signs of corrosion. Thereafter, the stainless steel bars were removed from the concrete by using split tensile loading. Photographs were taken

of broken concrete and the rebar, as shown in Figure 3.6. The bars were then removed from the concrete and then photographed on each side

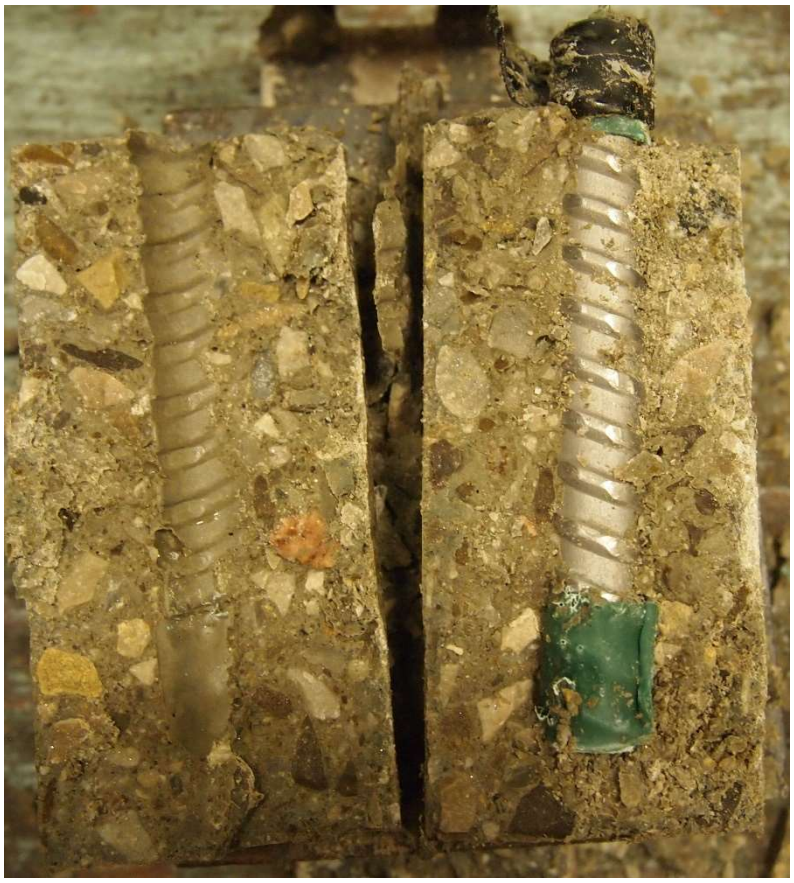

Figure 3.6: Broken 6% admixed chloride specimen cylinder with a 2205 bar after 96 hr at +300 mV polarization

The corrosion products on the stainless steels were removed using a 10-15% hydrochloric acid bath, as prescribed by the American Iron and Steel Institute for chromium-nickel stainless steels [71]. The bars were exposed to the acid bath for less than one minute, after which they were rinsed with distilled water. The corroded bars were not weighed after being cleaned due to the inability to remove pieces of concrete that had adhered to the steel's surface, which would skew the mass loss calculation. Photomicrographs were taken, at various magnifications, of the corroded stainless steel specimens upon removal of the corrosion products.

3.6 Testing of Concrete Cylinders

Concrete cylinders were made with each concrete batch in accordance ASTM C31/C31M [72], and their compressive strength was tested in accordance with ASTM C39 [73]. Bulk and surface resistivity measurements were also taken for each cylinder immediately prior to testing. The dimensions of the cylinders were 100 mm in diameter and 200 mm in length.

3.7 Summary of Parameters Tested

The number of specimens of each stainless steel grade tested in the RST at varying admixed chloride and polarization potential values is given in in Table 3.7. The minimum number of replicates was 6 specimens for a given admixed chloride and polarization potential, however, some additional specimens were tested for bars passivated in pore solution or for curing specimens in the humidity room.

Table 3.7: Number of Specimens of Each Stainless Steel Grade Tested

Polarization Potential (mV)	Admixed Chlorides by Mass of Cementitious Material (%)		
	4.0	6.0	7.5
100	10	6	0
200	0	8	6
300	0	6	6
400	6	6	6

For the sake of brevity, batches will be used to denote the admixed chloride content and polarization potential from here on in. For example, a 4-400 batch refers to the batch containing 4% admixed chloride by mass of cementitious material and tested with an applied overpotential of 400 mV.

For the 10 specimens in the 4-100 batch, 5 specimens were tested in their as-received condition and 5 specimens were tested after they had been passivated in synthetic pore solution for 24 hrs. For the 8 specimens in the 6-200 batch, 2 specimens were cured in the humidity room while the remaining 6 specimens were cured in the sealed environment. This is further discussed in Chapter 6.

Chapter 4 – Experimental Results

The following section describes the physical properties of the materials that were tested, as well as the results from the modified Rapid Screening Test (RST).

4.1 Concrete

Compression tests and electrical resistivity measurements were performed on the concrete cylinders cast together with the RST batch specimens. The tests were completed at 28 days after casting, and the average values of compressive strengths, surface resistivity and bulk resistivity of the concrete cylinders are presented in Table 4.1, Table 4.2, and Table 4.3, respectively.

Table 4.1: Average concrete compressive strength (MPa) by chloride content (wt.% by mass of cementitious material)

Chloride Content (wt. % by mass of cementitious material)	Average Compressive Strength (MPa)			
	3 Day	7 Day	14 Day	28 Day
4	28.01	37.87	43.02	50.87
6	19.76	27.52	36.32	44.46
7.5	12.67	21.76	-	36.87

Table 4.2: Average surface resistivity (kΩ cm) by chloride content (wt.% by mass of cementitious material)

Chloride Content (wt. % by mass of cementitious material)	Average Surface Resistivity (kΩ cm)			
	3 Day	7 Day	14 Day	28 Day
4	2.48	5.15	7.31	12.73
6	1.19	2.35	4.43	7.56
7.5	≤1.00	1.78	-	5.79

Table 4.3: Average bulk resistivity (kΩ cm) by chloride content (wt.% by mass of cementitious material)

Chloride Content (wt. % by mass of cementitious material)	Average Bulk Resistivity (kΩ cm)			
	3 Day	7 Day	14 Day	28 Day
4	1.36	3.01	4.27	7.54
6	0.77	-	2.92	5.14
7.5	0.53	1.05	-	3.72

4.2 Stainless Steel Alloys

The measured chemical composition of each of the stainless steel alloys used in the experimental procedure are shown in Table 4.4. These measurements were collected by using X-ray fluorescence (XRF), and all alloys fall within the acceptable ranges for chemical composition. It should be noted that XRF is unable to determine the composition of light elements (e.g. carbon and nitrogen) because it cannot accurately detect elements with an atomic mass less than aluminum [4].

Table 4.4: Chemical composition of stainless steels by XRF analysis

UNS Designation	Chemical Composition (%)									
	Type	C	Mn	P	S	Si	Cr	Ni	Mo	N
S32205	2205	<LOD	1.4	<LOD	<LOD	0.62	21.63	4.44	2.96	<LOD
S32304	2304	<LOD	1.79	<LOD	<LOD	0.69	22.44	3.19	0.32	<LOD
S24100	XM=28	<LOD	12.68	<LOD	<LOD	0.89	17.09	0.85	0.19	<LOD

Where "<LOD" represents element levels that are below the level of detection by the XRF

4.3 Passivation of Steel Specimens in Synthetic Pore Solution

To determine if any change in composition or character of the air-formed passive films on immersion in the highly alkaline test environment would significantly affect the corrosion behaviour of the tested stainless steel alloys, five sets of specimens were immersed in synthetic pore solution for 24 hours, as described in Chapter 3. Their open circuit potentials of the were measured during that period and are shown in Figure 4.1. One set of specimens was monitored for 48 hours to determine if the measured passivation potential of the specimens had reached a plateau and little change was noted between the 24 and 48 hrs. In all cases, there was a gradual increase in potential over the test period, suggesting the passive film was becoming more protective.

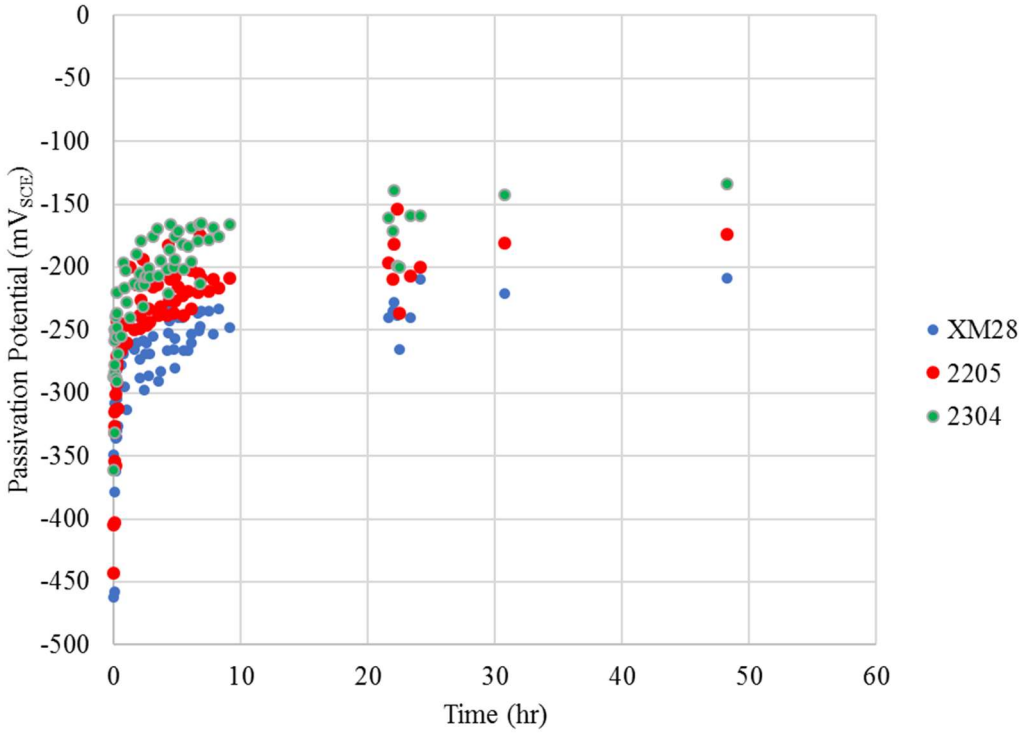

Figure 4.1: Stainless steel passivation potentials in a synthetic concrete pore solution. (75% GU/ 25% BFS mix with a 0.4 w/cm ratio)

4.4 Electrochemical Testing

The Rapid Screening test was performed on nine batches of specimens, as indicated in Table 3.7. The open circuit potential (E_{corr}), corrosion current density (i_{corr}), and time to corrosion were able to be determined. The following sections present the results of the Rapid Screening Test associated with each "batch" of the rapid screening test. A "batch" refers to the admixed chloride content and applied polarization potential of the set of specimens, as described in Section 3.7.

For the purpose of ranking of the steels, active corrosion of a specimen was considered to have initiated if its corrosion current density surpassed the proposed pass-fail limit of 25 mA/m^2 for 2 hours. Visual observations of corrosion are discussed in Section 4.5.

It should be noted that the 4-100 and 6-100 batches were kept, in their cylinders but without a cap, in a humidity room at 100% RH for the first 24 hours. All other specimens were kept in a sealed condition in the laboratory. The impact of these different procedures is discussed in Chapter 6.

Individual plots of open circuit potential (E_{corr}) and corrosion current density (i_{corr}) for a given casting week are shown in Appendix A. The concrete slump data that corresponds to each weekly batch are shown on each figure, when applicable. Note that the legend in each figure states the both the bar number and specimen number for a given specimen. For example, 2205 AR 1.1 denotes stainless steel grade 2205, the first specimen taken from bar one, and tested in its as-received state (AR).

4.4.1 RST 4-100 Batch

The 4% admixed Cl^-, +100 mV polarization (4-100) batch was used to determine whether any change in the air-formed passive film on the stainless steel during immersion in synthetic pore solution was sufficiently significant to justify this "pre-passivation" procedure for future batches. Five specimens of each stainless steel grade were tested in their as-received (AR) condition and another five specimens were tested after they had "pre-passivated" in synthetic pore solution (PP) for 24 hours. Individual plots of both E_{corr} and i_{corr} data are shown in Appendix A. The average E_{corr} of the AR and PP specimens are shown in Figure 4.2. The differences in the average and standard deviations of the open circuit potentials of the AR and PP stainless steel specimens measured shortly after immersion in the $Ca(OH)_2$ solution and, again 24 hr later, are shown in Table 4.5 and Table 4.6. It was concluded that the differences in potential were not significant enough to warrant further passivation of the stainless steel grades in synthetic pore solution for subsequent tests. The average OCP values between the replicates of each stainless steel grade were found to not vary by more than 58 mV at end of the 24 hr period.

By applying a polarization potential of +100 mV to the 4-100 batch specimens, the most positive potential was found to be -238 mV_{SCE}, which is well below the thermodynamic oxygen equilibrium potential of approximately +200 mV_{SCE} given the alkalinity of concrete medium. All 4-100 batch specimens were cured in the humidity room. A discussion of the impact of curing of the RST specimens in the humidity room is given in Chapter 6.

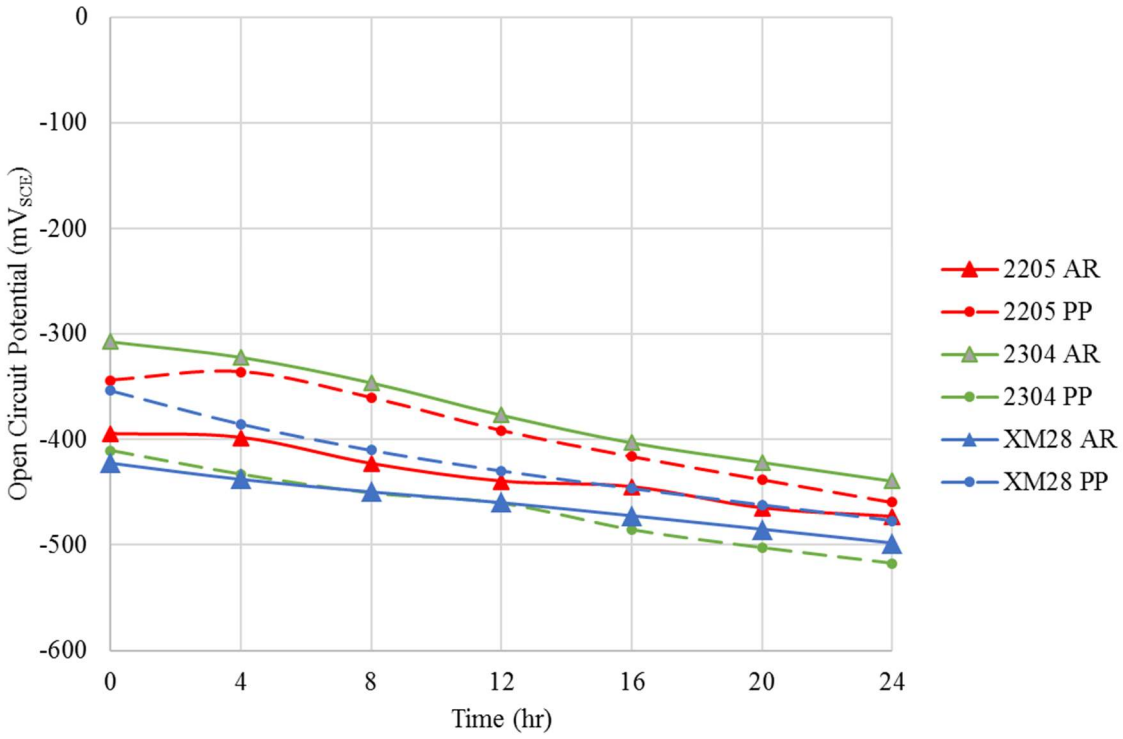

Figure 4.2: 4-100 Batch – Average Open Circuit Potentials over 24 hours (mV_{SCE}). Note that AR denotes the stainless steel specimens that were tested in their as-received condition, and that PP denotes the specimens that were tested after they were immersed in synthetic pore solution.

Table 4.5: 4-100 Batch – Averages of Open Circuit Potentials for the As-Received and Passivated in Synthetic Pore Solution Specimens

Time (h)	Average Open Circuit Potentials (mV_{SCE})					
	2205		2304		XM-28	
	AR	PP	AR	PP	AR	PP
0	-395	-344	-308	-411	-422	-354
24	-473	-460	-440	-517	-498	-477

Table 4.6: 4-100 Batch - Standard Deviation of Open Circuit Potentials for the As-Received and Passivated in Synthetic Pore Solution Specimens

Time (h)	Standard Deviation of Open Circuit Potentials (mV_{SCE})					
	2205		2304		XM-28	
	AR	PP	AR	PP	AR	PP
0	52	111	50	239	38	44
24	51	56	58	60	32	49

The corrosion current density values of all the specimens for the 4-100 batch were observed to be lower than the proposed pass-fail limit, indicating that active corrosion had not been initiated in any of the specimens.

For the RST specimens tested during the week of May 31, 2017, shown in Appendix A, two things should be noted. First, the electrical wire connected to the stainless steel 2304 PP 2.1 specimen was disconnected when the concrete formwork was removed, so, no data are shown for this specimen. Secondly, the electricity at the University of Waterloo went out sometime after 9:10 am on June 5, 2017. As a result, the corrosion current density data, shown in Figure A.10, are shown only to approximately 72 hours. Based on the performance of the other RST specimen sets for the 4-100 batch, it was believed that these specimens would not undergo corrosion initiation even if the test were to run for the full 96 hours.

For all subsequent batches, two specimens of each stainless steel grade in their as-received condition were tested at three weekly intervals for a total of six replicates. The plots of both the weekly E_{corr} and i_{corr} data are shown in in Appendix A. In the case of the 6% admixed Cl^-, +200 mV polarization (6-200) batch, eight specimens of each stainless steel grade were tested: 6 sets of specimens were cured in a sealed environment (similar to the other batches) and 2 sets were cured in the humidity room. Only the 6 sets of specimens cured in the sealed environment are considered for data analysis. A discussion of the impact of curing of the RST specimens in the humidity room is given in Chapter 6.

4.4.2 RST 4-400 Batch

The average E_{corr} values of specimens for the 4% Cl^-, +400 mV polarization (4-400) batch monitored over the first 24 hr after de-moulding the cylinders, are shown in Figure 4.3, The average OCP values for each stainless steel grade did not vary by more than 40 mV at the end of the OCP monitoring period. By applying a polarization potential of +400 mV to the 4-400 batch specimens, the most positive potential was found to be -17 mV_{SCE}.

The corrosion rates of three specimens of XM-28 were found to exceed the proposed pass-fail limit, as shown in Figure 4.3, and the bars were considered to have undergone active corrosion initiation. The times at which the specimens surpassed the proposed pass-fail limit, referred to as the corrosion initiation time, are shown in Table 4.7. The corrosion rate of all other specimens remained approximately an order of magnitude below the 0.025 A/m^2 level.

Table 4.7: 4-400 Batch – Corrosion Initiation Time (hr) of Corroded As-Received Specimens

Stainless Steel Grade	Specimen	Corrosion Initiation Time (hr)
XM-28	7.5	88.75
XM-28	7.6	7.75
XM-28	7.7	23.75

4.4.3 RST 6-100 Batch

The average E_{corr} values of the specimens for the 6% Cl^-, +100 mV polarization (6-100) batch, monitored over the first 24hrs after de-moulding the cylinders, are shown in Figure 4.4. The average OCP values between each stainless steel grade were found to not vary by more than 114 mV at the end of this period. At an anodic polarization of +100 mV, the most positive specimen potential was -208 mV_{SCE} at the end of the OCP monitoring period.

The corrosion current density values of all the specimens for the 6-100 batch were less than the proposed pass-fail limit over the 4-day polarization period, indicating that these conditions were not sufficient to initiate active corrosion.

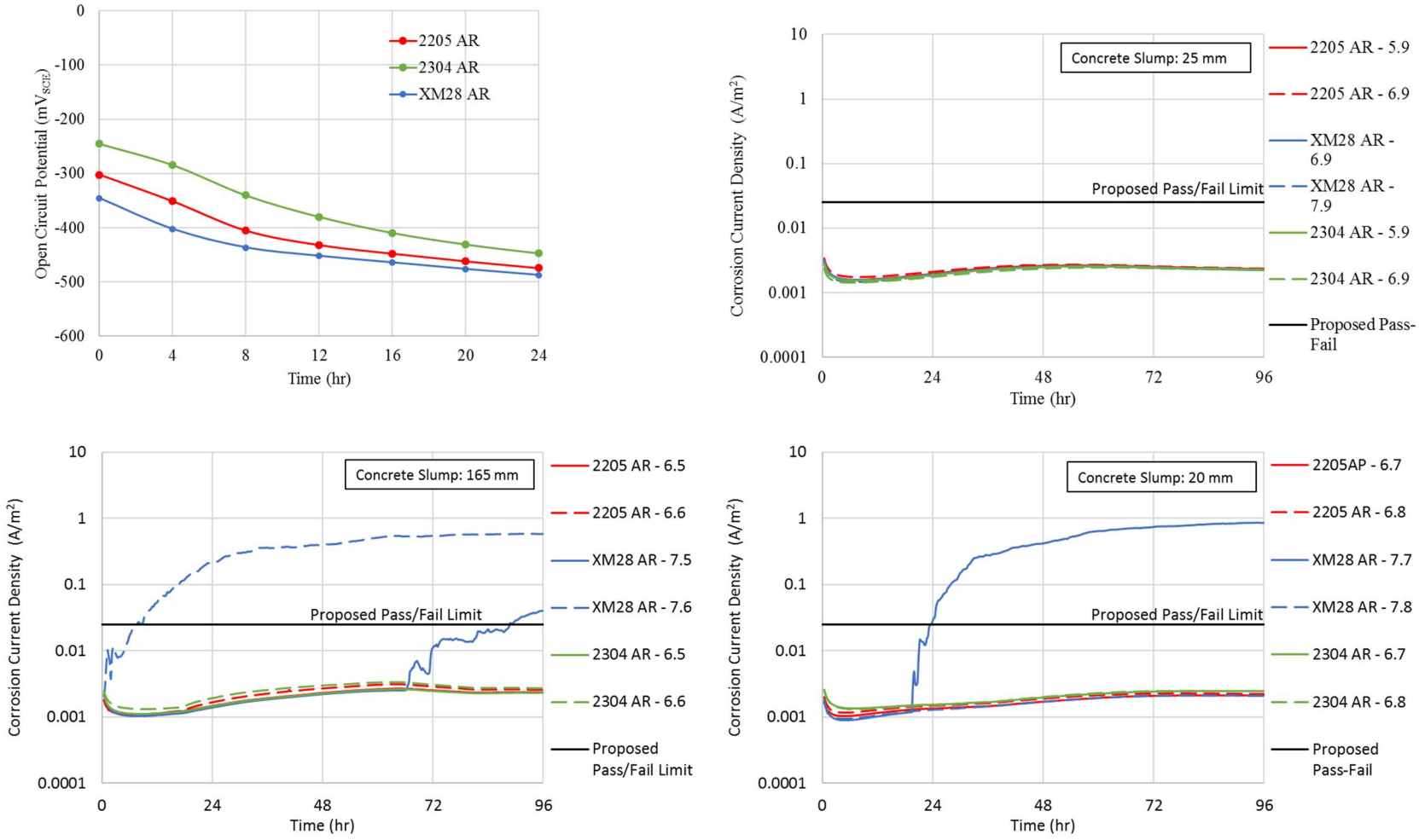

Figure 4.3: 4-400 Batch: Average Open Circuit Potentials over 24 hours (mV_{SCE}) [Top], Corrosion Current Densities over 96 hours [Bottom].

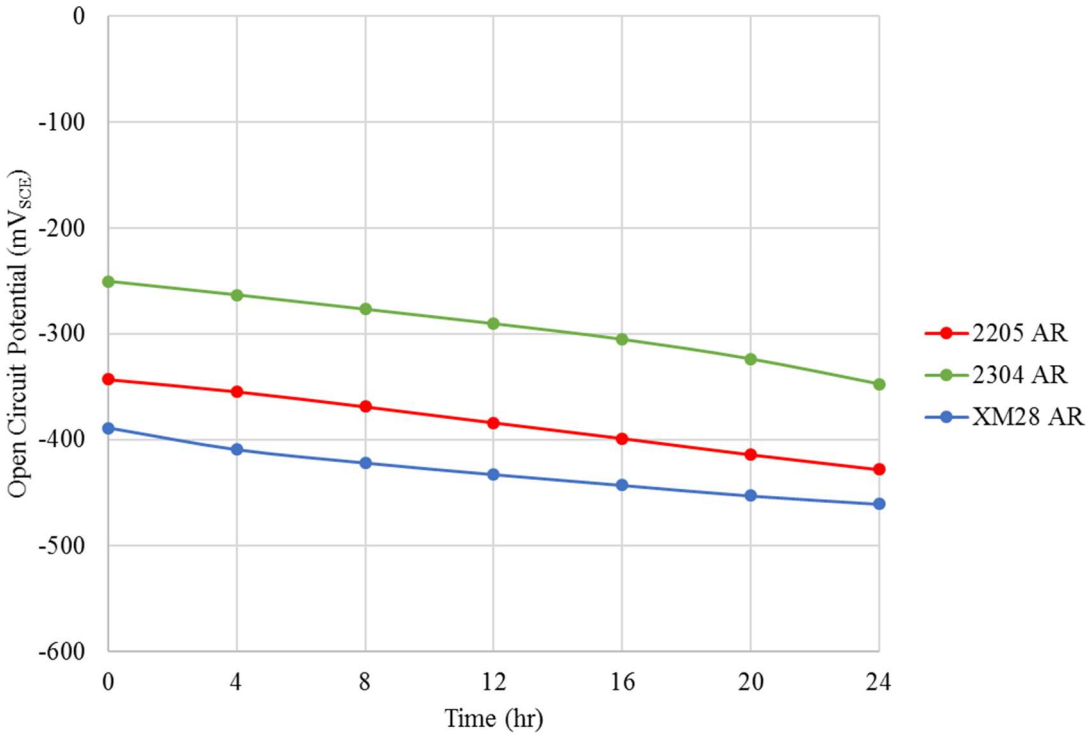

Figure 4.4: 6-100 Batch – Average Open Circuit Potentials over 24 hours (mV_{SCE})

4.4.4 RST 6-200 Batch

Eight specimens of each stainless steel grade were tested for the 6% Cl^-, +200 mV polarization (6-200) batch: 6 sets of specimens were cured in a sealed environment and 2 sets were cured in the humidity room. Only the 6 sets of specimens cured in the sealed environment are considered for data analysis. A discussion of the impact of curing of the RST specimens in the humidity room is given in Chapter 6. The average E_{corr} values of the six specimens are shown in Figure 4.5. The average OCP values between each stainless steel grade were found to not vary by more than 123 mV at the end of the OCP monitoring period. At a polarization potential of +200 mV the most positive potential of the specimens was -85 $mV_{SCE.}$

The corrosion rate of one specimen of XM-28 was found to exceed the proposed pass-fail limit at a corrosion initiation time of 27.92 hours, shown in Figure 4.5. None of the other specimens showed signs of initiation of active corrosion.

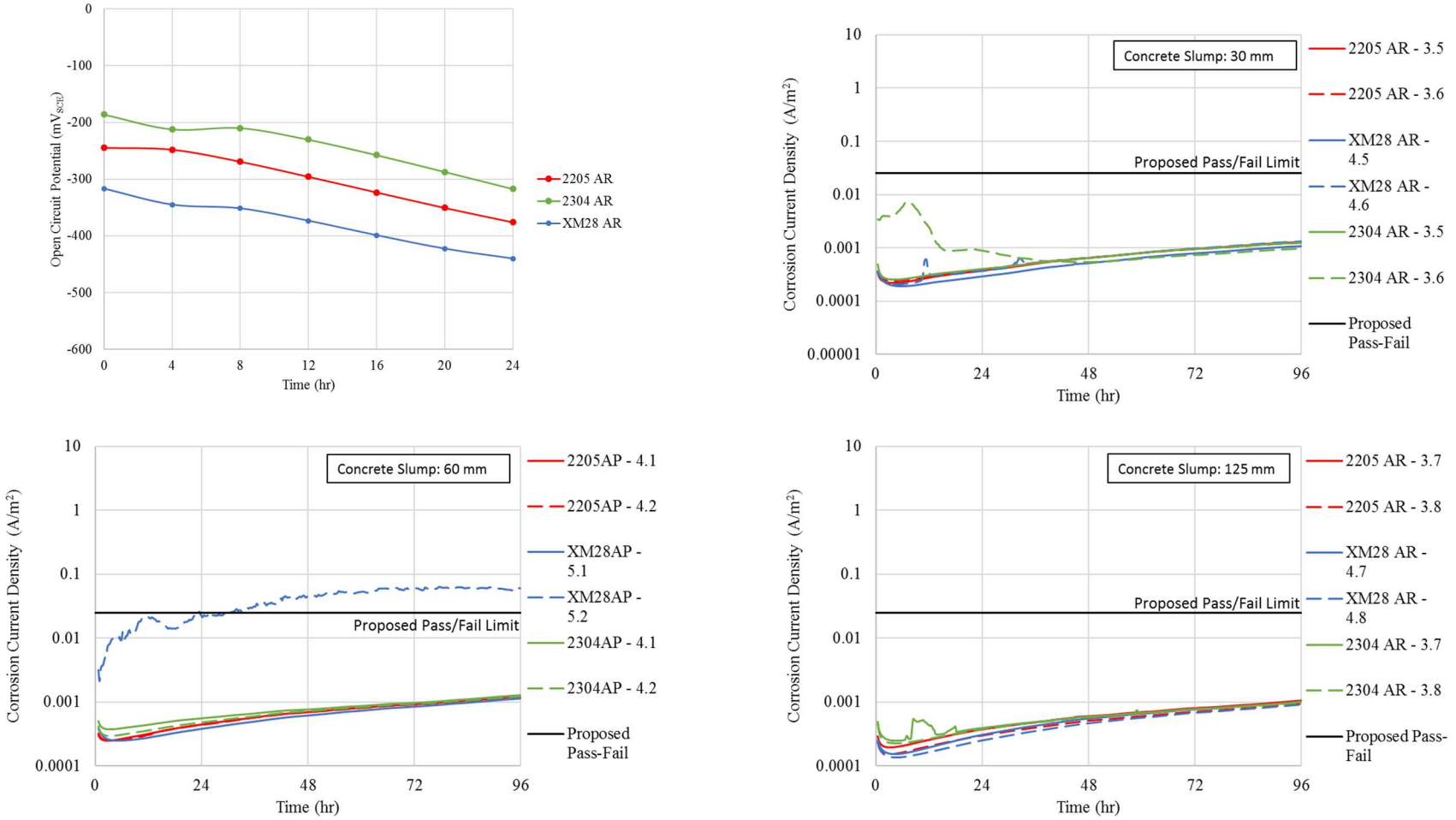

Figure 4.5: 6-200 Batch: Average Open Circuit Potentials over 24 hours (mV_{SCE}) [Top], Corrosion Current Densities over 96 hours [Bottom].

4.4.5 RST 6-300 Batch

The average E_{corr} of the 6% Cl^-, +300 mV polarization (6-300) batch specimens are shown in Figure 4.6. The average OCP values between each stainless steel grade were found to not vary by more than 103 mV at the end of the OCP monitoring period. At a polarization potential of +300 mV the most positive potential of the six specimens was -9 mV_{SCE}.

The corrosion rate of one specimen each of the XM-28 and the 2304 was found to exceed the proposed pass-fail limit at a corrosion initiation time of 4.50 hours and 38.50 hours, respectively, as shown in Figure 4.6.

4.4.6 RST 6-400 Batch

The average values of E_{corr} of 6% Cl^-, +400 mV polarization (6-400) specimens are shown in Figure 4.7. The variation of OCP within each stainless steel grade was found to not vary by more than 55 mV at the end of the 24 hr period. At an applied polarization potential of +400 mV to the 6-400 batch specimens, the most positive potential was found to be +109 mV_{SCE}, which is below the evolution potential of approximately +200 mV_{SCE} given the alkalinity of concrete media.

The corrosion rate of five specimens of XM-28 were found to exceed the proposed pass-fail limit at varying corrosion initiation times, shown in Table 4.8. The corrosion current density plots for each these specimens are shown in Figure 4.7.

Table 4.8: 6-400 Batch – Corrosion Initiation Time (hr) of Corroded As-Received Specimens

Stainless Steel Grade	Specimen	Corrosion Initiation Time (hr)
XM-28	6.1	2.75
XM-28	6.2	1.75
XM-28	6.3	56.50
XM-28	6.4	4.00
XM-28	6.5	16.75

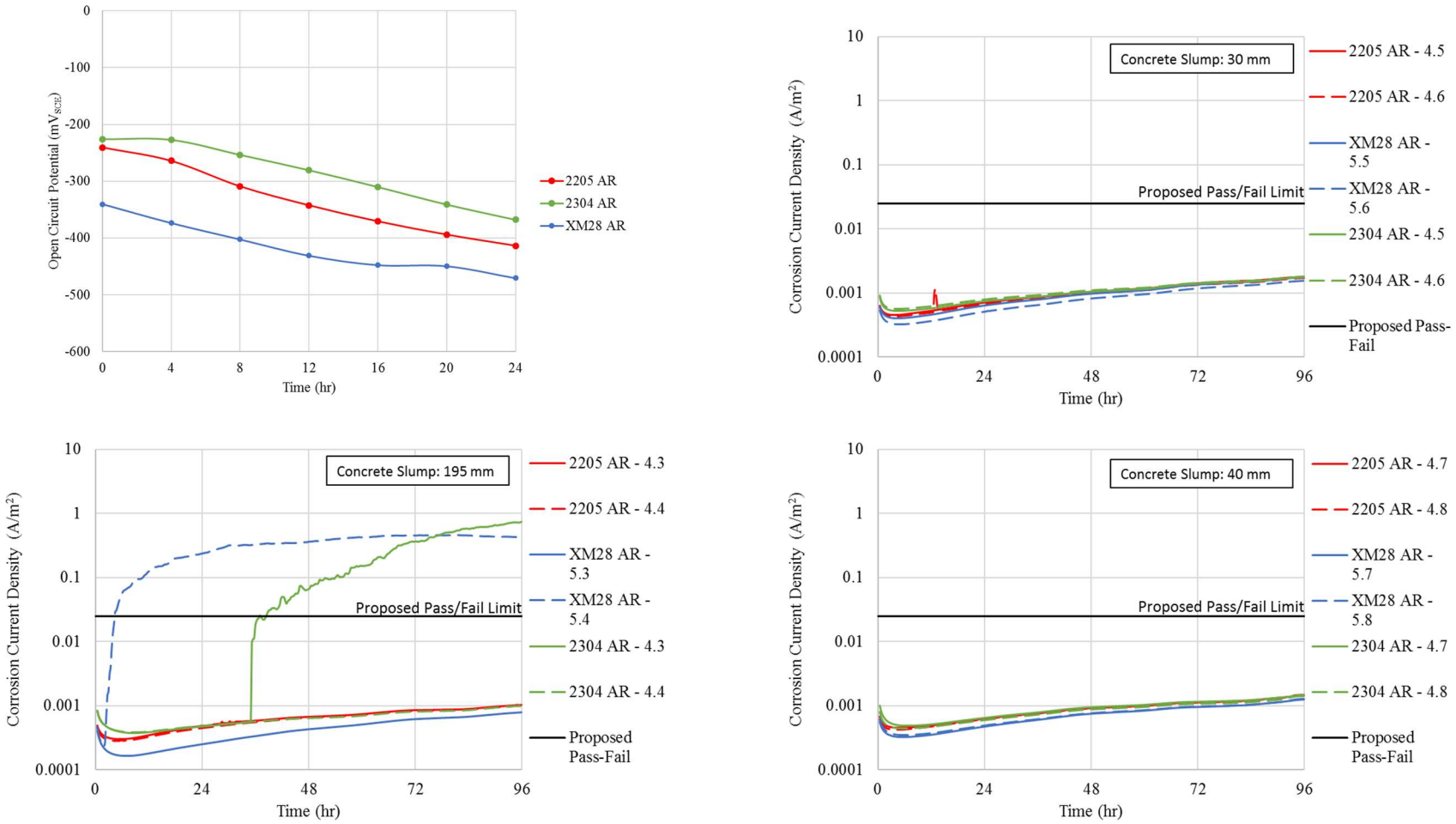

Figure 4.6: 6-300 Batch: Average Open Circuit Potentials over 24 hours (mV_{SCE}) [Top], Corrosion Current Densities over 96 hours [Bottom].

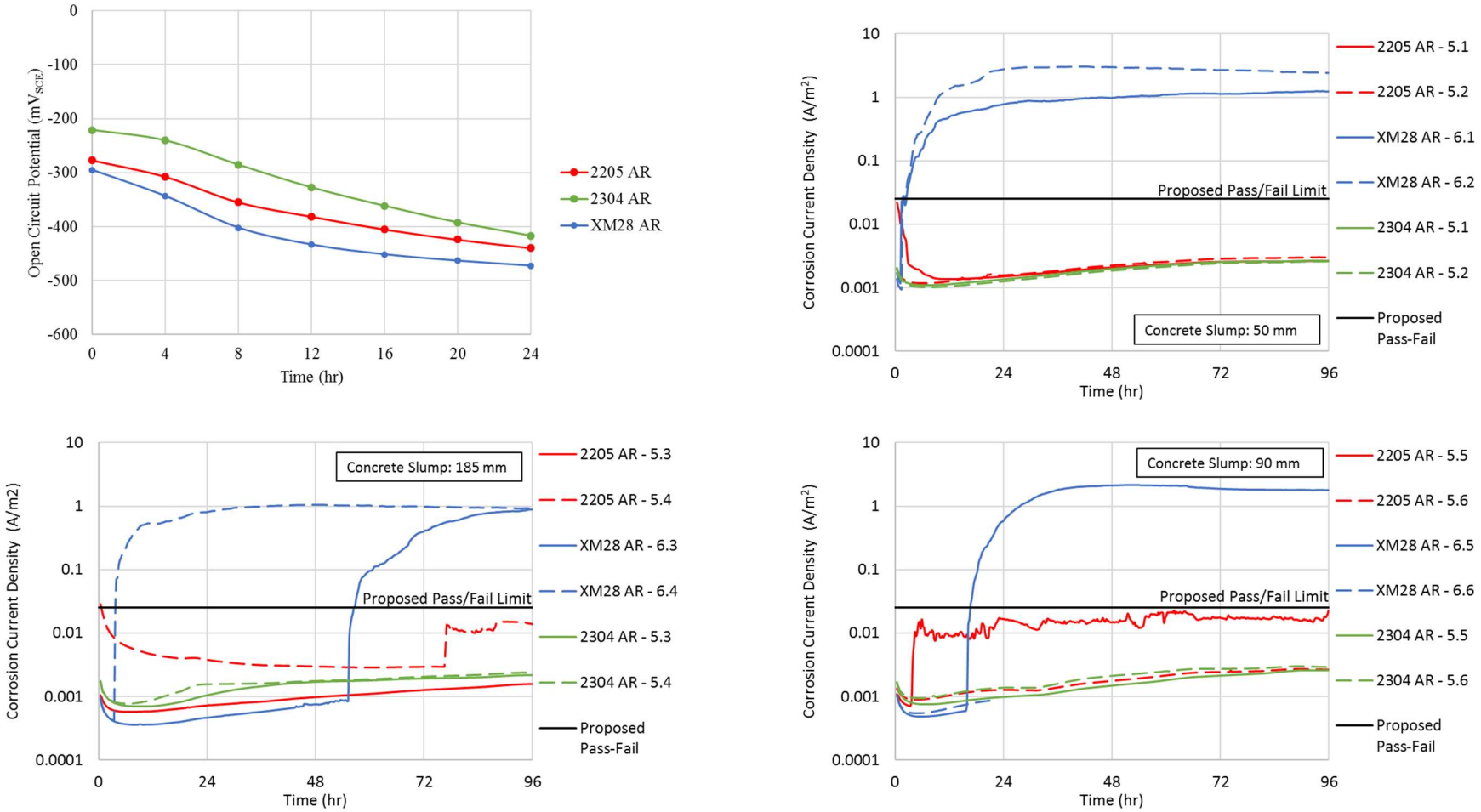

Figure 4.7: 6-400 Batch: Average Open Circuit Potentials over 24 hours (mV_{SCE}) [Top Left], Corrosion Current Densities over 96 hours [Top Right and Bottom].

4.4.7 RST 7.5-200 Batch

The average E_{corr} of the 7.5% Cl^-, +200 mV polarization (7.5-200) batch specimens are shown in Figure 4.8. The average OCP values between each stainless steel grade were found to not vary by more than 113 mV at the end of the OCP monitoring period. At an applied polarization potential of +200 mV to the 7.5-200 batch specimens, the most positive potential was found to be -166 mV_{SCE}, which is below the evolution potential of approximately +200 mV_{SCE} given the alkalinity of concrete media

The corrosion rate of six XM-28 specimens and three 2304 specimens were found to exceed the proposed pass-fail limit at varying corrosion initiation times, shown in Table 4.9. The corrosion current density plots for each these specimens are shown in Figure 4.8.

Table 4.9: 7.5-200 Batch – Corrosion Initiation Time (hr) of Corroded As-Received Specimens

Stainless Steel Grade	Specimen	Corrosion Initiation Time (hr)
XM-28	8.7	8.50
XM-28	8.8	10.50
XM-28	8.9	17.00
XM-28	9.0	2.50
XM-28	9.1	4.75
XM-28	9.2	11.50
2304	7.7	29.25
2304	8.0	59.50
2304	8.1	90.50

Large jumps in corrosion current density was observed for the 2205 7.7 and 7.8 specimens, as well as the 2304 7.9 and 8.2 specimens. However, each of these jumps were found to decay almost immediately. Since the corrosion current densities of each of these specimens were not sustained for more than 2 hours above the proposed pass/fail limit, active corrosion was considered to have not initiated in these specimens.

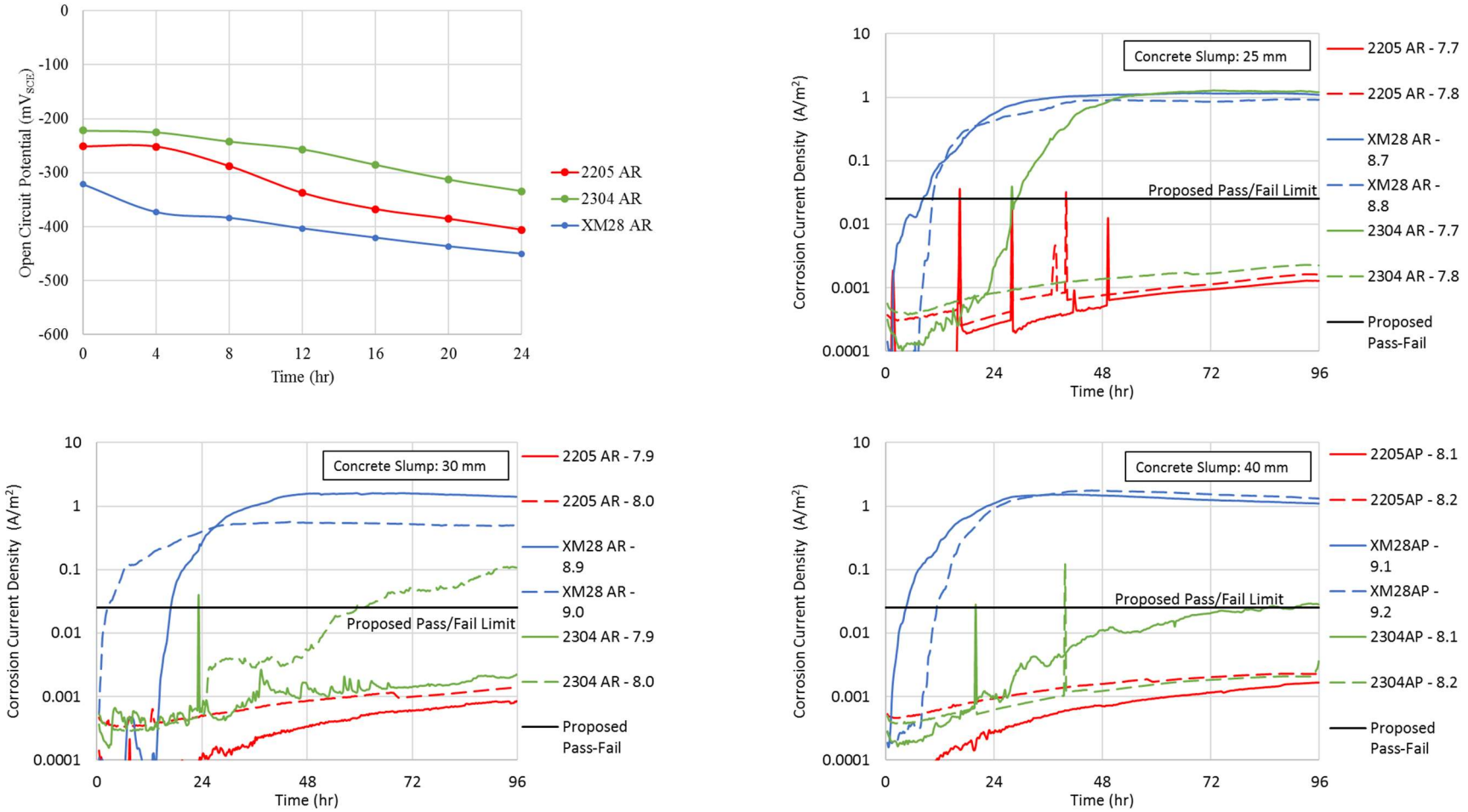

Figure 4.8: 7.5-200 Batch: Average Open Circuit Potentials over 24 hours (mV_{SCE}) [Top Left], Corrosion Current Densities over 96 hours [Top Right and Bottom].

4.4.8 RST 7.5-300 Batch

The average E_{corr} of the 7.5% Cl^-, +300 mV polarization (7.5-300) batch specimens are shown in Figure 4.9. The average OCP values between each stainless steel grade were found to not vary by more than 122 mV at the end of the OCP monitoring period. At an applied polarization potential of +300 mV to the 7.5-300 batch specimens, the most positive potential was found to be +34 mV_{SCE}.

The corrosion rates of four XM-28 specimens, four 2304 specimens, and two 2205 specimens were found to exceed the proposed pass-fail limit at varying corrosion initiation times, shown in Table 4.10. The corrosion current density plots for each these specimens are shown in Figure 4.9.

Table 4.10: 7.5-300 Batch – Corrosion Initiation Time (hr) of Corroded As-Received Specimens

Stainless Steel Grade	Specimen	Corrosion Initiation Time (hr)
XM-28	6.7	0.25
XM-28	6.8	2.75
XM-28	7.1	0.75
XM-28	7.4	12.25
2304	5.7	4.50
2304	5.8	2.00
2304	6.3	49.75
2304	6.4	42.25
2205	5.8	1.75

A large jump in the corrosion current density was observed for the 2205 5.7 specimen. However, this jump was also found to decay almost immediately. The corrosion current density of the 2205 6.4 specimen was found to have briefly surpassed the proposed pass/fail limit twice, and after each time it decreased and fell below the limit. Since the corrosion current density of these specimens were not sustained for more than 2 hours above the proposed pass/fail limit, active corrosion was considered to have not initiated in these specimens.

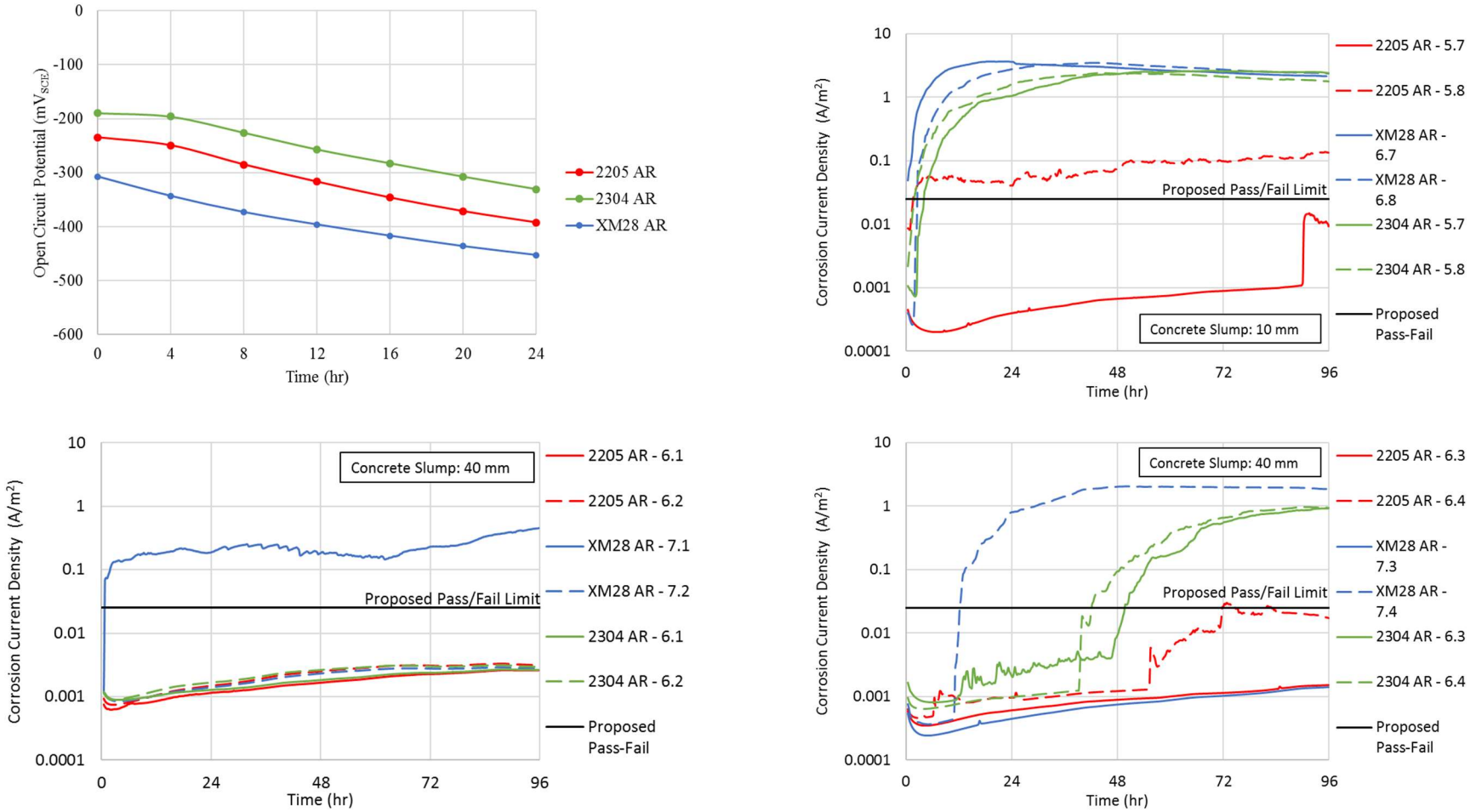

Figure 4.9: 7.5-300 Batch: Average Open Circuit Potentials over 24 hours (mV$_{SCE}$) [Top Left], Corrosion Current Densities over 96 hours [Top Right and Bottom].

4.4.9 RST 7.5-400 Batch

The average E_{corr} of the 7.5% Cl^-, +400 mV polarization (7.5-400) batch specimens are shown in Figure 4.10. The average OCP values between each stainless steel grade were found to not vary by more than 205 mV at the end of the OCP monitoring period. At an applied polarization potential of +400 mV to the 7.5-400 batch specimens, the most positive potential was found to be +137 mV_{SCE}, which is well below the thermodynamic oxygen equilibrium potential of approximately +200 mV_{SCE} given the alkalinity of concrete medium.

Six specimens of XM-28, six specimens of 2304, and three specimens of 2205 were found to exceed the proposed pass-fail limit at varying corrosion initiation times, shown in Table 4.11. The corrosion current density plots for each these specimens are shown in Figure 4.10.

Table 4.11: 7.5-400 Batch – Corrosion Initiation Time (hr) of Corroded As-Received Specimens

Stainless Steel Grade	Specimen	Corrosion Initiation Time (hr)
XM-28	8.1	0.25
XM-28	8.2	0.19
XM-28	8.3	0.25
XM-28	8.4	0.25
XM-28	8.5	0.25
XM-28	8.6	0.25
2304	7.1	0.25
2304	7.2	1.75
2304	7.3	2.50
2304	7.4	3.50
2304	7.5	2.25
2304	7.6	1.75
2205	7.3	3.75
2205	7.4	93.75
2205	7.6	39.25

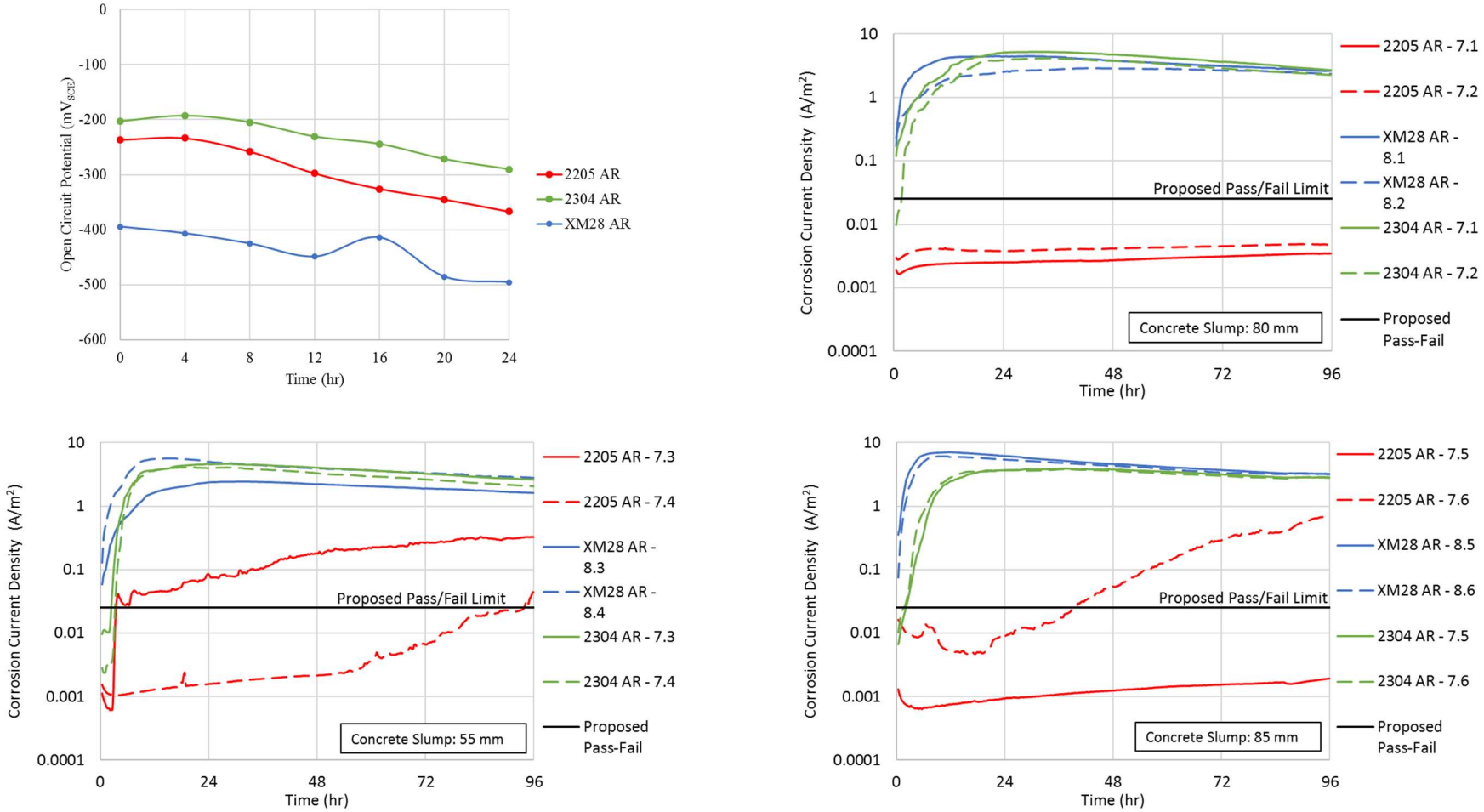

Figure 4.10: 7.5-400 Batch: Average Open Circuit Potentials over 24 hours (mV$_{SCE}$) [Top Left], Corrosion Current Densities over 96 hours [Top Right and Bottom].

4.4.10 Summary of Electrochemical Results

Summaries of the number of corroded bars based on the electrochemical testing results for each stainless steel grade are shown Table 4.12.

Table 4.12: Summary of Corroded Specimens based on Electrochemical Testing The number of corroded specimens is listed out of the total number of specimens tested.

Stainless steel grade XM-28.

Overpotential (mV)	Admixed Chloride Content (wt.% of cementitious material)		
	4%	6%	7.5%
100	0/5*	0/6	-
200	-	1/6**	6/6
300	-	1/6	4/6
400	3/6	5/6	6/6

Stainless steel grade 2304.

Overpotential (mV)	Admixed Chloride Content (wt.% of cementitious material)		
	4%	6%	7.5%
100	0/5*	0/6	-
200	-	0/6**	3/6
300	-	1/6	4/6
400	0/6	0/6	6/6

Stainless steel grade 2205.

Overpotential (mV)	Admixed Chloride Content (wt.% of cementitious material)		
	4%	6%	7.5%
100	0/5*	0/6	-
200	-	0/6**	0/6
300	-	0/6	1/6
400	0/6	0/6	3/6

*Note: Only the 5 AR specimens are listed
**Note: Only the 6 AR specimens cured in the sealed environment are shown.

4.5 Autopsy and Photomicrograph Results

All RST specimens were autopsied after the test, but only those specimens which were observed to have corrosion products are discussed in this section. As discussed in Chapter 3, the steel specimens were photographed after they were removed from the concrete. Once the corrosion products were removed using the acid bath and washed in distilled water, photographs and photomicrographs of the corroded specimens were taken at various magnifications. The lacquer under each of the ends for each stainless steel specimen was removed to confirm that crevice corrosion had not occurred at these locations, Figure 4.11. However, slight staining from the corrosion products on the exposed surface of the steel was sometimes observed in the lacquered regions at the top and/or bottom of the bar.

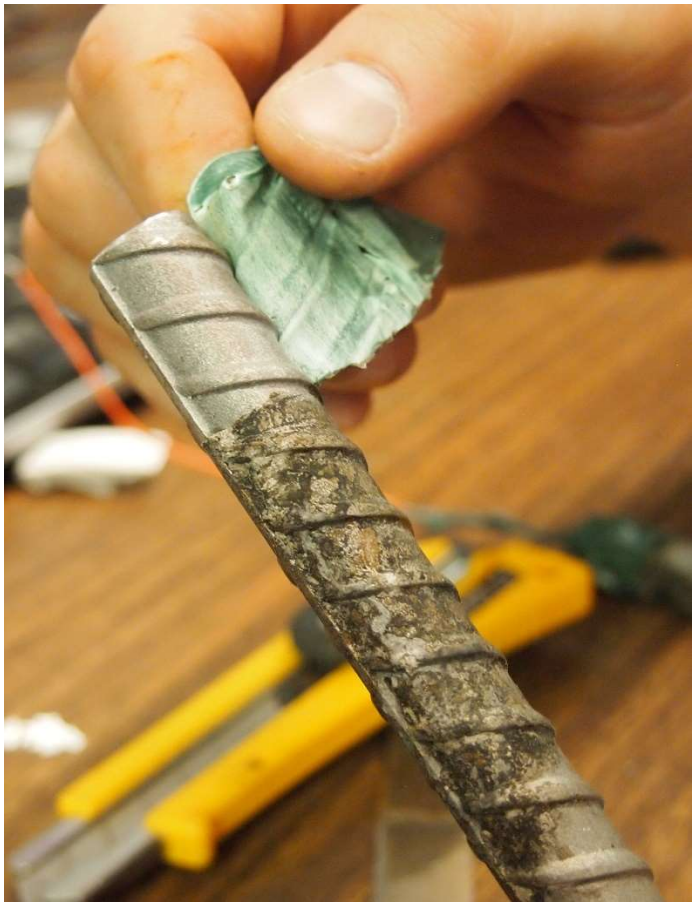

Figure 4.11: Inspection of RST 6-300 2304 AR 4.3 Specimen for crevice corrosion beneath lacquer

The corroded area for each stainless steel grade varied with the admixed chloride concentration and the polarization potential. The more aggressive conditions were found to yield both more extensive and more severe corrosion. Autopsy photographs and photomicrographs of typical cases of mild and severe corrosion of each of the steel grades are shown in Figures 4.12 to 4.19, and Figures 4.20, 4.21, and 4.22, respectively. Autopsy photographs and photomicrographs of all specimens are shown in Appendices C and D, respectively. Photographs showing cracking of the concrete specimens, caused by the corrosion products of their enclosed stainless steel grade, are shown alongside their respective autopsy photos.

Figure 4.12: RST 4-400 Batch – Corrosion Products on XM-28 AR 7.7. From top to bottom, a) original specimen, b) corrosion products on specimen upon removal from concrete, and c) pitting corrosion identification on a pickled specimen. Slight staining at the top of the bar from the soldering process was observed prior to casting the bar in concrete.

Figure 4.13: RST 7.5-400 Batch – XM-28 AR 8.1 Corrosion Products causing Cracking of Concrete Specimen

Figure 4.14: RST 7.5-400 Batch – Corrosion Products on XM-28 AR 8.1. From top to bottom, a) original specimen, b) & c) corrosion products on the specimen upon removal from concrete, and d) & e) pitting corrosion identification on the pickled specimen

Figure 4.15: RST 6-300 Batch – Corrosion Products on 2304 AR 4.3. From top to bottom, a) original specimen, b) corrosion products on specimen upon removal from concrete, and c) pitting corrosion identification on the pickled specimen

Figure 4.16: RST 7.5-400 Batch – 2304 AR 7.1 Corrosion Products causing Cracking of Concrete Specimen

Figure 4.17: RST 7.5-400 Batch – Corrosion Products on 2304 AR 7.1. From top to bottom, a) original specimen, b) & c) corrosion products on the specimen upon removal from concrete, and d) & e) pitting corrosion identification on the pickled specimen

Figure 4.18: 6-400 Batch – Evidence of Pitting Corrosion on 2205 AR 5.5. From top to bottom, a) original specimen, b) corrosion products on specimen upon removal from concrete, and c) & d) pitting corrosion identification on the pickled specimen. Identification of pitting corrosion was observed 1 week after autopsy.

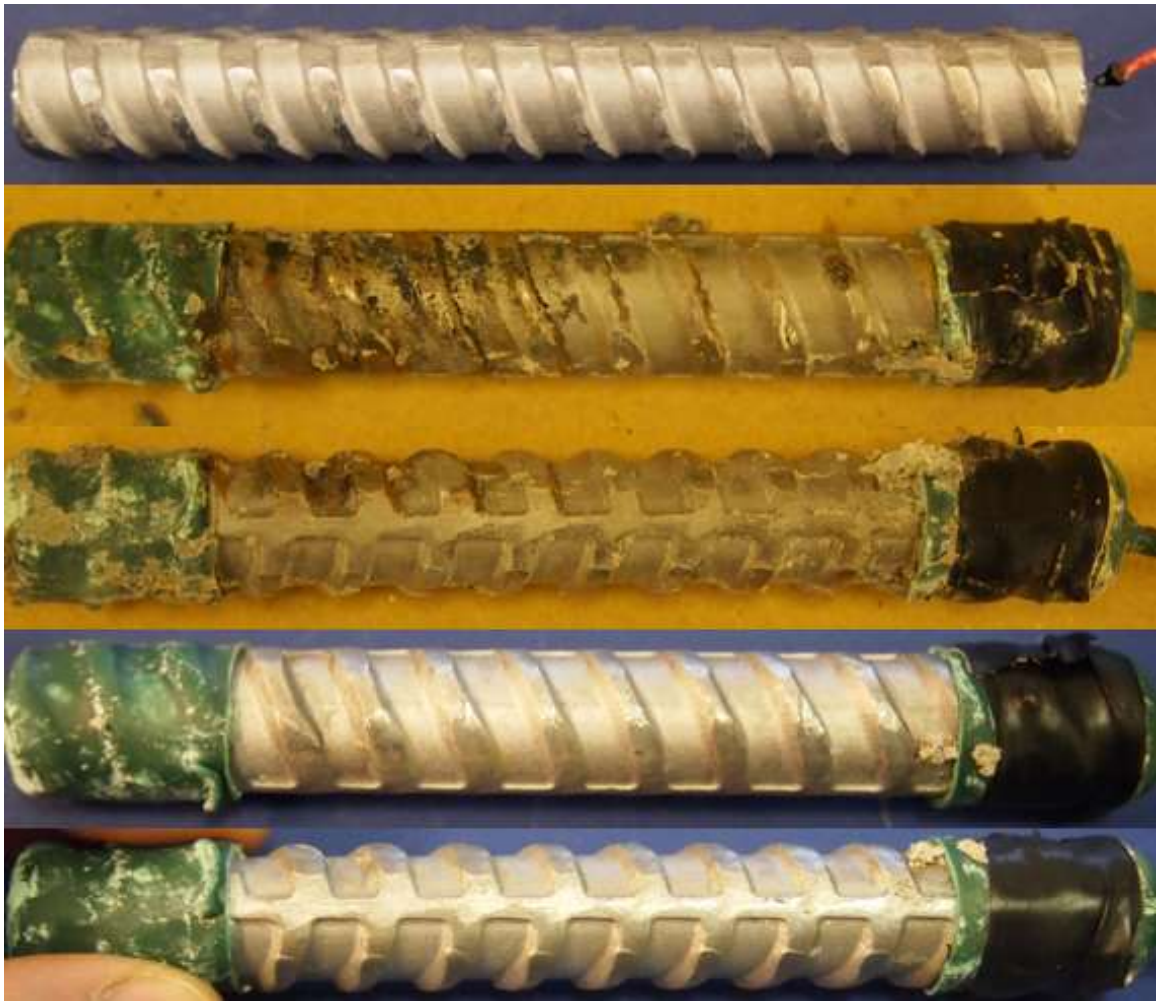

Figure 4.19: RST 7.5-400 Batch – Corrosion Products on 2205 AR 7.3. From top to bottom, a) original specimen, b) & c) corrosion products on the specimen upon removal from concrete, and d) & e) pitting corrosion identification on the pickled specimen

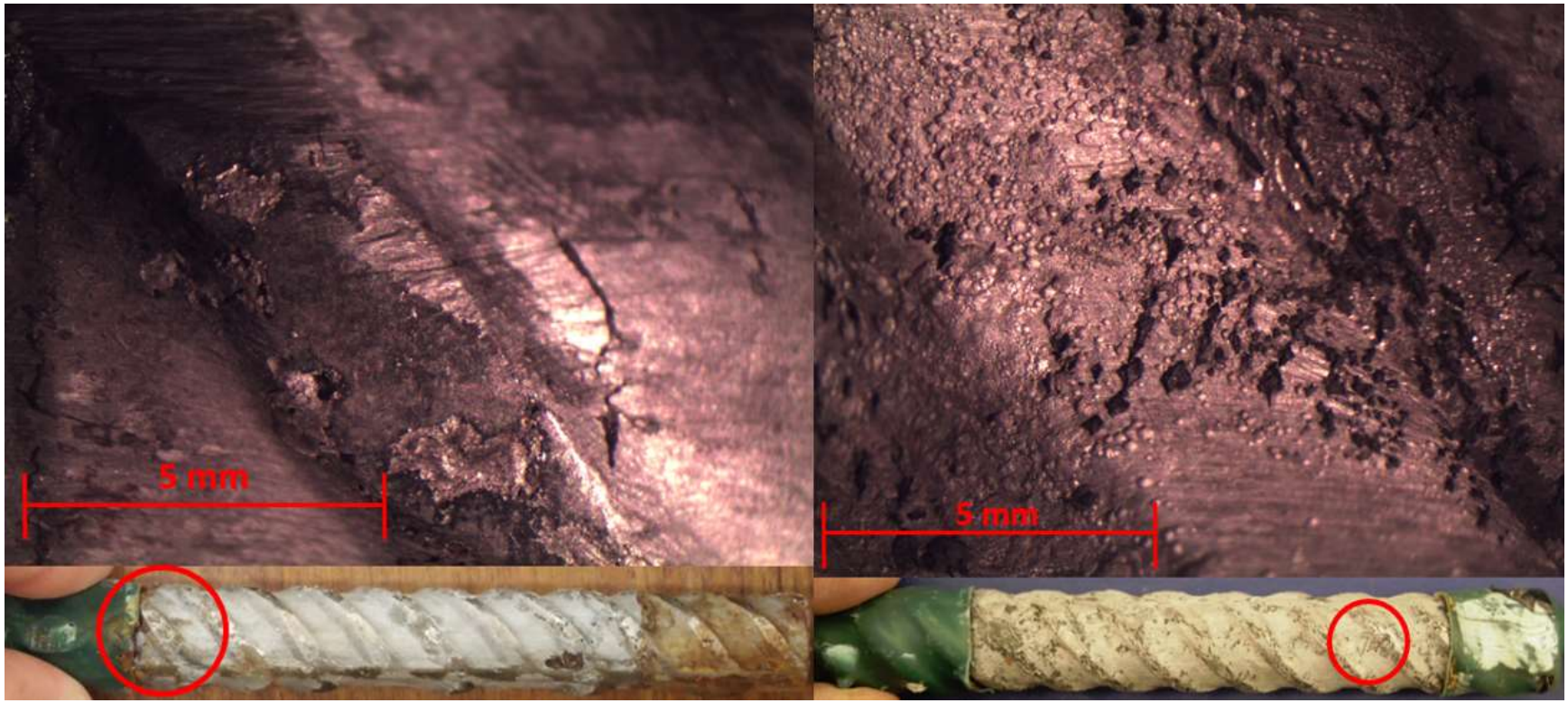

Figure 4.20:Photomicrographs of Corroded Areas on XM-28. A) RST 4-400 Batch XM-28 AR 7.8, and b) RST 7.5-400 Batch XM-28 AR 8.1

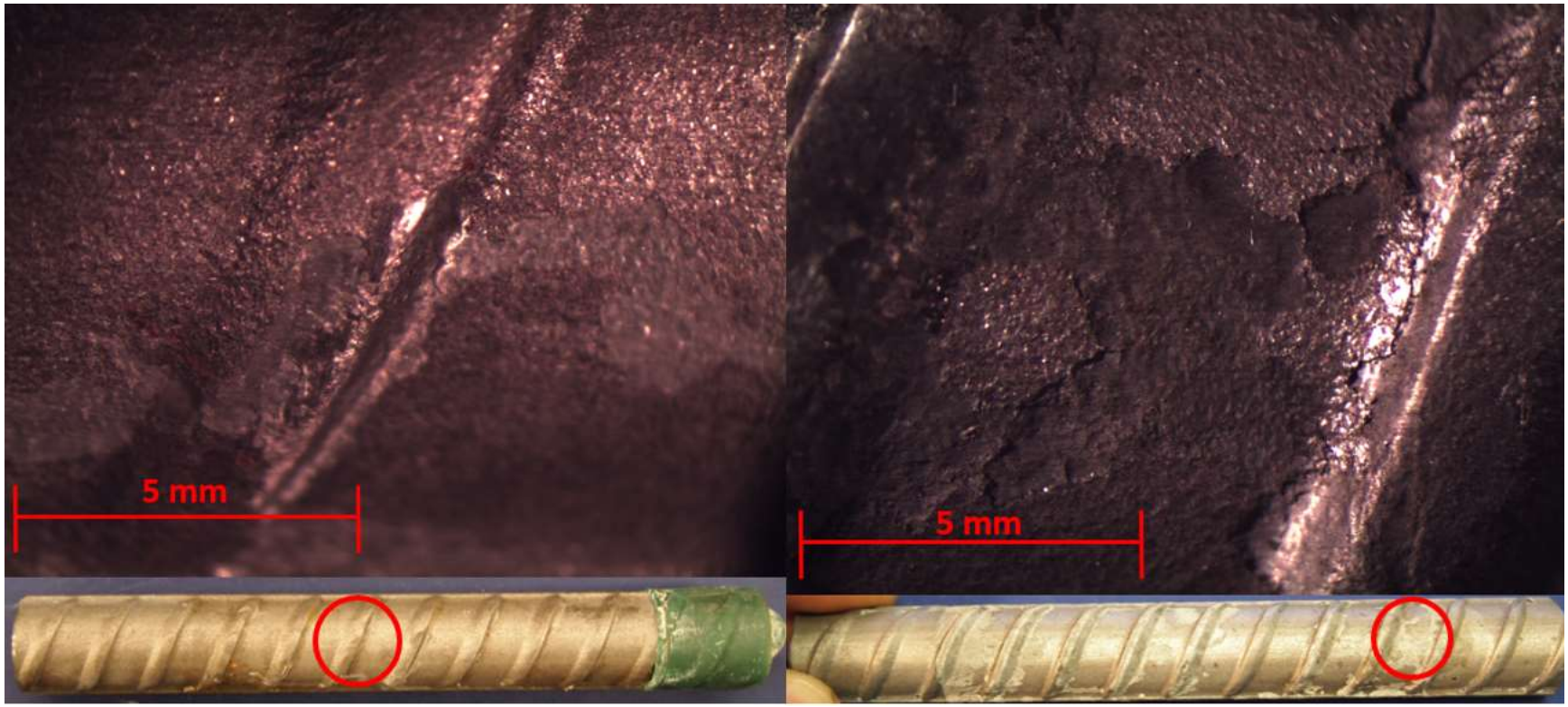

Figure 4.21: Photomicrographs of Corroded Areas on 2304. A) RST 6-300 Batch 2304 AR 4.3, and b) RST 7.5-400 Batch 2304 AR 7.3

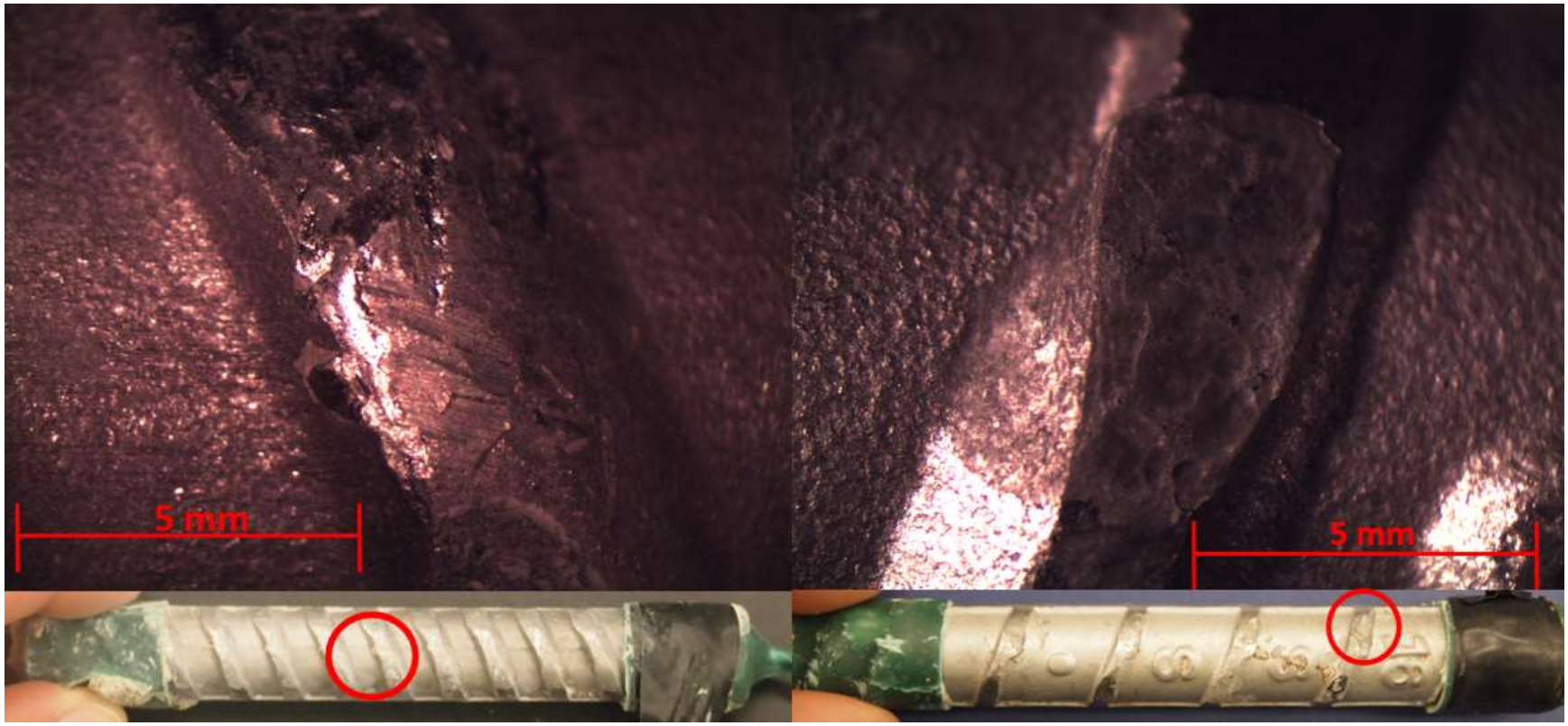

Figure 4.22: Photomicrographs of Corroded Areas on 2205. A) RST 7.5-200 Batch 2205 AR 7.7, and b) RST 7.5-400 Batch 2205 AR 7.6

4.5.1 Summary of Autopsy Results

Summaries of the autopsy results for the XM-28, 2304, and 2205 specimens are shown in Table 4.13. The following sections present the differences in corrosion detection between the electrochemical testing results and visual observation.

Table 4.13: Summary of Corroded Specimens based on Visual Observation

Stainless steel grade XM-28.

Overpotential (mV)	Admixed Chloride Content (wt.% of cementitious material)		
	4%	6%	7.50%
100	0/5*	0/6	-
200	-	1/6**	6/6
300	-	1/6	4/6
400	3/6	5/6	6/6

Stainless steel grade 2304.

Overpotential (mV)	Admixed Chloride Content (wt.% of cementitious material)		
	4%	6%	7.50%
100	0/5*	0/6	-
200	-	0/6**	6/6***
300	-	1/6	4/6
400	0/6	0/6	6/6

Stainless steel grade 2205.

Overpotential (mV)	Admixed Chloride Content (wt.% of cementitious material)		
	4%	6%	7.50%
100	0/5*	0/6	-
200	-	0/6**	2/6***
300	-	0/6	4/6***
400	0/6	2/6***	4/6***

*Note: Only the 5 AR specimens are listed
**Note: Only the 6 AR specimens cured in the sealed environment are shown.
*** Differs from electrochemical testing results

It should be noted that pitting corrosion was frequently observed along a “black defect line” on the 2304 specimens, shown in Figure 4.23. This defect line ran parallel to one of the longitudinal ribs on the bar, and it was observed on each 2304 specimen.

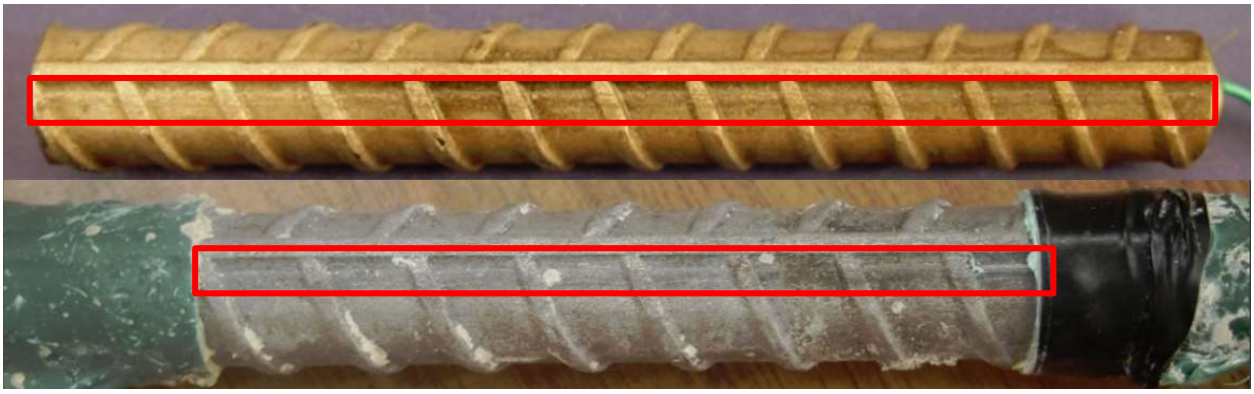

Figure 4.23: Black Defect Line observed in 2304 AR 7.7 (7.5-200 batch)

4.5.2 RST 6-400 Batch

When the specimens were originally autopsied, no other specimens showed signs of corrosion or corrosion products. However, once the bars were exposed to air, any corrosion products (oxides) became rust coloured. As a result, corrosion products were observed on two of the 2205 specimens: 2205 AR 5.4 and 5.5. The corrosion current density for each of these specimens did not surpass the proposed pass-fail limit. Their maximum corrosion current densities were found to only be 15 mA/m^2 and 21 mA/m^2, respectively. Periodic spikes in each bar’s corrosion current density were noted during potentiostatic polarization.

It should be noted that it was not possible for some of the concrete on the XM-28 AR 6.3 to be removed. Corrosion products were observed to stain the rebar, but pitting and general corrosion were found to be located primarily on the ribs adjacent to the adhered concrete. The phenomenon was observed on many bars in other RST batches as well. Slight staining of the bar was also observed underneath the lacquer at the top of the bar. This staining was attributed to the expansive corrosion products. No corrosion was observed on the area that was beneath the lacquer.

4.5.3 RST 7.5-200 Batch

Upon visual inspection, 2304 specimens 7.8, 7.9, 8.1, and 8.2 and 2205 specimens 7.7 and 7.8 were found to have corroded. The corrosion current density for each of the specimens was found to either not exceed the proposed pass/fail limit or to not exceed the limit for more than 2 hours. Periodic spikes of varying magnitude in each bar's corrosion current density were noted during potentiostatic polarization. It should be noted that evidence of corrosion was observed on 2304 specimens 8.1 and 8.2, and 2205 specimens 7.7 and 7.8 were noted approximately 5 months after the bars were autopsied.

4.5.4 RST 7.5-300 Batch

Upon visual inspection, 2205 AR 5.7 and 6.3 were found to have corroded. Based on the requirements of corrosion initiation for the electrochemical testing in the RST, these specimens were considered to not have corroded, as was similar to the case of the bars mentioned in Section 4.5.3. It should be noted that evidence of corrosion was observed on 2205 specimen 5.7 was noted approximately 7 months after the bar was autopsied.

4.5.5 RST 7.5-400 Batch

Upon visual inspection, 2205 AR 7.4 was found to have corroded. It should be noted that evidence of corrosion was observed on 2205 specimen 5.7 was noted approximately 7 months after the bar was autopsied.

The corrosion current density for the 2205 bar surpassed the proposed pass-fail limit at 93.75 hrs. However, at the time of the autopsy, the author was unable to identify any signs of corrosion products or pitting corrosion on the reinforcing bar. Evidence of corrosion was observed on 2205 specimen 5.7 was noted approximately 1 week after the bar was autopsied.

Chapter 5 – Statistical Analysis

5.1 Modelling Probability of Corrosion

In order to predict the probability of corrosion of the 2205, 2304, and XM-28 bars used in the RST, a probabilistic corrosion model was developed using logistic regression. The goal of this analysis was to find the best fitting, most reasonable model that exemplified the principle of parsimony between a dependent variable (DV) and its predictors, or independent variables (IV) [74]. A numerical regression model was not used to predict corrosion behaviour properties, such as corrosion current density, because that form of model is typically used to predict the mean value of a dependent variable. When studying the corrosion behaviour of any metal, mean values of most corrosion parameters (corrosion current density in particular) are not only unrepresentative, but very misleading. The following sections describe the process used to create the logistic regression model and the subsequent analysis of the model's outputs using the statistical analysis program "RStudio".

5.2 Logistic Regression

A separate logistic regression model was created for each stainless steel (SS) grade tested in the RST. The dependent variables that were input into the model were binary values based on whether an individual specimen of a stainless steel grade had corroded (i.e. a 1) or had not (i.e. a 0). The independent input variables were the applied overpotential (mV) and admixed chloride concentrations (wt. % by mass of cementitious material) that corresponded to their respective dependent variables. In order to proceed with the regression analysis, the degree of multicollinearity between the independent variables had to be determined. Unless otherwise specified, the following sections will discuss the statistical analysis process in detail for the XM-28 corrosion behaviour data. The abbreviated results of the 2304 and 2205 corrosion behaviour are shown in Sections 5.4 and 5.5**,** respectively.

5.3 XM-28 Regression Model

5.3.1 Multicollinearity

One of the basic assumptions of a regression model is that its independent variables (IV) are not correlated. If the IVs are correlated, or multicollinear, the model parameters are indeterminate and the standard errors of the estimated coefficients are infinitely large. One method to test the multicollinearity

of a regression model and its coefficients is the Farrar-Glauber (F-G) test [75]. This test consists of two tests which determine i) the existence and severity of multicollinearity as a function of the predictor variables (IVs), and ii) the source of the multicollinearity.

The first involves the following hypothesis test:

$$H_0: The\ predictors\ (x_i)\ are\ orthogonal \quad \text{vs.} \quad H_A: The\ predictors\ (x_i)\ are\ not\ orthogonal\ for\ all\ values\ of\ i$$

Where H_0 is the null hypothesis, and H_A is the alternate hypothesis. To determine the orthogonality of the IVs, they are standardized and used in a standardized determinant, also referred to as a correlation determinant. The general form for the standardized determinant is as follows:

$$\begin{vmatrix} 1 & r_{x_1x_2} & r_{x_1x_3} \\ r_{x_1x_2} & 1 & r_{x_2x_3} \\ r_{x_1x_3} & r_{x_2x_3} & 1 \end{vmatrix} \qquad \text{Equation 5.1}$$

where $r_{x_ix_j}$ represents the coefficient of correlation between predictors x_i and x_j. A standardized determinant value of 0 corresponds to the case of multicollinearity between all predictor variables, whereas a value of 1 corresponds to the case of orthogonality between all predictor variables. In practice however, the standardized determinant will lie somewhere between 0 and 1, with values closer to 0 and 1 corresponding to stronger degrees of multicollinearity and orthogonality, respectively. To test the severity of multicollinearity, Farrar and Glauber (1967) proposed the following Chi-squared test statistic:

$$\chi^2 = -\left[n - 1\left(\frac{1}{6}\right)(2k+5)\right] * log_e[value\ of\ the\ determinant] \qquad \text{Equation 5.2}$$

Where χ^2 is the Chi-square test statistic, n is the number of observations, and k is the number of independent variables in the model. The corresponding number of degrees of freedom (df) for the Chi-squared test statistic is as follows:

$$df = \frac{1}{2}k^*(k^* - 1) \qquad \text{Equation 5.3}$$

where k^* is the number of independent variables in the model, including the intercept. In the case of the data for the XM-28 specimens, the standardized determinant was found to be equal to one:

$$\begin{vmatrix} 1 & r_{yx_1} & r_{yx_2} \\ r_{yx_1} & 1 & r_{x_1x_2} \\ r_{yx_2} & r_{x_1x_2} & 1 \end{vmatrix} = \begin{vmatrix} 1 & 0 & 0 \\ 0.3 & 1 & 0 \\ 0.3 & 0 & 1 \end{vmatrix} = 1$$

Therefore, we accept the null hypothesis that the predictor variables are orthogonal.

As previously stated, the second part of the F-G test is used to detect the source of multicollinearity. However, since the first test found that there was no collinearity between any of the predictor variables, the second test is not required. Therefore, there are no issues of collinearity between the IVs for the XM-28 data.

5.3.2 Global Model

Prior to the selection of a usable model to predict the probability of corrosion for the XM-28 bars, a global model was constructed and its validity determined. The generalized formula for logistic regression, or the conditional distribution of the outcome variable y, is given as:

$$y = E(Y|\theta) + \varepsilon \qquad \text{Equation 5.4}$$

where ε is the error term, and $E(Y|\theta)$ is the conditional mean for logistic regression, or the expected value of Y given the set of independent variables θ. The conditional mean (π(x)) is denoted in Equation 5.6:

The logit transformation is used to transform the logistic regression model such that the independent variables resemble a linear regression model. The logit transformation is denoted as follows:

$$g(x) = \ln\left[\frac{\pi(x)}{1 - \pi(x)}\right] = \beta_0 + \beta_1 x_1 + \cdots \beta_i x_i \qquad \text{Equation 5.5}$$

where g(x) is used to denote the logit transformation, and β_i represent the estimated parameter coefficients.

The error term for the logistic regression follows a binomial distribution with a mean of zero and a variance equal to $\pi(x)[1 - \pi(x)]$ [74]. However, there is no common error term independent of the predictor values since the predicted values are constrained within the bounds of 0 and 1. Therefore, no error term was considered for the any of the logistic regression global models for each of the stainless steel grades.

The global model for the XM-28 specimens was determined to be as follows:

$$E(Y|x) = \pi(x) = \frac{e^{\beta_0+\beta_1 A+\beta_2 B+\beta_3 AB}}{1+e^{\beta_0+\beta_1 A+\beta_2 B+\beta_3 AB}} \quad \text{Equation 5.6}$$

$$g(x) = \ln\left[\frac{\pi(x)}{1-\pi(x)}\right] = \beta_0 + \beta_1 A + \beta_2 B + \beta_3 AB \quad \text{Equation 5.7}$$

where A represents the applied overpotential (mV), B represents the admixed chloride concentration (wt.% by mass of cementitious material), and AB represents the interaction term between the applied overpotential and the admixed chloride concentrations. Based on 53 observations, shown in Table 4.13, RStudio was able to predict the following model parameters, Table 5.1. Note that only the data pertaining to the specimens that were tested in their as-received condition was included for the statistical analysis. Akaike's Information Criterion (AIC) values are discussed in Section 5.3.3.

To determine the validity of the XM-28 global model Equation 5.7**,** a comparison of the observed to predicted values is required. This comparison uses a form of the log likelihood function called the likelihood ratio test:

$$D = -2\sum_{i=1}^{n}\left[y_i \ln\left(\frac{\hat{\pi}_i}{y_i}\right) + (1-y_i)\ln\left(\frac{1-\hat{\pi}_i}{1-y_i}\right)\right] \quad \text{Equation 5.8}$$

where D is the deviance, $\hat{\pi}_i = \hat{\pi}_i(x_i)$ which represents the maximum likelihood estimate of the conditional mean, and y_i represents the predicted value for the i^{th} observed value. To assess the significance of the IVs, the deviance of the model with the IVs (the residual deviance) is compared to the deviance of the model without the IVs (the null deviance):

$$G = D_{Residual} - D_{Null} \quad \text{Equation 5.9}$$

where G is a test statistic, $D_{Residual}$ is the residual deviance, and D_{Null} is the null deviance. Using a null hypothesis test that states that the β_i coefficients will equal zero, the statistic G follows a chi-square distribution, denoted by χ^2, with 1 degree of freedom. For the XM-28 global model, the statistic G was found to be $\chi^2(3) = 34.59$ with a p-value of 1.48×10^{-7}. Therefore, the null hypothesis was rejected, and the model was found to be significant at a 5% significance level.

Table 5.1: XM-28 Logistic Regression Global Model Estimated Coefficients from RStudio

Coefficients	Estimate	Std. Error	z-value	Pr(>|z|)	Significance Level
Intercept	-40.32	14.54	-2.78	0.006	0.1%
A	0.095	0.038	2.51	0.012	1%
B	5.68	2.17	2.60	0.0093	0.1%
A:B	-0.013	0.0057	-2.21	0.027	10%

5.3.3 Candidate Models

A set of candidate models were created based on the global model to determine the most appropriate regression model given the RST data. The candidate models were determined to be as follows:

Model 1: $$g(x) = ln\left[\frac{\pi(x)}{1 - \pi(x)}\right] = \beta_0 + \beta_1 A$$ Equation 5.10

Model 2: $$g(x) = ln\left[\frac{\pi(x)}{1 - \pi(x)}\right] = \beta_0 + \beta_1 B$$ Equation 5.11

Model 3: $$g(x) = ln\left[\frac{\pi(x)}{1 - \pi(x)}\right] = \beta_0 + \beta_1 A + \beta_2 B$$ Equation 5.12

Model 4: $$g(x) = ln\left[\frac{\pi(x)}{1 - \pi(x)}\right] = \beta_0 + \beta_1 A + \beta_2 B + \beta_3 AB$$ Equation 5.13

A common method for selecting candidate models is with information-theoretic methods, such as Akaike's Information Criterion (AIC) [76], [77]**.** Akaike's Information Criterion, Equation 5.14, is an approximate estimation of the relative distance between a given model, g(x), and the most optimal model, f(x). The optimal model, often referred to as the realistic model, is the model that reflects the complex nature of the process that is generated based on the observed data x. This complex function is not explicitly parameterized as it may not even have parameters analogous to the IVs in a modelling framework [76]. The lower the AIC value, the less information is lost between the approximate model and the real model.

$$AIC = -2\log(L(\hat{\theta}|y)) + 2k$$ Equation 5.14

Where $L(\hat{\theta}|y)$ is the likelihood function of the parameter vector θ, given the independent variable (IVs) x. However, the addition of more and more IVs to a regression model may have a detrimental effect as a result of an increase in "noise" from estimated parameters which are may not be needed to achieve a good model [76]–[78]. With this in mind, Sugiura (1978) derived c-AIC, otherwise known as the corrected Akaike's Information Criteria equation, or AIC_C:

$$AIC_c = AIC + \frac{2k^*(k^*+1)}{n-k^*-1} \qquad \text{Equation 5.15}$$

This corrected AIC penalizes over-fitted models in an attempt to abide by the principle of parsimony. The XM-28 candidate models were evaluated on the basis of AIC_c, and each model's respective AIC_c, Nagelkerke R^2 [79], and AIC differences, Equation 5.16, are shown in Table 5.2**.** For the purpose of this thesis, all models are evaluated on the basis of Nagelkerke R^2.

$$\Delta_i = AIC_{c_i} - min\ AIC_c \qquad \text{Equation 5.16}$$

where Δ_i represents the AIC_c differences, and AIC_{c_i} represents the AIC_c value for model i. Burnham and Anderson (1998) argue that the larger the Δ_i, the less plausible the fitted model is the best model for the given specimen set of data. They continue to describe that, as a general rule of thumb, models with an $\Delta_i \leq 2$ have substantial support of being plausible, models with an Δ_i between 4 and 7 have considerably less support, and that models with an Δ_i of greater than 10 have essentially no support [76].

Table 5.2: XM-28 Candidate model information-theoretic evaluation

Model	AIC_c	Nagelkerke R^2	Δ_i
1	63.94	0.305	16.244
2	65.041	0.283	17.345
3	51.82	0.549	4.124
4	47.696	0.639	0

Based on the results of the AIC_c, Table 5.2, Model 4 appears to be the model which best fits the given specimen set of data. Considering the models in terms of corrosion behaviour, logically it makes sense that the likelihood of corrosion in RST is a function of both the applied overpotential and the admixed chlorides, as well as the interaction between the two parameters.

5.3.4 Evaluation of the Selected Model

The estimated coefficients for the parameters used in Model 4 were determined using the maximum likelihood method in RStudio, and can be seen in Table 5.1. A hypothesis test, which states that the given variable's coefficient is zero, is constructed for each term in the regression model. The Z-values, Equation 5.17, for each variable are used to determine the associated p-value using a one-sided Z-test.

$$Z = \frac{\hat{\beta} - 0}{\hat{\sigma}_{\hat{\beta}}} = \frac{\hat{\beta}}{\hat{\sigma}_{\hat{\beta}}} \qquad \text{Equation 5.17}$$

Where Z is the Z-test statistic, $\hat{\beta}$ is the standardized regression coefficient for a given parameter, and $\hat{\sigma}_{\hat{\beta}}$ is the standardized error associated with $\hat{\beta}$. As can be seen in Table 5.1, all of the estimated coefficients for Model 4 were found to be significant at a 5% significance level. As a result, the null hypothesis tests associated with each parameter were rejected. Therefore, the estimated regression model to predict the probability of corrosion for XM-28 specimens in the RST is modelled by Equation 5.18:

$$g(x) = ln\left[\frac{\pi(x)}{1 - \pi(x)}\right] = -40.317 + 0.095A + 5.658B - 0.013AB \qquad \text{Equation 5.18}$$

A confusion matrix was then constructed to validate the performance of the regression model, Table 5.3.

Table 5.3: Confusion Matrix for XM-28 Regression Model No. 4

Experimental Observations	Predicted Values	
	Not Corroded	Corroded
Not Corroded	24 (AA)	3 (AB)
Corroded	5 (BA)	21 (BB)

For the XM-28 regression model, any predicted values with probabilities greater than or equal to 50% were considered to be "corroded". The true negative rate (i.e. sensitivity), false positive rate, true positive rate (i.e. specificity), the false negative rate, the accuracy, and the misclassification rate for Model 4 are shown in Equations 5.19 to 5.24, while their respective values are shown in Table 5.4.

$$True\ Negative\ Rate\ (TNR) = \frac{BB}{BA + BB} * 100\% \qquad \text{Equation 5.19}$$

$$False\ Positive\ Rate\ (FPR) = \frac{BA}{BA + BB} * 100\% \quad \text{Equation 5.20}$$

$$True\ Positive\ Rate\ (TPR) = \frac{AA}{AA + AB} * 100\% \quad \text{Equation 5.21}$$

$$False\ Negative\ Rate\ (FNR) = \frac{BB}{AA + AB} * 100\% \quad \text{Equation 5.22}$$

$$Accuracy = \frac{TNR + TPR}{2} \quad \text{Equation 5.23}$$

$$Misclassification\ rate = \frac{FPR + FNR}{2} \quad \text{Equation 5.24}$$

Table 5.4: XM-28 Model 4 Confusion Matrix Evaluation Parameters

Confusion Matrix Evaluators	Percentage (%)
True Negative Rate	88.89
False Negative Rate	11.11
True Positive Rate	80.77
False Positive Rate	19.23
Accuracy	84.83
Misclassification Rate	15.17

The corresponding Receiver Operating Characteristic (ROC) curve for Model 4 was generated using RStudio and is shown in Figure 5.1. The ROC curve plots the true positive rate (i.e. the ability of the model to detect whether specimens did not corrode) versus the false positive rate (i.e. the inability of the model to detect whether a specimen did not corrode). Each individual point on the curve represents the sensitivity and specificity associated with each predicted data point compared to its corresponding observed value (i.e. whether the model predicts for the 4-400 batch versus what the experimental data shows). The top left point on the graph (0,1) represents the best-case scenario where the model would predict only true positives and not contain any false positive errors. The diagonal grey line in Figure 5.1 (where y=x) represents the strategy of randomly guessing a set of predictor variables. Therefore, any model whose ROC curve appears above the diagonal is said to have useful information that is applied correctly [80].

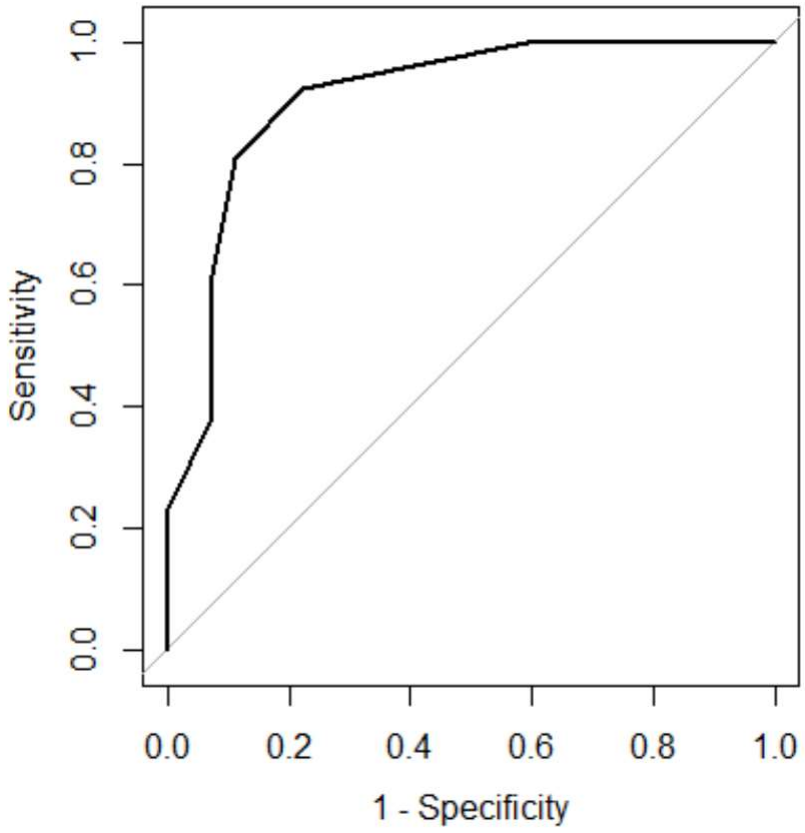

Figure 5.1: ROC curve for the XM-28 Model 4 Logistic Regression Model

The area under the ROC curve (AUROC) is often used as a summary of the accuracy of the test, with values between 0 and 1 [81]. However, because random guessing produces a diagonal with a corresponding AUROC of 0.5, any model with an AUROC less than 0.5 is impractical [80]. Model 4's ROC was found to be 0.909, and therefore the model is once again confirmed to better represent the data than a random guess.

5.3.5 Summary of the XM-28 Logistic Regression Model

Based on logistic regression Model 4, the prediction model for the probability of corrosion of the XM-28 specimens in the RST is given by Equation 5.18**.** A visual representation of the prediction model is shown in Figure 5.2. Note that none of the specimens for the 6-100 batch corroded, but the data point in Figure 5.2 was slightly moved to a probability value of 0.02 so that it could be easily seen by the reader.

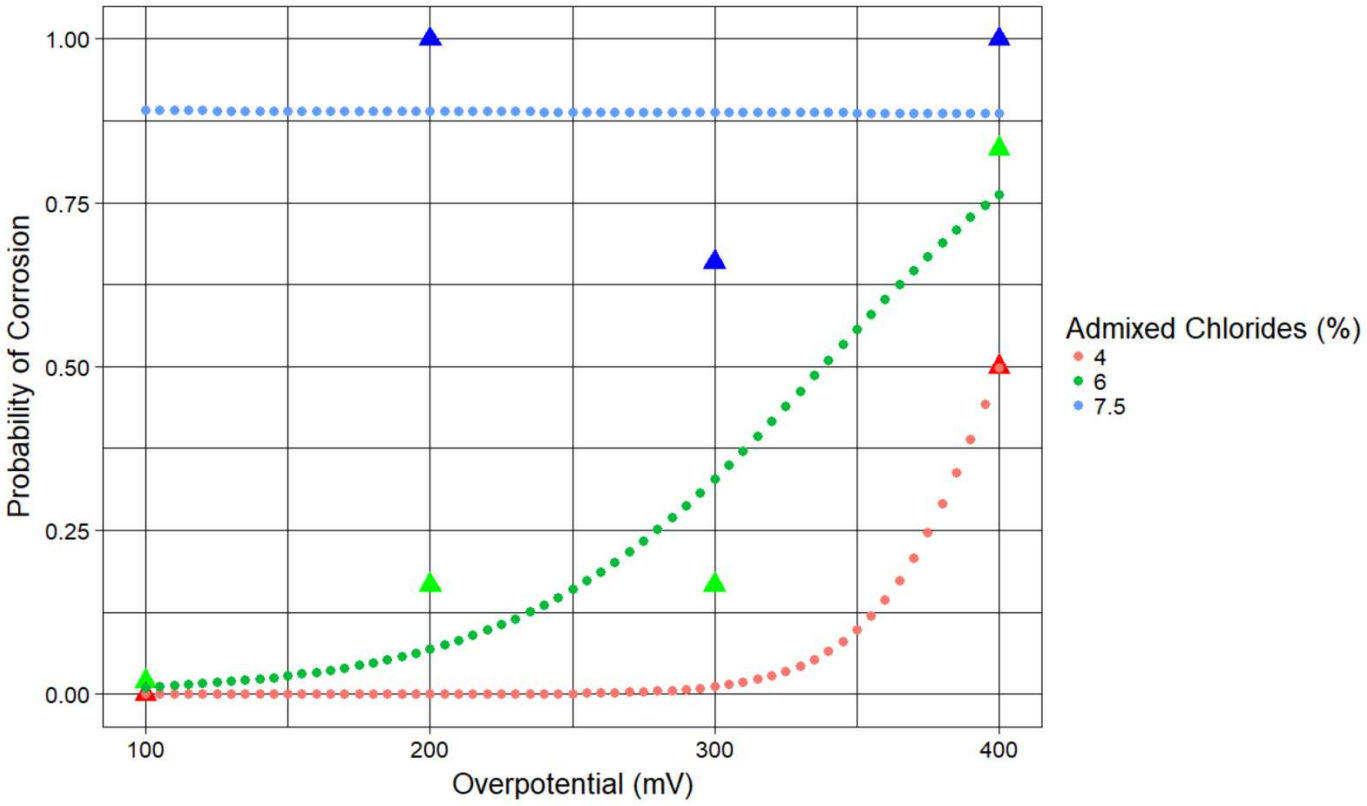

Figure 5.2: XM-28 Probabilistic Model based on RST data. Note that the triangular data points represent the fraction of observed specimens that corroded.

5.4 2304 Regression Model

5.4.1 Multicollinearity

By using a null hypothesis that states that the predictors are orthogonal, the 2304 specimen corrosion behavior data was tested for multicollinearity. The standardized determinant of the data was found to be equal to one:

$$\begin{vmatrix} 1 & r_{yx_1} & r_{yx_2} \\ r_{yx_1} & 1 & r_{x_1x_2} \\ r_{yx_2} & r_{x_1x_2} & 1 \end{vmatrix} = \begin{vmatrix} 1 & 0 & 0 \\ 0 & 1 & 0 \\ 0.3 & 0 & 1 \end{vmatrix} = 1$$

Therefore, we accept the null hypothesis that the predictor variables are orthogonal, and no further testing for multicollinearity is required for the 2304 data.

5.4.2 Global Model

Similar to the XM-28 data, the global model for the 2304 data was modelled by Equation 5.7. Based on 53 observations, shown in Table 4.15 of Chapter 4, RStudio was able to predict the following model parameters, Table 5.5.

Table 5.5: 2304 Logistic Regression Global Model Parameters from RStudio

Coefficients	Estimate	Standard Error	z-value	Pr(>|z|)	Significance Level
Intercept	-29.99	19.24	-1.56	0.12	100%
A	0.022	0.061	0.36	0.72	100%
B	4.28	2.81	1.52	0.13	100%
A:B	-0.0029	0.0089	-0.33	0.75	100%

Once again, a null hypothesis test, similar to that of the one in Section 5.3.2, was used that states that the β_i coefficients will equal zero. For the 2304 global model, the statistic G was found to be $\chi^2(3) = 45.85$ with a p-value of 6.1×10^{-10}. Therefore, the null hypothesis was rejected, and the model was found to be significant at a 5% significance level.

5.4.3 Candidate Models

A set of candidate models were created based on the global model to determine the most appropriate regression model given the RST data. The candidate models were determined to be the same as Models 1-4 in Equations 5.10 to 5.14. The information-theoretics for each model are shown in Table 5.6.

Table 5.6: 2304 Candidate model information-theoretic evaluation

Model	AIC_c	Nagelkerke R^2	Δ_i
1	68.96	0.0464	41.70
2	31.67	0.808	4.41
3	27.26	0.809	0
4	29.49	0.810	2.23

Based on the results of the AIC_c, Table 5.6, Model 3 was chosen to be the model for the given specimen set of data.

5.4.4 Evaluation of Selected Model

The estimated coefficients for Model 3 were determined using the maximum likelihood method in RStudio and are shown in Table 5.7.

Table 5.7: 2304 Logistic Regression Model 3 Estimated Coefficients from RStudio

Coefficients	Estimate	Standard Error	z-value	Pr(>|z|)	Significance Level
Intercept	-24.28	6.09	-3.99	6.64×10^{-5}	0%
A	0.0021	0.0066	0.32	0.75	100%
B	3.43	0.85	4.05	5.12×10^{-5}	0%

As can be seen in Table 5.7, two of the three estimated coefficients for Model 3 were found to be significant at a 5% significance level. As a result, the null hypothesis tests associated with each parameter were rejected. However, the p-value for the estimated coefficient for the polarization potential term ("A") was found to be insignificant at 5% significance level. As previously stated, the author believes that the polarization potential does influence the corrosion behaviour of the 2304 specimens. The insignificance of the estimated coefficient for the "a" term was attributed to the lack of balanced data (i.e. 15 specimens corroded and 38 specimens did not corrode). As a result, the author believes that, for the given specimen set of data, the estimated coefficient for the "a" is insignificant, but it may be significant for a larger and more balanced specimen set of data. Therefore, the estimated regression model to predict the probability of corrosion for 2304 specimens in the RST is modelled by Equation 5.25:

$$g(x) = ln\left[\frac{\pi(x)}{1 - \pi(x)}\right] = -24.283 + 0.002A + 3.432B \qquad \text{Equation 5.25}$$

A confusion matrix was then constructed to validate the performance of the regression model, Table 5.8.

Table 5.8: Confusion Matrix for 2304 Regression Model No. 3

Experimental Observations	Predicted Values	
	Not Corroded	Corroded
Not Corroded	34 (AA)	2 (AB)
Corroded	1 (BA)	16 (BB)

Similar to the XM-28 model, any predicted values with probabilities greater than or equal to 50% were considered to be "corroded". The confusion matrix evaluation parameters were determined using Equations 5.19 to 5.24, while their respective values are shown in Table 5.9.

Table 5.9: 2304 Model 3 Confusion Matrix Evaluation Parameters

Confusion Matrix Evaluators	Percentage (%)
True Negative Rate	94.12
False Negative Rate	5.88
True Positive Rate	94.44
False Positive Rate	5.55
Accuracy	94.28
Misclassification Rate	5.72

The corresponding Receiver Operating Characteristic (ROC) curve for Model 3 was generated using RStudio and is shown in Figure 5.3. Model 3's ROC was found to be 0.96, and therefore the model is once again confirmed to better represent the data than a random guess.

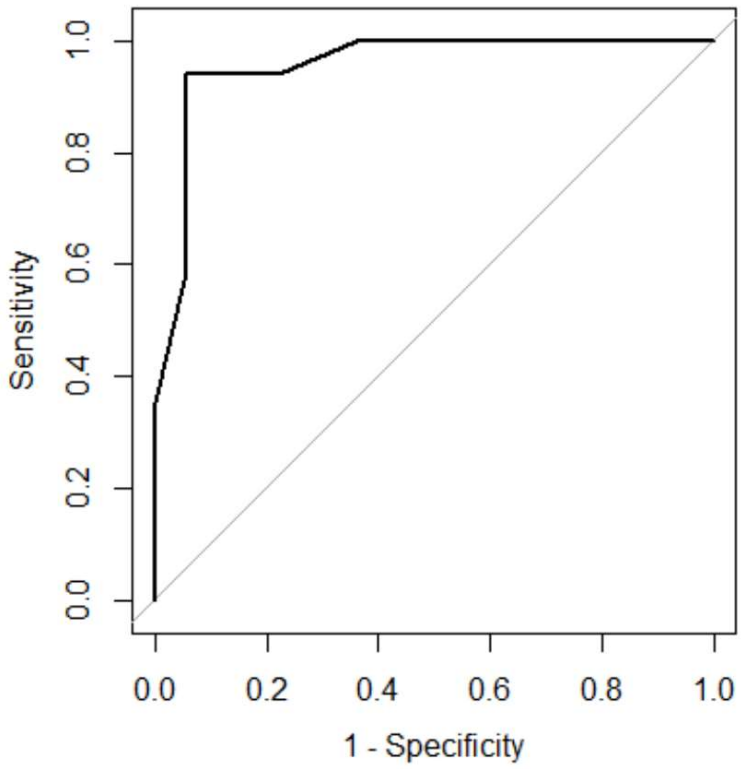

Figure 5.3: ROC curve for the 2304 Model 3 Logistic Regression Model

5.4.5 Summary of the 2304 Logistic Regression Model

Based on logistic regression Model 3, the prediction model for the probability of corrosion of the 2304 specimens in the RST is given by Equation 5.25**.** A visual representation of the prediction model is shown in Figure 5.4. Note that none of the specimens for the 6-100 or the 6-400 batches corroded, but the data point in Figure 5.4 were slightly moved to a probability value of 0.02 so that it could be easily seen by the reader.

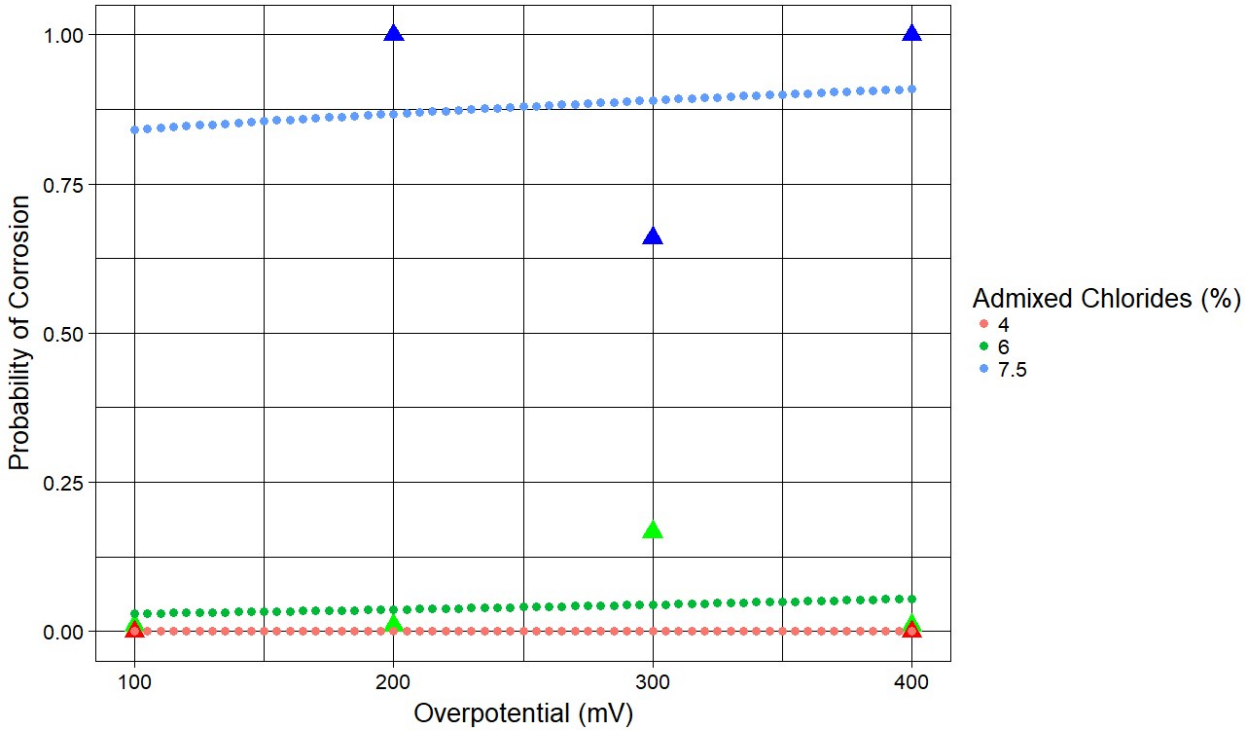

Figure 5.4: 2304 Probabilistic Model based on RST data. Note that the triangular data points represent the fraction of observed specimens that corroded.

5.5 2205 Regression Model

5.5.1 Multicollinearity

By using a null hypothesis that states that the predictors are orthogonal, the 2205 specimen corrosion behavior data was tested for multicollinearity. The standardized determinant of the data was found to be equal to one:

$$\begin{vmatrix} 1 & r_{yx_1} & r_{yx_2} \\ r_{yx_1} & 1 & r_{x_1x_2} \\ r_{yx_2} & r_{x_1x_2} & 1 \end{vmatrix} = \begin{vmatrix} 1 & 0 & 0 \\ 0 & 1 & 0 \\ 0.3 & 0 & 1 \end{vmatrix} = 1$$

Therefore, we accept the null hypothesis that the predictor variables are orthogonal, and no further testing for multicollinearity is required for the 2205 data.

5.5.2 Global Model

Similar to the XM-28 and 2304 data, the global model for the 2205 data was modelled by Equation 5.7. Based on 53 observations, shown in Table 4.16 of Chapter 4, RStudio was able to predict the following model parameters, Table 5.10.

Table 5.10: 2205 Logistic Regression Global Model Parameters from RStudio

Coefficients	Estimate	Standard Error	z-value	Pr(>|z|)	Significance Level
Intercept	-342.48	46789.91	-0.007	0.994	100%
A	0.84	116.97	0.007	0.994	100%
B	45.46	6238.66	0.01	0.994	100%
A:B	-0.11	15.6	-0.007	0.994	100%

Once again, a null hypothesis test, similar to that of the one in Section 5.3.2, was used that states that the β_i coefficients will equal zero. For the 2205 global model, the statistic G was found to be $\chi^2(3) = 18.45$ with a p-value of 3.55×10^{-4}. Therefore, the null hypothesis was rejected, and the model was found to be significant at a 5% significance level.

5.5.3 Candidate Models

A set of candidate models were created based on the global model to determine the most appropriate regression model given the RST data. The candidate models were determined to be the same as Models 1-4 in Equations 5.10 to 5.14. The information-theoretics for each model are shown in Table 5.11.

Table 5.11: 2205 Candidate model information-theoretic evaluation

Model	AIC_c	Nagelkerke R^2	Δ_i
1	51.89	0.108	10.16
2	42.84	0.344	1.11
3	41.95	0.417	0.22
4	41.73	0.474	0

Based on the results of the AIC_c, Table 5.11, Model 4 appears to be the model which best fits the given specimen set of data. However, based on the Δ_i values, Models 2 and 3 should also be considered. However, Model 2, shown in Table 5.12, does take the polarization potential into account, which is believed to affect the corrosion behaviour of the bar. The estimated coefficients of Model's 3 and 4 are shown in Table 5.13 and Table 5.14, respectively. Even though the Model 4's Δ_i and Nagelkerke R^2 values are better than that of Model 3, the significance of Model 4's estimated coefficients appear to only be significant at the 95% significance level. As a result, Model 3 was chosen to be the model for the given specimen set of data.

Table 5.12: 2205 Logistic Regression Model 2 Estimated Coefficients from RStudio

Coefficients	Estimate	Standard Error	z-value	Pr(>|z|)	Significance Level
Intercept	-11.46	3.93	-2.91	0.0036	0.1%
A	1.50	0.55	2.71	0.0068	0.1%

Table 5.13: 2205 Logistic Regression Model 3 Estimated Coefficients from RStudio

Coefficients	Estimate	Standard Error	z-value	Pr(>|z|)	Significance Level
Intercept	-13.69	4.49	-3.05	0.0023	0.1%
A	0.0083	0.0051	1.64	0.1	100%
B	1.46	0.56	2.56	0.0094	0.1%

Table 5.14: 2205 Logistic Regression Model 4 Estimated Coefficients from RStudio

Coefficients	Estimate	Standard Error	z-value	Pr(>|z|)	Significance Level
Intercept	-342.48	46789.91	-0.007	0.994	100%
A	0.84	116.97	0.007	0.994	100%
B	45.46	6238.66	0.01	0.994	100%
A:B	-0.11	15.6	-0.007	0.994	100%

5.5.4 Evaluation of the Selected Model

The estimated coefficients for Model 3 were determined using the maximum likelihood method in RStudio and are shown in Table 5.13. All the estimated coefficients for Model 3 were found to be significant at a 5% significance level. As a result, the null hypothesis tests associated with each parameter

were rejected. Therefore, the estimated regression model to predict the probability of corrosion for 2304 specimens in the RST is modelled by Equation 5.26:

$$g(x) = ln\left[\frac{\pi(x)}{1 - \pi(x)}\right] = -13.688 + 0.0083A + 1.461B \qquad \text{Equation 5.26}$$

A confusion matrix was then constructed to validate the performance of the regression model, Table 5.15.

Table 5.15: Confusion Matrix for 2205 Regression Model No. 3

Experimental Observations	Predicted Values	
	Not Corroded	Corroded
Not Corroded	40 (AA)	3 (AB)
Corroded	7 (BA)	3 (BB)

Similar to the XM-28 model, any predicted values with probabilities greater than or equal to 50% were considered to be "corroded". The confusion matrix evaluation parameters were determined using Equations 5.19 to 5.24, while their respective values are shown in Table 5.16.

Table 5.16: 2205 Model 3 Confusion Matrix Evaluation Parameters

Confusion Matrix Evaluators	Percentage (%)
True Negative Rate	30.00
False Negative Rate	70.00
True Positive Rate	93.02
False Positive Rate	6.98
Accuracy	61.51
Misclassification Rate	38.49

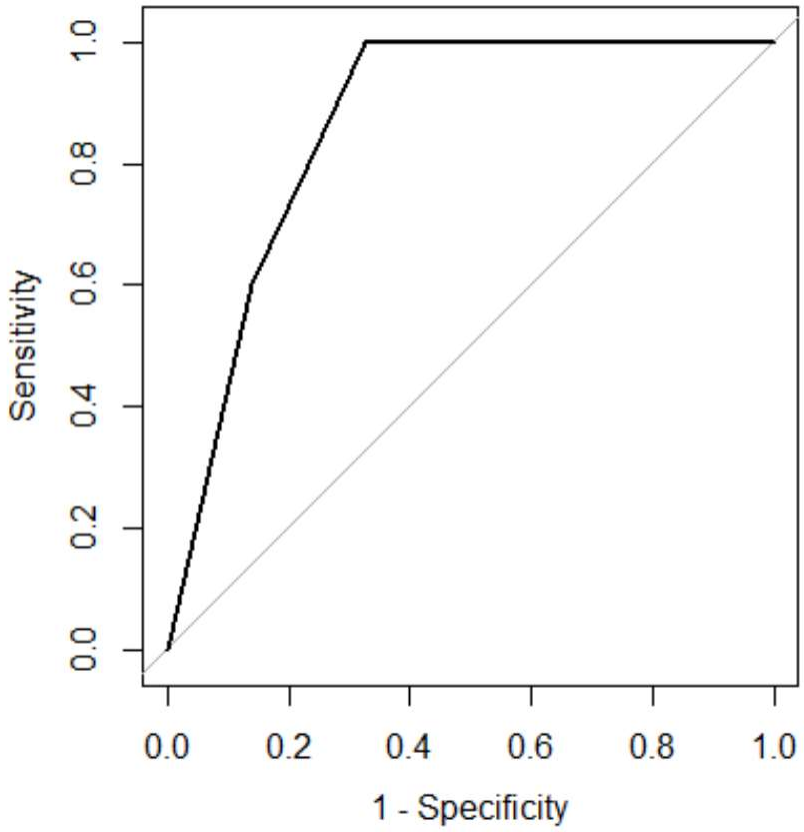

Figure 5.5: ROC curve for the 2205 Model 3 Logistic Regression Model

The corresponding Receiver Operating Characteristic (ROC) curve for Model 3 was generated using RStudio and is shown in Figure 5.5. Model 3's ROC was found to be 0.87, and therefore the model is once again confirmed to better represent the data than a random guess.

5.5.5 Summary of the 2205 Logistic Regression Model

Based on logistic regression Model 3, the prediction model for the probability of corrosion of the 2205 specimens in the RST is given by Equation 5.25**.** A visual representation of the prediction model is shown in Figure 5.6. Note that none of the specimens for the 6-100 or the 7.5-200 batches corroded, but the data point in Figure 5.6 were slightly moved to a probability value of 0.02 so that it could be easily seen by the reader.

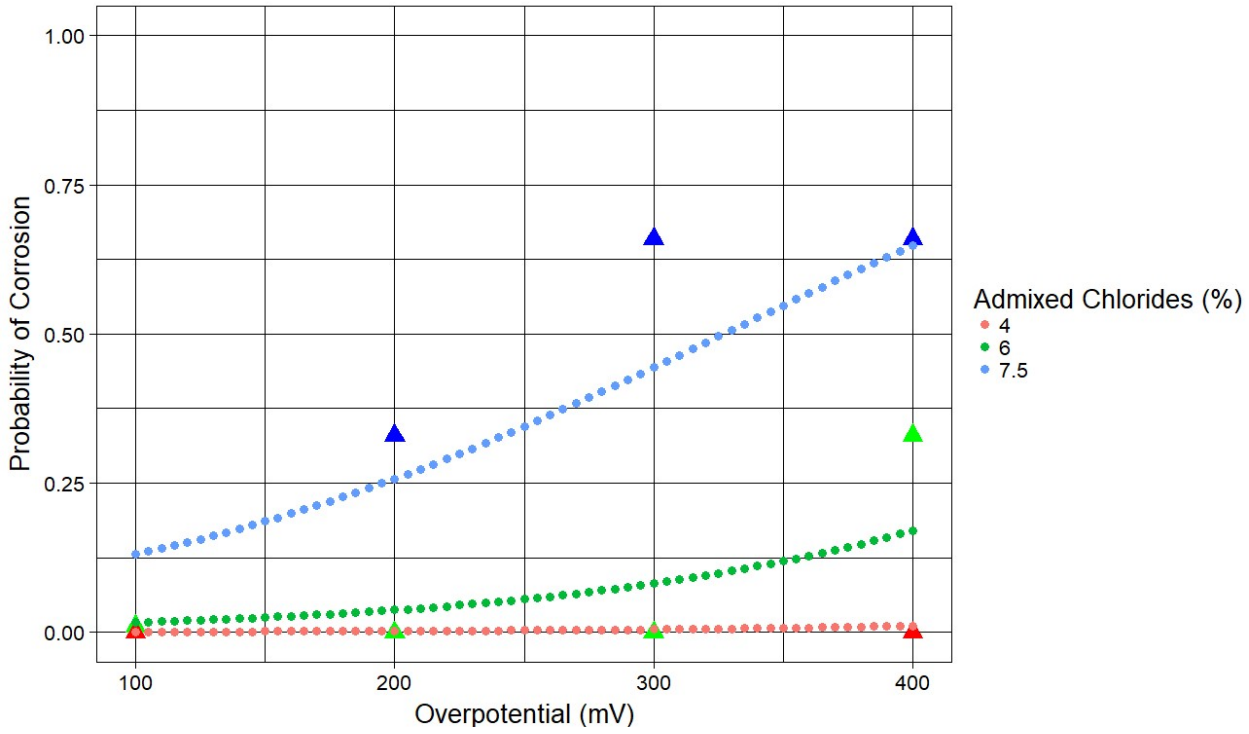

Figure 5.6: 2304 Probabilistic Model based on RST data. Note that the triangular data points represent the fraction of observed specimens that corroded.

5.6 Summary of Logistic Regression Models

In general, the logistic regression models for the XM-28 and 2304 corrosion behaviour data seem fairly accurate, with Nagelkerke R^2 values of 0.64 and 0.73, respectively. However, the logistic regression model for the 2205 corrosion behaviour data appears to be less accurate, with a Nagelkerke R^2 value of 0.39. Furthermore, the accuracy of the 2205 regression model was found to be approximately 58%, whereas the accuracy of the XM-28 and 2304 regression models were found to be approximately 85% and 91.5%, respectively. This disparity in accuracy for the 2205 regression model can be attributed to severely disproportionate data; 8 specimens were observed to corrosion and 45 were found to not corrode.

5.6.1 Theoretical Critical Chloride Thresholds

Using the logistic regression models for the XM-28, 2304, and 2205 data, one can theoretically predict the critical chloride threshold of each of the tested stainless steel grades. By setting the polarization potential value in each of their respective equations to 0 and setting the probability of corrosion to 50%,

one can solve for the supposed critical chloride threshold (C_T). The values for the theoretical critical chloride thresholds are shown in Table 5.17.

Table 5.17: Theoretical Critical Chloride Thresholds for the Tested Stainless Steel Grades

Stainless Steel Grade	Theoretical Critical Chloride Threshold (wt.% by mass of cementitious material)
2205	9.4
2304	7.1
XM-28	7.1

Note that these threshold values are based only on the data gathered for this adapted Rapid Screening Test and are discussed further in Chapter 6. These values are not representative of stainless steels used in reinforced concrete in reality. The bars used in reinforced concrete structures are allowed to develop a passive film in an alkaline medium for many years prior to coming into contact with chlorides. A more accurate estimate of the critical chloride threshold values for each of the stainless steel grades exposed to admixed chlorides in concrete would require more data.

Chapter 6 – Discussion

The following section discusses any trends, outliers, or observations related to the results presented in Chapter 4 and Chapter 5.

6.1 Rapid Screening Test Parameters

The parameters used for the Rapid Screening Test may not be representative of conditions in reality. To the author's knowledge, the maximum chloride concentration by mass of cementitious material observed in the field is approximately 5%. However, the application of highly concentrated chloride brines in recent years is expected to increase the chloride content in the concrete cover of highway structures. This topic will be discussed in more detail by Van Niejenhuis and Hansson [66]. Regarding the applied polarization potentials, it is unlikely that reinforcing bars would experience anodic polarization in service but could do so if subject to stray currents, for example from electrified rail trains and power stations in the locale [82].

6.2 The Effect of Admixed Chlorides by NaCl

The decrease in concrete resistivity with higher admixed chloride concentrations is expected due the increased concentration of ions in the concrete pore solution, leading to increased ionic conduction. However, the measurable decrease in the strength of the concrete with increased NaCl salt was not expected and is currently under investigation by Van Niejenhuis and Hansson [66].

6.3 Open Circuit Potential

6.3.1 The Effect of Passivation in Pore Solution on the Open Circuit Potentials of the Steel Embedded in Concrete

The open circuit potentials (OCP) of the 2205 and XM28 bars passivated in synthetic concrete pore solution were found to be more positive than their as-received counterparts. The 2304 specimens that had been passivated in synthetic pore solution, or pre-passivated, were observed to wildly fluctuate when they were initially measured during the OCP monitoring period of the RST (i.e. 24 to 48 hours after casting), as shown in Appendix A and B. One can theorize that the 2304 specimens that were tested may have had some material defects or different surface treatment of the specimens (i.e. pickling, sandblasting, etc.) by

the manufacturer compared to the 2205 and XM-28 bars, and as a result, their interaction with the synthetic pore solution yielded varied results. However, the exact reason as to why this phenomenon may have occurred is currently unknown to the author. The influence of various surface treatments and finishes is currently being investigated by Ibrahim Ogunsanya [83].

The difference in open circuit potentials obtained from passivating the stainless steel specimens in synthetic concrete pore solution compared to the as-received specimens is considered to generally be insignificant. If the specimens were allowed reach equilibrium in concrete prior to encountering chlorides, the results of this test may be different and would simulate real-world conditions more accurately. However, as previously stated, one of the main advantages of this test is its rapid test duration, and by pre-passivating the bars, unnecessary time is added to said duration. Therefore, testing of the specimens in their as-received condition with an air-formed passive film was conducted and is recommended for future applications of the test.

6.3.2 The Effect of Slump and Moist Curing

Both the effect of curing the RST specimens in a moist environment and the effect of variable slump were investigated to determine if these factors influenced the open circuit potentials of the bars. The OCP values of the 2205, XM-28, and 2304 bars are plotted against the slump data in Figures 6.1, 6.2, and 6.3 for their respective concrete mixes. Aside from the outliers listed below, the effects of increased slump and moist curing the specimens do not appear to significantly affect the open circuit potentials of the bars. However, it should be noted that there was significantly less scatter in the OPC values for all three grades in concrete with 4% admixed Cl^- than in concretes with 6 0r 7.5% Cl^-. This suggests the steels in the higher chloride concentrations experienced some degree of non-uniform chloride attack.

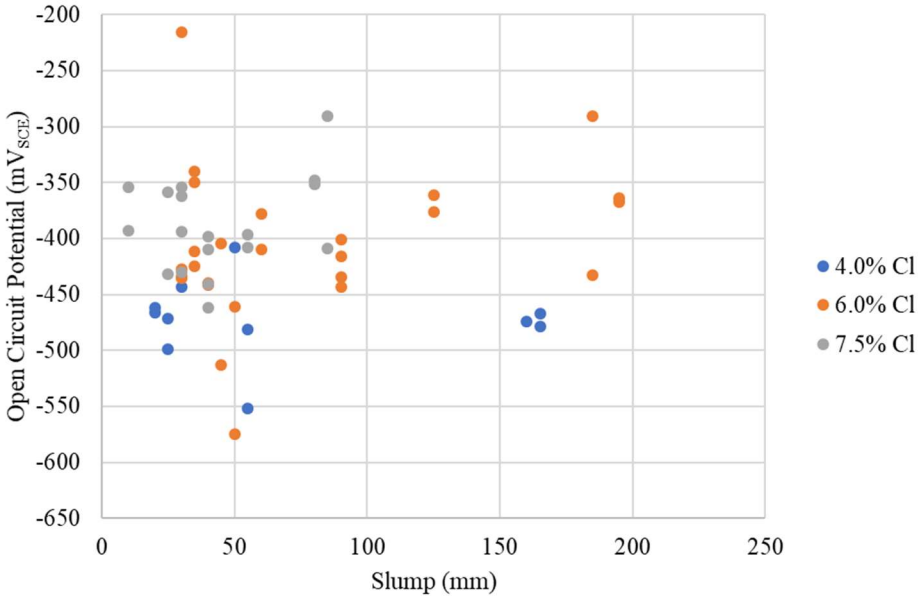

Figure 6.1: Open Circuit Potentials (mV$_{SCE}$) of all 2205 AR specimens versus the slump (mm) of the concrete they were cast in. Open circuit potential values were taken 48 hours after casting.

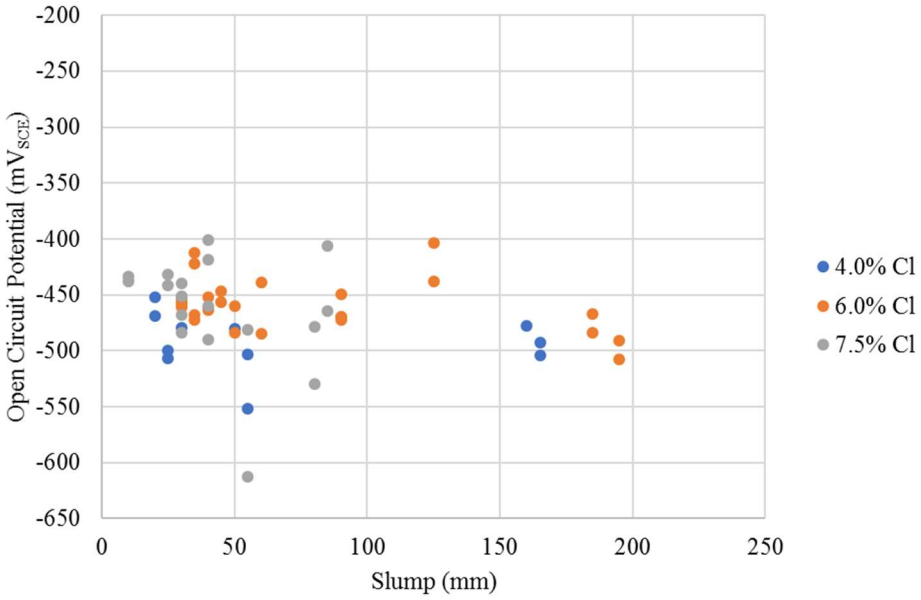

Figure 6.2: Open Circuit Potentials (mV$_{SCE}$) of all XM-28 AR specimens versus the slump (mm) of the concrete they were cast in. Open circuit potential values were taken 48 hours after casting

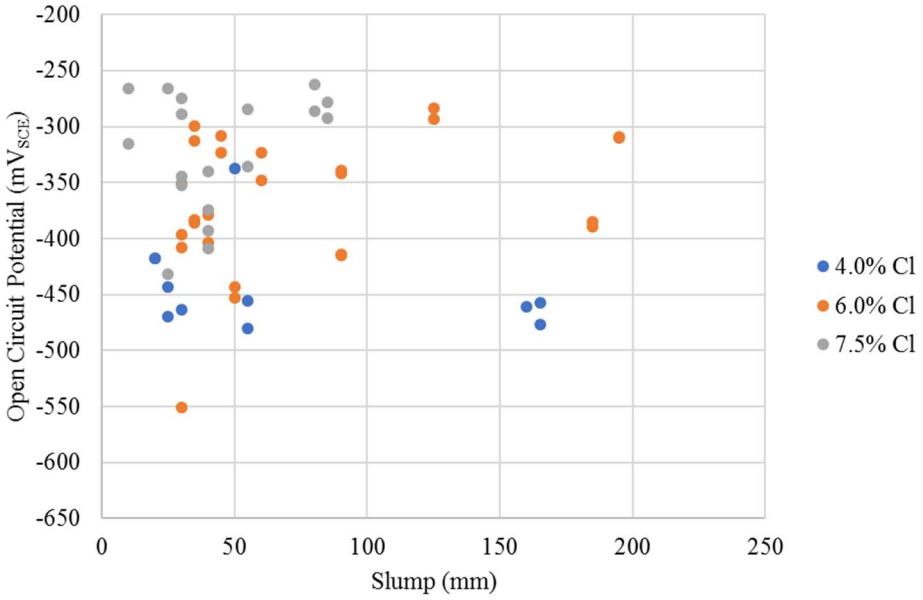

Figure 6.3: Open Circuit Potentials (mV_{SCE}) of all 2304 AR specimens versus the slump (mm) of the concrete they were cast in. Open circuit potential values were taken 48 hours after casting

The outliers in Figures 6.1, 6.2, and 6.3 are as follows. The OCP of 2205 AR 3.6 in the 6-200 batch was found to be -216 mV_{SCE}, while the OCP of the replicate bar cast in the same week was found to be -428 mV_{SCE}. Both specimens were found to have approximately the same passive i_{corr} values. The OCP of XM-28 AR 8.3 in the 7.5-400 batch was observed to be -613 mV_{SCE}, while that of the replicate bar cast in the same week was -482 mV_{SCE}. Both bars corroded under the applied 400 mV polarization with the same initiation time but the latter exhibited the higher i_{corr} despite its less negative potential. Finally, the OCP of 2304 AR 3.6 in the 6-200 batch was found to be -551 mV_{SCE}, while the OCP of the replicate bar cast in the same week was found to be -350 mV_{SCE}. Both specimens were found to have approximately the same passive i_{corr} values.

6.3.3 The Effect of Admixed Chlorides on the Open Circuit Potentials

A summary of the average and standard deviations of the OCP values of each stainless steel grade is shown in Table 6.1. The average and standard deviations of the OCP values by each batch are shown in Appendix B to illustrate any effect of concrete mix. The average, maximum, and minimum OCP values for each of the stainless steel grades are shown in Figure 6.4.

Table 6.1: Open Circuit Potential (mV_{SCE}) Statistics 48 hours after Casting

RST Batch	Open Circuit Potential (mV_{SCE}) Statistics 48 hours after Casting					
	2205 AR		XM-28 AR		2304 AR	
	Average	Standard Deviation	Average	Standard Deviation	Average	Standard Deviation
4-100	-473	51	-498	32	-440	58
4-400	-474	14	-447	22	-487	26
6-100	-428	42	-461	12	-347	32
6-200	-376	33	-440	37	-317	32
6-300	-414	37	-471	23	-368	46
6-400	-439	90	-472	10	-417	27
7.5-200	-406	43	-450	14	-334	48
7.5-300	-392	32	-453	29	-331	56
7.5-400	-367	36	-395	70	-290	25

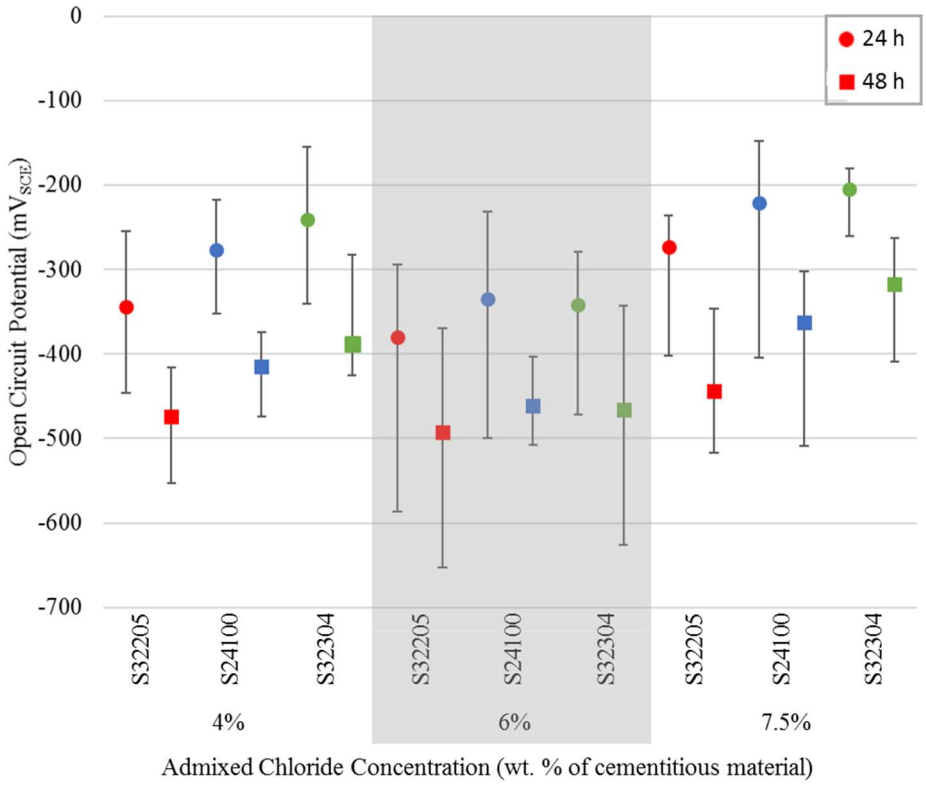

Figure 6.4: The average, maximum, and minimum open circuit potentials of the bars measured immediately on immersion in a saturated $Ca(OH)_2$ solution (i.e. 24 hours after casting – circular symbols) and after a further 24 hours (i.e. 48 hours after casting – square symbols).

In general, the OCP of all of the bars became more negative over the 24 hour OCP monitoring period, although there was considerable variation between the minimum and maximum values. The cathodic shift over the 24 hour period suggests that the passive film on each bar is degrading with increased contact with the admixed chlorides. Marcus et al. [84] proposed that when the passive film is completely dissolved at a given location, the potential drop that occurs is at the metal-electrolyte interface, resulting in an active corrosion site. Localized thinning of the passive film results in significant metal dissolution, causing a large drop in potential.

The variability within the OCP values for a given stainless steel grade can be attributed to the stochastic nature of corrosion in concrete. Factors such as the non-uniformity of the surface films on the ribbed bars and the heterogeneous nature of concrete contribute to the variability of the OCP values.

There is no indication from the open circuit potential measurements that increasing the admixed chloride concentration from 6 to 7.5 wt. % of cementitious materials resulted in corrosion initiation prior to the application of the polarization potential. The maximum and minimum OCP values for each of the stainless steel types are in the same range for the different admixed chloride concentrations. However, the average OCP values for the XM-28 and 2304 specimens were found to become more negative from 4% to 6% admixed chlorides, but to become more positive from 6% to 7.5% admixed chlorides. This could be attributed to corrosion initiating in the XM-28 and 2304 specimens in the 7.5% admixed chloride concrete batches prior to the application of the polarization potentials. The build-up of corrosion products on the XM-28 and 2304 bars would affect the OCP readings, leading to more positive OCP values. However, the OCP values for the 2205 specimens remained consistent from all three chloride contents suggesting that chlorides had little effect on the resistance of the passive film. This theory corresponds to the theoretical C_T values of each the stainless steel grades calculated using the logistic regression models for each grade. Both XM-28 and 2304 grades were found to have threshold values of 7.1 and 7.1, respectively, while the 2205 grade was found to have a threshold value of 9.4, again suggesting that corrosion may have initiated on the XM-28 and 2304 specimens prior to the application of the polarization potentials.

6.4 Corrosion Initiation

Based on the electrochemical test and autopsy results presented in Chapter 4, several observations can be made regarding corrosion initiation. Corrosion products were observed on the surface of all the specimens whose corrosion current density exceeded the proposed pass/fail limit for more than 2 hours (i.e. active

corrosion initiation had occurred). Moreover, all specimens whose corrosion current density jumped by approximately one order of magnitude, even briefly, had visible evidence of corrosion, even if they did not exceed the pass/fail limit. The only observed exception from these statements was the 2304 AR 7.8 specimen in the 7.5-200 batch, shown in Figure 6.5. The bar's corrosion current density did not experience any "jumps", and its i_{corr} was found to be at least one order of magnitude lower than the 25 mA/m^2 proposed pass/fail limit, remaining at a passive i_{corr} value. However, corrosion was apparent on visual inspection of the autopsied bar.

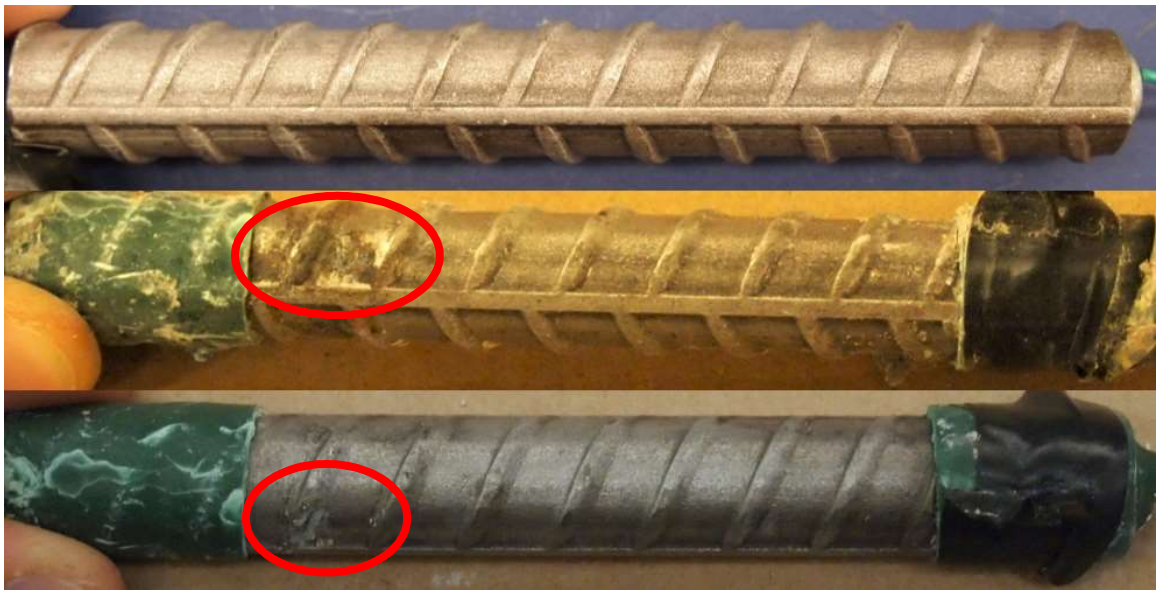

Figure 6.5: 7.5-200 Batch – Corrosion Products on 2304 AR 7.8. From top to bottom, a) original specimen, b) corrosion products on the specimen upon removal from concrete, and c) pitting corrosion identification on the pickled specimen

After the momentary jumps in corrosion current density, the corrosion rates of the 2304 and 2205 specimens reverted to their "pre-jump" values by the next set of readings, i.e. within 15 minutes. This behaviour is be attributed to momentary pitting of the bars, followed by the immediate repassivation of the bars. In concrete, this critical concentration of chlorides is often referred to as the critical chloride threshold.

An alternative explanation for the spikes in the i_{corr} plots for some of the 2304 and 2205 specimens is possible contamination of the bars. One example of potential contamination of the specimens could be the

"dark line" observed on the 2304 specimens Figure 4.23 in Section 4. These corroding areas were too small for any analysis that was within the scope of this project.

The effect of the OCP values of the bars 48 hours after casting was investigated to determine its influence on the corrosion initiation of the specimens, shown in Figures 6.6, 6.7, and 6.8 for the 2205, XM-28, and 2304 specimens, respectively. Only the specimens that had undergone corrosion initiation based on the electrochemical results (i.e. had surpassed the 25 mA/m^2 limit for more than 2 hours) were considered in this investigation. It was determined that the OCP values immediately prior to the application of the polarization potential had no measurable effect on the corrosion initiation of the bars.

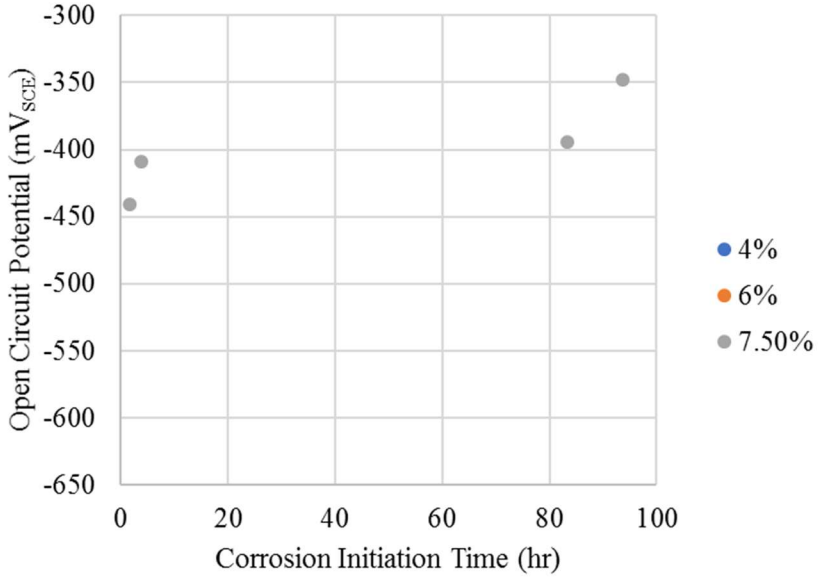

Figure 6.6: 2205 AR Specimens: Open Circuit Potentials (mV_{SCE}) of bars that surpassed the proposed pass/fail limit

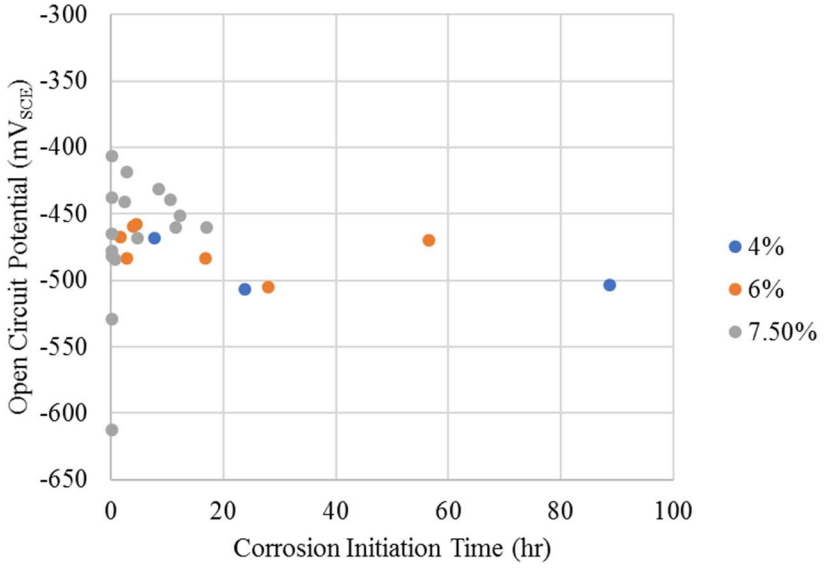

Figure 6.7: XM-28 AR Specimens: Open Circuit Potentials (mV$_{SCE}$) of bars that surpassed the proposed pass/fail limit

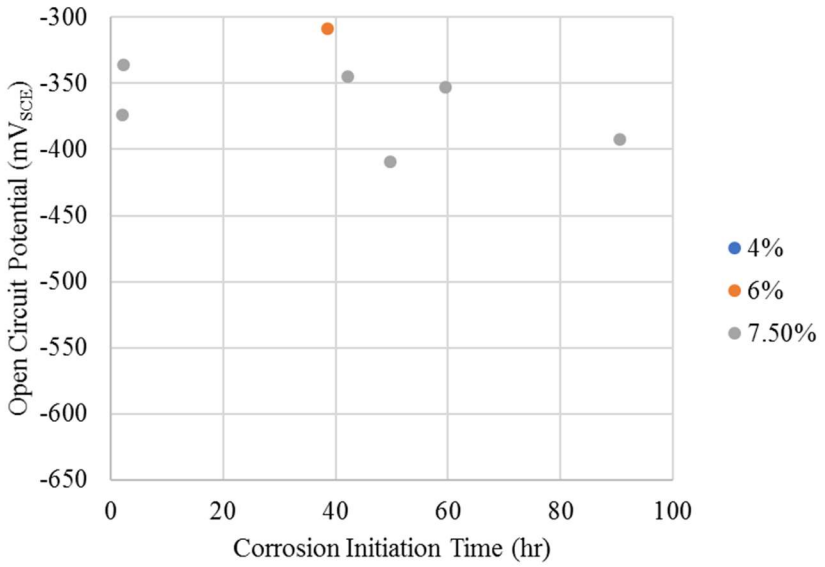

Figure 6.8: 2304 AR Specimens: Open Circuit Potentials (mV$_{SCE}$) of bars that surpassed the proposed pass/fail limit

Although corrosion initiation has been previously defined as the corrosion current exceeding 25 mA/m^2 for more than 2 hours, an alternative definition of corrosion initiation is proposed. For the purpose of this

project, corrosion initiation is now defined as a jump in a bar's i_{corr} by at least one order of magnitude. The reasoning is as follows. Based on the original definition, the electrochemical results indicate that corrosion initiation has only occurred in the bars shown in Table 4.12. Observations noted during the autopsy of the bars did not show any visible evidence that corrosion had occurred. However, post-autopsy examinations of the bars (ranging from 1 week to 5 months after autopsy) showed relatively small areas of rust-coloured oxidation, indicating that corrosion had initiated, contrary to the original definition of corrosion initiation.

6.5 Corrosion Current Density

The selected logistic regression models for each stainless steel grade found that the corrosion initiation of the bars was significantly affected more by increasingly higher admixed chloride concentrations than the applied polarization potentials. This conclusion from the statistical analysis agrees with the experimental results. In general, higher admixed chlorides concentrations resulted in more bars actively corroding, as well as higher active i_{corr} and passive i_{corr} values for each bar, regardless of the applied polarization potential. Photomicrographs of pitting corrosion damage by varying the admixed chloride content per stainless steel grade are shown in Figure 6.10. Please note that no 2304 specimens corroded in the 6-400 batch, so the 6-300 batch and 7.5-300 batch were used for the comparison in Figure 6.10.

For a given chloride concentration, once a bar's i_{corr} surpassed the proposed pass/fail limit of 25 mA/m^2, higher applied polarization potentials resulted in higher active i_{corr} and passive i_{corr} values. Note that the "passive" i_{corr} values are considered to be the i_{corr} values of any bar that is below the proposed pass/fail limit by at least one order of magnitude at the end of the applied polarization period (96 h). Photomicrographs of pitting corrosion damage by varying the polarization potential for a given admixed chloride content are shown in Figure 6.11.

A comparison between the average passive i_{corr} values of each stainless steel grade and the applied polarization potential for the 6% admixed chloride concentration batches are shown in Figure 6.9. Note that the specimens for the 4% and 7.5% admixed chloride concentrations were not considered due to the lack of tested polarization potential batches and the high number of actively corroding bars, respectively. Active i_{corr} values were not compared in the same manner as the passive i_{corr} values because of the high variability of their values as a result of the various factors that affect said values, such as bar defects, the heterogeneous nature of concrete, and chloride concentration gradients within the concrete.

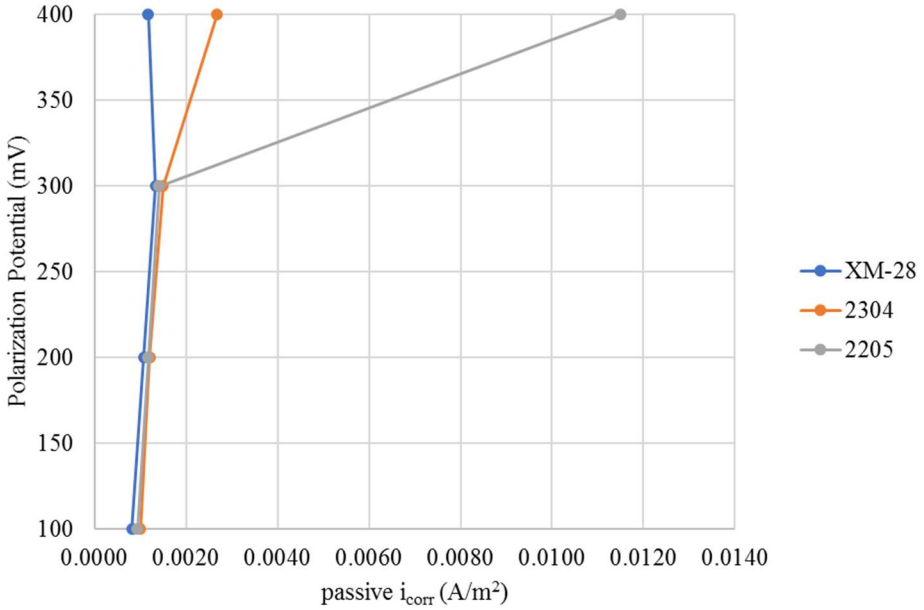

Figure 6.9: Average passive I_{corr} (A/m^2) of each Stainless Steel Grade versus Applied Polarization Potential (mV)

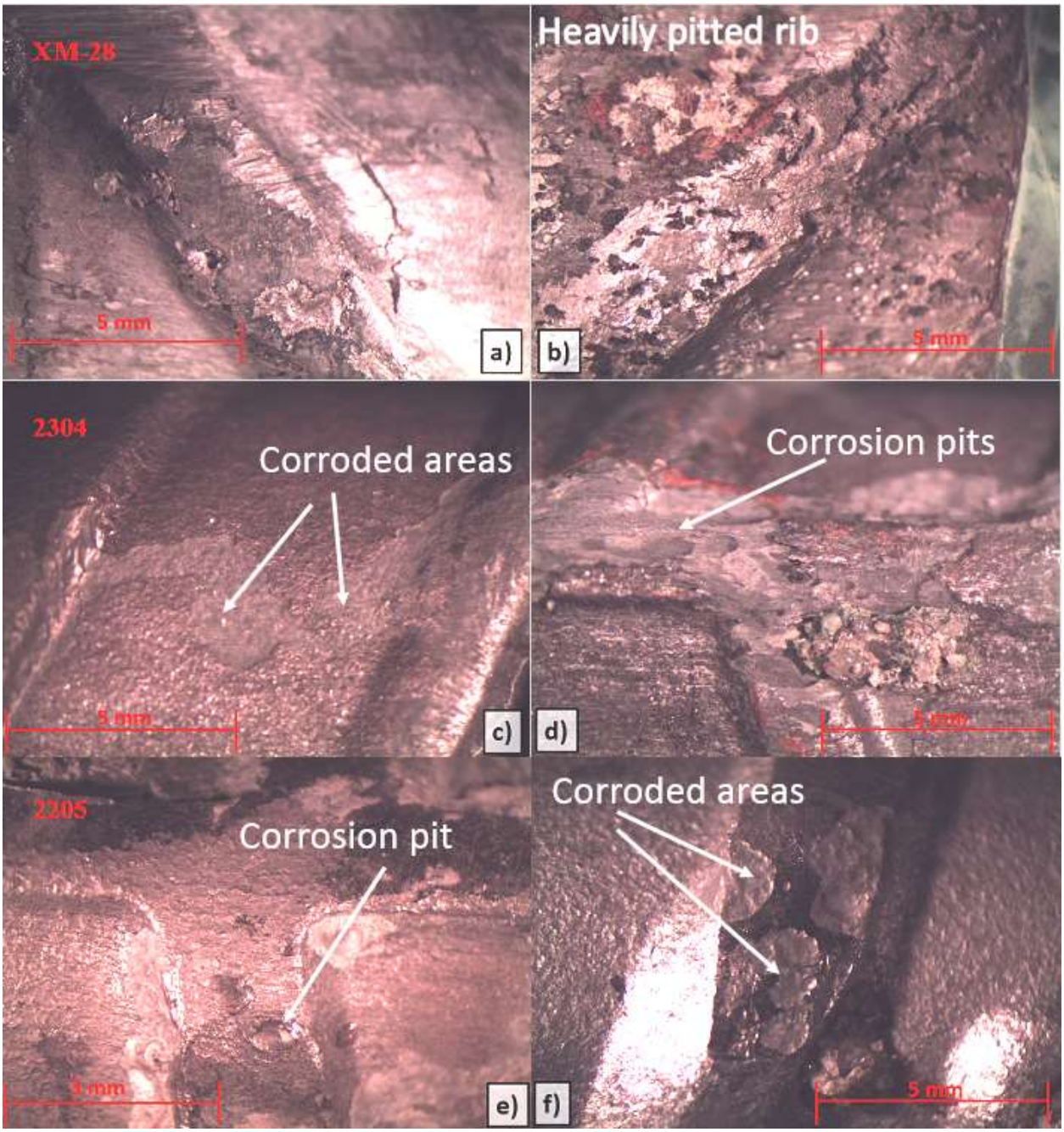

Figure 6.10: Photomicrograph Comparison of Pitting Corrosion Damage by Increasing the Admixed Chloride Concentration. The specimens, read from left to right, are as follows: a) XM-28 AR 7.6 (4-400 batch), b) XM-28 AR 8.2 (7.5-400 batch), c) 2304 AR 4.3 (6-300 batch), d) 2304 AR 5.8 (7.5-300 batch), e) 2205 AR 5.4 (6-400 batch), f) 2205 AR 7.6 (7.5-400 batch)

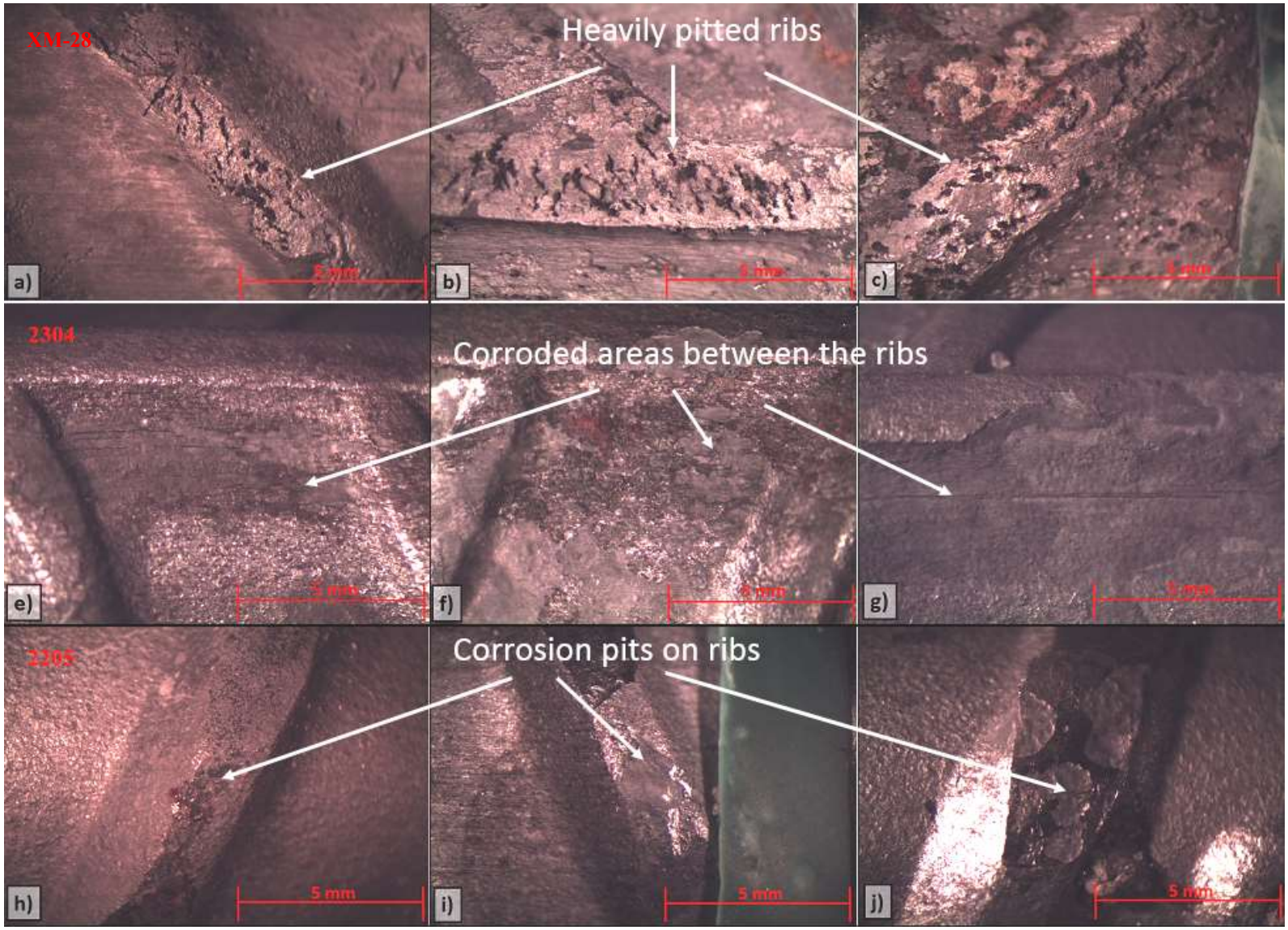

Figure 6.11: Photomicrograph Comparison of Pitting Corrosion Damage by Increasing the Polarization Potential. The specimens, read from left to right, are as follows: a) XM-28 AR 8.7 (7.5-200 batch), b) XM-28 AR 6.8 (7.5-300 batch), c) XM-28 AR 8.2 (7.5-400 batch), e) 2304 AR 7.9 (7.5-200 batch), f) 2304 AR 5.7 (7.5-300 batch), g) 2304 AR 7.5 (7.5-400 batch), h) 2205 AR 7.8 (7.5-200 batch), i) 2205 AR 7.6 (7.5-300 batch), and j) 2205 AR 7.6 (7.5-400 batch)

6.6 Cracking of the Concrete Specimens by Corrosion Products

Cracking of the concrete specimens was only observed in the 6-400 batch and all the 7.5% admixed chloride batches. The general trend appears to be that if the corrosion current density of the bars was at least 1 A/m^2 for more than 48 hours, the concrete specimens containing the bars would crack because of the corrosion products. None of the bars in the batches that were less aggressive than the 6-400 batch were observed to have a corrosion current density greater than 1 A/m^2.

6.7 Corrosion Behaviour of the Stainless Steel Grades

The current densities reported correspond to the measured current divided by the whole area of steel exposed to the concrete. While this gives correct values for the passive current densities, it is incorrect once active corrosion is initiated. To be accurate, after initiation the measured current should be divided by the area of bar that is actively corroding. In general, higher corrosion current densities were found to correspond to more frequent and severe pitting corrosion across the bars. Based on the statistical analysis, the theoretical C_T of the XM-28 specimens was approximately the same as the 2304. However, based on the pitting corrosion of the XM-28 bars, the author believes that XM-28 is far more susceptible to severe pitting corrosion once corrosion has initiated, as shown in Figure 6.10 and Figure 6.11.

In contrast to the deep pits observed on the XM-28 bars, corrosion of the 2304 specimens appears to be restricted to a shallow surface layer; it appears that the outermost layer of the steel was the only layer that corroded. The improved corrosion resistance of the 2304 specimens could be attributed to the higher chromium and nickel, and the small amount of molybdenum of this alloy compared to the XM-28 bars.

When pitting corrosion was observed on the 2205 specimens, it was very mild in nature compared to the XM-28 and 2304 specimens. This improved corrosion resistance could be attributed to the higher nickel and molybdenum contents of the bar compared to both the XM-28 and 2304 bars.

Chapter 7 – Summary, Conclusions and Recommendations

This chapter presents conclusions and recommendations based on the research presented in the previous chapters. Section 7.1 summarizes the conclusion of this project based on the experimental and analytical research. The recommendations based on this research are presented in Section 7.2, which is divided into subsections which summarize the recommendations for industry practice and the recommendations for future research.

7.1 Summary and Conclusions

Passivation of the stainless steels in the synthetic concrete pore solution suggests that the passive films developed on the tested bars were becoming more protective than the air-formed films on the "as-received" bars. However, the differences in potentials between the as-received specimens and the "pre-passivated" specimens were found to be insignificant. Therefore, all Rapid Screening Test batches after the 4% admixed Cl^-, +100 mV polarization (4-100) batch tested the stainless steels in their as-received condition.

The corrosion initiation results of the electrochemical testing and the observations made during and after autopsying the bars were found to differ. For this reason, a new definition of corrosion initiation was proposed for use in the electrochemical portion of the Rapid Screening Test: any increase in corrosion current density by at least one order of magnitude should be considered as corrosion initiation at a pit, even if the pit is found to re-passivate. Therefore, a relative comparison of the 2205, 2304, and XM-28 specimens was determined by the number of specimens that have corroded in the Rapid Screening Test, as well as the order of magnitude of their respective corrosion current densities. The experimental results can be summarized as follows:

- The higher the admixed chloride concentration in concrete, the more likely that a bar will initiate corrosion. Corrosion initiation was more frequent at higher admixed chloride concentrations and corrosion current density values, averaged over the whole bar area, were observed to be higher as well. The susceptibility of each of the stainless steel grades to chloride attack, in order of the most to least susceptible, are as follows: XM-28 ≈ 2304 > 2205. Corrosion initiation was found be more influenced by the admixed chloride concentration than the applied polarization potential.

- The higher the polarization potential, the more severe the pitting corrosion was on each of the stainless steel grades. Higher corrosion current density values correlated with higher polarization potentials once corrosion initiation had occurred. More severe cases of pitting corrosion were also observed with higher corrosion current density values. A ranking of the stainless steel grades based on the severity of corrosion, in order of the most to least damaged, is as follows: XM-28 >> 2304 > 2205.
- The open circuit potential of the bars immediately prior to the application of polarization potential did not significantly influence corrosion initiation. The variability of the open circuit potential values between the specimens of a given stainless steel grade can be attributed to many factors such as non-uniform chemical composition, irregular surface and surface roughness of the bars, and the heterogeneous nature of concrete. Varying the slump content and curing conditions does not appear to have a significant effect on the open circuit potential of the different stainless steel grades for any of the admixed chloride concentrations.
- The corrosion products from steel specimens whose corrosion current densities were at least 1 A/m^2 for a minimum of 48 hours were found to crack the concrete specimens. This phenomenon was observed in all the batches that were more aggressive than the 6% admixed Cl^-, +300 mV polarization (6-300) batch.

A statistical analysis of the corrosion data for each of the stainless steel grades was conducted. It was determined that increasing the admixed chloride content of the concrete mixture has a far more significant impact on the corrosion initiation of the bars than does the applied polarization potentials. Based on the results of the logistic regression models, theoretical critical chloride thresholds were predicted. The values for these thresholds, by wt.% of cementitious material, are 7.1%, 7.1%, and 9.4% for XM-28, 2304, and 2205, respectively. Note that the number of corroded versus non-corroded specimens for 2304 and 2205 are imbalanced and as a result, the thresholds may be vastly different than the calculated values. Based on the severity of the pitting corrosion seen in the photomicrographs, it is believed that 2304 has a higher chloride threshold than XM-28. It must be emphasized that these threshold values should be used as relative values in the Rapid Screening Test, and not as an accurate estimate of the critical chloride threshold values for each of these stainless steel grades in reality. The table below, Table 7.1, summarizes the ranking of the reinforcing bars based on the results of the Rapid Screening Test.

Table 7.1: Ranking of Rapid Screening Test Specimens in terms of Corrosion Resistance

Stainless Steel Grade	Overall Ranking	Electrochemical Results	Autopsy Results	Statistical Analyses Results
S32205	1	1	1	1
S32304	2	2	2	2
S24100	3	3	3	2

7.2 Recommendations

7.2.1 Recommendations based on Experimental and Analytical Results

Due to the short duration of the Rapid Screening Test, it is recommended that the stainless steels be tested in their as-received condition instead of pre-passivating the bars in synthetic concrete pore solution. Based on the definition of corrosion initiation stated in Section 6.4, the recommended parameters for testing new and existing grades of stainless steel are 7.5% admixed chlorides by mass of cementitious material and +300 mV of applied polarization potential. These parameters have been found to initiate corrosion in at least approximately 50% of the specimens of each of the stainless steel grades that were tested. In particular, 50% of the control specimens were observed to have corroded using these parameters. Using the recommended parameters, the proposed relative ranking of stainless steel specimens is based on the number of specimens that have corroded, the order of magnitude of the specimen's corrosion current density, and the severity of the pitting corrosion observed on the specimens.

Both the experimental results and the statistical analyses demonstrate that 2205 outperforms both 2304 and XM-28, which is attributed to its chemical composition. The 2304 bars appear to undergo corrosion initiation similarly to the XM-28 specimens in the 7.5% admixed chloride conditions, but they appear to be far less susceptible to severe pitting corrosion than the XM-28 bars based on the corrosion damage shown in the photomicrographs. It is concluded that 2304 reinforcing bars can be specified in highway structures made of reinforced concrete to minimize maintenance and associated costs such as user delay and lane closures for the service life of the highway structure. Based on the autopsy results of the Rapid Screening Test, XM-28 appears to be far more susceptible to pitting corrosion than 2304 or 2205. It should be noted that chloride concentrations in excess of 5% by mass of cementitious material in concrete highway structures have not been reported in the available literature to date.

7.2.2 Recommendations for Future Work

Although the work presented here is based on the best available information at the time of completing this work, future research could be done to improve upon the value of the results. This research could include improvements to both the experimental design as well as the statistical analysis of the data.

7.2.3 Improved Experimental Design

Various considerations could be made to improve upon the Rapid Screening Test, however, one must consider the short testing duration when trying to re-design the test to more accurately simulate realistic conditions for stainless steel reinforcing bars in concrete highway infrastructure. Specific improvements to enhance the corrosion behaviour knowledge of various stainless steel grades in reinforced concrete are detailed in the following paragraphs.

7.2.4 Concrete Mix Design and Testing

The concrete mix design that was used for the experimental work of this project met the specifications of the Ministry of Transportation of Ontario for highway bridges. The effect of other and or additional cementitious material contents, as well as lower w/cm ratios, on the corrosion performance of stainless steel bars in the Rapid Screening Test is currently unknown.

Admixed chlorides were introduced into the concrete mix by admixed sodium chloride into the concrete mixing water. However, highly concentrated chloride brines have been used in recent years for deicing applications on Canadian highway infrastructure. These brines can include various combinations of the salts magnesium chloride, calcium chloride, and sodium chloride. The effect of these individual salts, or the combination thereof, on the corrosion behaviour of stainless steels in the Rapid Screening Test is currently unknown. Knowledge of their impact would be invaluable when trying to accurately simulate the realistic conditions of stainless steel reinforcing bars in highway concrete infrastructure.

Finally, it is recommended that moisture content analyses of each concrete mix used for the Rapid Screening Test be conducted. By testing the moisture content of the concrete, one could more accurately determine if there is a correlation between additional water content in the concrete mix and the corrosion behaviour of the stainless steel bars.

7.2.5 Stainless Steel Grades

The stainless steel reinforcing bar grades used for this project were limited to 2205, 2304, and XM-28. These grades have been used in highway infrastructure, but their corrosion performance over extended periods of time (i.e. 75 to 100 years) is currently unknown. Testing a stainless steel grade with a known service life, such as 304, would be useful for determining a baseline for the Rapid Screening Test for benchmarking purposes. The corrosion performance of other stainless steel grades relative to the 304 grade could give some indication of their relative corrosion performance, which could be useful when determining the applicability of a given stainless steel grade for highway infrastructure projects.

7.2.6 Recommendations for Statistical Analyses

The logistic regression models used to predict the probability of corrosion for each of the stainless steel grades were based on two independent predictors: the admixed chloride concentration in the concrete, and the applied polarization potential. By following the recommendations for the improved experimental design in Section 7.2.3, additional data could be gathered to increase the number of independent predictors. These predictors could be, and are not limited to: cement content, cementitious material composition, moisture content in the concrete, the variation in a bar's chemical composition, or even specific manufacturing processes related to the surface finishes and preparation of the bars. By using these metrics to predict the probability of corrosion in the tested stainless steel grades, one could more accurately predict the probability of corrosion. The relative comparison of the corrosion behaviour between the tested stainless steel grades could have not only a valid experimental basis, but it could be based on a statistical analysis that could more accurately simulate realistic conditions.

Letters of Copyright Permission

American Concrete Institute

Always advancing

Peter Loudfoot
University of Waterloo
200 University Avenue West
Waterloo, ON, N2L 3G1
CANADA

July 9, 2018

Subject: Use of ACI Copyrighted Material

Your request to:

___X___ Use information/figures/tables indicated below. Please credit American Concrete Institute, author(s) and publication.

___X___ Reprint the information described in the quantity indicated. Please add a note to the reprint similar to: *Authorized reprint from (publication) (issue/volume/year as appropriate.)*

_____ Payment of Right-to-Reprint fee of (\$0) is required.

Permission is granted to reference and reprint:

Figure 3 Layout of ACT test setup from *Nov–Dec 2003 ACI Materials Journal, Vol. 100 No. 6, Title No. 100-M60 "Accelerated Chloride Threshold Testing: Part I-ASTM A 615 and A 706 Reinforcement"*

Signed: Angela Matthews Date: 9 July 2018

Angela Matthews
Editor, Publishing Services
Angela.Matthews@Concrete.org

Peter Loudfoot

From: reportcard <reportcard@asce.org>
Sent: Tuesday, July 17, 2018 11:29 AM
To: Peter Loudfoot
Subject: RE: New submission from Contact Us

Peter,

Permission to use the two infrastructure report card figures is granted. Please use the following citation: 2017 ASCE Infrastructure Report Card. www.infrastructurereportcard.org

Thank you,

American Society of Civil Engineers

From: Infrastructure Report Card <infrastructurereportcard@mail01.dev1-ironistic.com>
Sent: Tuesday, July 17, 2018 10:03 AM
To: reportcard <reportcard@asce.org>
Subject: New submission from Contact Us

Name
Peter Loudfoot
Email
pghloudf@uwaterloo.ca
Organization
University of Waterloo
Message
I was wondering who I should contact regarding permissions for some of the figures from the following document: American Society of Civil Engineers, “2017 Infrastructure Report Card,” p. 111, 2017. I would like permission to include these figures and tables in my thesis, which will be available on the University of Waterloo’s institutional repository. Proper citation will be included with the reproduction of the table. If you could please let me know, I would appreciate it. Thank you.

ASTM INTERNATIONAL

Standard: ASTM A955-18 Standard Specification for Deformed and Plain Stainless Steel Bars for Concrete Reinforcement

Publisher: ASTM International

Issue Date: Jan 1, 2018

Order Completed

Thank you for your order.

This Agreement between Peter Loudfoot ("You") and ASTM International ("ASTM International") consists of your order details and the terms and conditions provided by ASTM International and Copyright Clearance Center.

License number	Reference confirmation email for license number
License date	Jul, 24 2018
Licensed Content Publisher	ASTM International
Licensed Content Publication	ASTM Standard
Licensed Content Title	ASTM A955-18 Standard Specification for Deformed and Plain Stainless Steel Bars for Concrete Reinforcement
Licensed Content Date	Jan 1, 2018
Type of use	Thesis/Dissertation
Requestor type	Academic institution
Format	Print, Electronic
Portion	chart/graph/table/figure
Number of charts/graphs/tables/figures	2
Rights for	Main product
Duration of use	Life of current/future editions
Creation of copies for the disabled	no
With minor editing privileges	yes
For distribution to	United States and Canada
In the following language(s)	Original language of publication
With incidental promotional use	no
Lifetime unit quantity of new product	0 to 499
Order reference number	
Title	Graduate Student
Instructor name	Carolyn Hansson
Institution name	University of Waterloo
Expected presentation date	Aug 2018
Portions	Fig A2.1 Fig A3.1
Requestor Location	Mr. Peter Loudfoot 2346 Reid Road Newtonville, ON L0A1J0

	Canada Attn: Mr. Peter Loudfoot
Billing Type	Invoice
Billing address	Mr. Peter Loudfoot 2346 Reid Road Newtonville, ON L0A1J0 Canada Attn: Mr. Peter Loudfoot
Total	0.00 CAD

CLOSE WINDOW

NACE International
15835 Park Ten Place
Houston, TX 77084
Tel: 281-228-6200
Fax: 281-228-6300

NACE INTERNATIONAL
The Worldwide Corrosion Authority

Permission to Reproduce Figures, Photos, and Tables from Copyrighted Works

Date: August 2, 2018

Name: Peter Loudfoot Title: Graduate Student

Company ("Publisher"): University of Waterloo

Address: 200 University Ave W., Waterloo, Ontario, Canada N2L 3G1

Tel: 226-792-0077 Fax:

Email: pghloudf@uwaterloo.ca

Material to be Reproduced ("Work"): Please provide a complete description of the material involved. Include the following elements where applicable: publication name, issue date, page number, figure/photo/table number, paper number, conference name, etc.

Corrosion Journal Volume 72 Issue 6 pgs 834-842 (Primary Author: Van Niejenhuis)

Figure 2 and Figure 3

Table 3 and 4

Reproduction Method ("Publication Media"): Please provide a complete description of how and where the Work will be used. Include the following elements as applicable: publication name, issue, circulation, print run, web site address, conference name, presentation time and place, etc.

Masters Thesis located in the University of Waterloo's institutional repository: https://uwspace.uwate

Title: The Adaption of a Rapid Screening Test to Rank the Corrosion Behaviour of Stainless Steel R

NACE International ("NACE") hereby grants to "Publisher" the right to publish the Work utilizing the Publication Media described above. The publication right granted herein is limited the specific Publication Media described above. To the extent the publication of the Work is to occur by an above-specified date, such as in a particular periodical or at a particular conference, the right granted herein shall automatically terminate upon the date of such occurrence, whether or not the Work is actually published. To the extent the Publication Media is a web site, the publication right is limited to publication at the specific web site URL identified above. Any right granted herein is a limited, non-transferable, non-exclusive right. No other rights in the Work are granted herein.

Publisher shall not edit or modify the Work except to meet the style and graphic requirements of the individual media involved.

The Publisher shall include the following notation with any publication of the Work:*

A. Conference Paper
Reproduced with permission from NACE International, Houston, TX. All rights reserved. Author(s), Paper NUMBER presented at CORROSION/YEAR, City, State. © NACE International FIRST YEAR OF PUBLICATION.

B. Journal Article
Reproduced with permission from NACE International, Houston, TX. All rights reserved. Author(s) name, Article title, Journal title, Vol. no., Issue no., and publication year. © NACE International FIRST YEAR OF PUBLICATION.

C. Magazine Article
Reproduced with permission from NACE International, Houston, TX. All rights reserved. Author(s) name, Article title, Magazine title, Vol. no., Issue no., and publication year. © NACE International FIRST YEAR OF PUBLICATION.

D. Standards
STANDARDS/TECHNICAL COMMITTEE REPORT NAME. © NACE International YEAR. All rights reserved by NACE. Reprinted with permission. NACE standards are revised periodically. Users are cautioned to obtain the latest edition; information in an outdated version of the standard may not be accurate.

* Modifications to Notations: Other reference wording can be used, but must be approved by NACE in writing *in advance*.

The Publisher shall include full bibliographic citations of or references to the original NACE source, where applicable.

Publisher shall obtain a copy of the original Work directly from NACE International and shall not utilize copies of the Work from other sources, including the author(s).

To the extent the Work is published on a web site as authorized herein, the Work shall be posted in a file format that does not allow the content of the Work to be easily copied from the Web Site or changed.

As between NACE and Publisher, Publisher acknowledges that NACE owns all rights in the Works.

Publisher shall not be entitled to any compensation for its efforts in promoting the Work.

THE WORK IS PROVIDED "AS IS." ALL EXPRESS OR IMPLIED COVENANTS, CONDITIONS, REPRESENTATIONS OR WARRANTIES, INCLUDING ANY IMPLIED WARRANTY OF MERCHANTABILITY OR FITNESS FOR A PARTICULAR PURPOSE OR CONDITIONS OF ACCURACY, COMPLETENESS OR QUALITY AND THOSE ARISING BY STATUTE OR OTHERWISE IN LAW, ARE HEREBY DISCLAIMED.

IN NO EVENT WILL NACE BE LIABLE FOR ANY DIRECT, INDIRECT, PUNITIVE, SPECIAL, INCIDENTAL OR CONSEQUENTIAL DAMAGES IN CONNECTION WITH OR RELATED TO THIS AGREEMENT (INCLUDING LOSS OF PROFITS, USE, DATA, OR OTHER ECONOMIC ADVANTAGE), HOWSOEVER ARISING.

This Agreement and the rights granted herein may be terminated immediately by NACE upon breach of this Agreement by Publisher. Unless earlier terminated, this Agreement and the rights granted herein will automatically terminate 6 months from the Date set forth above. If the Work has not been published within that time period, a new Agreement must be obtained.

Publisher may not, directly or indirectly, sell, assign, sublicense, lease, rent, distribute, or otherwise transfer this Agreement or any rights granted herein, without the prior written consent of NACE.

If any provision of this Agreement is found to be unenforceable, then this Agreement shall be deemed to be amended by modifying such provision to the extent necessary to make it legal and enforceable while preserving its intent. The remainder of this Agreement shall not be affected by such modification.

This Agreement does not create, and shall not be construed to create, any employer-employee, joint venture or partnership relationship between the parties. No officer, employee, agent, servant or independent contractor of either party shall at any time be deemed to be an employee, servant, agent or contractor of any other party for any purpose whatsoever.

This Agreement shall be governed by, and construed and enforced in accordance with, the laws of the State of Texas, without regard to the choice of law provisions of that State.

This Agreement shall only be effective if signed by authorized representatives of both parties. This Agreement constitutes the entire Agreement between the parties with respect to the subject matter of this Agreement. Any change, modification or waiver hereto must be in writing and signed by authorized representatives of both parties.

Other Terms & Conditions: _____

Publisher hereby requests permission to publish the Work described above and agrees to comply with all Terms and Conditions listed above.

Request submitted by:

Peter Loudfoot

Printed Name

Peter Loudfoot

Title

Graduate Student

Signature

Date

August 2, 2018

Request approved by NACE:

Daniela Freeman

Printed Name

Daniela Freeman

Title

Copyright Permissions

Signature

daniela.freeman@nace.org Digitally signed by daniela.freeman@nace.org DN: cn=daniela.freeman@nace.org Date: 2018.08.06 10:56:27 -05'00'

Date

8/6/2018

Request agreed to by:

Colin Van Niejenhuis

Lead Author Printed Name

Colin Van Niejenhuis

Lead Author Title

Graduate Student

Lead Author Signature

Date

August 2, 2018

References

[1] Ontario Provincial Standard Specification, *OPSS 1440: Material Specification for Organic Coatings for Steel Reinforcement*. Canada, 2014, pp. 1–8.

[2] Ontario Provincial Standard Specification, *OPSS 905: Construction Specification for Steel Reinforcement for Concrete*. Canada, 2007, pp. 1–15.

[3] N. J. Delatte, "Lessons from Roman Cement and Concrete," *J. Prof. Issues Eng. Educ. Pract.*, vol. 127, no. July, pp. 109–115, 2001.

[4] C. B. Van Niejenhuis, "The Case for Stainless Steel Reinforcing Bars," University of Waterloo, 2015.

[5] Y. Zhou, B. Gencturk, K. Willam, and A. Attar, "Carbonation-Induced and Chloride-Induced Corrosion in Reinforced Concrete Structures," *Am. Soc. Civ. Eng.*, vol. 27, no. 9, pp. 1–17, 2015.

[6] G. H. Koch, M. P. H. Brongers, N. G. Thompson, Y. P. Virmani, and J. H. Payer, "Corrosion costs and preventive strategies in the United States," *NACE Int.*, pp. 1–12, 2002.

[7] C. Hansson, R. Haas, R. Green, R. Evers, O. Gepraegs, and R. Al-Assar, "Corrosion Protection Strategies for Ministry Bridges," 2000.

[8] A. Ranjith, K. Balaji Rao, and K. Manjunath, "Evaluating the effect of corrosion on service life prediction of RC structures - A parametric study," *Int. J. Sustain. Built Environ.*, vol. 5, no. 2, pp. 587–603, 2016.

[9] K. Bhargava, A. K. Ghosh, Y. Mori, and S. Ramanujam, "Modeling of time to corrosion-induced cover cracking in reinforced concrete structures," *Cem. Concr. Res.*, vol. 35, no. 11, pp. 2203–2218, 2005.

[10] American Society of Civil Engineers, "2017 Infrastructure Report Card," 2017.

[11] I. Ahmad, "The State of Ontario's Roads and Bridges: An Analysis of 93 Municipalities," 2015.

[12] CSA Group, *Canadian Highway Bridge Design Code S6-14*. Canada, 2014.

[13] M. Schönning, S. Randström, and O. S. Ab, "Adaption of EN 480-14 : 2006 as a test method for determining a critical chloride threshold level for stainless steel rebar," in *Eurocorr 2011*, 2011.

[14] A. K. Moruza and S. R. Sharp, "The Use of Corrosion Resistant Reinforcement as a Sustainable Technology for Bridge Deck Construction," *TRB 2010 Annu. Meet.*, vol. 4, no. 434, 2010.

[15] R. E. Schnell and M. P. Bergmann, "Improving Tomorrow's Infrastructure: Extending the life of concrete structures with solid stainless steel reinforcing bar," in *New York City Bridge Engineering Conference*, 2007, pp. 1–11.

[16] G. G. Clemeña, "Investigations of the resistance of several new metallic reigorcing bars to chloride-induced corrosion in concrete," no. December, p. 24, 2003.

[17] G. G. Clemena and Y. P. Virmani, "Comparing the Chloride Resistances of Reinforcing Bars," *Concr. Int.*, vol. November, no. November, pp. 39–49, 2004.

[18] W. Hartt, R. Powers, and F. Presuel-Moreno, "Corrosion Resistant Alloys for Reinforced Concrete; Interim Report," 2007.

[19] N. Mohamed, M. Boulfiza, and R. Evitts, "Corrosion of Carbon Steel and Corrosion-Resistant Rebars in Concrete Structures Under Chloride Ion Attack," vol. 22, no. March, pp. 787–795, 2013.

[20] A. Azizinamini, E. H. Power, G. F. Myers, and H. C. Ozyildirim, "Bridges for Service Life Beyond 100 Years: Innovative Systems, Subsystems, and Components," Miami, FL, 2013.

[21] Arminox, “Pier in Progreso, Mexico: Inspection Report - Evaluation of the Stainless Steel Reinforcement,” 1999.
[22] Acerinox, “Acerinox Annual Report: 2015,” 2015.
[23] N. R. Baddoo, “Stainless steel in construction: A review of research, applications, challenges and opportunities,” *J. Constr. Steel Res.*, vol. 64, no. 11, pp. 1199–1206, 2008.
[24] W. H. Hartt, R. G. Powers, and R. J. Kessler, “Performance of Corrosion Resistant Reinforcements in Concrete and Application of Results to Service Life Projection,” *NACE Int.*, pp. 1–26, 2009.
[25] G. Markeset, S. Rostam, and O. Klinghoffer, *Guide for the use of stainless steel reinforcement in concrete structures*. 2006.
[26] A. D. Jones, *Principles and Prevention of Corrosion*, Second Edi. Upper Saddle River: Prentice-Hall, Inc., 1996.
[27] B. Elsener, D. Addari, S. Coray, and A. Rossi, “Nickel-free manganese bearing stainless steel in alkaline media — Electrochemistry and surface chemistry,” *Electrochim. Acta*, vol. 56, no. 12, pp. 4489–4497, 2011.
[28] J. R. Scully and M. F. Hurley, “Investigation of the Corrosion Propagation Characteristics of New Metallic Reinforcing Bars,” Charlottesville, Virginia, 2007.
[29] B. O. Elfström, “The effect of chloride ions on passive layers on stainless steels,” *Mater. Sci. Eng.*, vol. 42, no. C, pp. 173–180, 1980.
[30] J. A. Sedriks, *Corrosion of Stainless Steels*. Canada: John Wiley & Sons, 1979.
[31] J. L. Kepler and C. E. Locke, “Evaluation of Corrosion Protection Methods for Reinforced Concrete Highway Structures,” *Corrosion*, no. 58, p. 231, 2000.
[32] J. A. Magee and R. E. Schnell, “Stainless Steel Rebar,” *Adv. Mater. Process.*, vol. October, pp. 43–45, 2002.
[33] L. Bertolini and M. Gastaldi, “Corrosion resistance of low-nickel duplex stainless steel rebars,” *Mater. Corros.*, vol. 62, no. 2, pp. 120–129, 2011.
[34] J. A. Sedriks, *Corrosion of Stainless Steels*, Second. New York: Wiley & Sons, 1996.
[35] M. Serdar, L. V. Zulj, and D. Bjegovic, “Long-term corrosion behaviour of stainless reinforcing steel in mortar exposed to chloride environment,” vol. 69, pp. 149–157, 2012.
[36] A. Fahim, A. E. Dean, M. D. A. Thomas, and E. G. Moffatt, “Corrosion resistance of chromium-steel and stainless steel reinforcement in concrete,” *Mater. Corros.*, no. December 2017, pp. 1–17, 2018.
[37] S. D. Cramer *et al.*, “Prevention of chloride-induced corrosion damage to bridges.,” *ISIJ Int.*, vol. 42, no. 12, pp. 1376–1385, 2002.
[38] S. Randstrom, M. Almen, R. Pettersson, and M. Adair, “Reproducibility of critical chloride threshold levels for stainless steel reinforcement,” *Struct. Faults*, 2010.
[39] M. F. Hurley and J. R. Scully, “Threshold Chloride Concentrations of Selected Corrosion-Resistant Rebar Materials Compared to Carbon Steel,” *Corros. Sci.*, vol. 62, pp. 892–904, 2006.
[40] D. Trejo, C. Halmen, and K. Reinschmidt, “Corrosion Performance Tests for Reinforcing Steel in Concrete: Technical Report (FHWA/TX-09/0-4825-1),” vol. 7, no. 2, p. 254, 2009.
[41] ASTM International, *ASTM A955 / A955M-18, Standard Specification for Deformed and Plain Stainless Steel Bars for Concrete Reinforcement*. West Conshohocken, PA, 2018.
[42] B. Sederholm, J. Almqvist, and S. Randström, “Corrosion Properties of Stainless Steels as Reinforcement in Concrete in Swedish Outdoor Environment,” *NACE Int.*, 2009.
[43] D. Trejo and R. G. Pillai, “Accelerated Chloride Threshold Testing: Part I-ASTM A 615 and

A 706 Reinforcement," *ACI Mater. J.*, vol. 100, no. 6, pp. 519–527, 2003.
[44] M. Castellote, C. Andrade, and C. Alonso, "Accelerated simultaneous determination of the chloride depassivation threshold and of the non-stationary diffusion coefficient values," *Corros. Sci.*, vol. 44, no. 11, pp. 2409–2424, 2002.
[45] P. V. Nygaard and M. R. Geiker, "A method for measuring the chloride threshold level required to initiate reinforcement corrosion in concrete," *Mater. Struct. Constr.*, vol. 38, no. 278, pp. 489–494, 2005.
[46] H. R. Soleymani and M. E. Ismail, "Comparing corrosion measurement methods to assess the corrosion activity of laboratory OPC and HPC concrete specimens," *Cem. Concr. Res.*, vol. 34, no. 11, pp. 2037–2044, 2004.
[47] H. Song and V. Saraswathy, "Corrosion Monitoring of Reinforced Concrete Structures - A Review," *Int. J. Electrochem. Sci.*, vol. 2, pp. 1–28, 2007.
[48] D. Trejo and R. G. Pillai, "Accelerated Chloride Threshold Testing: Part I-ASTM A 615 and A 706 Reinforcement," *ACI Mater. J.*, vol. 100, no. 6, pp. 519–527, 2003.
[49] M. Pourbaix, *Atlas of Electrochemical Equilibria in Aqueous Solutions*. Houston, Texas: NACE, 1984.
[50] C. Alonso, M. Castellote, and C. Andrade, "Chloride threshold dependence of pitting potential of reinforcements," *Electrochim. Acta*, vol. 47, no. 21, pp. 3469–3481, 2002.
[51] D. Izquierdo, C. Alonso, C. Andrade, and M. Castellote, "Potentiostatic determination of chloride threshold values for rebar depassivation - Experimental and statistical study," *Electrochim. Acta*, vol. 49, no. 17–18, pp. 2731–2739, 2004.
[52] C. B. Van Niejenhuis, T. W. Bandura, and C. M. Hansson, "Evaluation of the proposed European test procedure for ranking stainless steel rebar," *Corros. Eng.*, vol. 72, no. 6, pp. 834–842, 2016.
[53] T. D. Marcotte, "Characterization of chloride-induced corrosion products that form in steel - reinforced cementitious materials," University of Waterloo, 1991.
[54] U. M. Angst *et al.*, "The steel – concrete interface," 2017.
[55] M. F. Hurley and J. R. Scully, "Threshold Chloride Concentrations of Selected Corrosion Resistant Rebar Materials Compared to Carbon Steel," *NACE Int.*, vol. 32, no. 05457, pp. 1–13, 2005.
[56] L. Bertolini, F. Bolzoni, T. Pastore, and P. Pedeferri, "Behaviour of stainless steel in simulated concrete pore solution," *Br. Corros. J.*, vol. 31, no. 3, pp. 218–222, 1996.
[57] A. Bautista, G. Blanco, and F. Velasco, "Corrosion behaviour of low-nickel austenitic stainless steels reinforcements : A comparative study in simulated pore solutions," vol. 36, pp. 1922–1930, 2006.
[58] D. Addari, B. Elsener, and A. Rossi, "Electrochemistry and surface chemistry of stainless steels in alkaline media simulating concrete pore solutions," *Electrochim. Acta*, vol. 53, no. 27, pp. 8078–8086, 2008.
[59] R. D. Granata and W. H. Hartt, "Integrity of Infrastructure Materials and Structures," Dania Beach, Florida, 2009.
[60] J. T. Pérez-Quiroz, J. Terán, M. J. Herrera, M. Martínez, and J. Genescá, "Assessment of stainless steel reinforcement for concrete structures rehabilitation," *J. Constr. Steel Res.*, vol. 64, no. 11, pp. 1317–1324, 2008.
[61] ASTM International, *ASTM A955 / A955M-18, Standard Specification for Deformed and Plain Stainless Steel Bars for Concrete Reinforcement*. West Conshohocken, PA, 2018.
[62] C. M. Hansson and B. Sørensen, "The Threshold Concentration of Chloride in Concrete for

the Initiation of Reinforcement Corrosion," in *Corrosion Rates of Steel in Concrete, ASTM STP 1065*, N. S. Berke, V. Chaker, and D. Whiting, Eds. Philadelphia: American Society for Testing and Materials, 1990, pp. 3–16.
[63] B. Sørensen, P. B. Jensen, and E. Maahn, "The Corrosion Properties of Stainless Steel Reinforcement," in *Corrosion of Reinforcement in Concrete*, 1990.
[64] C. B. Van Niejenhuis, S. Walbridge, and C. M. Hansson, "The performance of austenitic and duplex stainless steels in cracked concrete exposed to concentrated chloride brine," *J. Mater. Sci.*, vol. 51, no. 1, pp. 362–374, 2016.
[65] ASTM International, *ASTM A276/A276M - 17: Standard Specification for Stainless Steel Bars for Shapes*. West Conshohocken, PA, 2017.
[66] C. B. Van Niejenhuis, I. Ogunsanya, and C. M. Hansson, "To be Published."
[67] Ontario Provincial Standard Specification, *OPSS 1002: Material Specification for Aggregates - Concrete*. 2011, pp. 1–20.
[68] Ontario Provincial Standard Specification, *OPSS 1350: Material Specification for Concrete - Materials and Production*. 2013, pp. 1–28.
[69] Ontario Provincial Standard Specification, *OPSS 904: Construction Specification for Concrete Structures*. 2008, pp. 1–17.
[70] R. Myrdal, "Reference electrodes for concrete," in *The electrochemistry and characteristics of embeddable reference electrodes for concrete*, Cambridge: Woodhead Publishing Limited, 2007, pp. 13–24.
[71] American Iron and Steel Institute, "Cleaning an descaling stainless steels," *A Des. Handb. Ser. Des. Handb. Ser.*, vol. 9001, pp. 1–38, 1982.
[72] ASTM International, *ASTM C31/C31M-18: Standard Practice for Making and Curing Concrete Test Specimens in the Field*. West Conshohocken, PA, 2018.
[73] ASTM International, *ASTM C39/C39M-18: Standard Test Method for Compressive Strength of Cylindrical Concrete Specimens*. West Conshohocken, PA, 2018.
[74] D. W. Hosmer and S. Lemeshow, *Applied Logistic Regression*. Canada: John Wiley & Sons, 1989.
[75] D. E. Farrar and R. R. Glauber, "Multicollinearity in Regression Analysis : The Problem Revisited," *Rev. Econ. Stat.*, vol. 49, no. 1, pp. 92–107, 1967.
[76] K. P. Burnham and D. R. Anderson, *Model Selection and Inference: A Partical Information-Theoretic Approach*. New York: Springer-Verlag New York Inc., 1998.
[77] Y. Sakamoto, M. Ishiguro, and G. Kitagawa, *Akaike Information Criterion Statistics*. Tokyo, Japan: KTK Scientific Publishers, 1986.
[78] N. Sugiura, "Further analysts of the data by akaike' s information criterion and the finite corrections," *Commun. Stat. - Theory Methods*, vol. 7, no. 1, pp. 13–26, 1978.
[79] N. J. D. Nagelkerke, "A Note on a General Definition of the Coefficient of Determination," *Biometrika*, vol. 78, no. 3, pp. 691–692, 1991.
[80] T. Fawcett, "An introduction to ROC analysis," *Pattern Recognit. Lett.*, vol. 27, no. 8, pp. 861–874, 2006.
[81] P. Martínez-Camblor, C. Carleos, and N. Corral, "Powerful nonparametric statistics to compare k independent ROC curves," *J. Appl. Stat.*, vol. 38, no. 7, pp. 1317–1332, 2011.
[82] S. S. Wyer, *Digest of publications of Bureau of Standards on electrolysis of underground structures caused by the disintegrating action of stray electric currents from electric railways*. Washington: National Bureau of Standards, 1918.
[83] I. Ogunsanya, "To be Published."

[84] P. Marcus, V. Maurice, and H. H. Strehblow, “Localized corrosion (pitting): A model of passivity breakdown including the role of the oxide layer nanostructure,” *Corros. Sci.*, vol. 50, no. 9, pp. 2698–2704, 2008.

Appendix A

Open Circuit Potential and Corrosion Current Density Plots by Batch

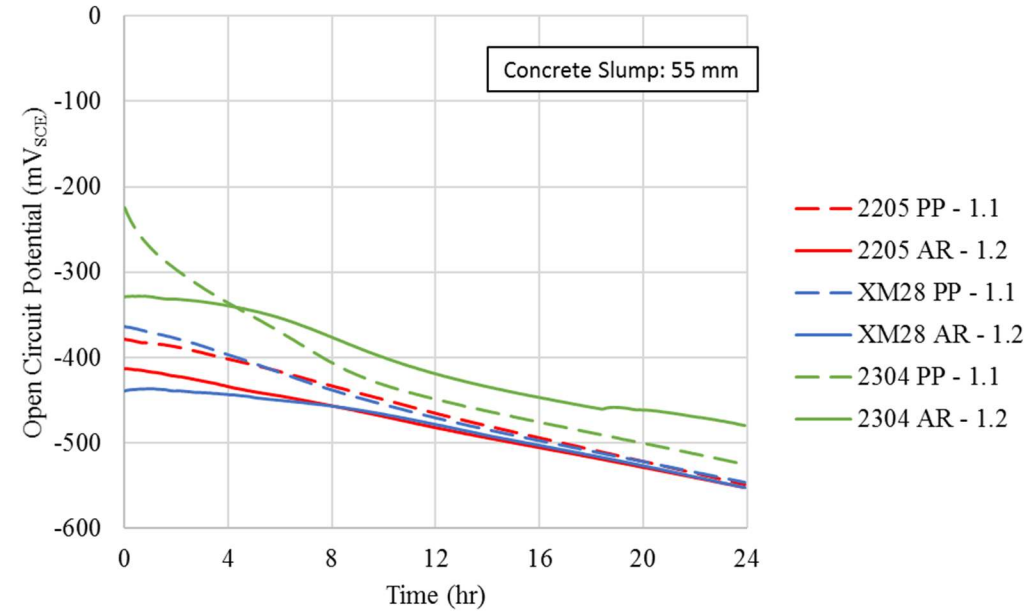

Figure A.1: -100 Batch Open Circuit Potential over 24 hours – Week of April 25, 2017

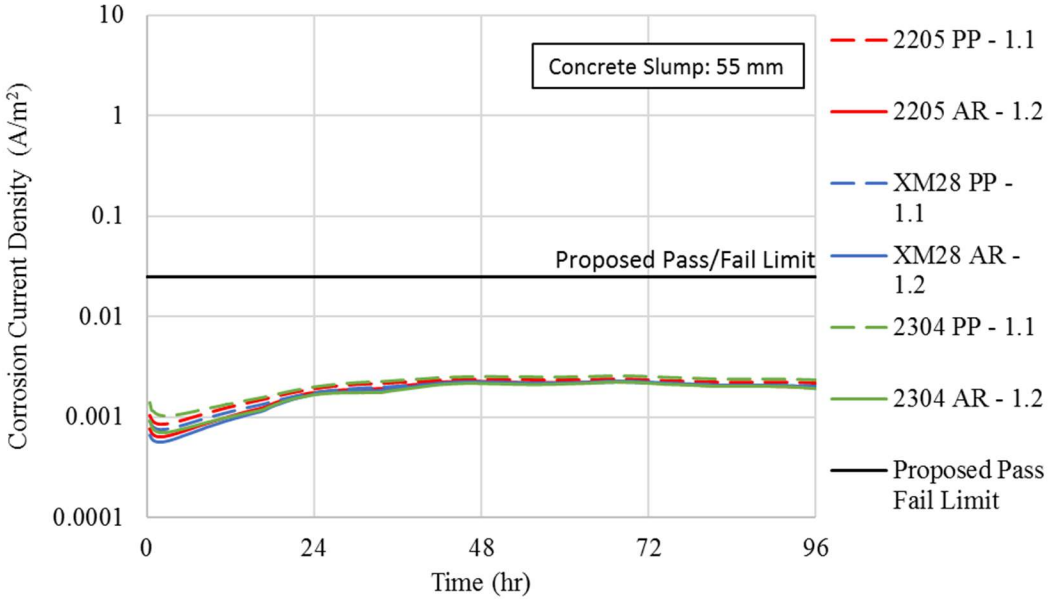

Figure A.2: -4-100 Batch Corrosion Current Densities over 96 hours – Week of April 25, 2017

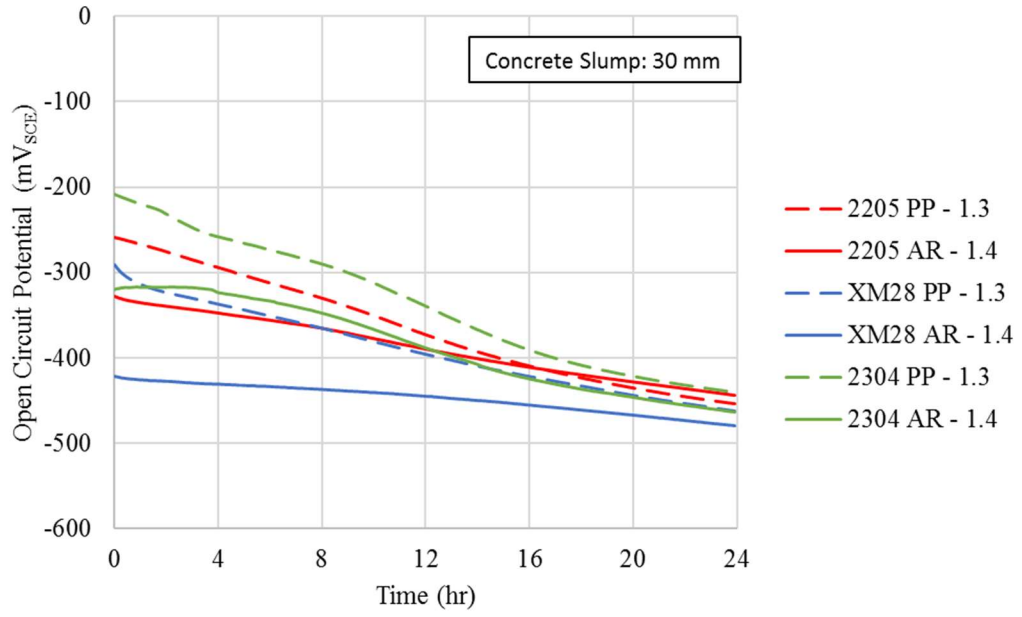

Figure A.3: -4-100 Batch Open Circuit Potential over 24 hours – Week of May 4, 2017

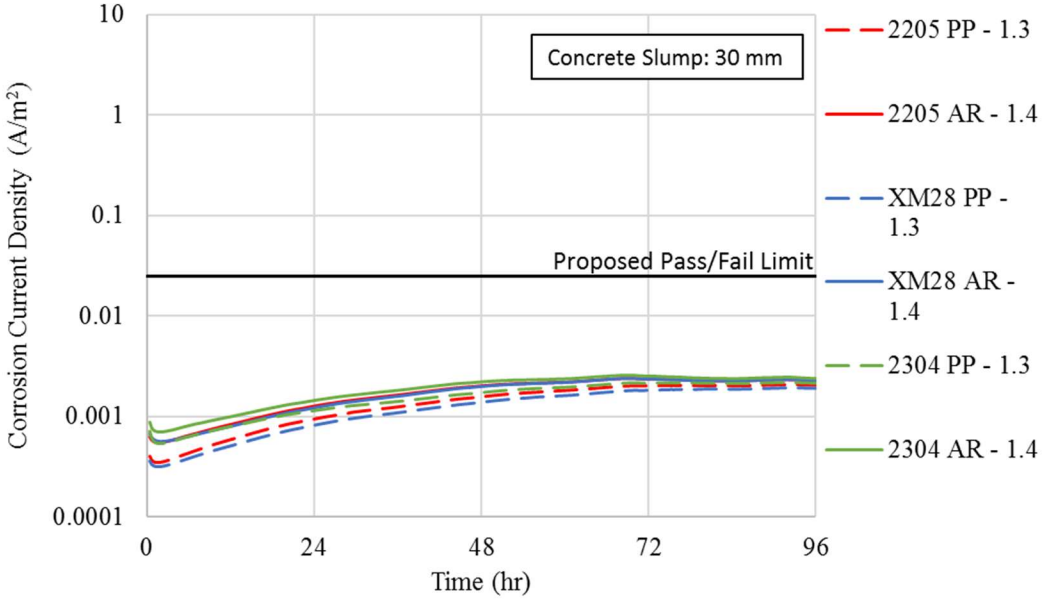

Figure A.4: 4-100 Batch Corrosion Current Densities over 96 hours – Week of May 4, 2017

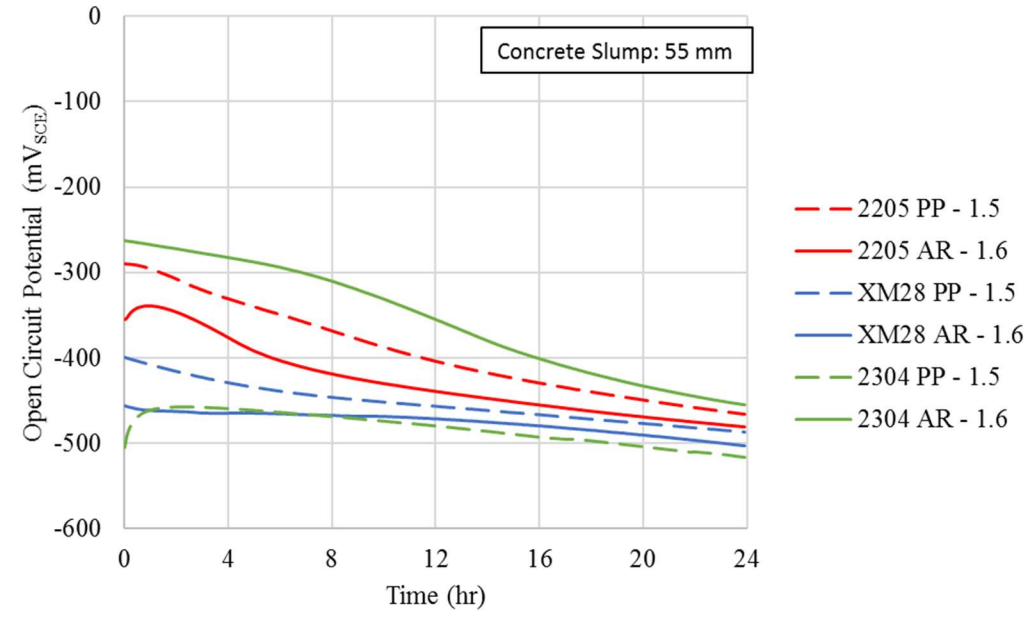

Figure A.5: 4-100 Batch Open Circuit Potential over 24 hours – Week of May 9, 2017

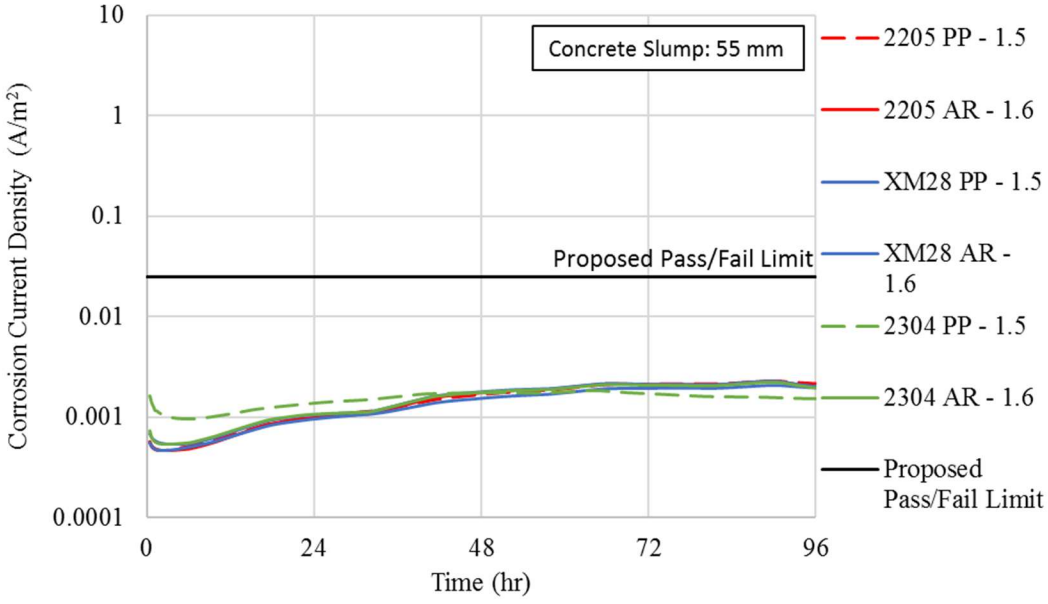

Figure A.6: 4-100 Batch Corrosion Current Densities over 96 hours – Week of May 9, 2017

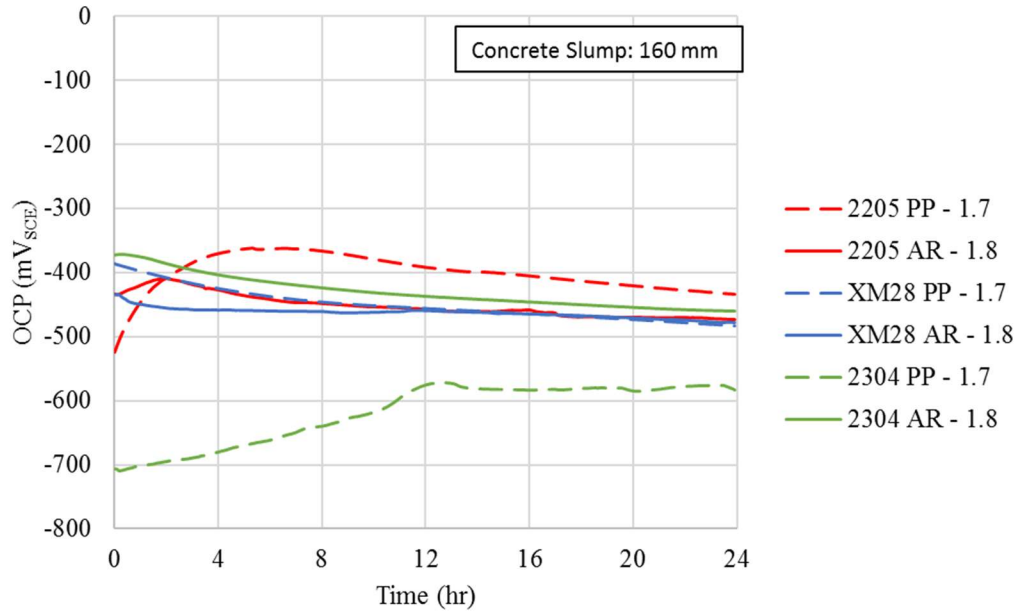

Figure A.7: 4-100 Batch Open Circuit Potential over 24 hours – Week of May 17, 2017

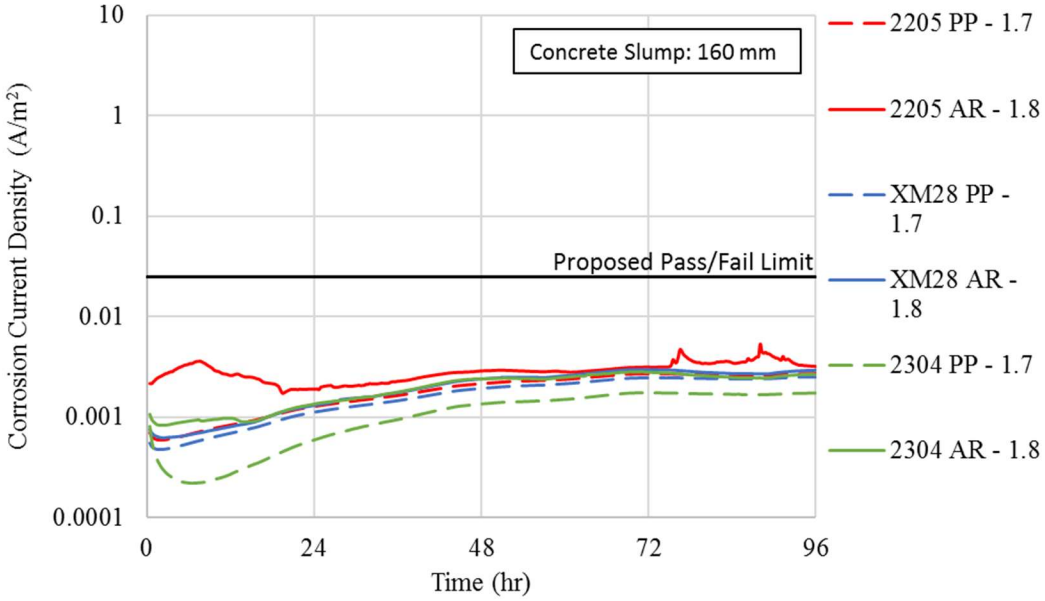

Figure A.8: 4-100 Batch Corrosion Current Densities over 96 hours – Week of May 17, 2017

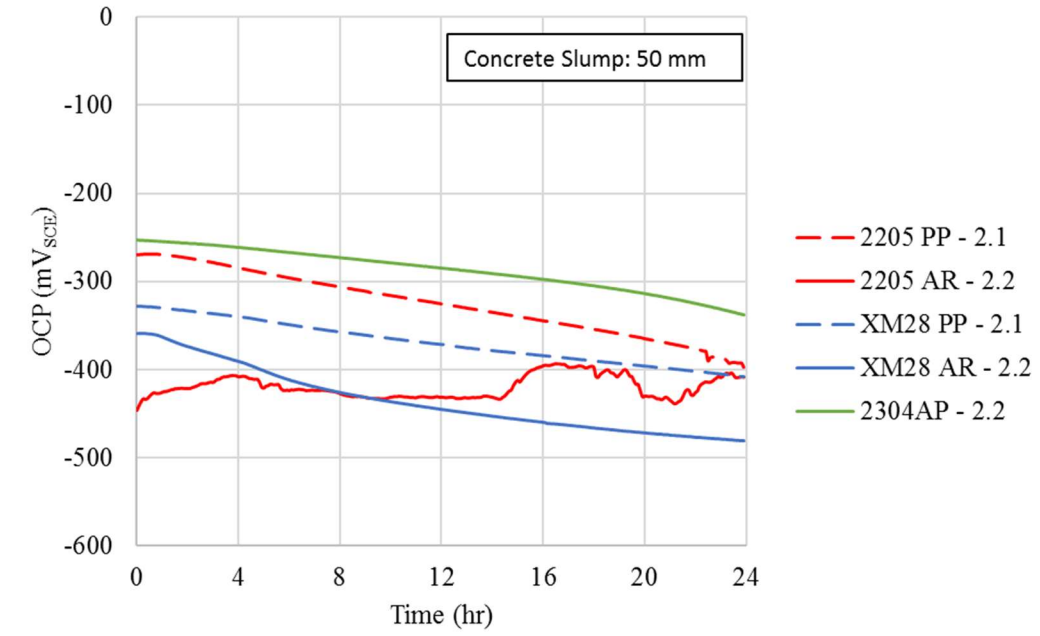

Figure A.9: 4-100 Batch Open Circuit Potential over 24 hours – Week of May 31, 2017

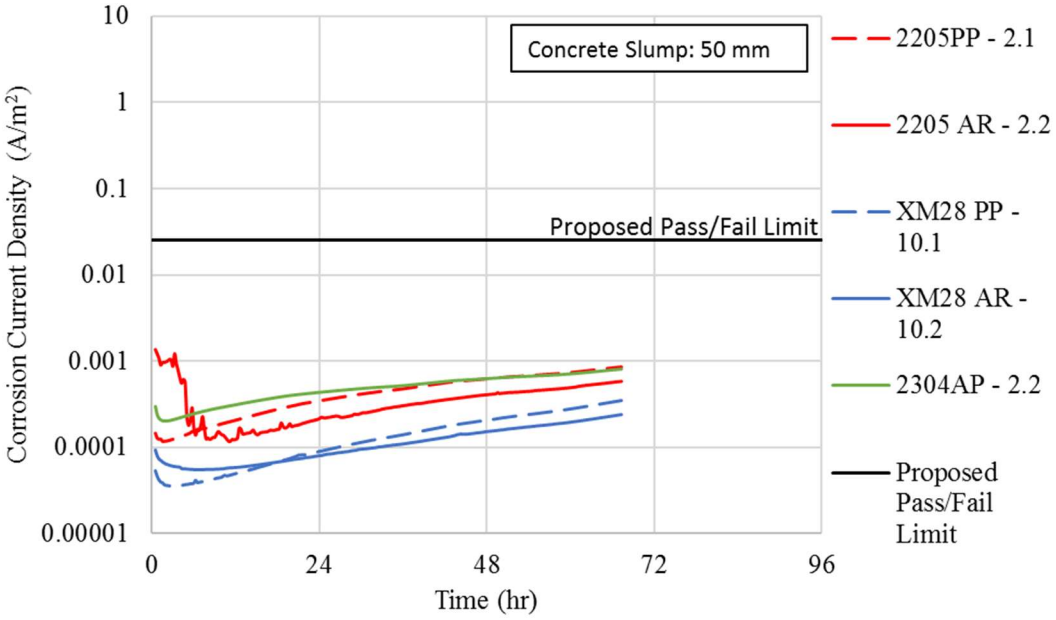

Figure A.10: 4-100 Batch Corrosion Current Densities over 96 hours – Week of May 31, 2017

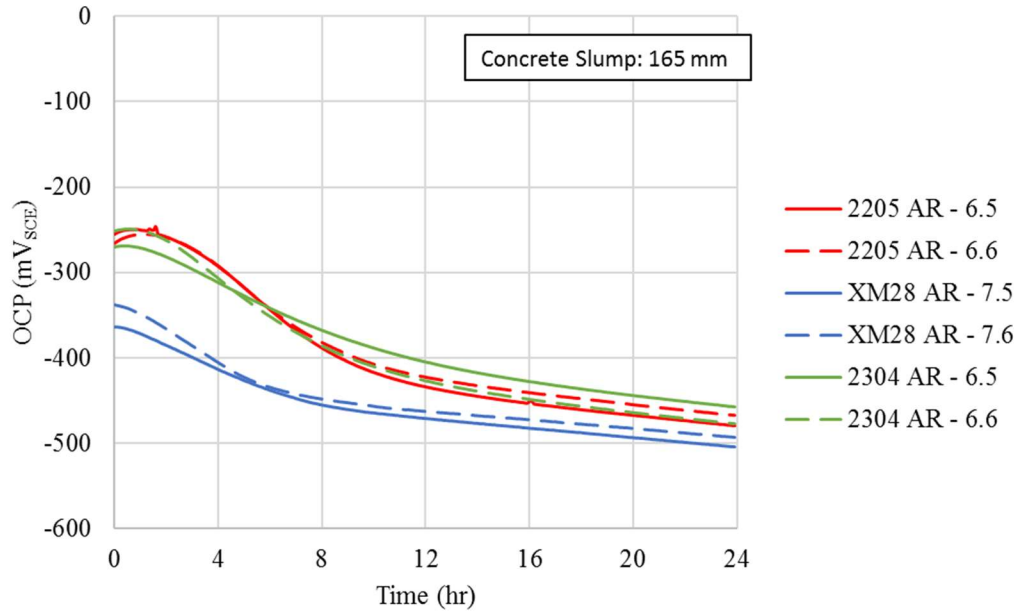

Figure A.11: 4-400 Batch Open Circuit Potential over 24 hours – Week of November 21, 2017

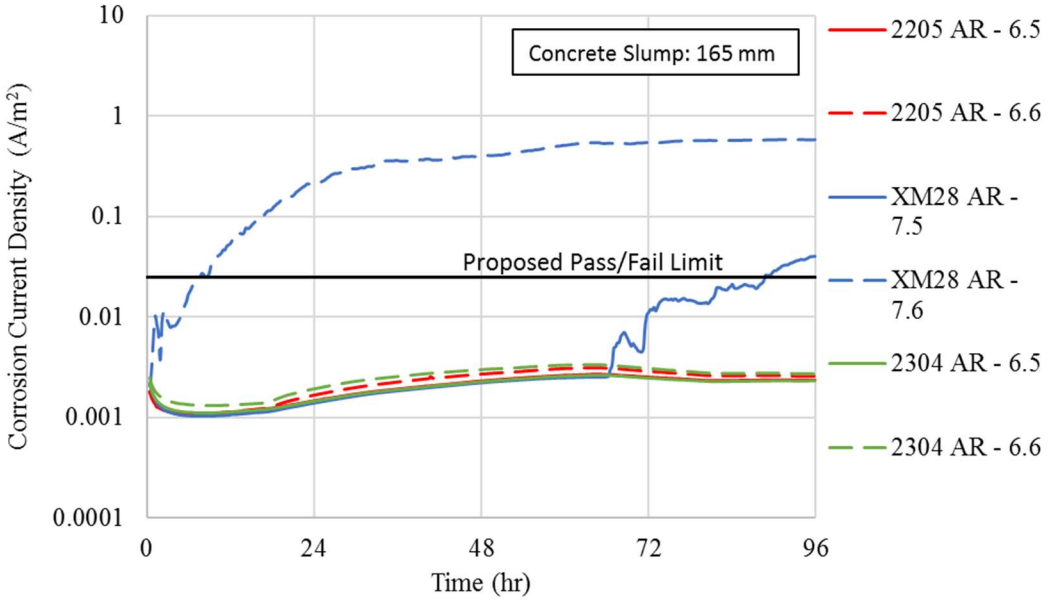

Figure A.12: 4-400 Batch Corrosion Current Densities over 96 hours – Week of November 21, 2017

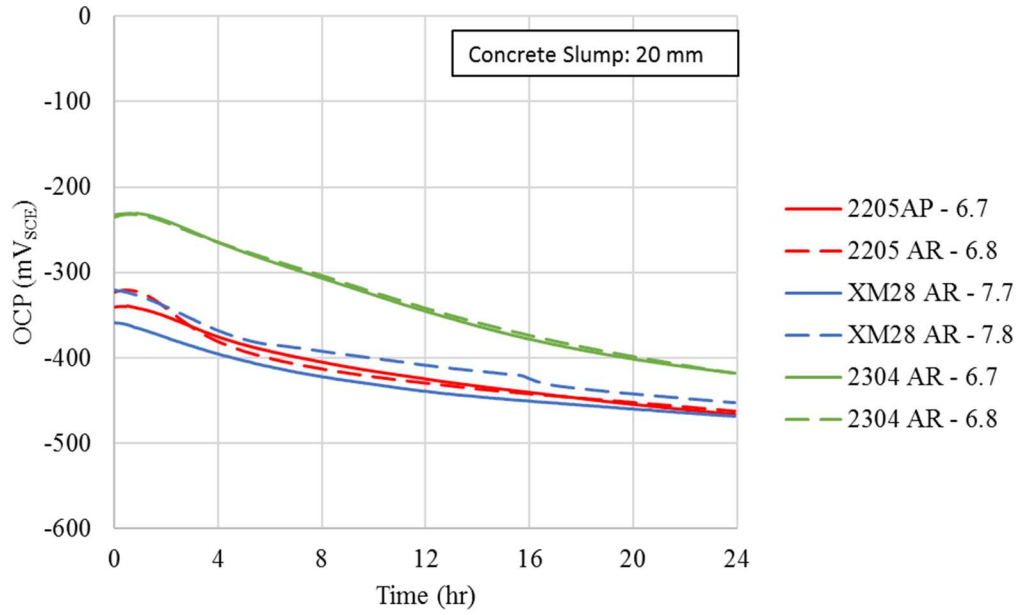

Figure A.13: 4-400 Batch Open Circuit Potential over 24 hours – Week of December 5, 2017

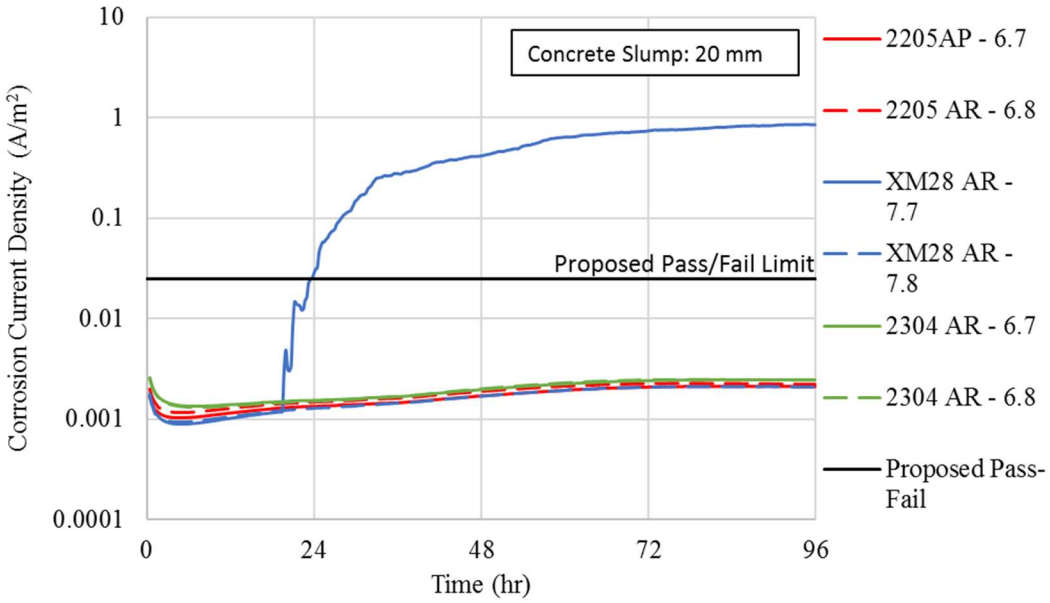

Figure A.14: 4-400 Batch Corrosion Current Densities over 96 hours – Week of December 5, 2017

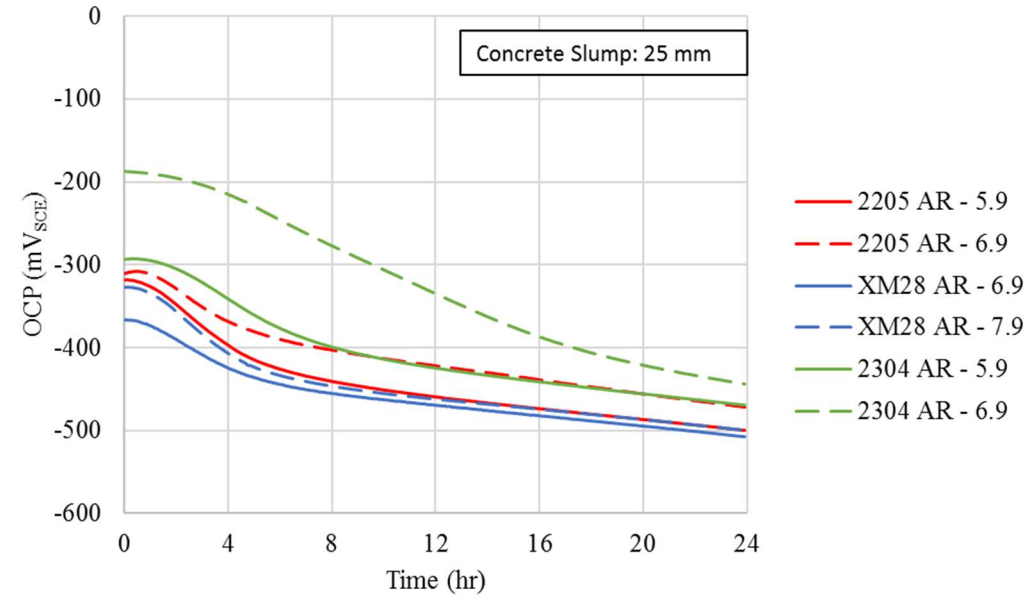

Figure A.15: 4-400 Batch Open Circuit Potential over 24 hours – Week of December 12, 2017

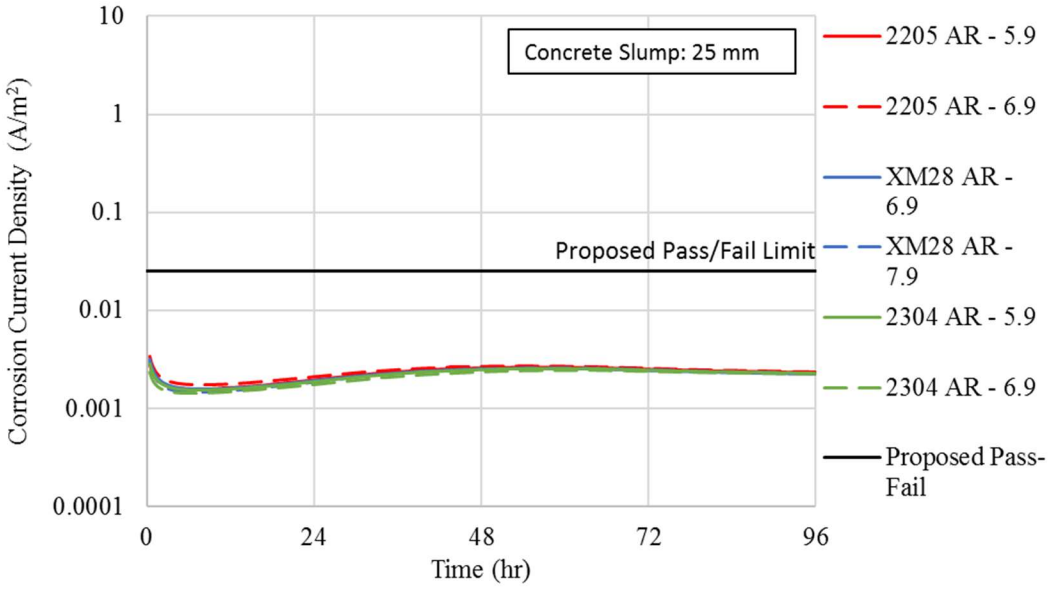

Figure A.16: 4-400 Batch Corrosion Current Densities over 96 hours – Week of December 12, 2017

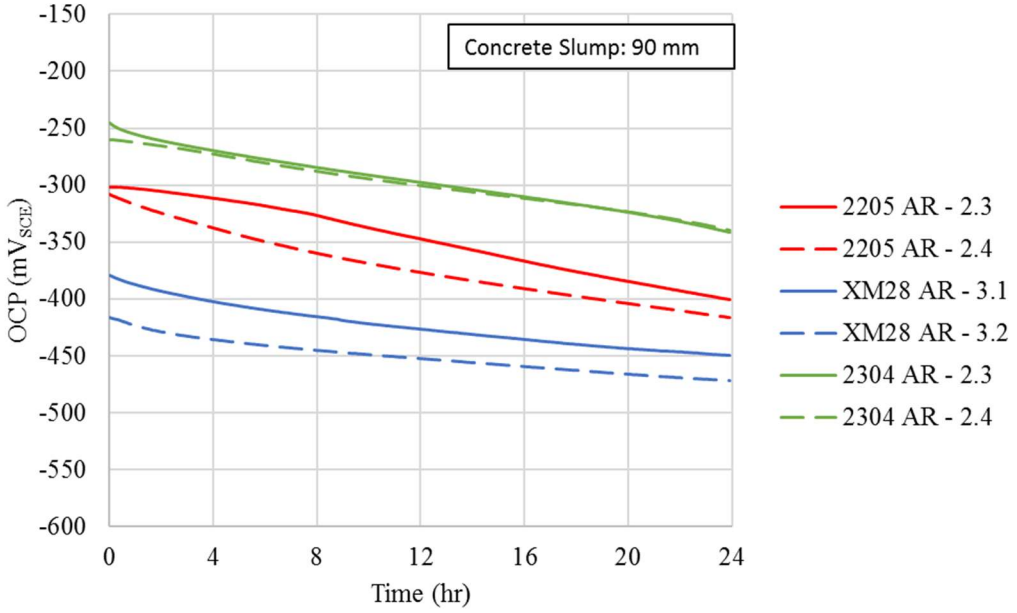

Figure A.17: 6-100 Batch Open Circuit Potential over 24 hours – Week of June 7, 2017

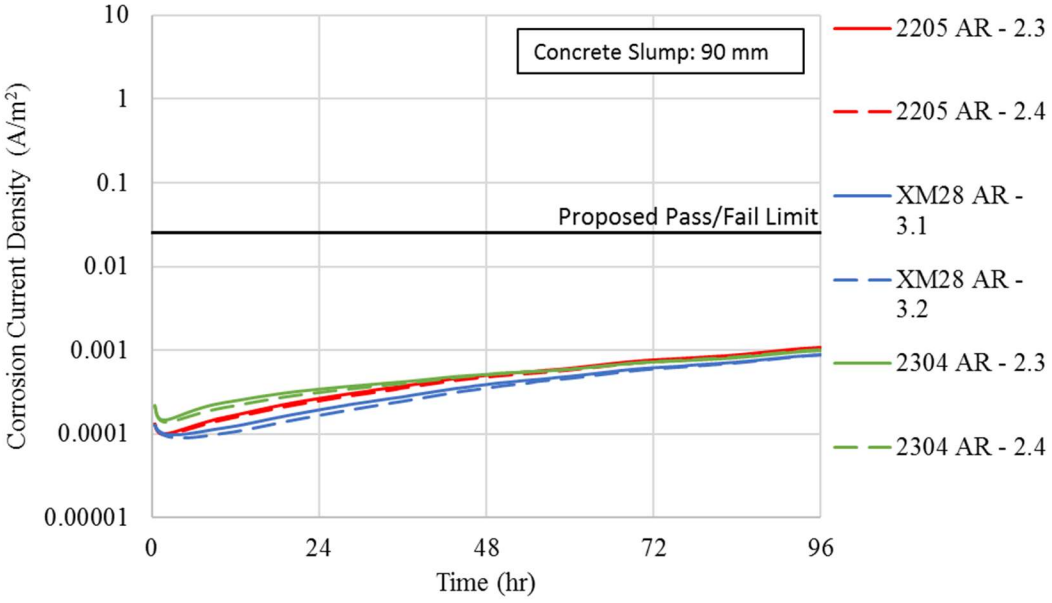

Figure A.18: 6-100 Batch Corrosion Current Densities over 96 hours – Week of June 7, 2017

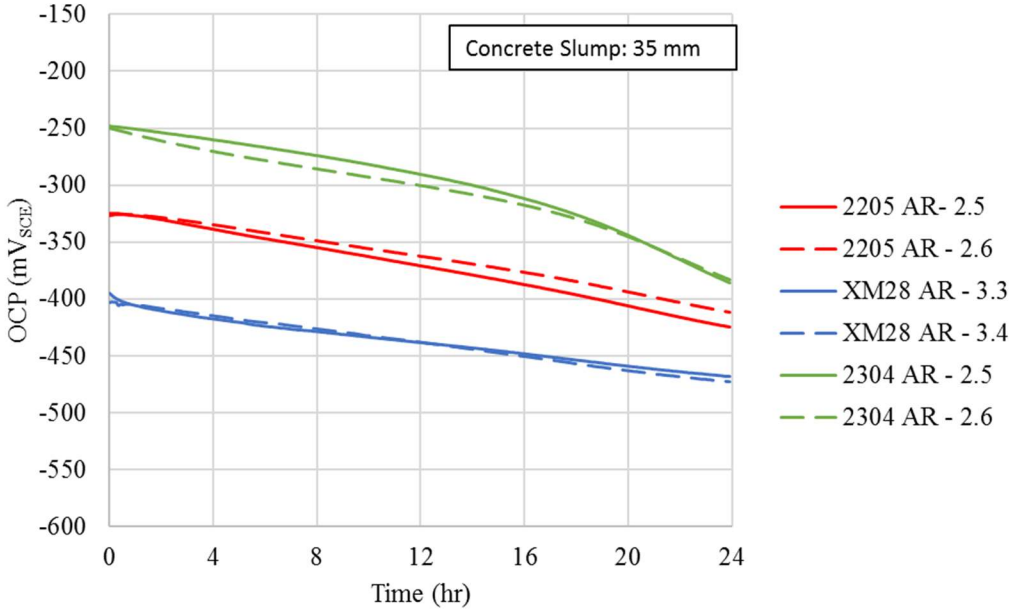

Figure A.19: 6-100 Batch Open Circuit Potential over 24 hours – Week of June 13, 2017

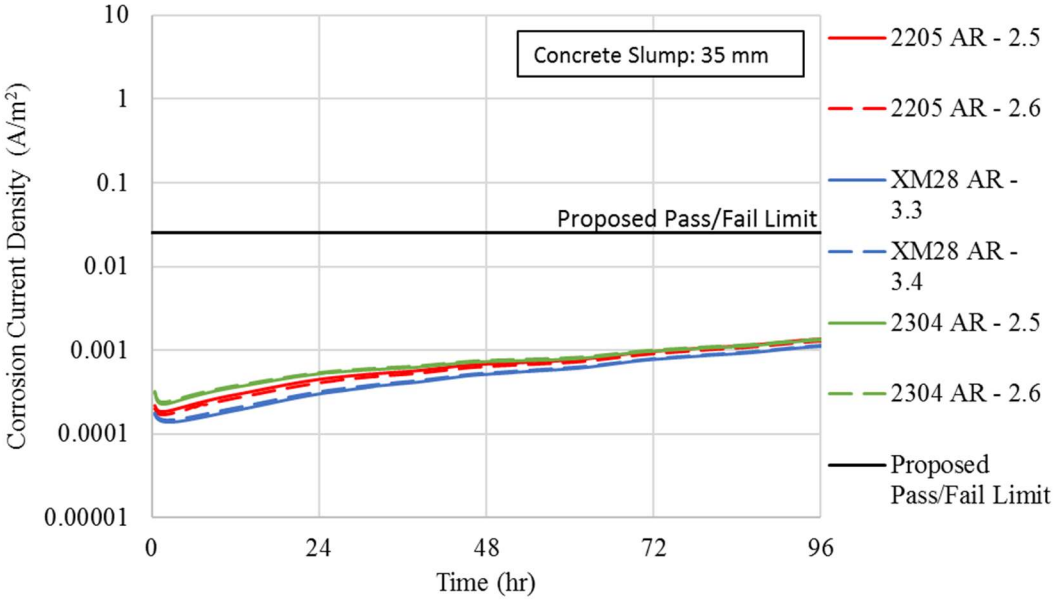

Figure A.20: 6-100 Batch Corrosion Current Densities over 96 hours – Week of June 13, 2017

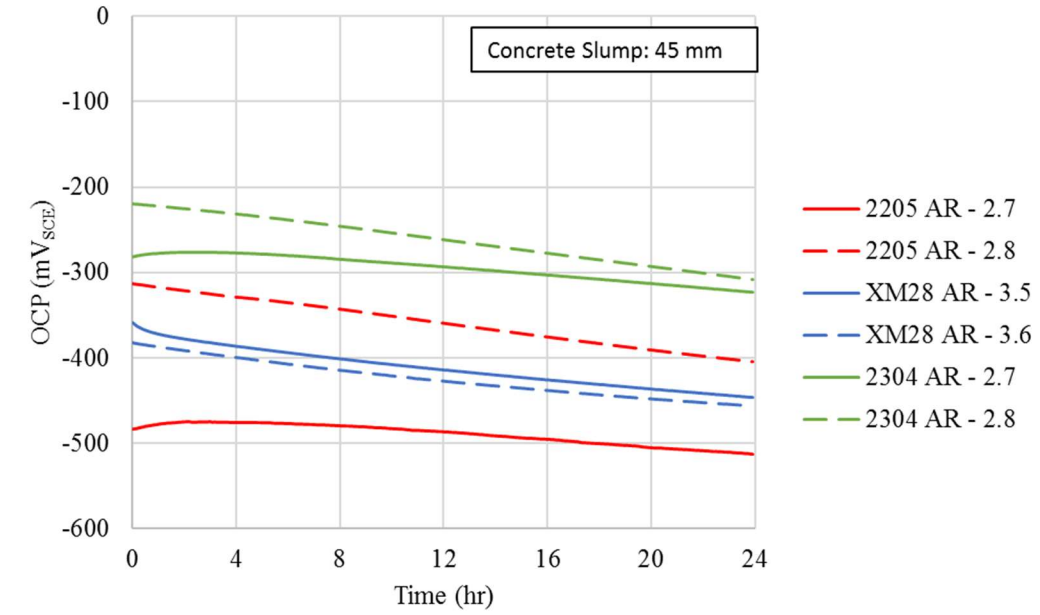

Figure A.21: 6-100 Batch Open Circuit Potential over 24 hours – Week of June 20, 2017

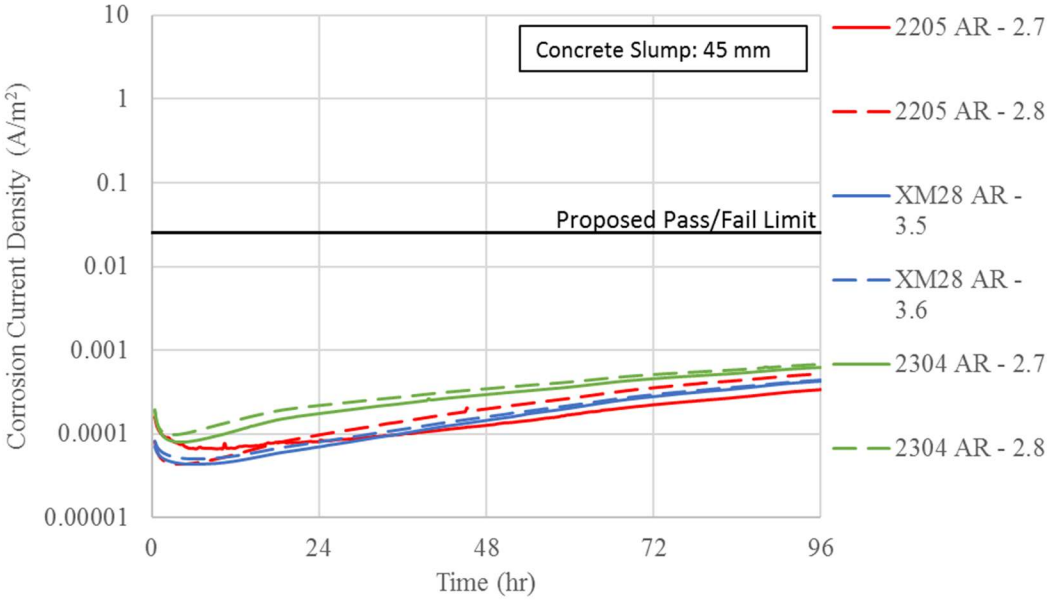

Figure A.22: 6-100 Batch Corrosion Current Densities over 96 hours – Week of June 20, 2017

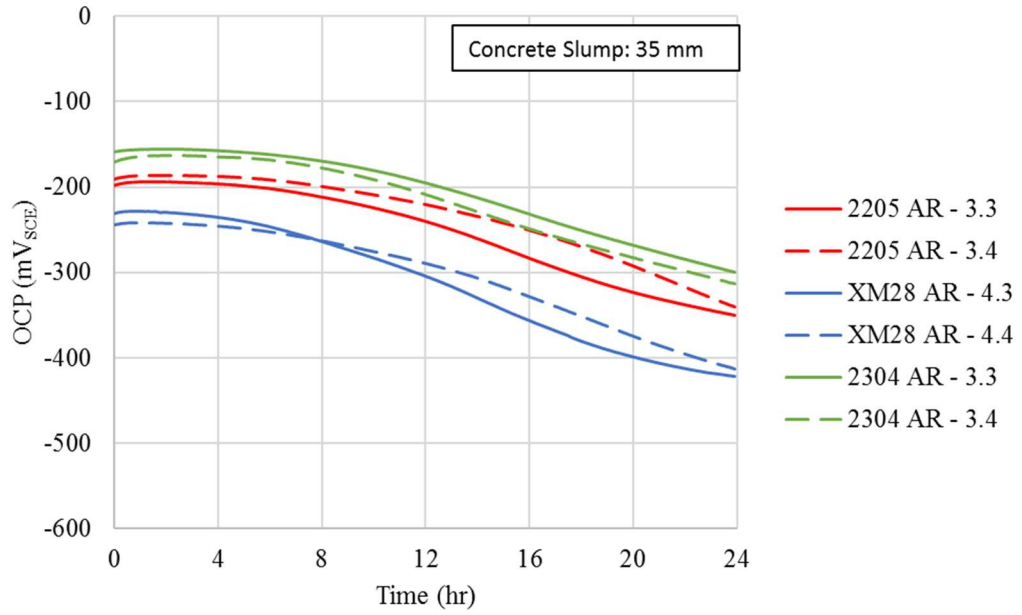

Figure A.23: 6-200 Batch Open Circuit Potential over 24 hours – Week of August 2, 2017

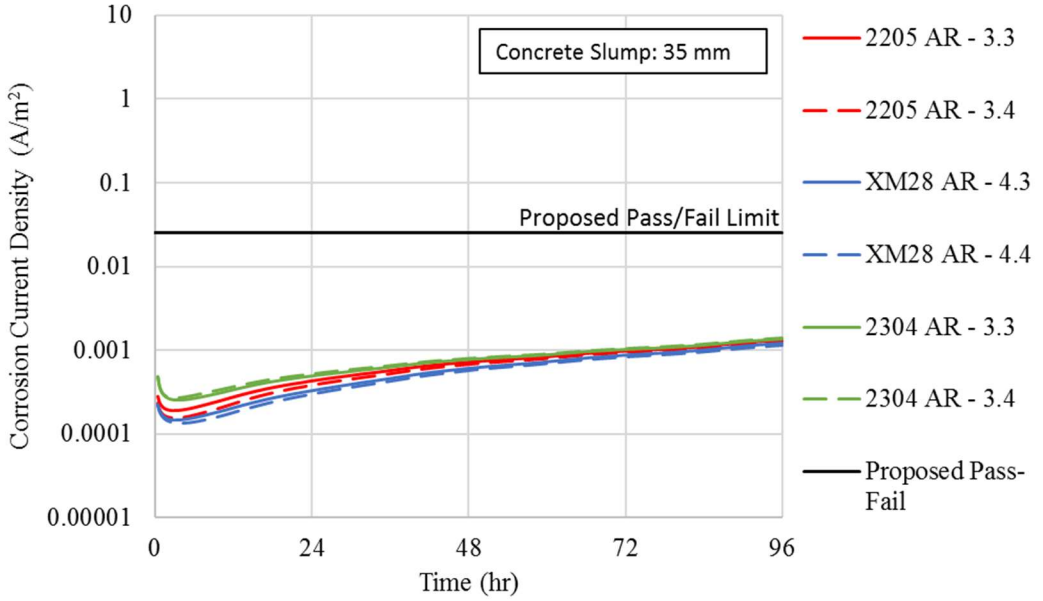

Figure A.24: 6-200 Batch Corrosion Current Densities over 96 hours – Week of August 2, 2017

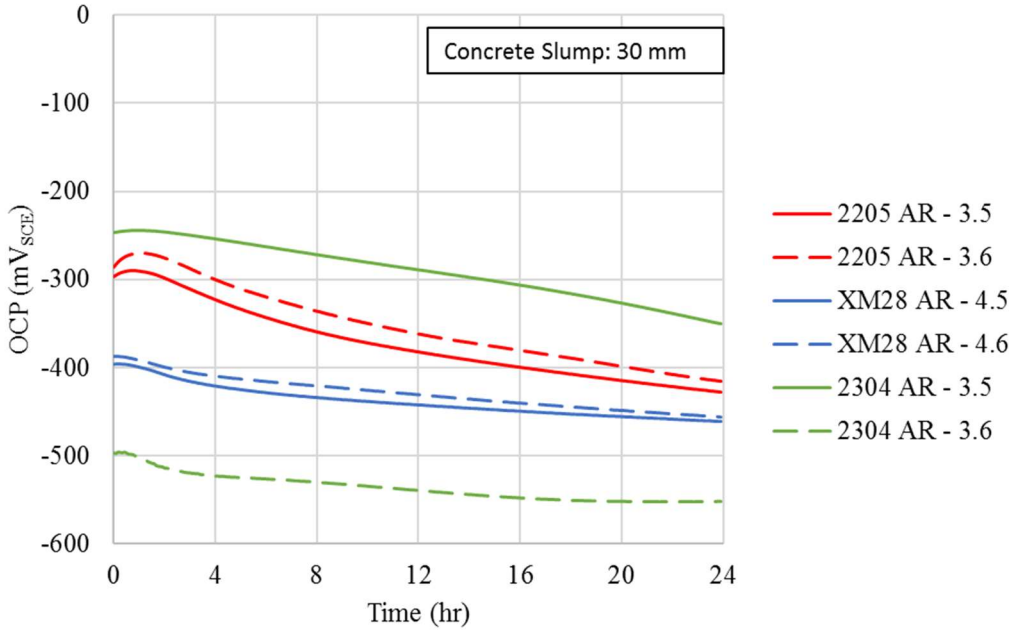

Figure A.25: 6 -200 Batch Specimens Cured in Humidity Room- Open Circuit Potentials over 24 hours – Week of August 9, 2017

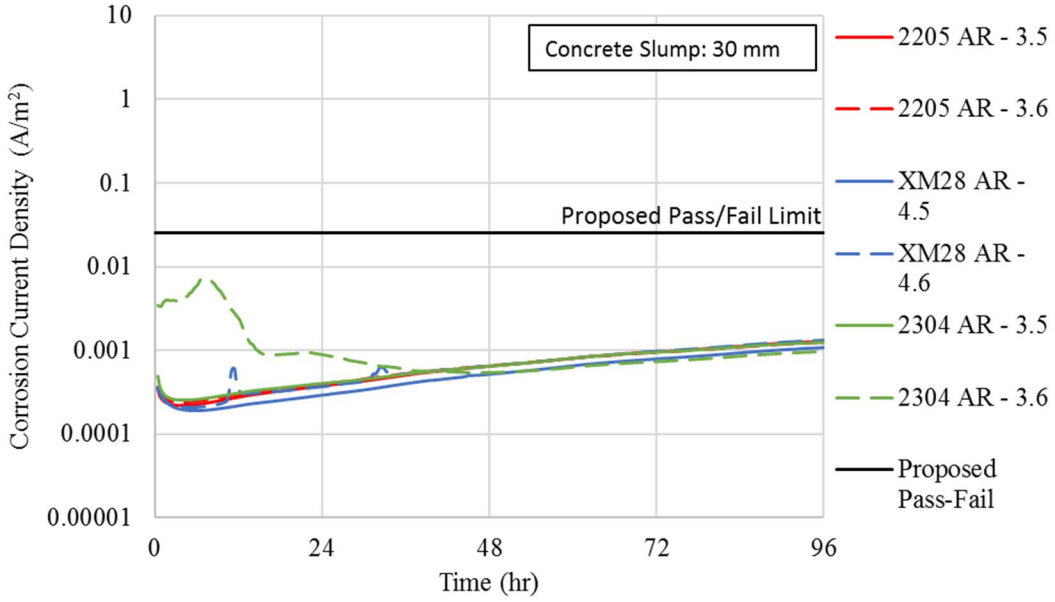

Figure A.26: 6 -200 Batch Specimens Cured in Humidity Room Corrosion Current Densities over 96 hours – Week of August 9, 2017

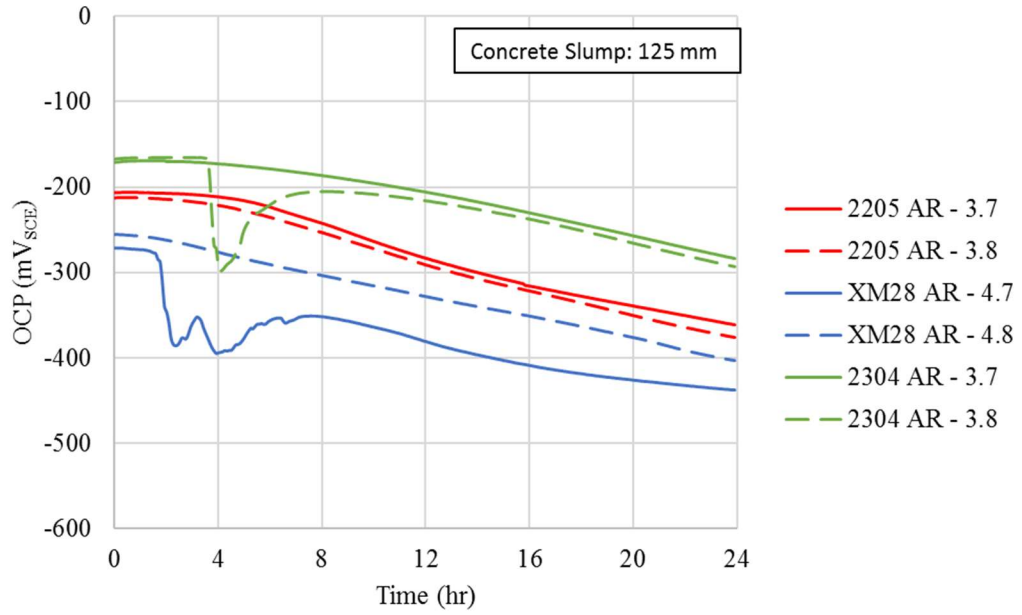

Figure A.27: 6-200 Batch Open Circuit Potentials over 24 hours – Week of August 29, 2017

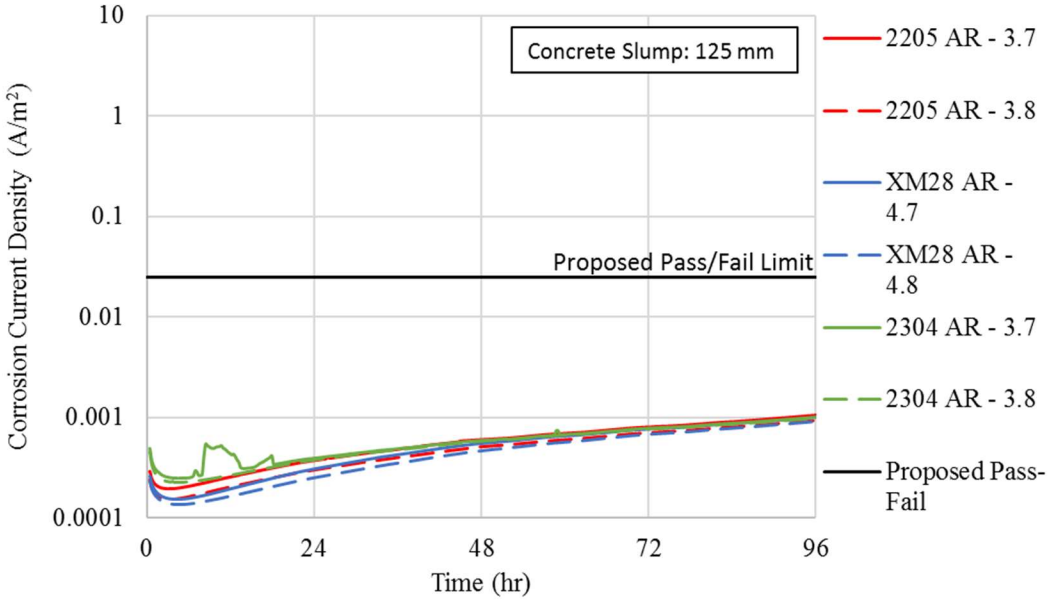

Figure A.28: 6-200 Batch Corrosion Current Densities over 96 hours – Week of August 29, 2017

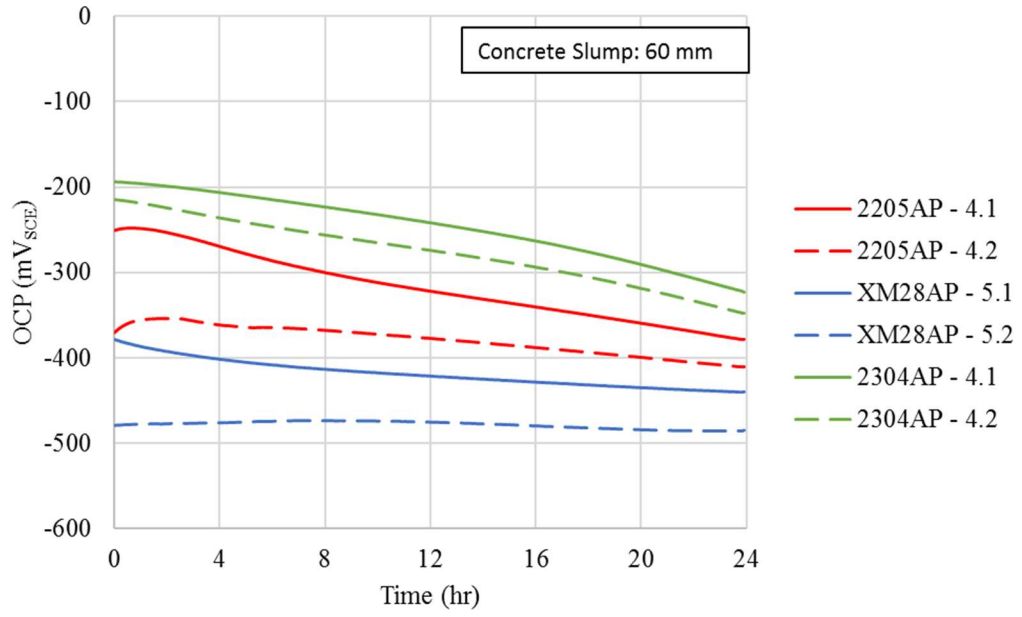

Figure A.29: 6-200 Batch Open Circuit Potentials over 24 hours – Week of September 5, 2017

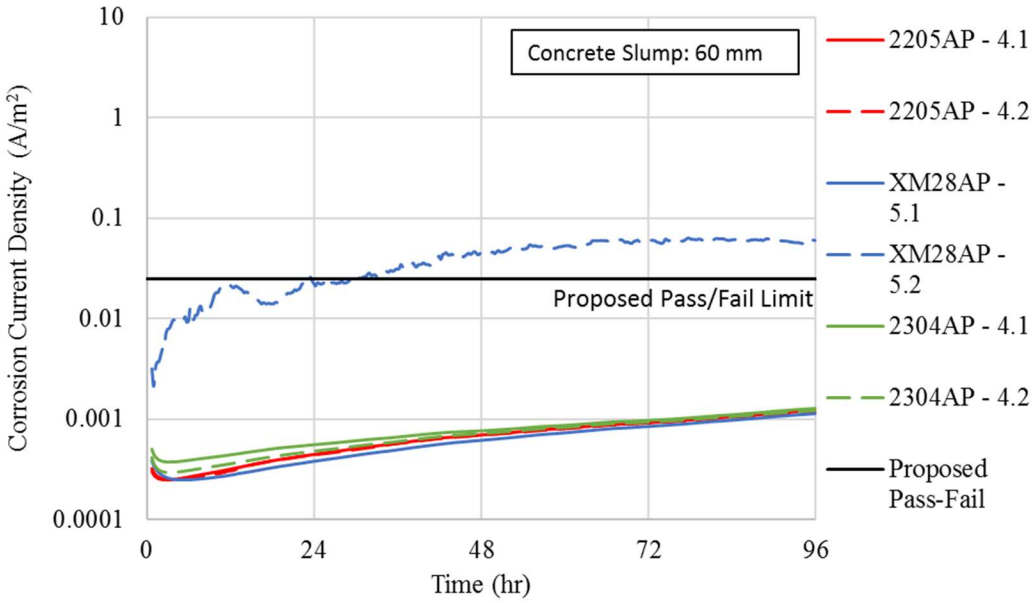

Figure A.30: 6-200 Batch Corrosion Current Densities over 96 hours – Week of September 5, 2017

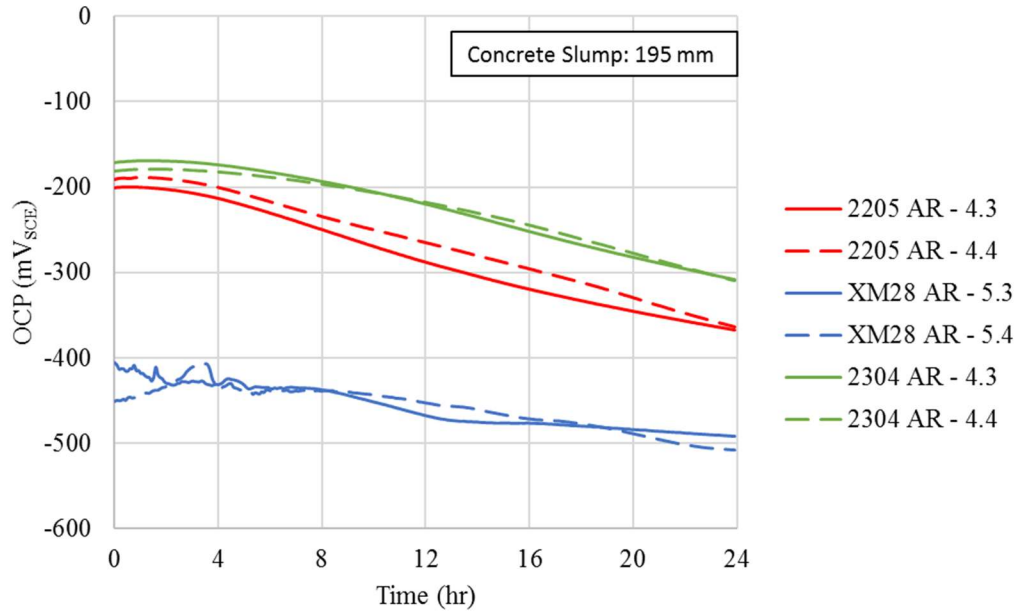

Figure A.31: 6-300 Batch Open Circuit Potentials over 24 hours – Week of September 12, 2017

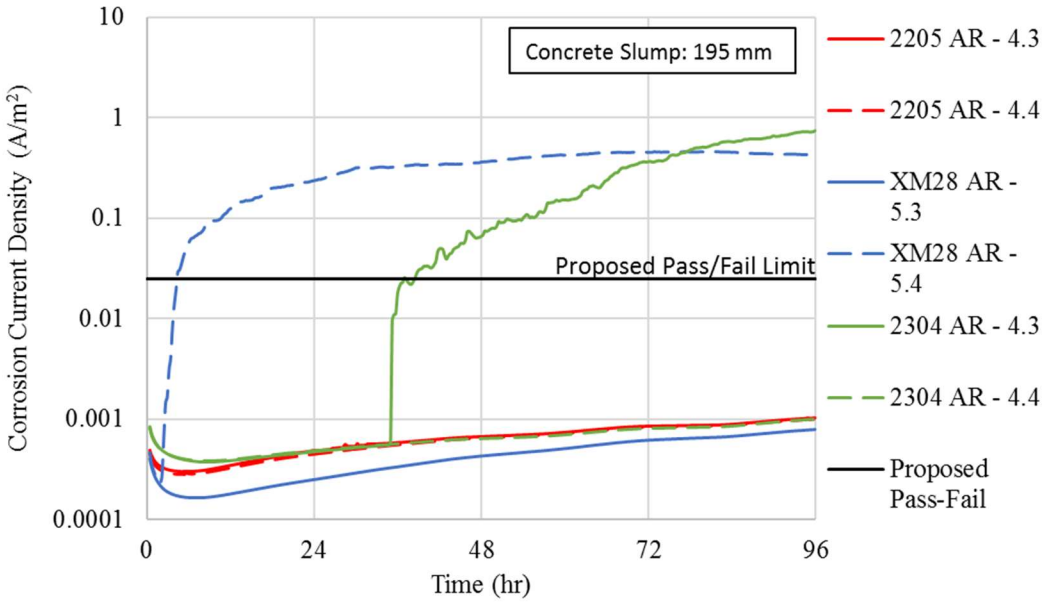

Figure A.32: 6-300 Batch Corrosion Current Densities over 96 hours – Week of September 12, 2017

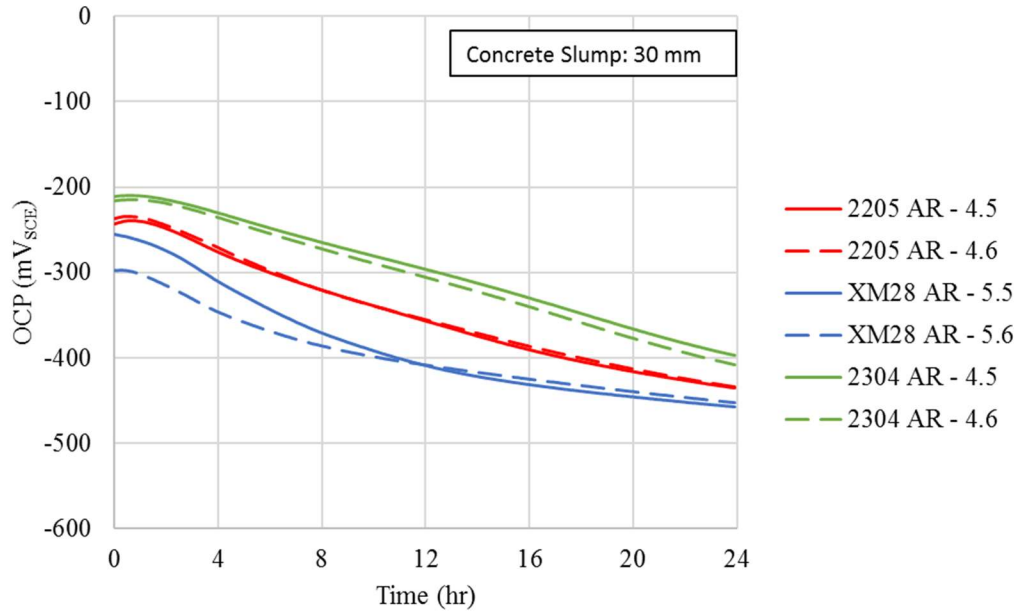

Figure A.33: 6-300 Batch Open Circuit Potentials over 24 hours – Week of September 19, 2017

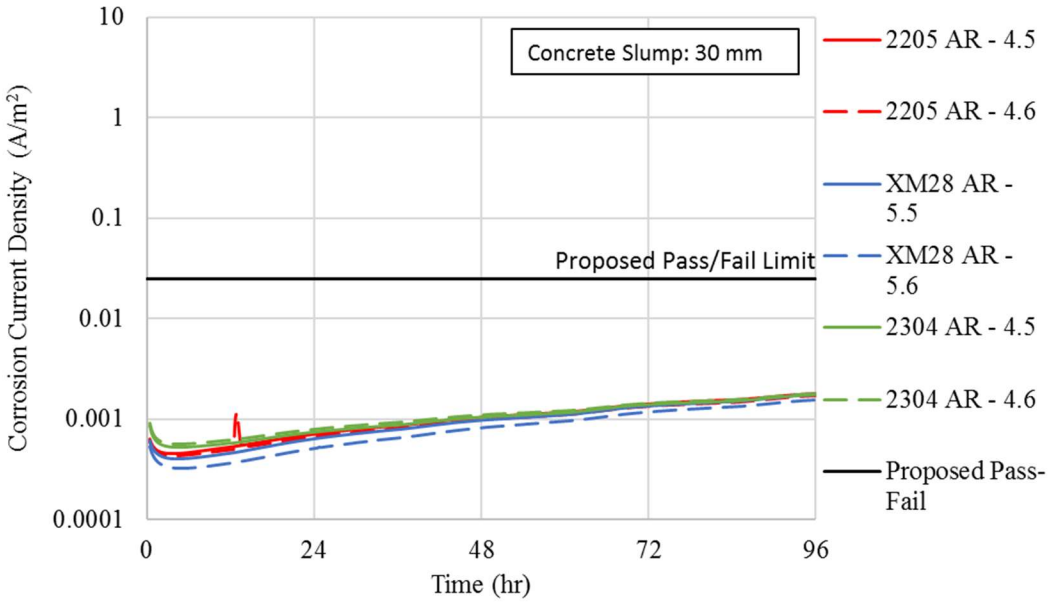

Figure A.34: 6-300 Batch Corrosion Current Densities over 96 hours – Week of September 19, 2017

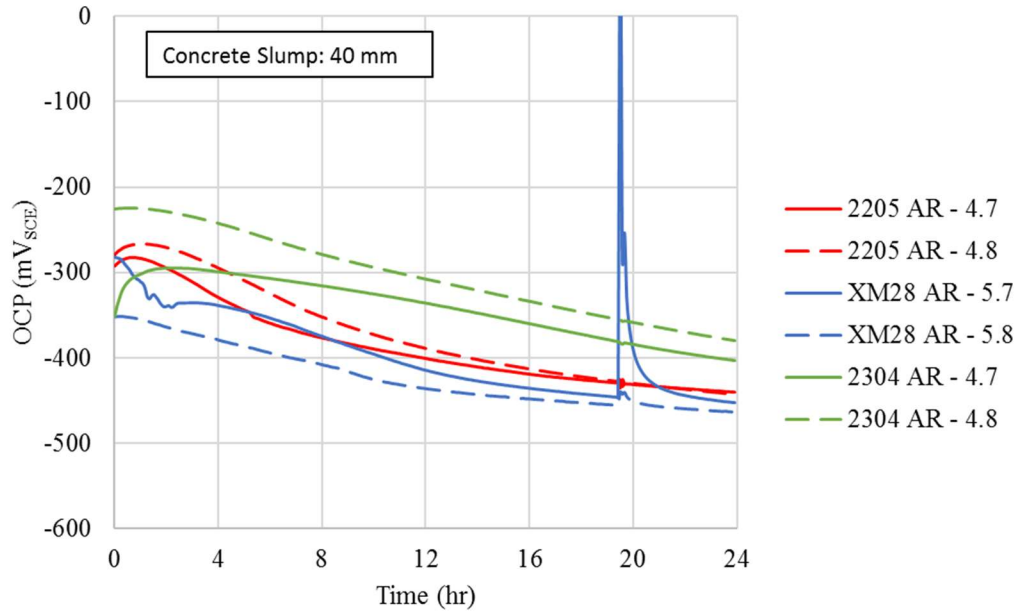

Figure A.35: 6-300 Batch Open Circuit Potentials over 24 hours – Week of September 26, 2017

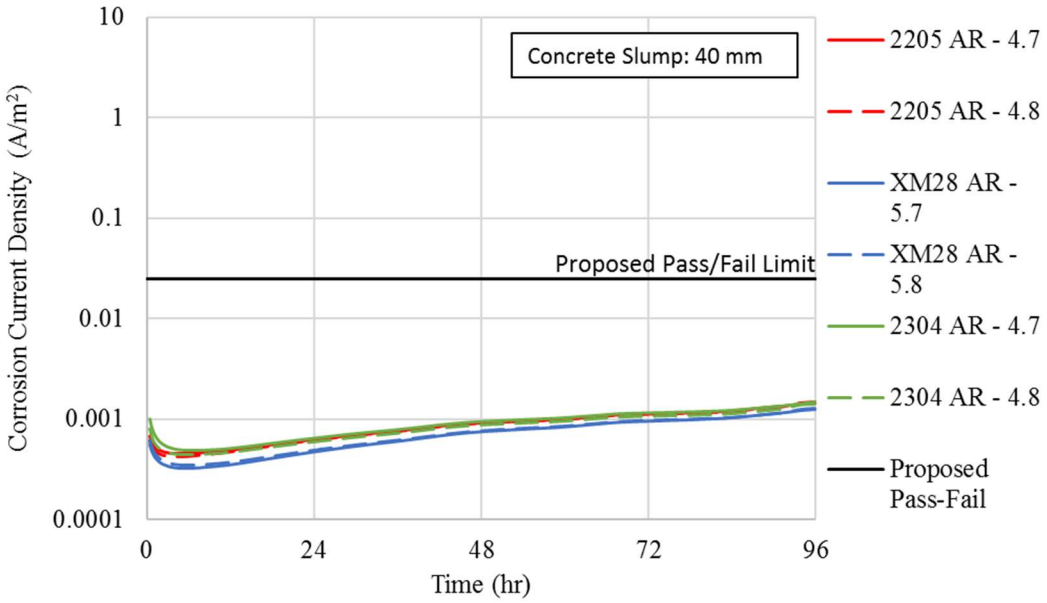

Figure A.36: 6-300 Batch Corrosion Current Densities over 96 hours – Week of September 26, 2017

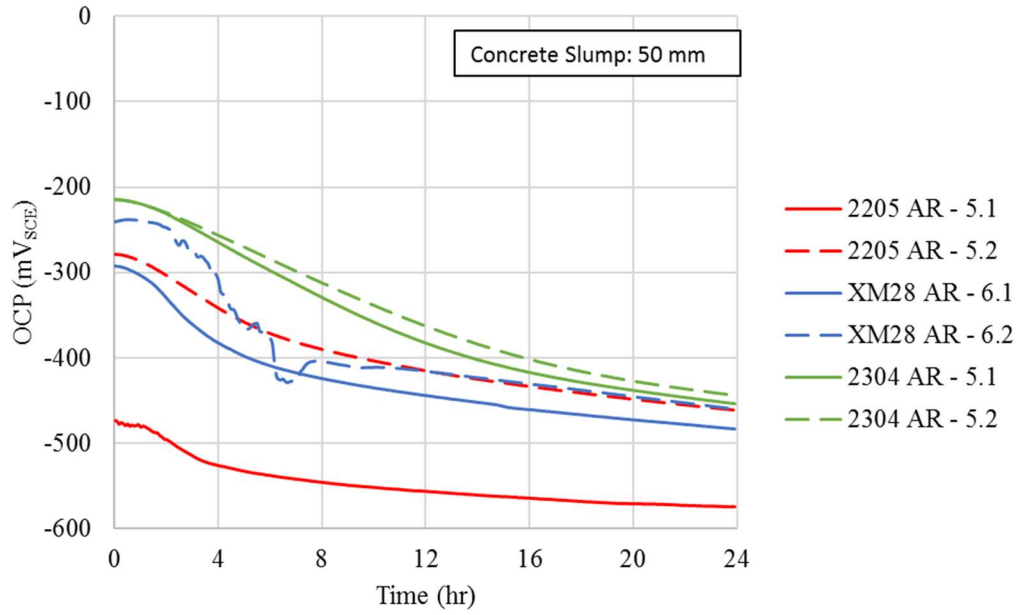

Figure A.37: 6-400 Batch Open Circuit Potentials over 24 hours – Week of October 10, 2017

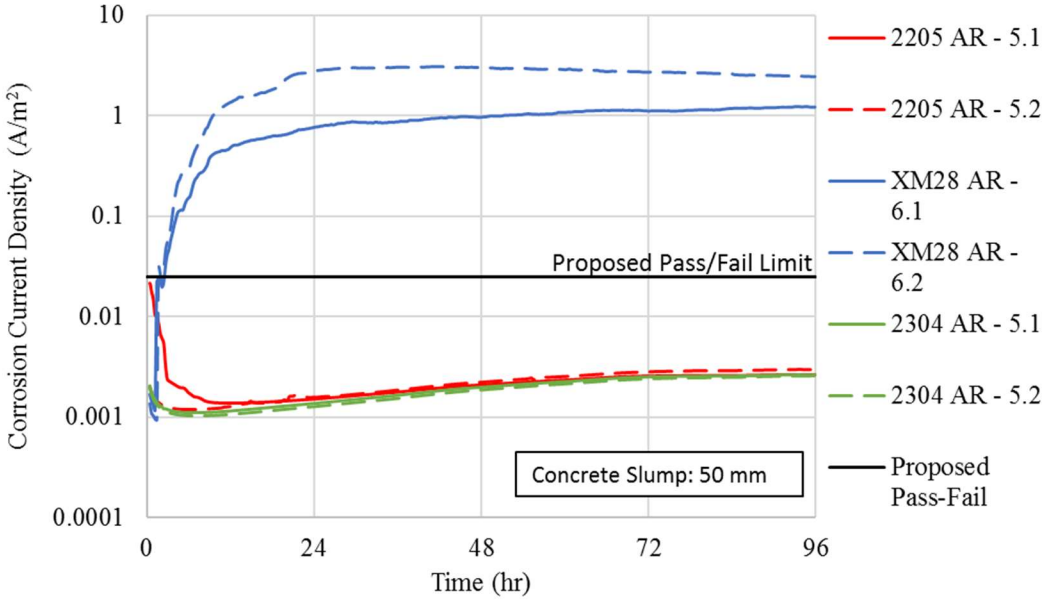

Figure A.38: 6-400 Batch Corrosion Current Densities over 96 hours – Week of October 10, 2017

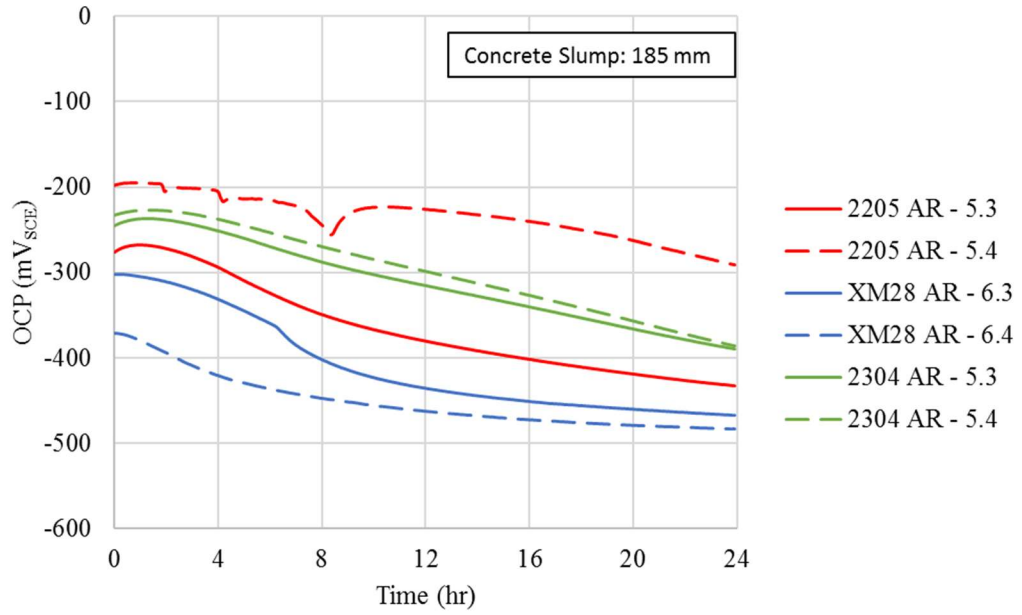

Figure A.39: 6-400 Batch Open Circuit Potentials over 24 hours – Week of October 17, 2017

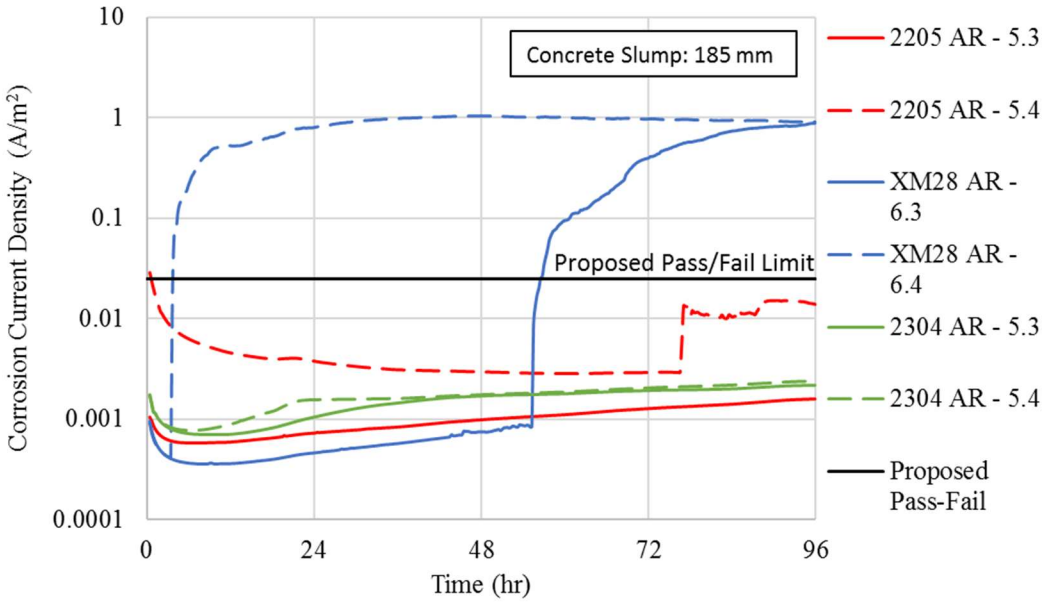

Figure A.40: 6-400 Batch Corrosion Current Densities over 96 hours – Week of October 17, 2017

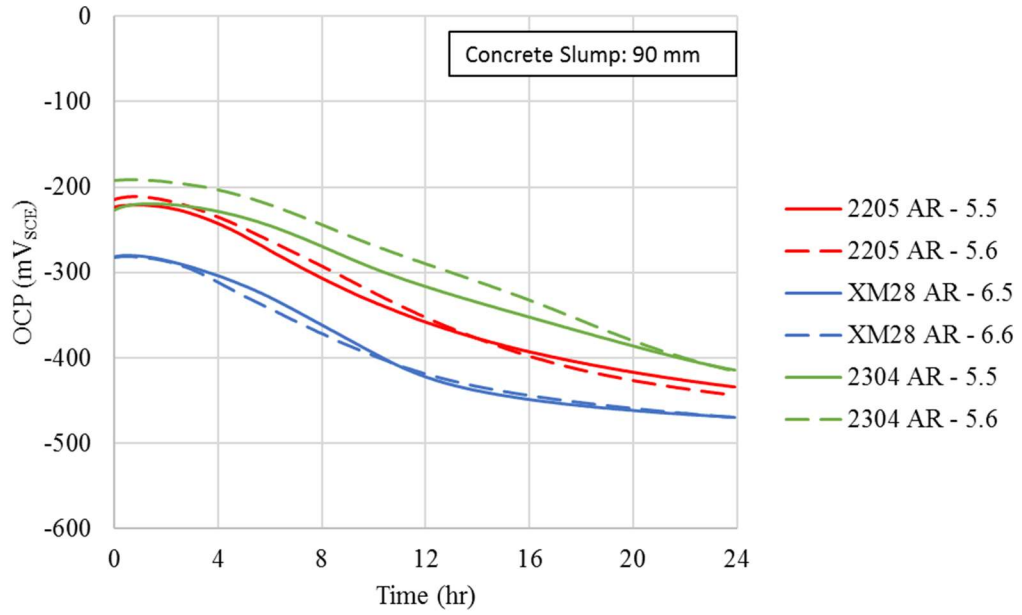

Figure A.41: 6-400 Batch Open Circuit Potentials over 24 hours – Week of October 24, 2017

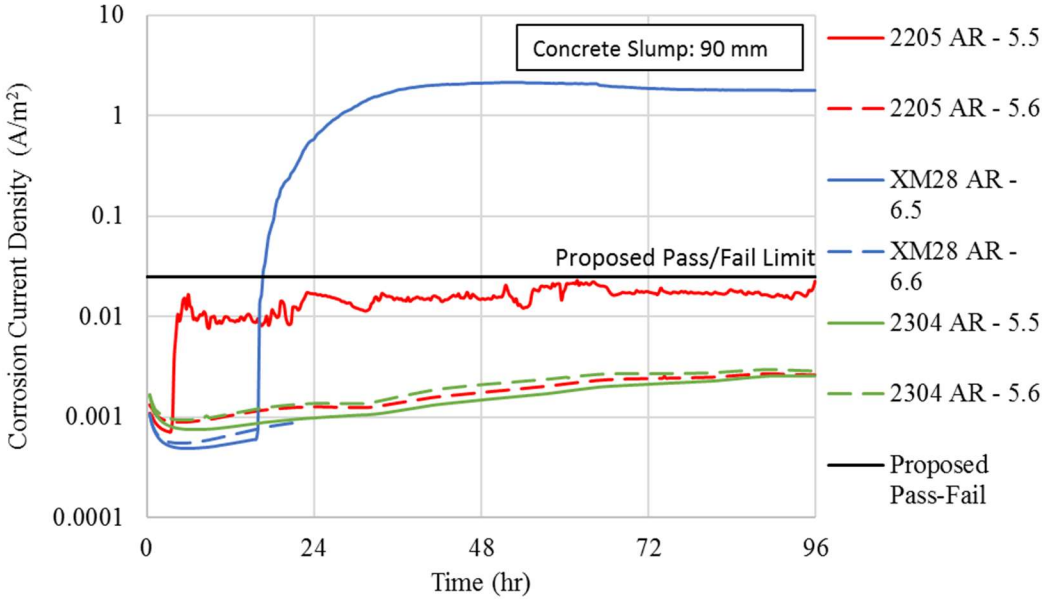

Figure A.42: 6-400 Batch Corrosion Current Densities over 96 hours – Week of October 24, 2017

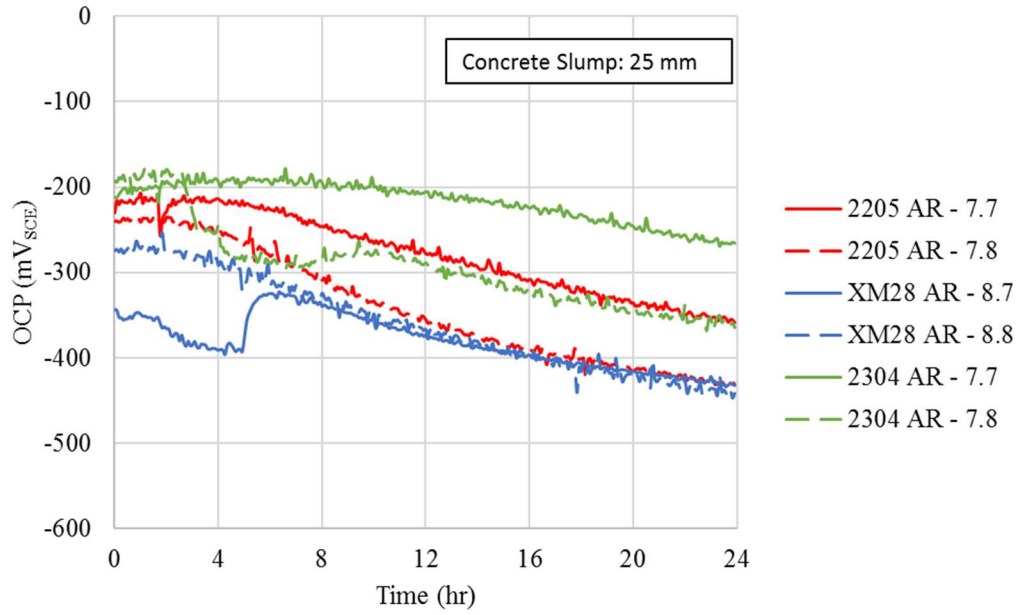

Figure A.43: 7.5-200 Batch Open Circuit Potentials over 24 hours – Week of January 23, 2018

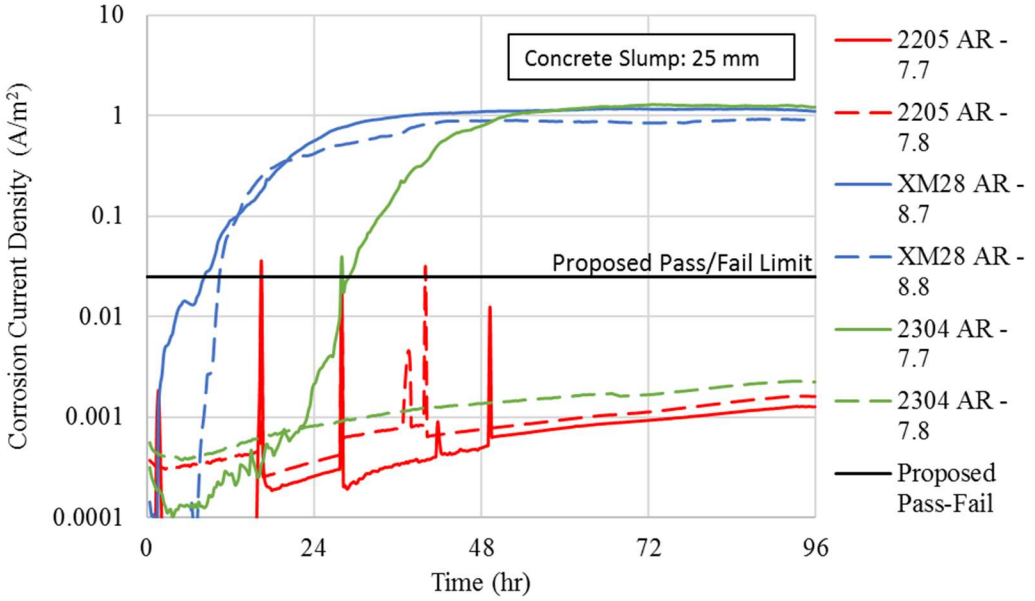

Figure A.44: 7.5-200 Batch Corrosion Current Densities over 96 hours – Week of January 23, 2018

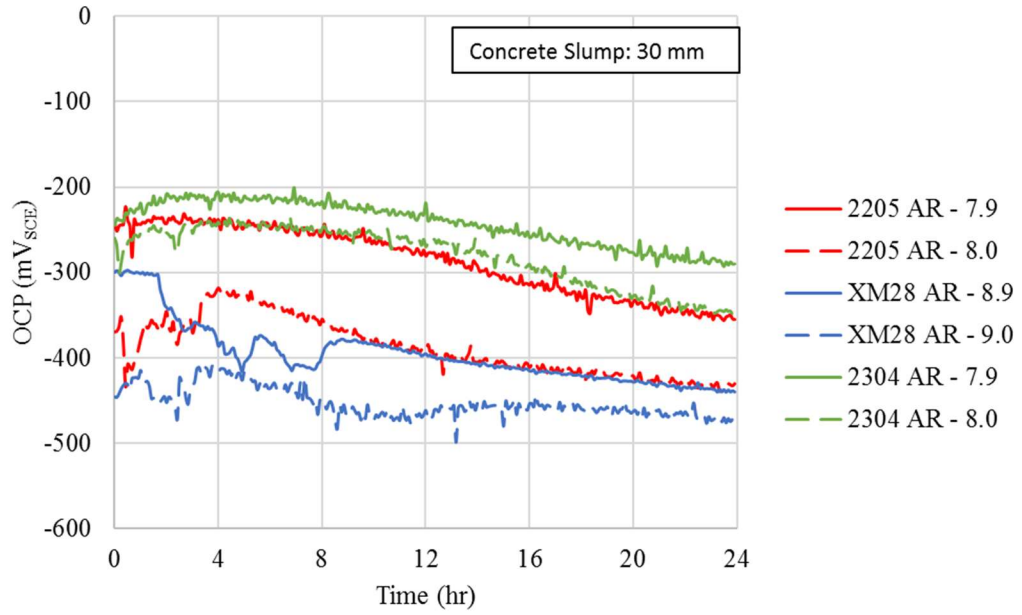

Figure A.45: 7.5-200 Batch Open Circuit Potentials over 24 hours – Week of February 7, 2018

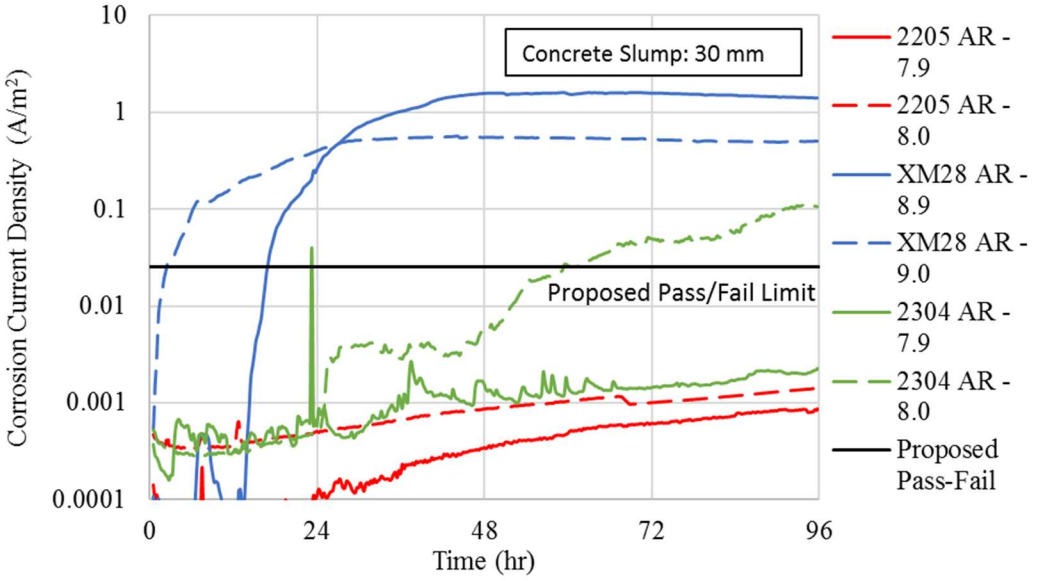

Figure A.46: 7.5-200 Batch Corrosion Current Densities over 96 hours – Week of February 7, 2018

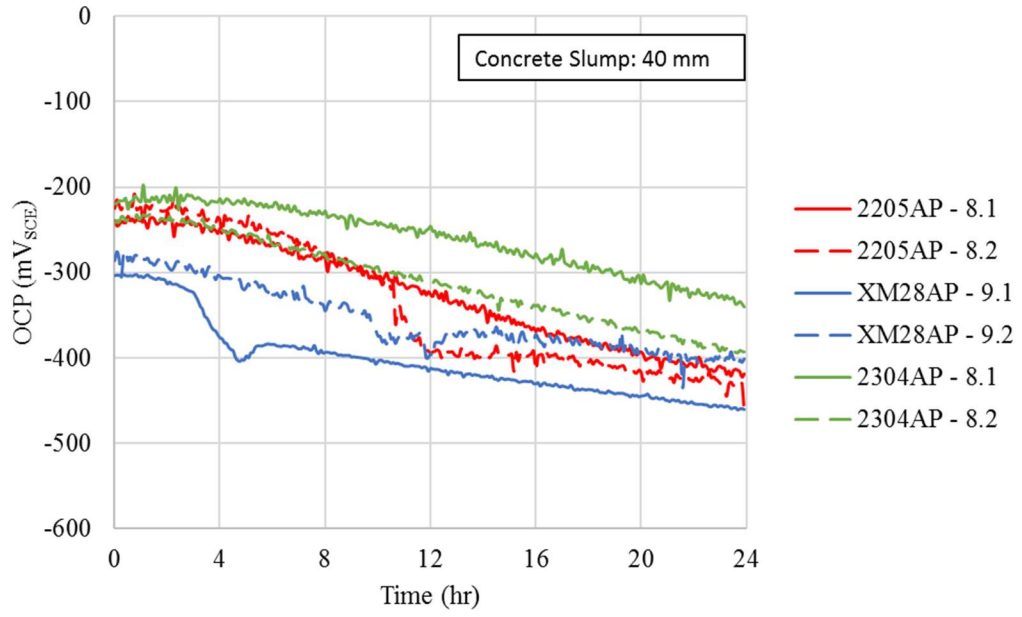

Figure A.47: 7.5-200 Batch Open Circuit Potentials over 24 hours – Week of February 14, 2018

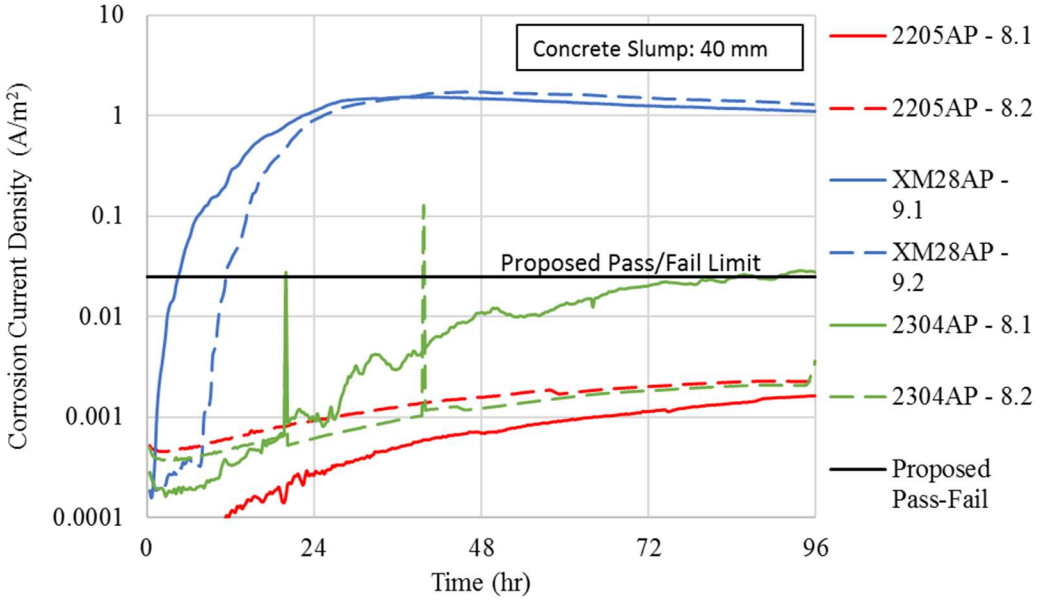

Figure A.48: 7.5-200 Batch Corrosion Current Densities over 96 hours – Week of February 14, 2018

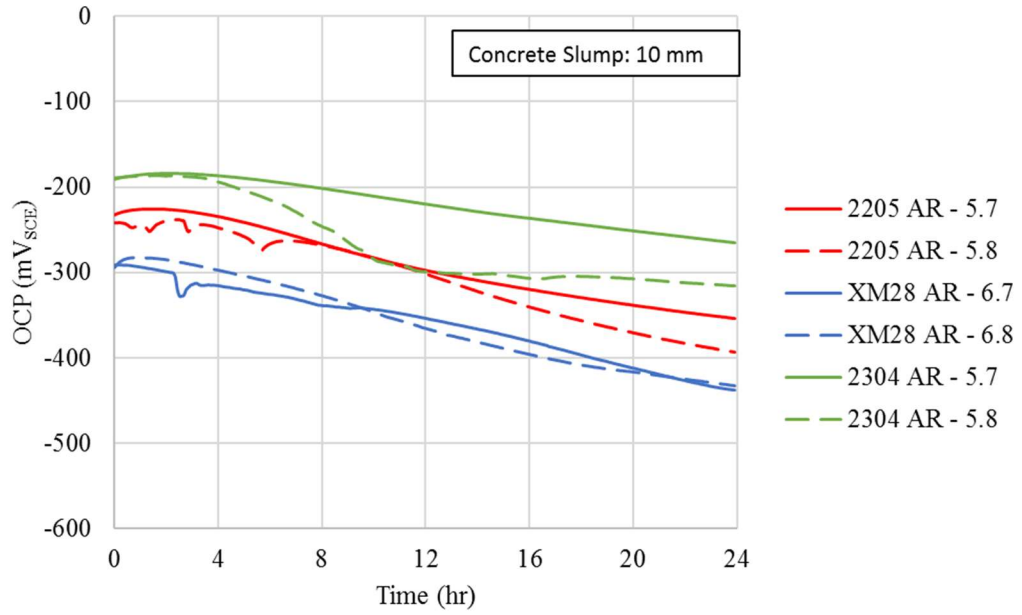

Figure A.49: 7.5-300 Batch Open Circuit Potentials over 24 hours – Week of October 31, 2017

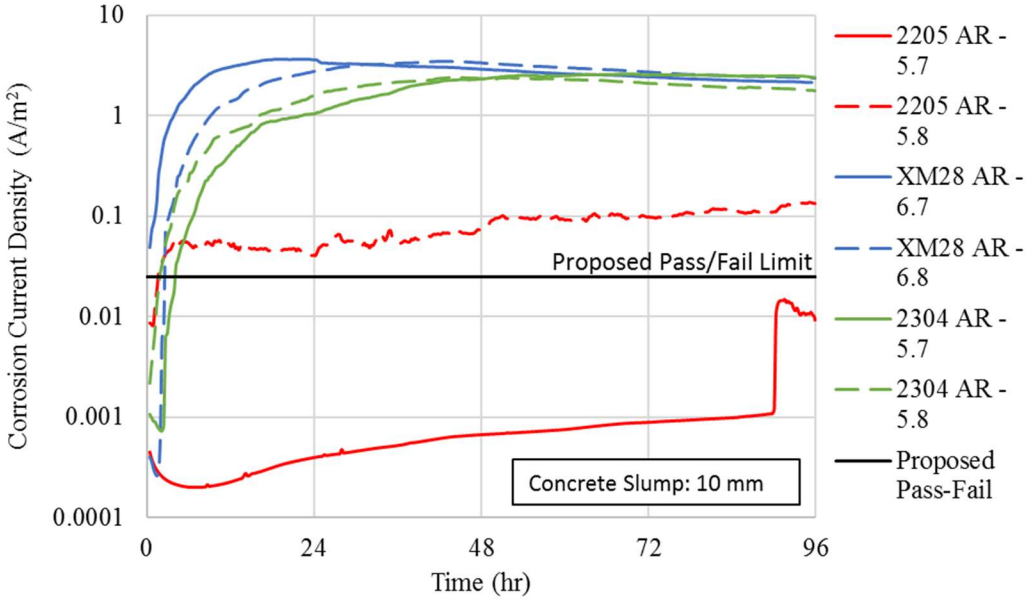

Figure A.50: 7.5-300 Batch Corrosion Current Densities over 96 hours – Week of October 31, 2017

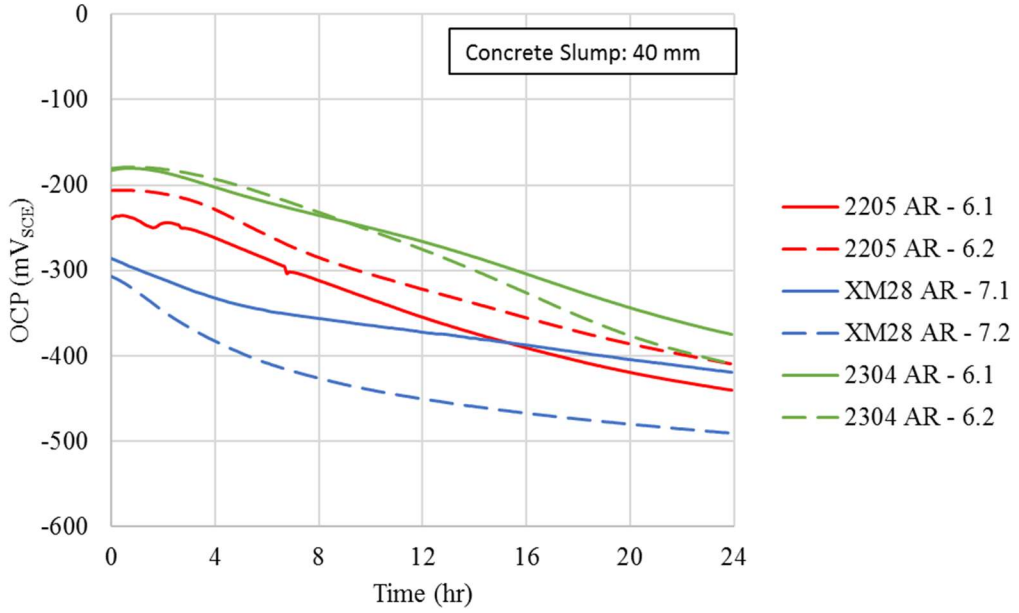

Figure A.51: 7.5-300 Batch Open Circuit Potentials over 24 hours – Week of November 7, 2017

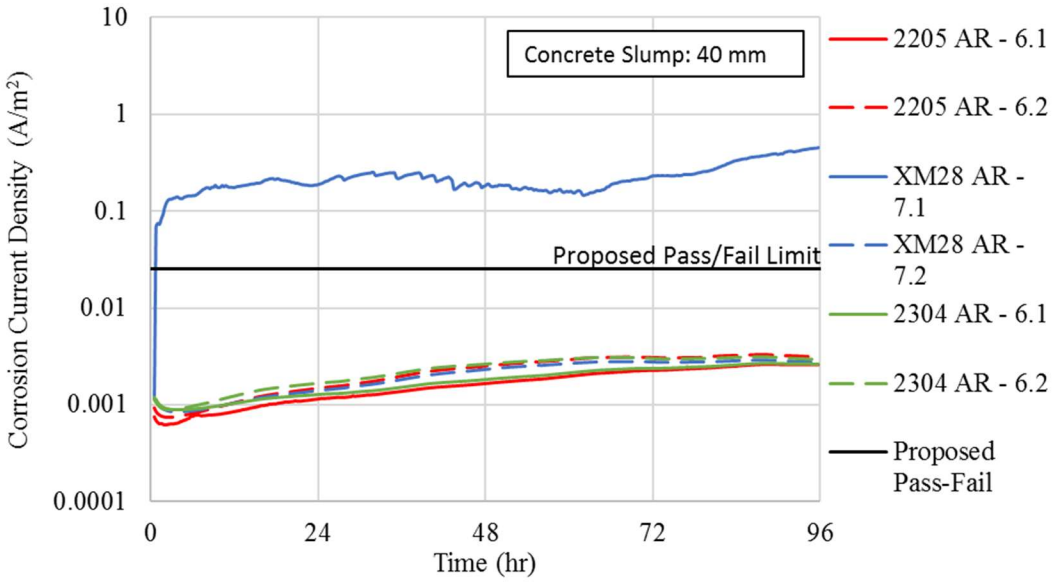

Figure A.52: 7.5-300 Batch Corrosion Current Densities over 96 hours – Week of November 7, 2017

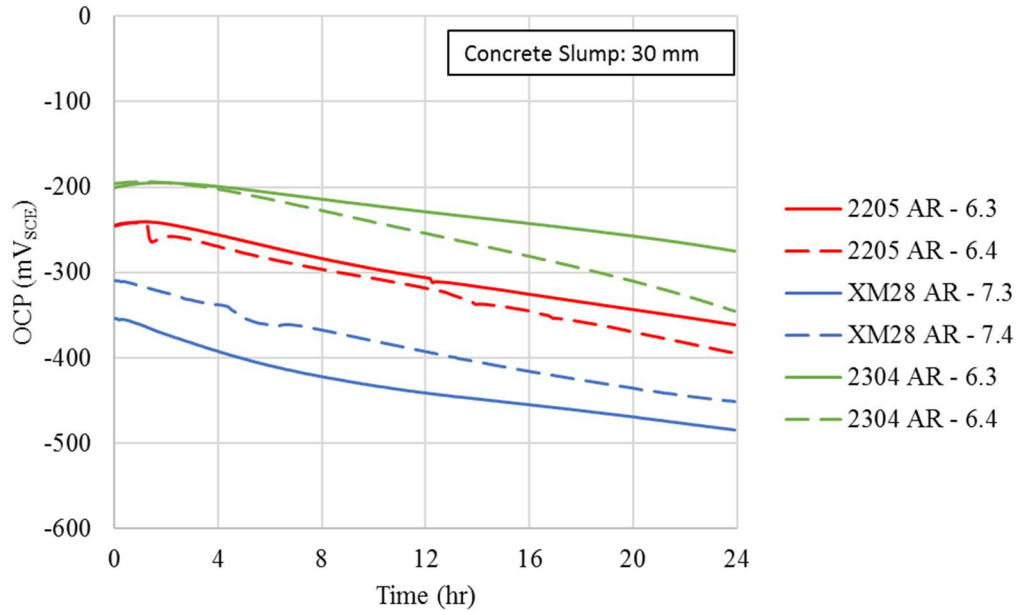

Figure A.53: 7.5-300 Batch Open Circuit Potentials over 24 hours – Week of November 14, 2017

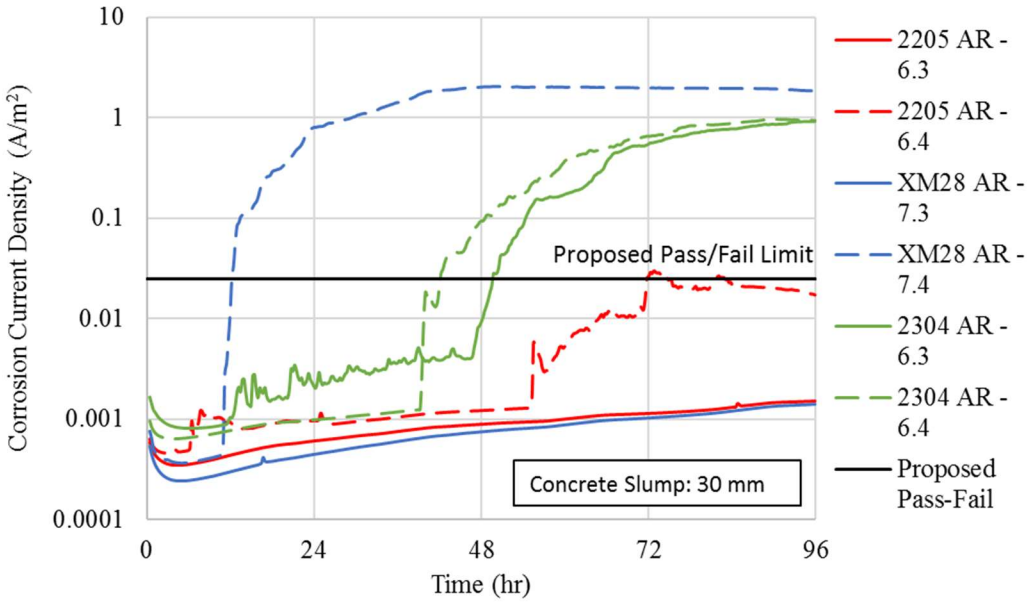

Figure A.54: 7.5-300 Batch - Corrosion Current Densities over 96 hours – Week of November 14, 2017

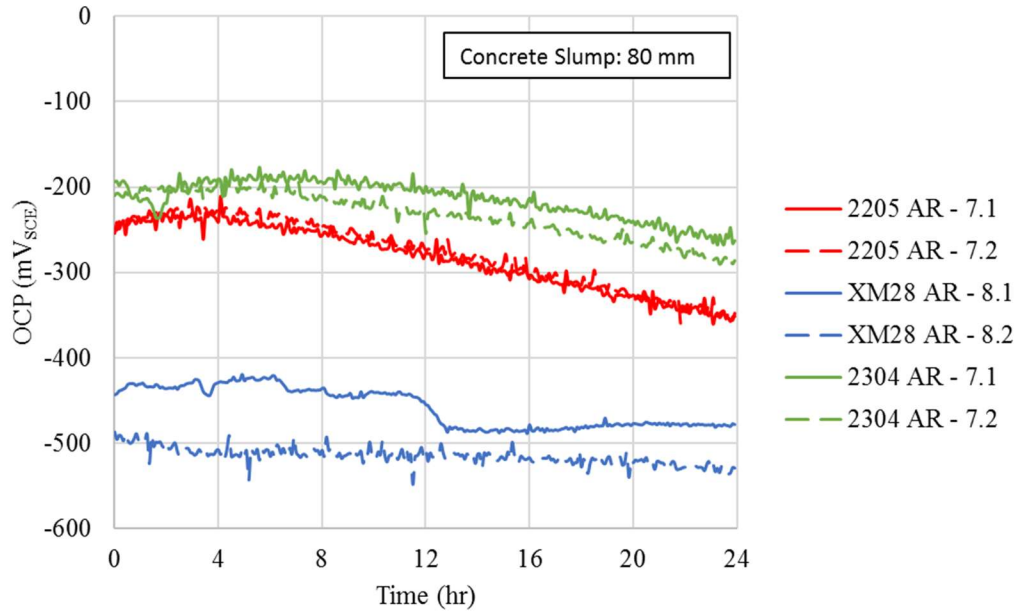

Figure A.55: 7.5-400 Batch Open Circuit Potentials over 24 hours – Week of January 10, 2018

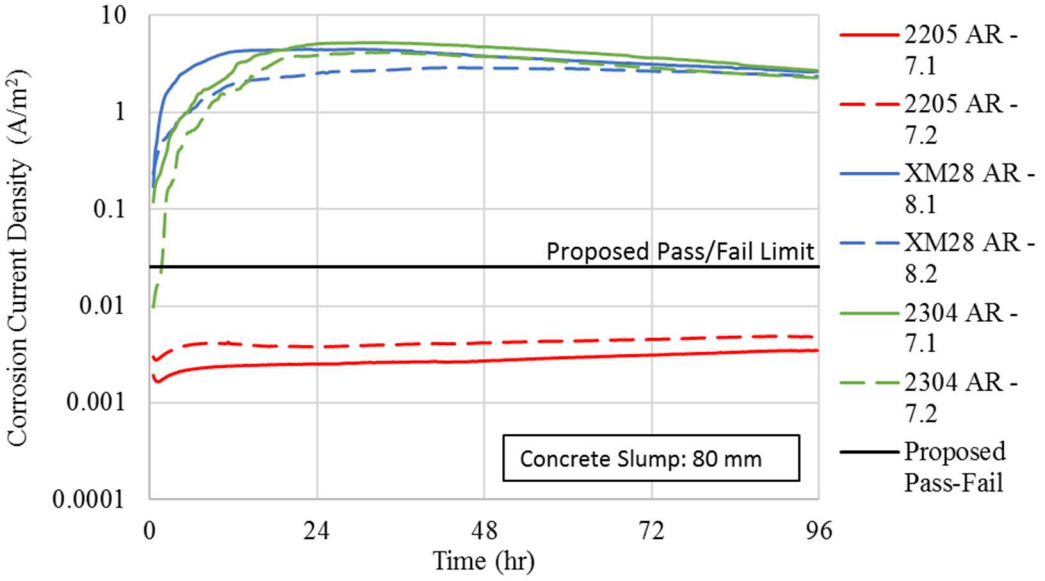

Figure A.56: 7.5-400 Batch - Corrosion Current Densities over 96 hours – Week of January 10, 2018

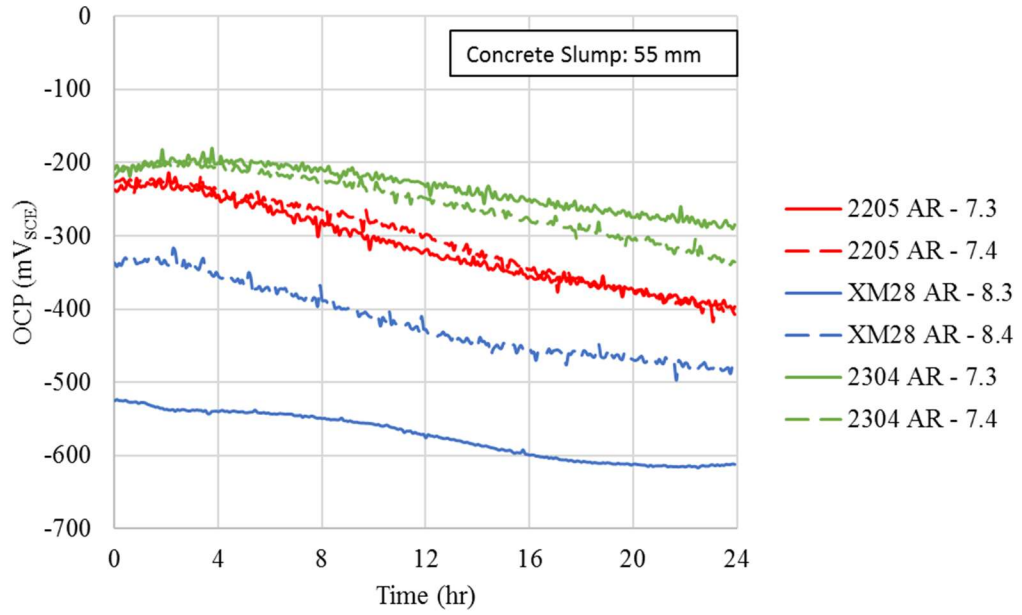

Figure A.57: 7.5-400 Batch Open Circuit Potentials over 24 hours – Week of January 17, 2018

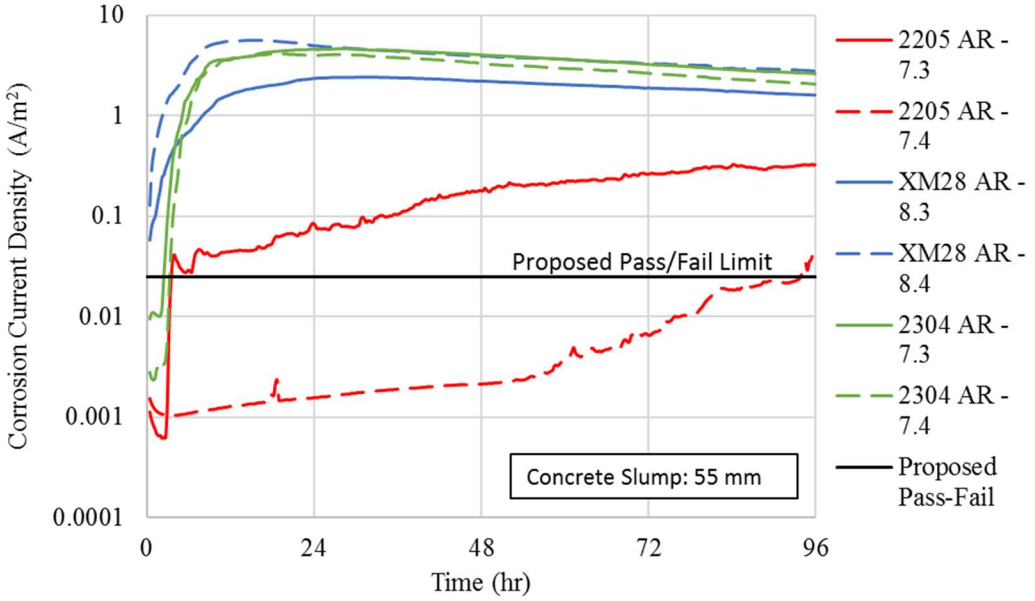

Figure A.58: 7.5-400 Batch - Corrosion Current Densities over 96 hours – Week of January 17, 2018

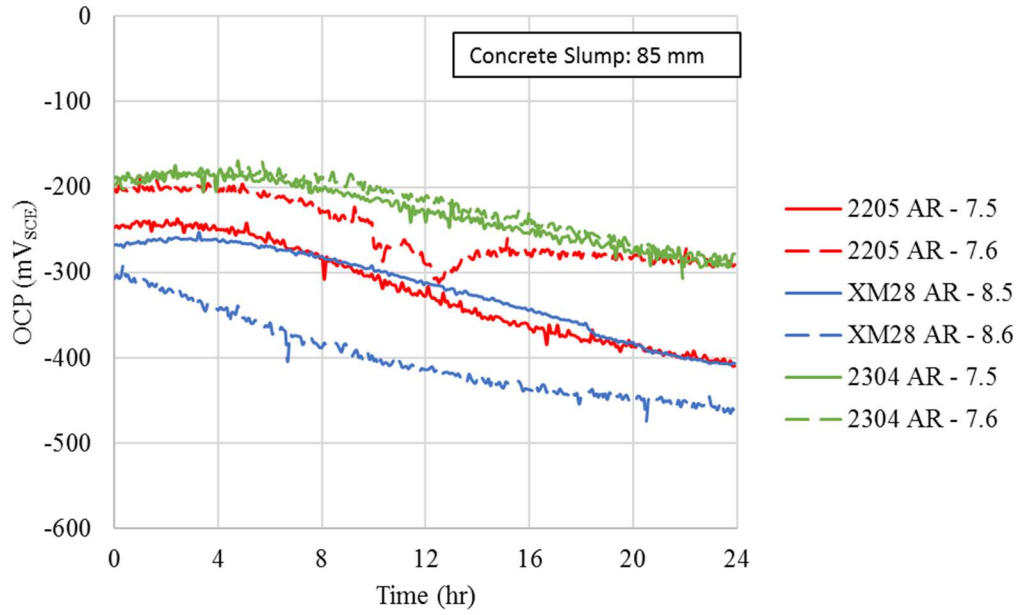

Figure A.59: 7.5-400 Batch Open Circuit Potentials over 24 hours – Week of January 23, 2018

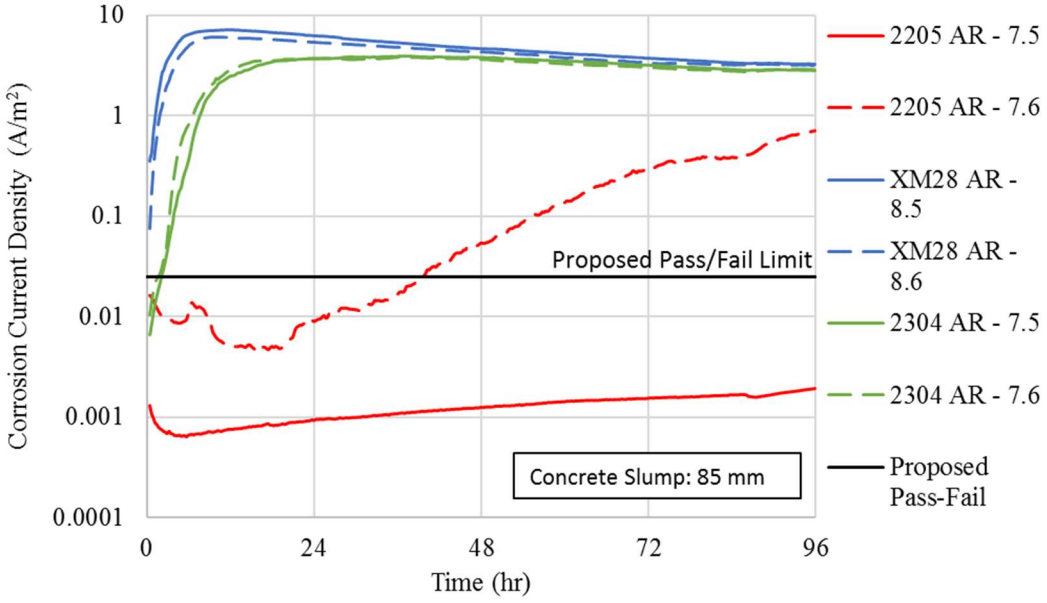

Figure A.60: 7.5-400 Batch - Corrosion Current Densities over 96 hours – Week of January 17, 2018

Appendix B

Open Circuit Potential Statistics: Averages and Standard Deviations

Table B.1: 4-100 Batch – Average Open Circuit Potentials (mV_{SCE})

Time (hr)	Average Open Circuit Potential (mVSCE)					
	2205 AR	2205 PP	XM28 AR	XM28 PP	2304 AR	2304 PP
0	-395	-344	-422	-354	-308	-411
4	-398	-336	-438	-385	-322	-433
8	-423	-361	-450	-410	-346	-451
12	-440	-392	-460	-430	-377	-461
16	-445	-416	-472	-447	-403	-486
20	-465	-438	-485	-462	-422	-503
24	-473	-460	-498	-477	-440	-517

Table B.2: 4-100 Batch – Standard Deviation of Open Circuit Potentials (mV_{SCE})

Time (hr)	Standard Deviations of Circuit Potential (mVSCE)					
	2205 AR	2205 PP	XM28 AR	XM28 PP	2304 AR	2304 PP
0	52	111	38	44	50	239
4	37	50	30	45	55	184
8	36	48	18	45	58	146
12	34	51	15	44	60	97
16	43	54	19	44	62	79
20	41	56	25	46	61	67
24	51	56	32	49	58	60

Table B.3: 4-400 Batch – Average Open Circuit Potentials (mV_{SCE})

Time (hr)	Average Open Circuit Potential (mVSCE)		
	2205 AR	XM28 AR	2304 AR
0	-302	-345	-245
4	-351	-402	-284
8	-405	-436	-340
12	-432	-452	-380
16	-447	-464	-409
20	-462	-476	-431
24	-474	-487	-447

Table B.4: 4-400 Batch – Standard Deviations of Open Circuit Potentials (mV_{SCE})

Time (hr)	Standard Deviation of Open Circuit Potential (mV_{SCE})		
	2205 AR	XM28 AR	2304 AR
0	34	20	36
4	46	19	45
8	21	25	51
12	14	24	44
16	13	23	34
20	13	21	28
24	14	22	26

Table B.5: 6-100 Batch – Average Open Circuit Potentials (mV_{SCE})

Time (hr)	Average Open Circuit Potential (mVSCE)		
	2205 AR	XM28 AR	2304 AR
0	-343	-389	-251
4	-354	-409	-264
8	-369	-422	-277
12	-384	-433	-291
16	-399	-443	-305
20	-414	-453	-324
24	-428	-461	-347

Table B.6: 6-100 Batch – Standard Deviations of Open Circuit Potentials (mV_{SCE})

Time (hr)	Standard Deviation of Open Circuit Potential (mVSCE)		
	2205 AR	XM28 AR	2304 AR
0	69	20	20
4	60	17	17
8	55	15	16
12	51	13	15
16	48	12	15
20	45	12	20
24	42	12	32

Table B.7: 6-200 Batch – Average Open Circuit Potentials (mV_{SCE})

Time (hr)	Average Open Circuit Potential (mV SCE)		
	2205 AR	XM28 AR	2304 AR
0	-245	-317	-186
4	-248	-345	-212
8	-269	-352	-210
12	-296	-373	-230
16	-323	-399	-257
20	-351	-422	-287
24	-376	-440	-317

Table B.8: 6-200 Batch – Standard Deviations of Open Circuit Potentials (mV_{SCE})

Time (hr)	Standard Deviation of Open Circuit Potential (mV SCE)		
	2205 AR	XM28 AR	2304 AR
0	77	108	31
4	75	107	56
8	72	94	42
12	65	82	39
16	56	66	34
20	44	50	32
24	33	37	32

Table B.9: 6-300 Batch – Average Open Circuit Potentials (mV_{SCE})

Time (hr)	Average Open Circuit Potential (mVSCE)		
	2205 AR	XM28 AR	2304 AR
0	-240	-340	-226
4	-264	-374	-227
8	-309	-402	-254
12	-342	-431	-281
16	-371	-448	-310
20	-394	-450	-341
24	-414	-471	-368

Table B.10: 6-300 Batch – Standard Deviations of Open Circuit Potentials (mV_{SCE})

Time (hr)	Standard Deviation of Open Circuit Potential (mVSCE)		
	2205 AR	XM28 AR	2304 AR
0	40	76	65
4	49	52	45
8	56	30	49
12	54	25	49
16	51	21	49
20	45	36	48
24	37	23	46

Table B.11: 6-400 Batch – Average Open Circuit Potentials (mV_{SCE})

Time (hr)	Average Open Circuit Potential (mVSCE)		
	2205 AR	XM28 AR	2304 AR
0	-277	-295	-221
4	-308	-343	-240
8	-355	-402	-285
12	-381	-433	-327
16	-405	-451	-361
20	-424	-463	-392
24	-439	-472	-417

Table B.12: 6-400 Batch – Standard Deviations of Open Circuit Potentials (mV_{SCE})

Time (hr)	Standard Deviation of Open Circuit Potential (mVSCE)		
	2205 AR	XM28 AR	2304 AR
0	101	43	18
4	117	48	23
8	106	32	31
12	107	18	37
16	104	15	38
20	98	12	33
24	90	10	27

Table B.13: 7.5-200 Batch – Average Open Circuit Potentials (mV_{SCE})

Time (hr)	Average Open Circuit Potential (mVSCE)		
	2205 AR	XM28 AR	2304 AR
0	-251	-322	-222
4	-252	-373	-225
8	-288	-384	-242
12	-338	-403	-257
16	-368	-420	-285
20	-386	-436	-313
24	-406	-450	-334

Table B.14: 7.5-200 Batch – Standard Deviations of Open Circuit Potentials (mV_{SCE})

Time (hr)	Standard Deviation of Open Circuit Potential (mVSCE)		
	2205 AR	XM28 AR	2304 AR
0	60	65	26
4	35	43	23
8	39	47	36
12	52	34	41
16	47	22	42
20	41	17	45
24	43	14	48

Table B.15: 7.5-300 Batch – Average Open Circuit Potentials (mV_{SCE})

Time (hr)	Average Open Circuit Potential (mVSCE)		
	2205 AR	XM28 AR	2304 AR
0	-235	-307	-190
4	-250	-343	-196
8	-285	-373	-226
12	-317	-396	-257
16	-346	-417	-283
20	-371	-436	-307
24	-392	-453	-331

Table B.16: 7.5-300 Batch – Standard Deviations of Open Circuit Potentials (mV_{SCE})

Time (hr)	Standard Deviation of Open Circuit Potential (mVSCE)		
	2205 AR	XM28 AR	2304 AR
0	15	25	8
4	16	37	6
8	17	42	16
12	21	41	30
16	25	36	36
20	30	31	48
24	32	29	56

Table B.17: 7.5-400 Batch – Average Open Circuit Potentials (mV_{SCE})

Time (hr)	Average Open Circuit Potential (mVSCE)		
	2205 AR	XM28 AR	2304 AR
0	-236	-395	-203
4	-234	-407	-193
8	-258	-425	-205
12	-298	-449	-231
16	-326	-414	-244
20	-345	-485	-272
24	-367	-495	-290

Table B.18: 7.5-400 Batch – Standard Deviations of Open Circuit Potentials (mV_{SCE})

Time (hr)	Standard Deviation of Open Circuit Potential (mVSCE)		
	2205 AR	XM28 AR	2304 AR
0	19	105	11
4	16	106	10
8	20	95	14
12	21	90	22
16	35	211	23
20	41	77	21
24	46	70	25

Appendix C

Rapid Screening Test Autopsy Pictures

Figure C.1: RST 4-400 Batch – Corrosion Products on XM-28 AR 7.5. From top to bottom, a) original specimen, b) corrosion products on specimen upon removal from concrete, and c) pitting corrosion identification on a pickled specimen

Figure C.2: RST 4-400 Batch – Corrosion Products on XM-28 AR 7.6. From top to bottom, a) original specimen, b) corrosion products on specimen upon removal from concrete, and c) pitting corrosion identification on a pickled specimen

Figure C.3: RST 4-400 Batch – Corrosion Products on XM-28 AR 7.7. From top to bottom, a) original specimen, b) corrosion products on specimen upon removal from concrete, and c) pitting corrosion identification on a pickled specimen

Figure C.4: RST 6-200 Batch – Corrosion Products on XM-28 AR 5.2. From top to bottom, a) original specimen, b) corrosion products on specimen upon removal from concrete, and c) pitting corrosion identification on a pickled specimen

Figure C.5: RST 6-300 Batch – Corrosion Products on 2304 AR 4.3. From top to bottom, a) original specimen, b) corrosion products on specimen upon removal from concrete, and c) pitting corrosion identification on the pickled specimen

Figure C.6: RST 6-300 Batch – Corrosion Products on XM-28 AR 5.4. From top to bottom, a) original specimen, b) corrosion products on specimen upon removal from concrete, and c) pitting corrosion identification on the pickled specimen

Figure C.7: RST 6-400 Batch – XM-28 AR 6.1 Corrosion Products Observed on Concrete Specimen

Figure C.8: 6-400 Batch – Corrosion Products on XM-28 AR 6.1. From top to bottom, a) original specimen, b) corrosion products on specimen upon removal from concrete, and c) pitting corrosion identification on the pickled specimen

Figure C.9: RST 6-400 Batch – XM-28 AR 6.2 Corrosion Products causing Cracking of Concrete Specimen

Figure C.10: 6-400 Batch – Corrosion Products on XM-28 AR 6.2. From top to bottom, a) original specimen, b) corrosion products on specimen upon removal from concrete, and c) pitting corrosion identification on the pickled specimen

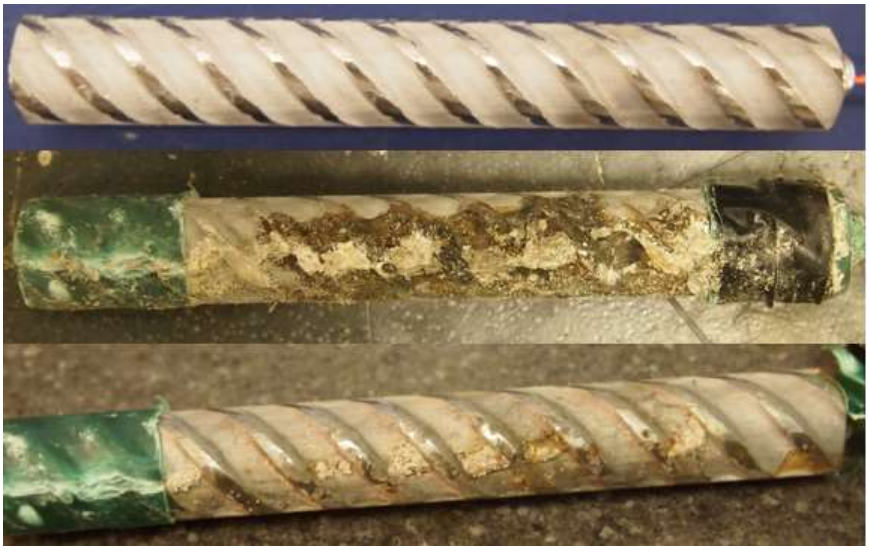

Figure C.11: 6-400 Batch – Corrosion Products on XM-28 AR 6.3. From top to bottom, a) original specimen, b) corrosion products on specimen upon removal from concrete, and c) pitting corrosion identification on a pickled specimen

Figure C.12: RST 6-400 Batch – XM-28 AR 6.4 Corrosion Products causing Cracking of Concrete Specimen

Figure C.13: 6-400 Batch – Corrosion Products on XM-28 AR 6.4. From top to bottom, a) original specimen, b) corrosion products on specimen upon removal from concrete, and c) pitting corrosion identification on the pickled specimen

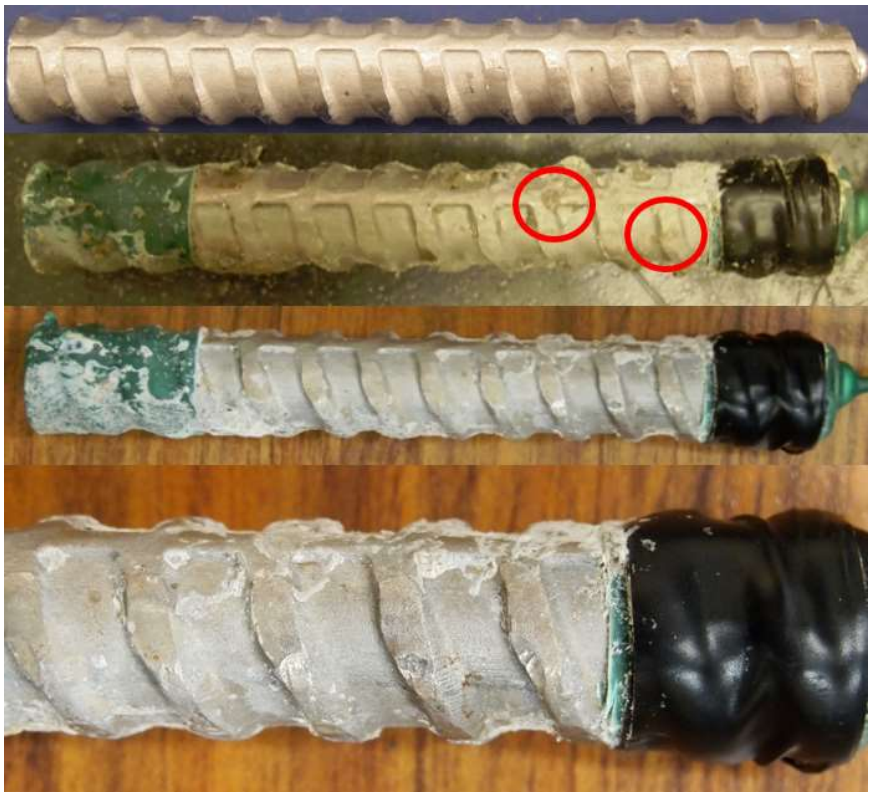

Figure C.14: 6-400 Batch – Evidence of Pitting Corrosion on 2205 AR 5.4. From top to bottom, a) original specimen, b) corrosion products on specimen upon removal from concrete, and c) & d) pitting corrosion identification on the pickled specimen. Identification of pitting corrosion was observed 2 weeks after the autopsy.

Figure C.15: RST 6-400 Batch – XM-28 AR 6.5 Corrosion Products causing Cracking of Concrete Specimen

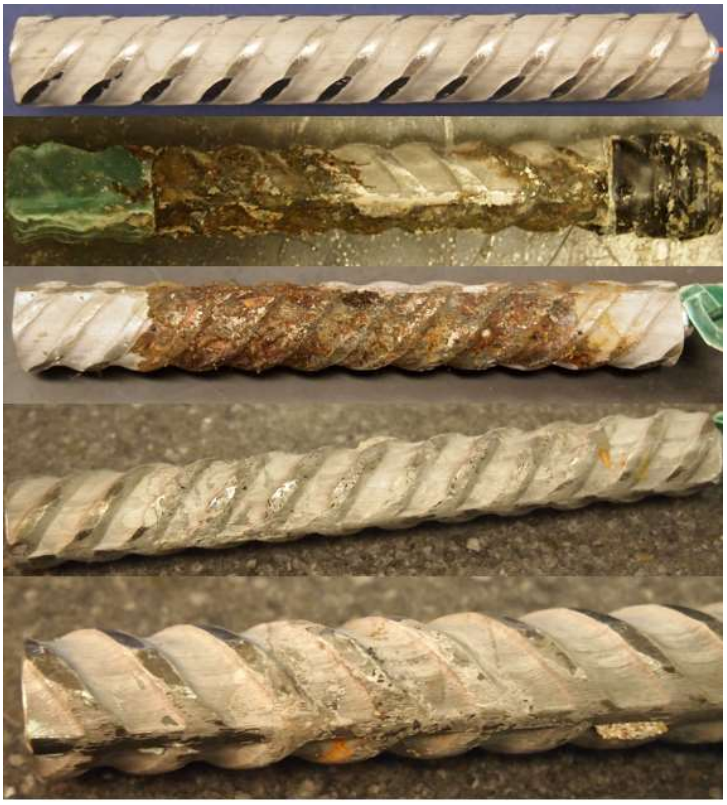

Figure C.16: 6-400 Batch – Corrosion Products on XM-28 AR 6.5. From top to bottom, a) original specimen, b) corrosion products on the specimen upon removal from concrete, c) oxidized corrosion products, and d) & e) pitting corrosion identification on the pickled specimen

Figure C.17: 6-400 Batch – Evidence of Pitting Corrosion on 2205 AR 5.5. From top to bottom, a) original specimen, b) corrosion products on specimen upon removal from concrete, and c) & d) pitting corrosion identification on the pickled specimen. Identification of pitting corrosion was observed 1 week after the autopsy.

Figure C.18: RST 7.5-200 Batch – XM-28AR 8.7 Corrosion Products causing Cracking of Concrete Specimen

Figure C.19: 7.5-200 Batch – Corrosion Products on XM-28 AR 8.7. From top to bottom, a) original specimen, b) & c) corrosion products on the specimen upon removal from concrete, and d) & e) pitting corrosion identification on the pickled specimen

Figure C.20: RST 7.5-200 Batch – XM-28 AR 8.8 Corrosion Products causing Cracking of Concrete Specimen

Figure C.21: 7.5-200 Batch – Corrosion Products on XM-28 AR 8.8. From top to bottom, a) original specimen, b) corrosion products on the specimen upon removal from concrete, and c) pitting corrosion identification on the pickled specimen

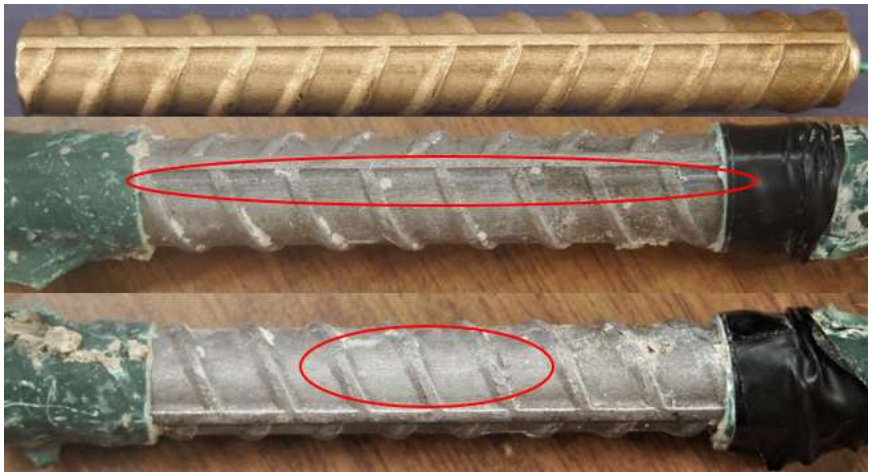

Figure C.22: 7.5-200 Batch – Corrosion Products on 2304 AR 7.7. From top to bottom, a) original specimen, and b) & c) corrosion products on the specimen upon removal from concrete. Identification of pitting corrosion was observed 5 months after the autopsy.

Figure C.23: 7.5-200 Batch – Corrosion Products on 2304 AR 7.8. From top to bottom, a) original specimen, b) corrosion products on the specimen upon removal from concrete, and c) pitting corrosion identification on the pickled specimen

Figure C.24: RST 7.5-200 Batch – 2304 AR 7.9 Corrosion Products causing Cracking of Concrete Specimen

Figure C.25: 7.5-200 Batch – Corrosion Products on 2304 AR 7.9. From top to bottom, a) original specimen, b) corrosion products on the specimen upon removal from concrete, and c) pitting corrosion identification on the pickled specimen

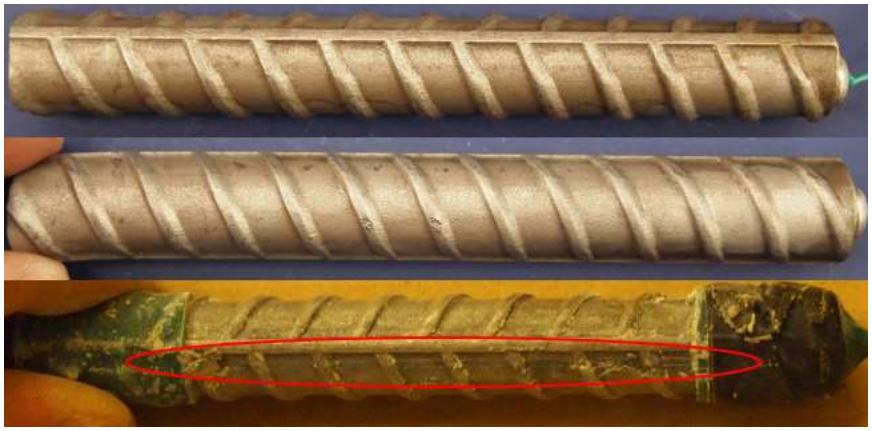

Figure C.26: 7.5-200 Batch – Corrosion Products on 2304 AR 8.0. From top to bottom, a) & b) original specimen, and c) corrosion products on the specimen upon removal from concrete. The slight staining at the top of the bar in a) is due to soldering flux.

Figure C.27: RST 7.5-200 Batch – XM-28 AR 8.9 Corrosion Products causing Cracking of Concrete Specimen

Figure C.28: 7.5-200 Batch – Corrosion Products on XM-28 AR 8.9. From top to bottom, a) original specimen, b) & c) corrosion products on the specimen upon removal from concrete, and d) & e) pitting corrosion identification on the pickled specimen. The slight staining at the top of the bar in a) is due to soldering flux.

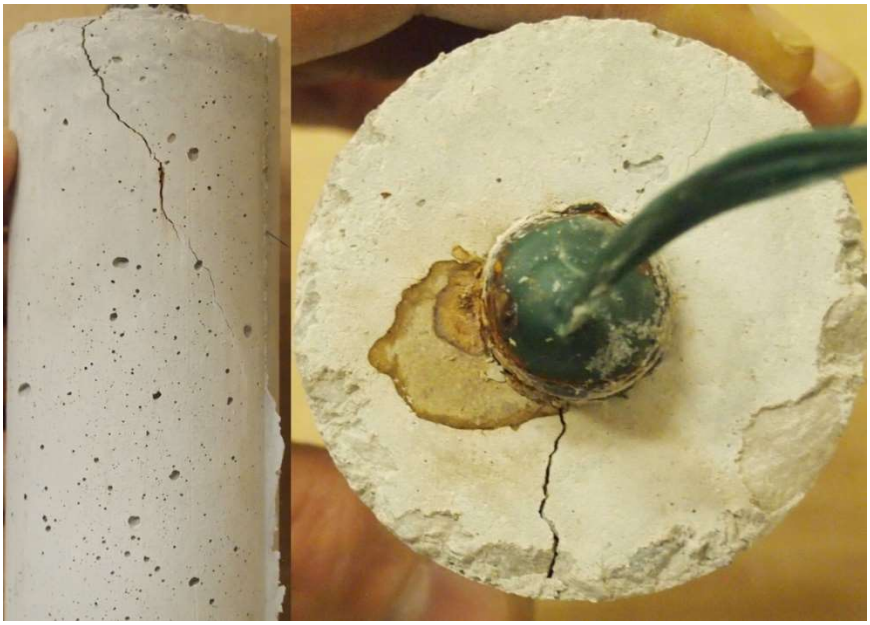

Figure C.29: RST 7.5-200 Batch – XM-28 AR 9.0 Corrosion Products causing Cracking of Concrete Specimen

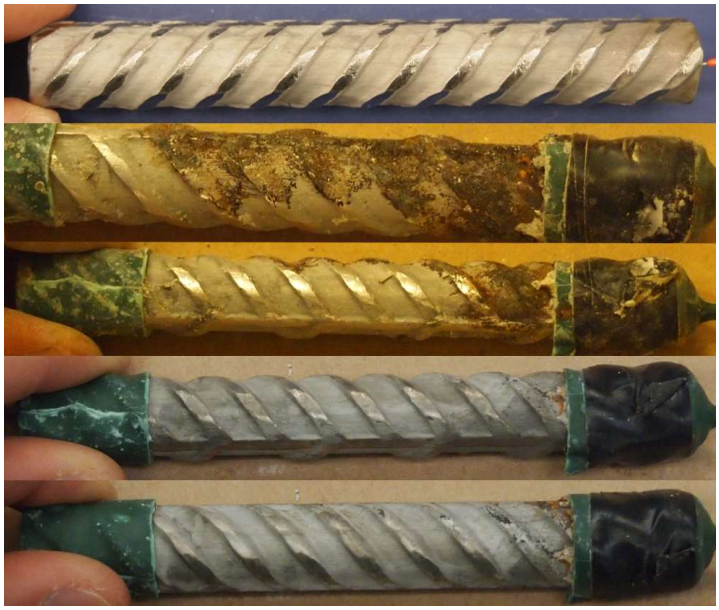

Figure C.30: 7.5-200 Batch – Corrosion Products on XM-28 AR 9.0. From top to bottom, a) original specimen, b) & c) corrosion products on the specimen upon removal from concrete, and d) & e) pitting corrosion identification on the pickled specimen. The slight staining at the top of the bar in a) is due to soldering flux.

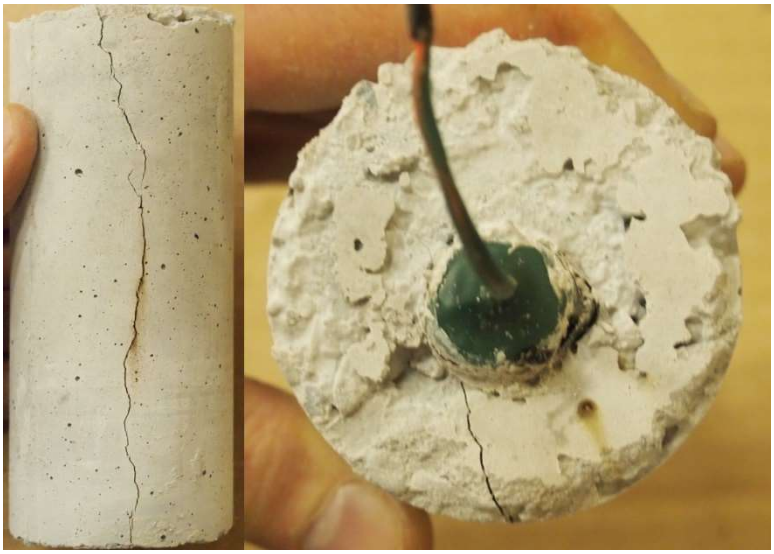

Figure C.31: RST 7.5-200 Batch – XM-28 AR 9.1 Corrosion Products causing Cracking of Concrete Specimen

Figure C.32: 7.5-200 Batch – Corrosion Products on XM-28 AR 9.1. From top to bottom, a) original specimen, b) & c) corrosion products on the specimen upon removal from concrete, and d) & e) pitting corrosion identification on the pickled specimen

Figure C.33: RST 7.5-200 Batch – XM-28 AR 9.2 Corrosion Products causing Cracking of Concrete Specimen

Figure C.34: 7.5-200 Batch – Corrosion Products on XM-28 AR 9.2. From top to bottom, a) original specimen, b) & c) corrosion products on the specimen upon removal from concrete, and d) & e) pitting corrosion identification on the pickled specimen

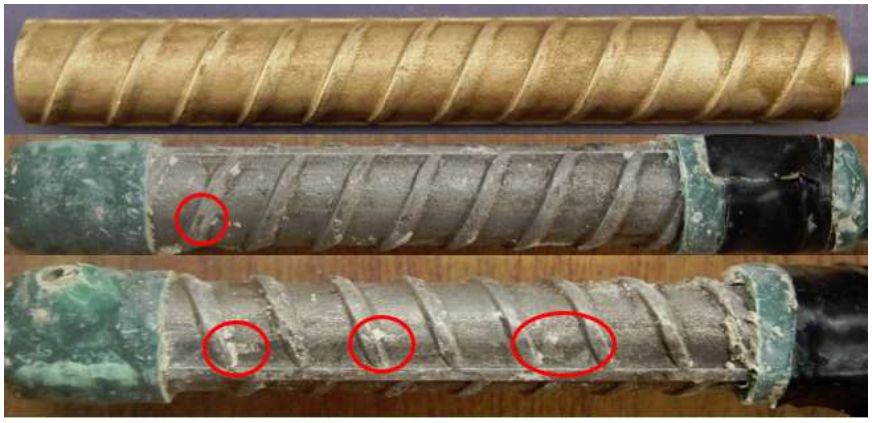

Figure C.35: 7.5-200 Batch – Corrosion Products on 2304 AR 8.1. From top to bottom, a) original specimen, and b) & c) corrosion products on the specimen upon removal from concrete. Identification of pitting corrosion was observed 4 months after the autopsy. The slight staining at the top of the bar in a) is due to soldering flux.

Figure C.36: 7.5-200 Batch – Corrosion Products on 2304 AR 8.2. From top to bottom, a) original specimen, b) & c) corrosion products on the specimen upon removal from concrete, and d) & e) pitting corrosion identification on the pickled specimen

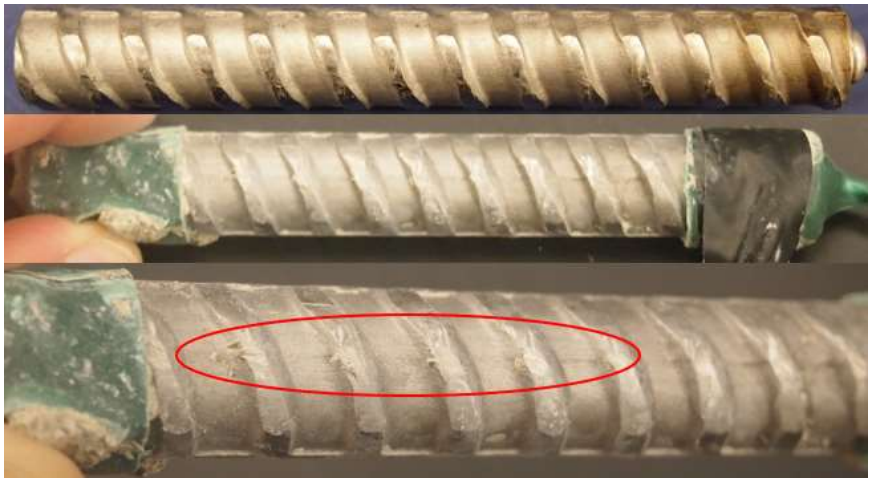

Figure C.37: 7.5-200 Batch – Corrosion Products on 2205 AR 7.7. From top to bottom, a) original specimen, and b) & c) corrosion products on the specimen upon removal from concrete. Identification of pitting corrosion was observed 4 months after the autopsy. The slight staining at the top of the bar in a) is due to soldering flux.

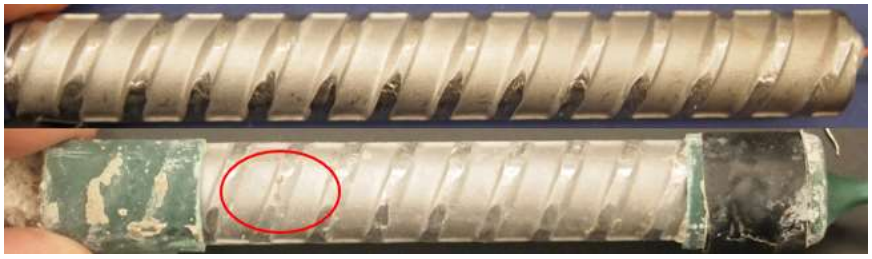

Figure C.38: Corrosion Products on 2205 AR 7.8. From top to bottom, a) original specimen, and b) corrosion products on the specimen upon removal from concrete. Identification of pitting corrosion was observed 4 months after the autopsy.

Figure C.39: RST 7.5-300 Batch – 2304 AR 5.7 Corrosion Products Leaking through Concrete Specimen

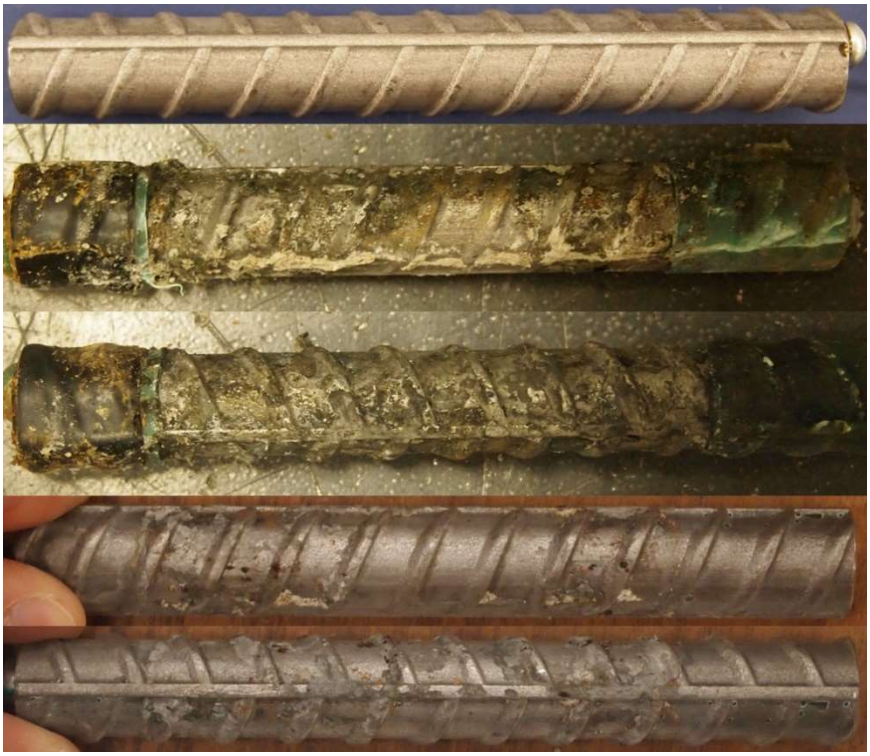

Figure C.40: 7.5-300 Batch – Corrosion Products on 2304 AR 5.7. From top to bottom, a) original specimen, b) & c) corrosion products on the specimen upon removal from concrete, and d) & e) pitting corrosion identification on the pickled specimen

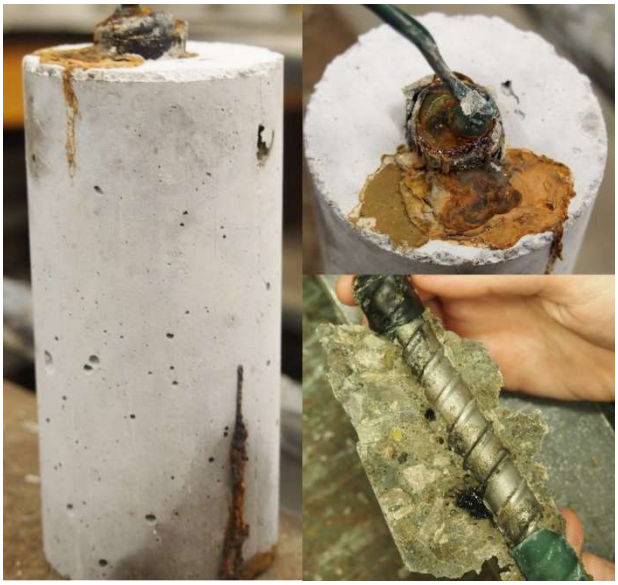

Figure C.41: RST 7.5-300 Batch – 2304 AR 5.8 Corrosion Products Leaking through Concrete Specimen, a) & b). Black corrosion products staining concrete, c).

Figure C.42: 7.5-300 Batch – Corrosion Products on 2304 AR 5.8. From top to bottom, a) original specimen, b) & c) corrosion products on the specimen upon removal from concrete, and d) & e) pitting corrosion identification on the pickled specimen. The slight staining at the top of the bar in a) is due to soldering flux.

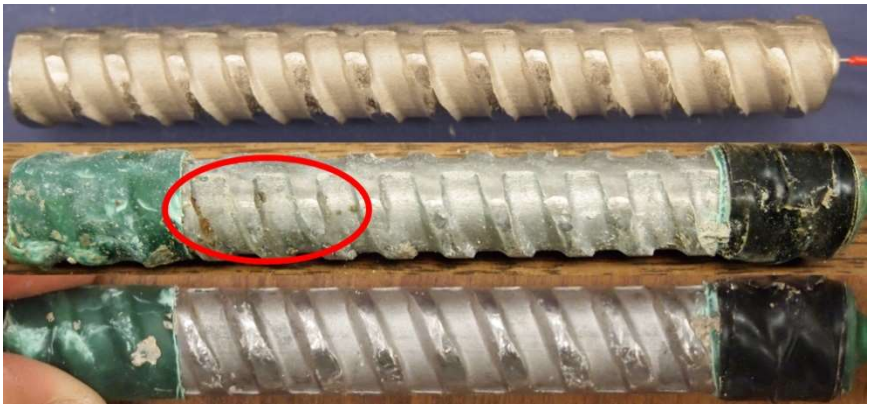

Figure C.43: 7.5-300 Batch – Corrosion Products on 2205 AR 5.7. From top to bottom, a) original specimen, b) corrosion products on the specimen upon removal from concrete, and c) pitting corrosion identification on the pickled specimen

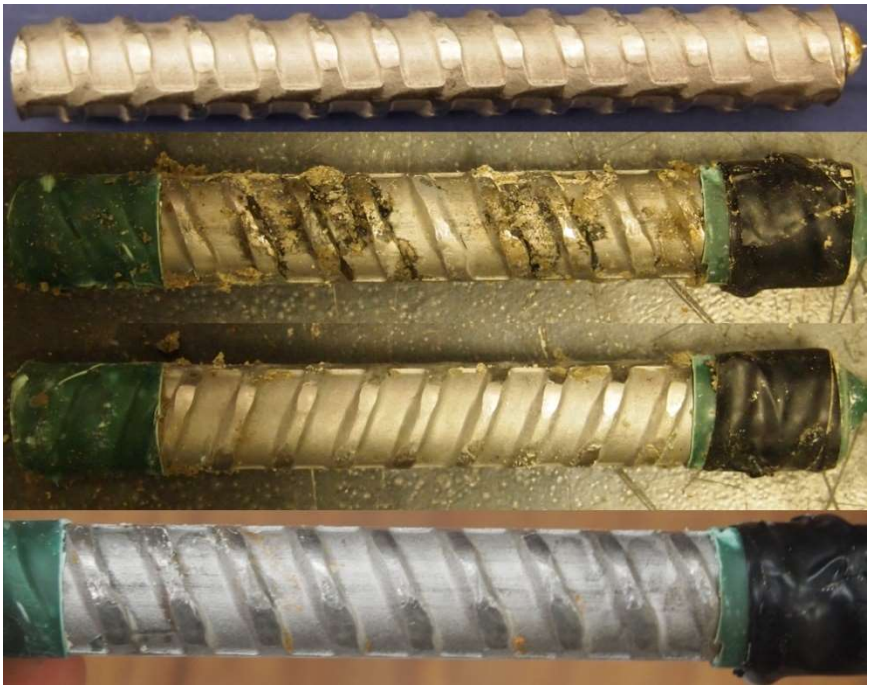

Figure C.44: 7.5-300 Batch – Corrosion Products on 2205 AR 5.8. From top to bottom, a) original specimen, b) & c) corrosion products on the specimen upon removal from concrete, and d) pitting corrosion identification on the pickled specimen

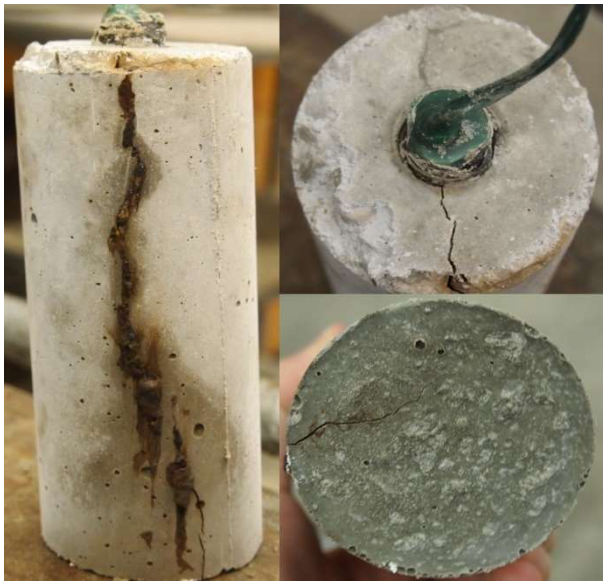

Figure C.45: RST 7.5-300 Batch – XM-28 AR 6.7 Corrosion Products Cracking the Concrete Specimen

Figure C.46: 7.5-300 Batch – Corrosion Products on XM-28 AR 6.7. From top to bottom, a) original specimen, b) & c) corrosion products on the specimen upon removal from concrete, and d) & e) pitting corrosion identification on the pickled specimen

Figure C.47: RST 7.5-300 Batch – XM-28 AR 6.8 Corrosion Products Cracking the Concrete Specimen

Figure C.48: 7.5-300 Batch – Corrosion Products on XM-28 AR 6.8. From top to bottom, a) original specimen, b) & c) corrosion products on the specimen upon removal from concrete, and d) & e) pitting corrosion identification on the pickled specimen

Figure C.49: 7.5-300 Batch – Corrosion Products on XM-28 AR 7.1. From top to bottom, a) original specimen, b) & c) corrosion products on the specimen upon removal from concrete, and d) & e) pitting corrosion identification on the pickled specimen. The slight staining at the top of the bar in a) is due to soldering flux.

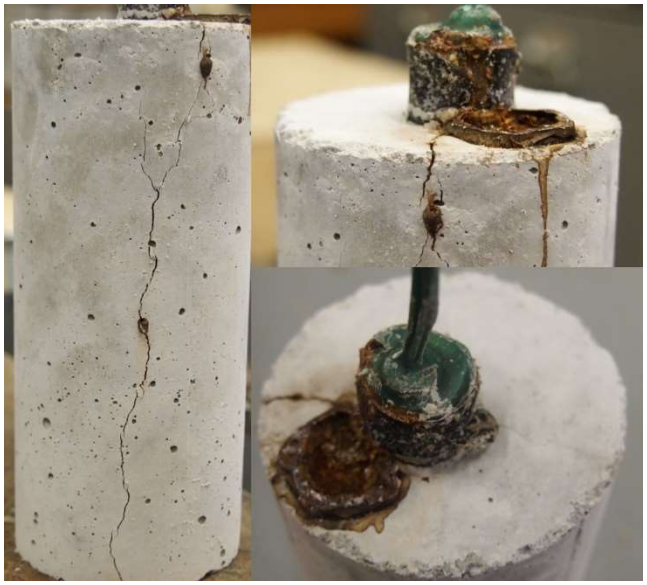

Figure C.50: RST 7.5-300 Batch – XM-28 AR 7.4 Corrosion Products Cracking the Concrete Specimen

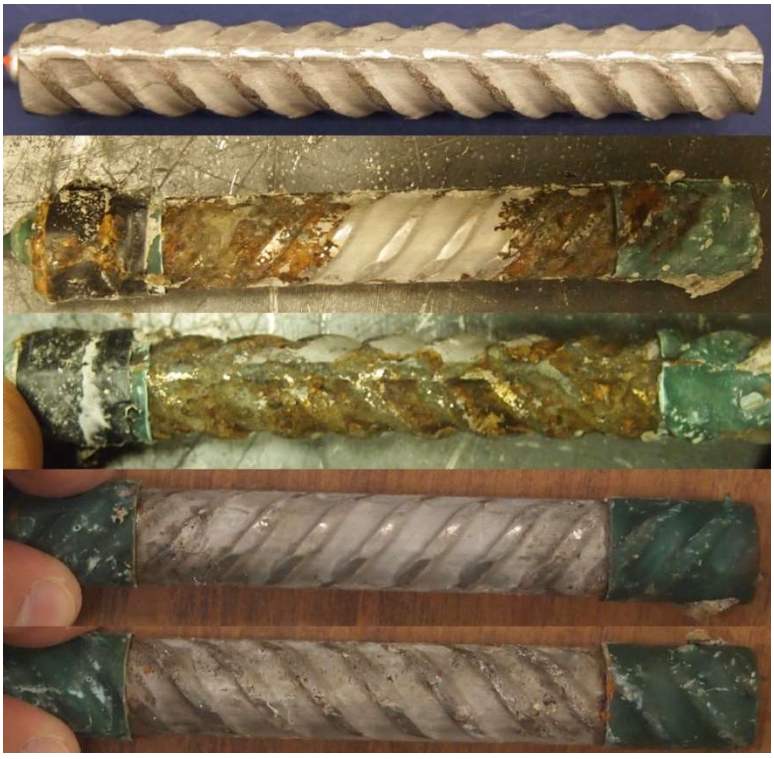

Figure C.51: 7.5-300 Batch – Corrosion Products on XM-28 AR 7.4. From top to bottom, a) original specimen, b) & c) corrosion products on the specimen upon removal from concrete, and d) & e) pitting corrosion identification on the pickled specimen

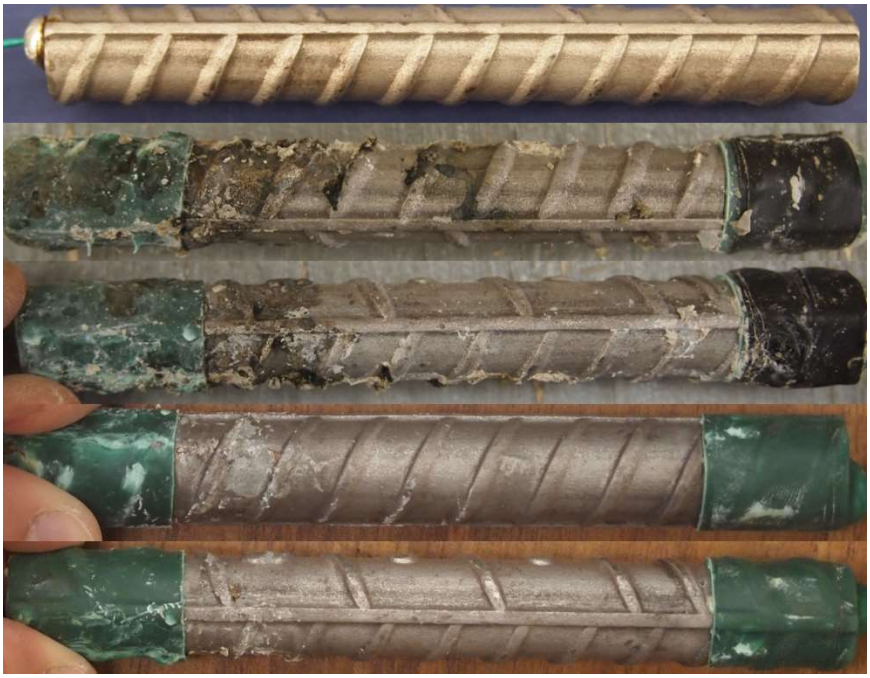

Figure C.52: 7.5-300 Batch – Corrosion Products on 2304 AR 6.3. From top to bottom, a) original specimen, b) & c) corrosion products on the specimen upon removal from concrete, and d) & e) pitting corrosion identification on the pickled specimen

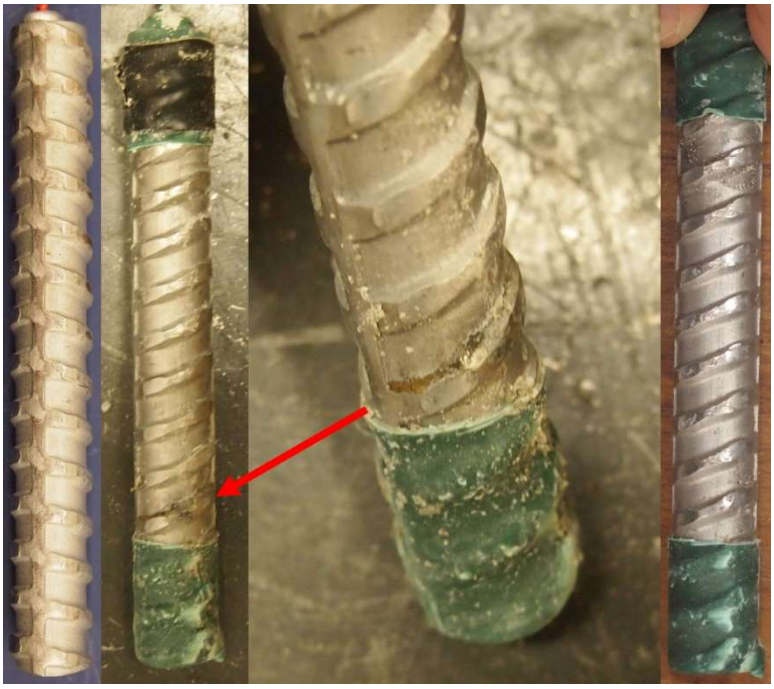

Figure C.53: 7.5-300 Batch – Corrosion Products on 2205 AR 6.4. From left to right, a) original specimen, b) & c) corrosion products on the specimen upon removal from concrete, and d) pitting corrosion identification on the pickled specimen

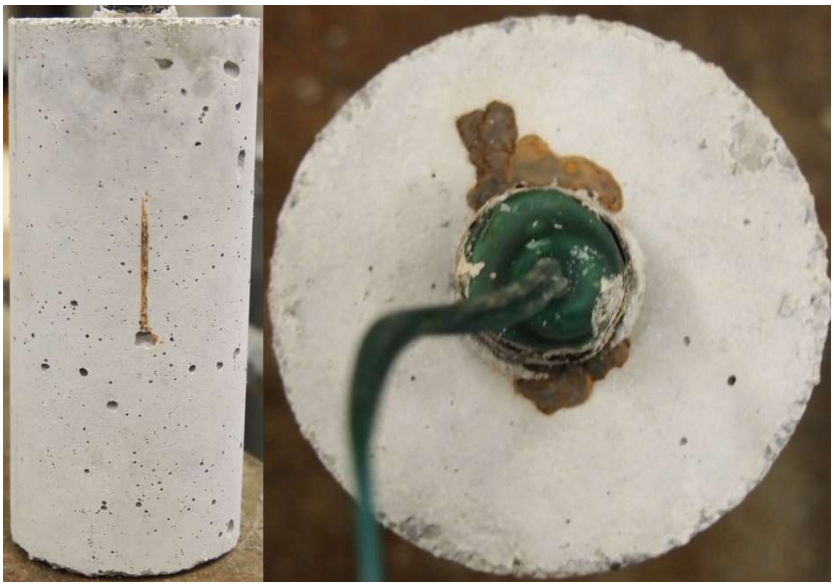

Figure C.54: RST 7.5-300 Batch – 2304 AR 6.4 Corrosion Products Cracking the Concrete Specimen

Figure C.55: 7.5-300 Batch – Corrosion Products on 2304 AR 6.4. From top to bottom, a) original specimen, b) & c) corrosion products on the specimen upon removal from concrete, and d) & e) pitting corrosion identification on the pickled specimen

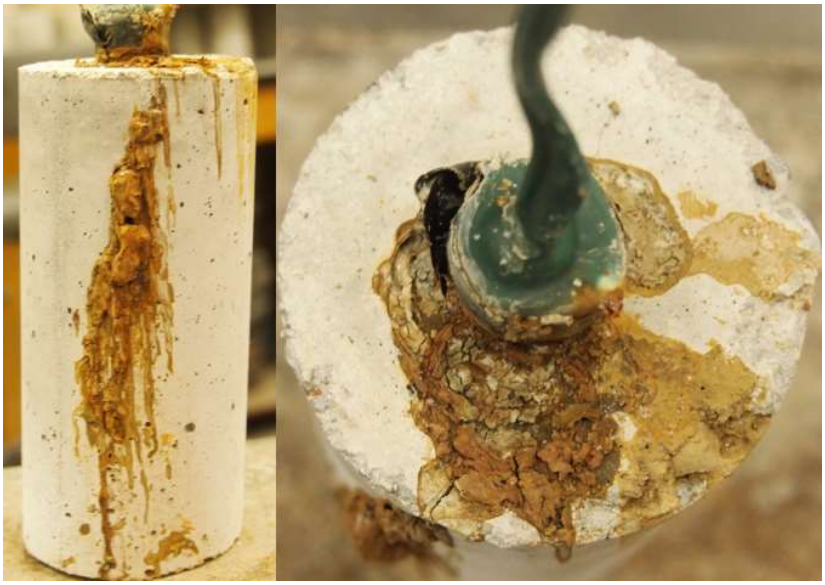

Figure C.56: RST 7.5-400 Batch – 2304 AR 7.1 Corrosion Products causing Cracking of Concrete Specimen

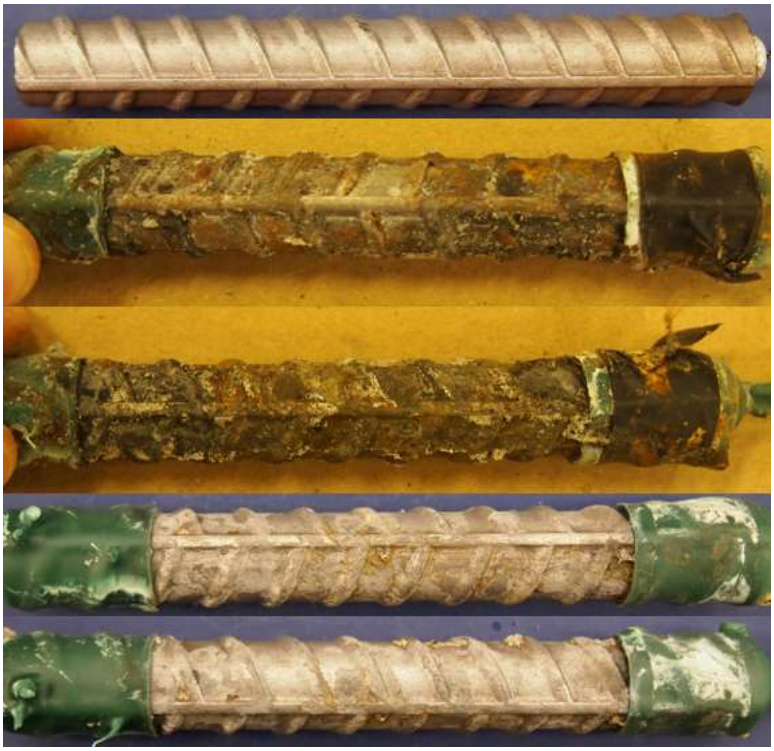

Figure C.57: 7.5-400 Batch – Corrosion Products on 2304 AR 7.1. From top to bottom, a) original specimen, b) & c) corrosion products on the specimen upon removal from concrete, and d) & e) pitting corrosion identification on the pickled specimen. The slight staining at the top of the bar in a) is due to soldering flux.

Figure C.58: RST 7.5-400 Batch – 2304 AR 7.2 Corrosion Products causing Cracking of Concrete Specimen

Figure C.59: 7.5-400 Batch – Corrosion Products on 2304 AR 7.2. From top to bottom, a) original specimen, b) & c) corrosion products on the specimen upon removal from concrete, and d) & e) pitting corrosion identification on the pickled specimen

Figure C.60: RST 7.5-400 Batch – XM-28 AR 8.1 Corrosion Products causing Cracking of Concrete Specimen

Figure C.61: 7.5-400 Batch – Corrosion Products on XM-28 AR 8.1. From top to bottom, a) original specimen, b) & c) corrosion products on the specimen upon removal from concrete, and d) & e) pitting corrosion identification on the pickled specimen

Figure C.62: RST 7.5-400 Batch – XM-28 AR 8.2 Corrosion Products causing Cracking of Concrete Specimen

Figure C.63: 7.5-400 Batch – Corrosion Products on XM-28 AR 8.2. From top to bottom, a) original specimen, b) & c) corrosion products on the specimen upon removal from concrete, and d) & e) pitting corrosion identification on the pickled specimen

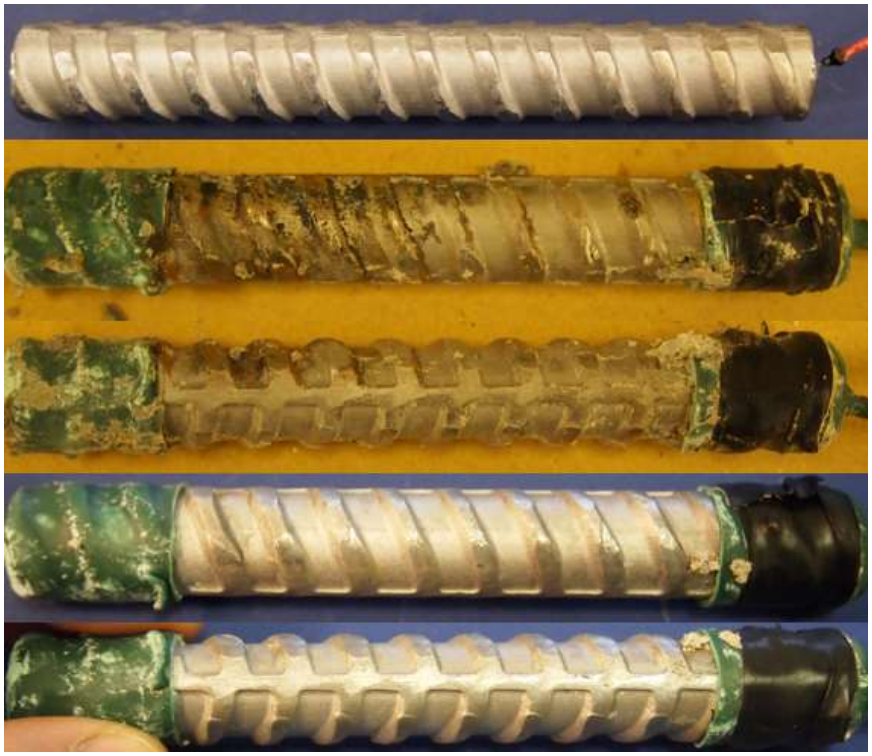

Figure C.64: 7.5-400 Batch – Corrosion Products on 2205 AR 7.3. From top to bottom, a) original specimen, b) & c) corrosion products on the specimen upon removal from concrete, and d) & e) pitting corrosion identification on the pickled specimen

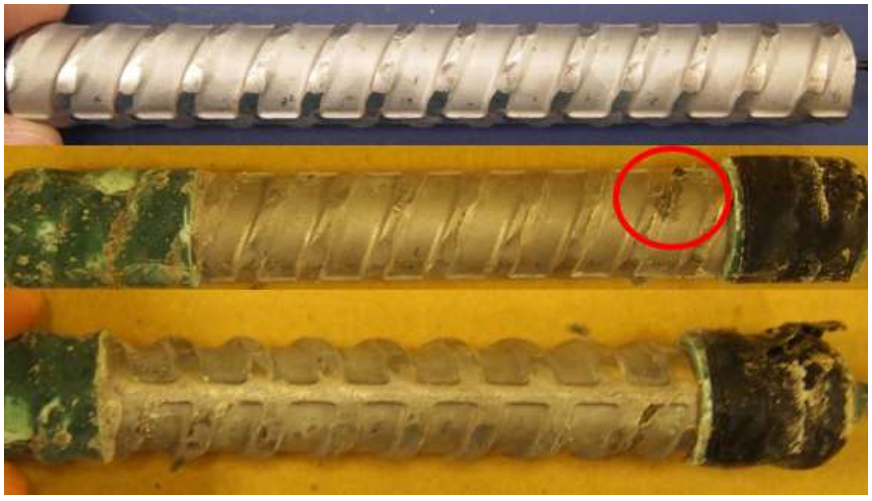

Figure C.65: 7.5-400 Batch – Corrosion Products on 2205 AR 7.4. From top to bottom, a) original specimen, and b) & c) corrosion products on the specimen after removal from concrete

Figure C.66: RST 7.5-400 Batch – 2304 AR 7.3 Corrosion Products causing Cracking of Concrete Specimen

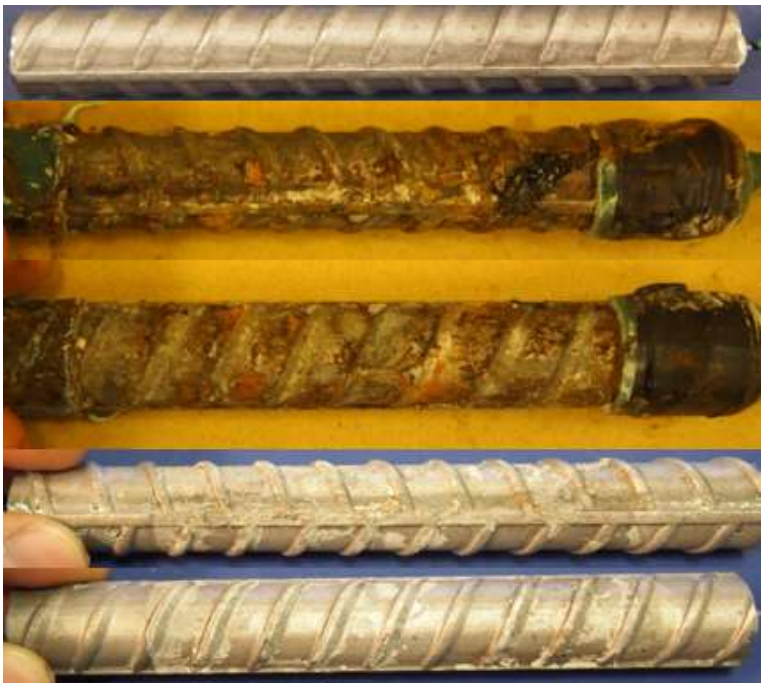

Figure C.67: 7.5-400 Batch – Corrosion Products on 2304 AR 7.3. From top to bottom, a) original specimen, b) & c) corrosion products on the specimen upon removal from concrete, and d) & e) pitting corrosion identification on the pickled specimen

Figure C.68: RST 7.5-400 Batch – 2304 AR 7.4 Corrosion Products causing Cracking of Concrete Specimen

Figure C.69: 7.5-400 Batch – Corrosion Products on 2304 AR 7.4. From top to bottom, a) original specimen, b) & c) corrosion products on the specimen upon removal from concrete, and d) & e) pitting corrosion identification on the pickled specimen

Figure C.70: RST 7.5-400 Batch – XM-28 AR 8.3 Corrosion Products causing Cracking of Concrete Specimen

Figure C.71: 7.5-400 Batch – Corrosion Products on XM-28 AR 8.3. From top to bottom, a) original specimen, b) & c) corrosion products on the specimen upon removal from concrete, and d) & e) pitting corrosion identification on the pickled specimen

Figure C.72: RST 7.5-400 Batch – XM-28 AR 8.4 Corrosion Products causing Cracking of Concrete Specimen

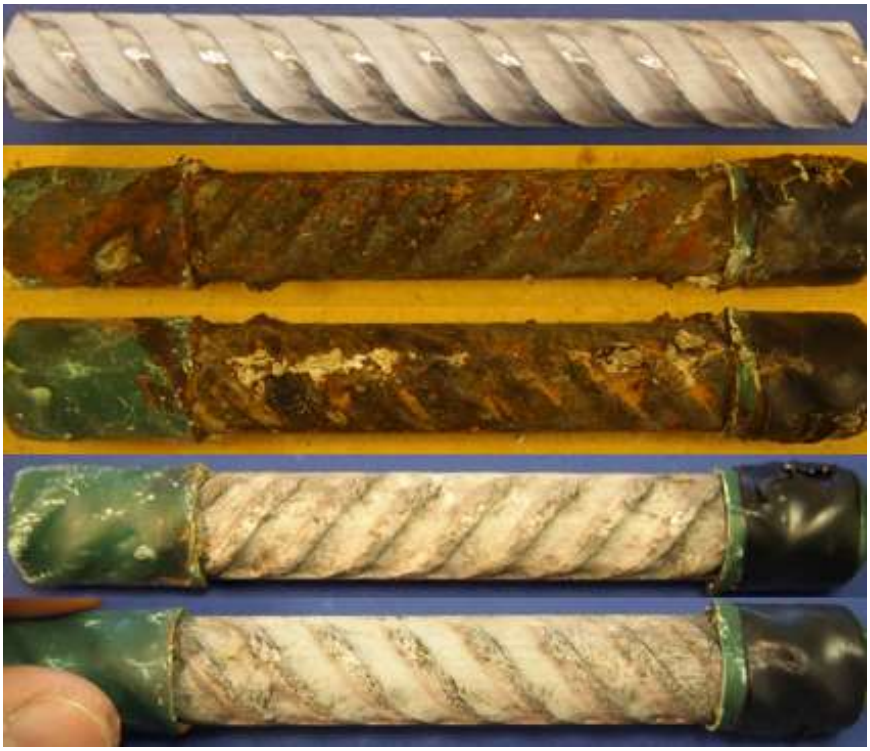

Figure C.73: 7.5-400 Batch – Corrosion Products on XM-28 AR 8.4. From top to bottom, a) original specimen, b) & c) corrosion products on the specimen upon removal from concrete, and d) & e) pitting corrosion identification on the pickled specimen

Figure C.74: 7.5-400 Batch – Corrosion Products on 2205 AR 7.6. From top to bottom, a) original specimen, b) & c) corrosion products on the specimen upon removal from concrete, and d) & e) pitting corrosion identification on the pickled specimen

Figure C.75: RST 7.5-400 Batch – 2304 AR 7.5 Corrosion Products causing Cracking of Concrete Specimen

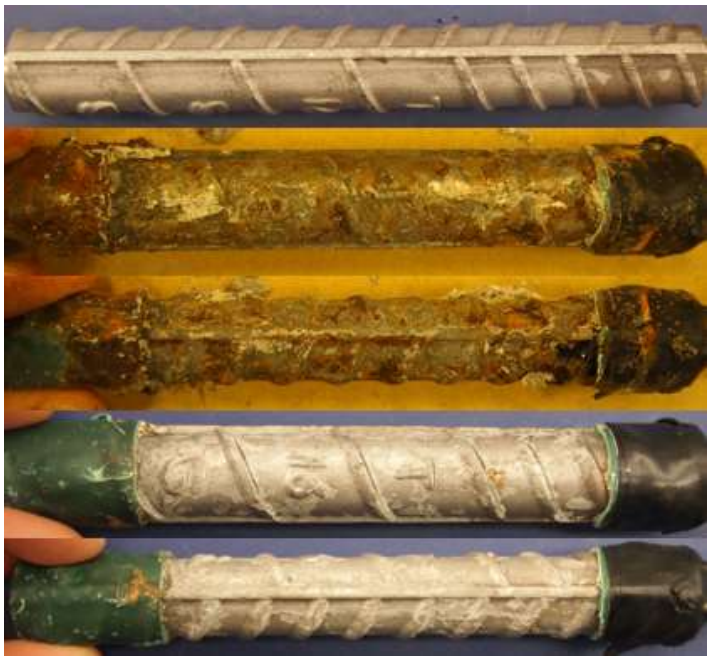

Figure C.76: 7.5-400 Batch – Corrosion Products on 2304 AR 7.5. From top to bottom, a) original specimen, b) & c) corrosion products on the specimen upon removal from concrete, and d) & e) pitting corrosion identification on the pickled specimen

Figure C.77: RST 7.5-400 Batch – 2304 AR 7.6 Corrosion Products causing Cracking of Concrete Specimen

Figure C.78: 7.5-400 Batch – Corrosion Products on 2304 AR 7.6. From top to bottom, a) original specimen, b) & c) corrosion products on the specimen upon removal from concrete, and d) & e) pitting corrosion identification on the pickled specimen

Figure C.79: RST 7.5-400 Batch – XM-28 AR 8.5 Corrosion Products causing Cracking of Concrete Specimen

Figure C.80: 7.5-400 Batch – Corrosion Products on XM-28 AR 8.5. From top to bottom, a) original specimen, b) & c) corrosion products on the specimen upon removal from concrete, and d) & e) pitting corrosion identification on the pickled specimen. The slight staining at the top of the bar in a) is due to soldering flux.

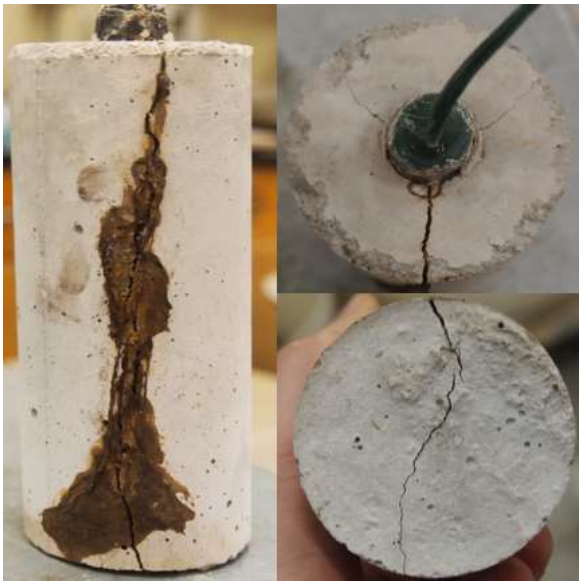

Figure C.81: RST 7.5-400 Batch – XM-28 AR 8.6 Corrosion Products causing Cracking of Concrete Specimen

Figure C.82: 7.5-400 Batch – Corrosion Products on XM-28 AR 8.6. From top to bottom, a) original specimen, b) & c) corrosion products on the specimen upon removal from concrete, and d) & e) pitting corrosion identification on the pickled specimen. The slight staining at the top of the bar in a) is due to soldering flux.

Appendix D
Rapid Screening Test Photomicrographs

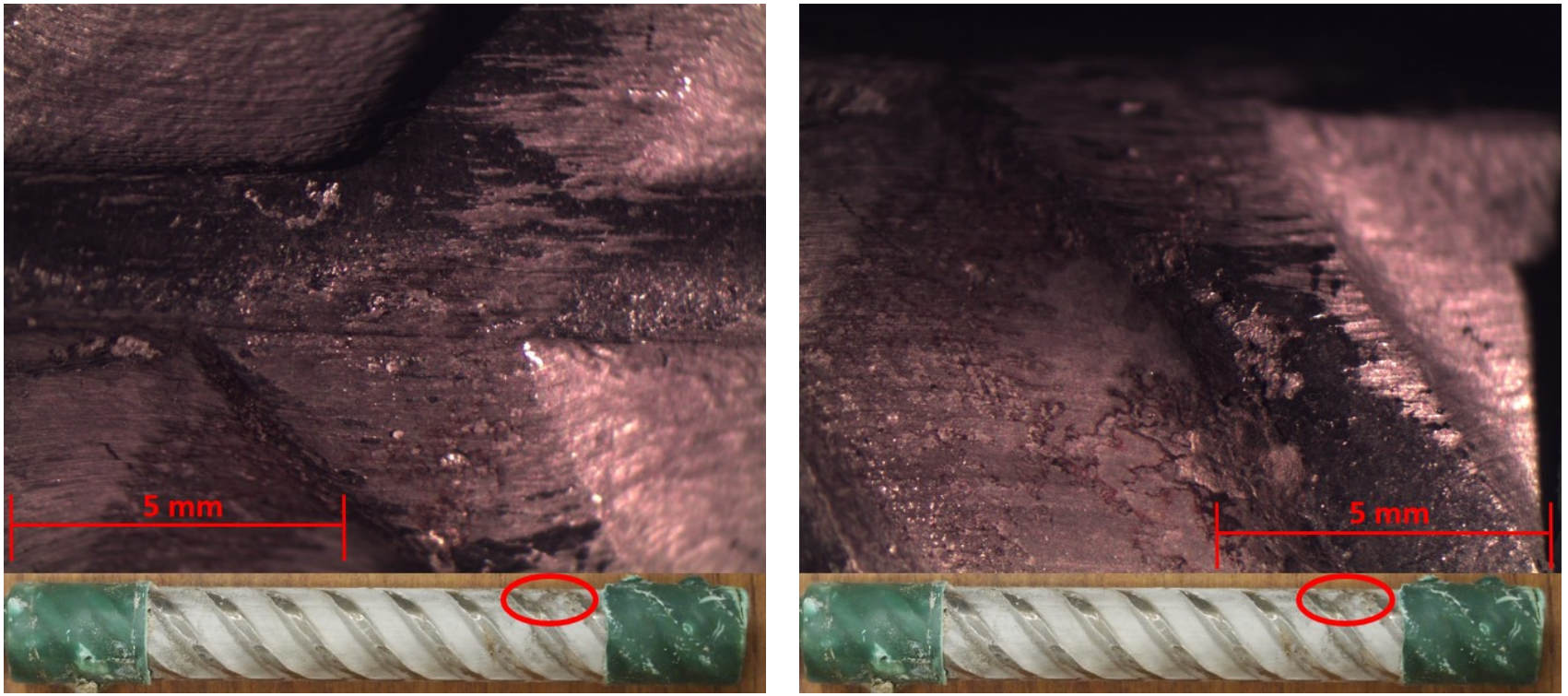

Figure D.1: RST Batch 4-400 Photomicrographs: a) pickled XM-28 AR 7.5.

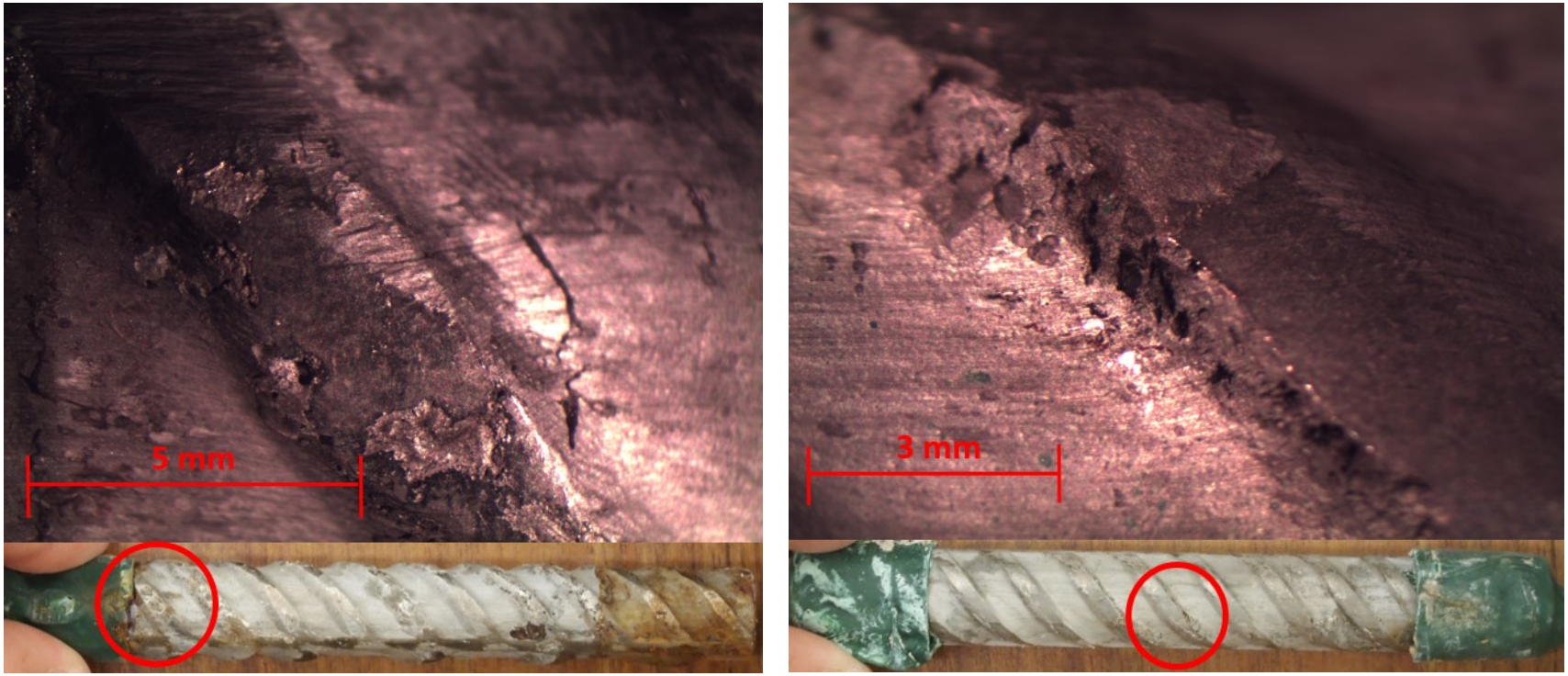

Figure D.2: RST Batch 4-400 Photomicrographs: a) pickled XM-28 AR 7.6 and b) pickled XM-28 AR 7.7. Staining from corrosion products observed underneath the lacquer on XM-28 AR 7.6

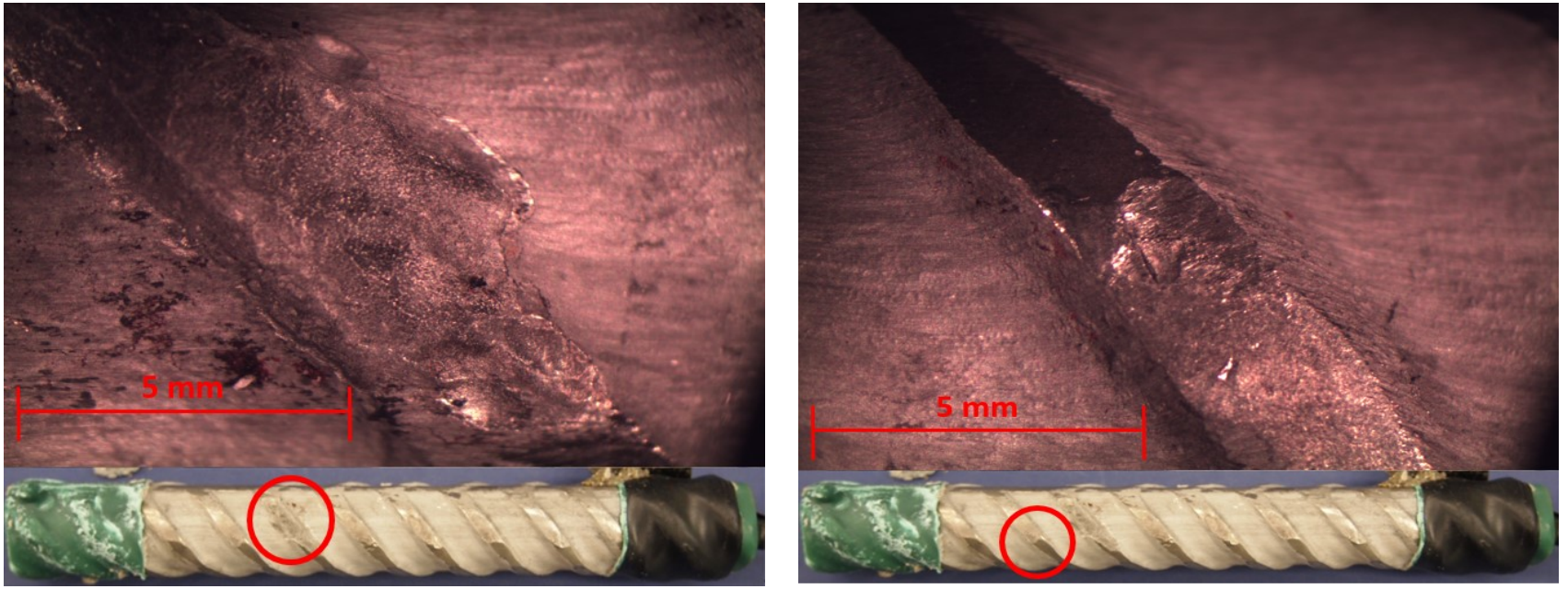

Figure D.3: RST Batch 6-200 Photomicrographs: pickled XM-28 AR 5.2

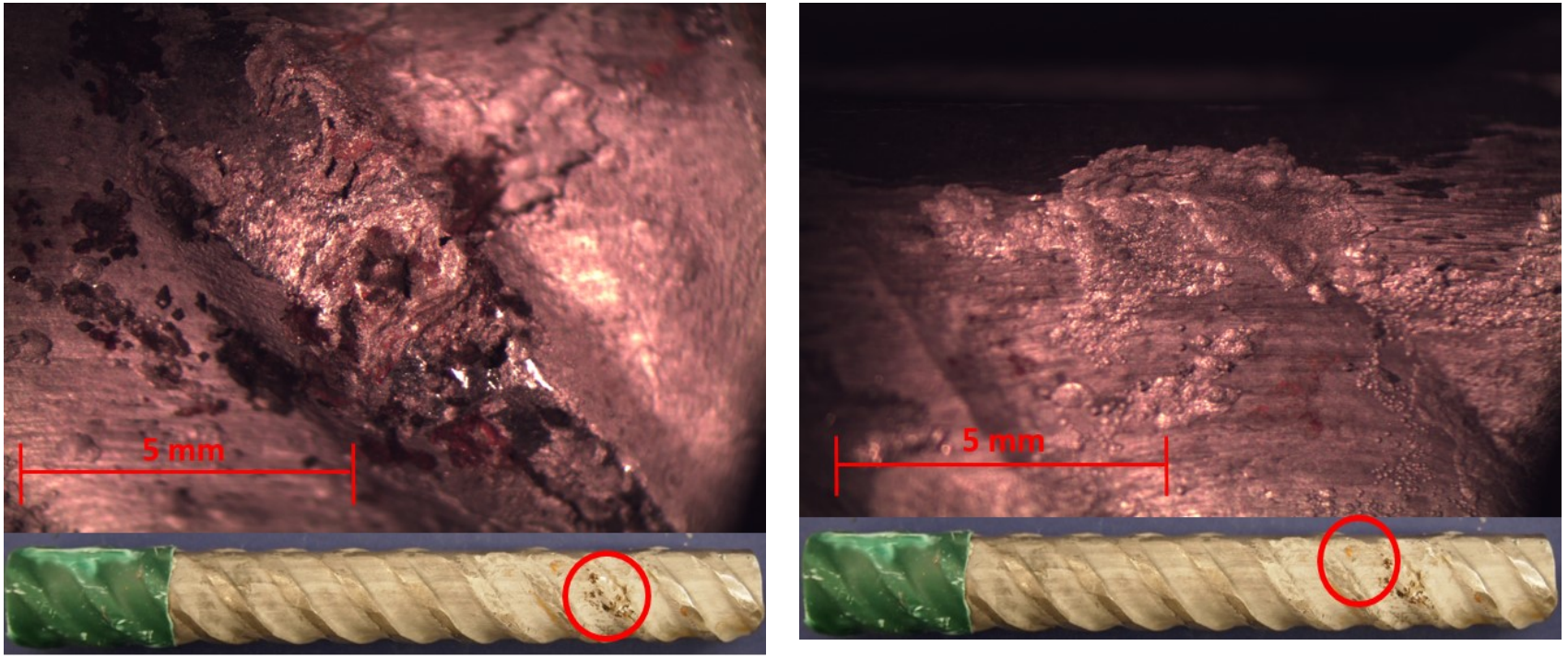

Figure D.4: RST Batch 6-300 Photomicrographs: pickled XM-28 AR 5.4

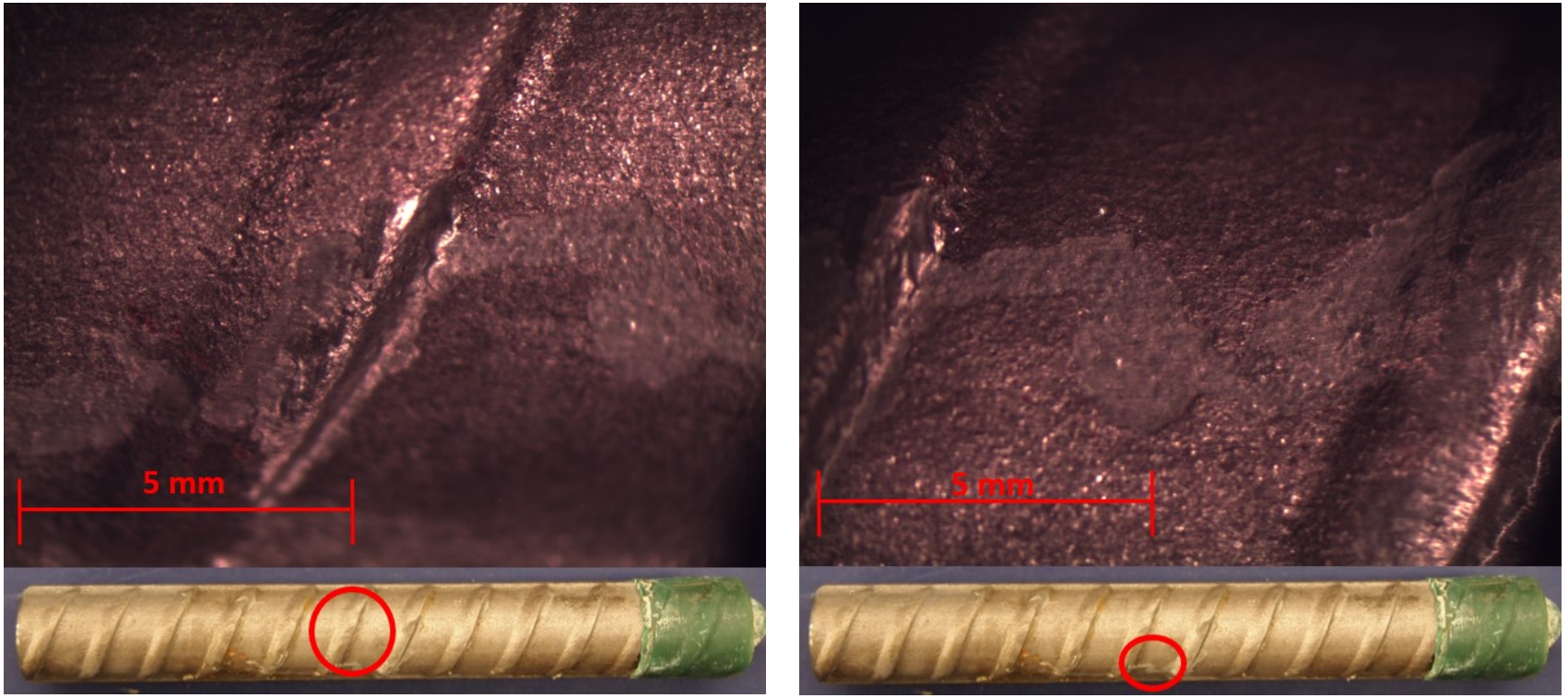

Figure D.5: RST Batch 6-300 Photomicrographs: pickled 2304 AR 4.3

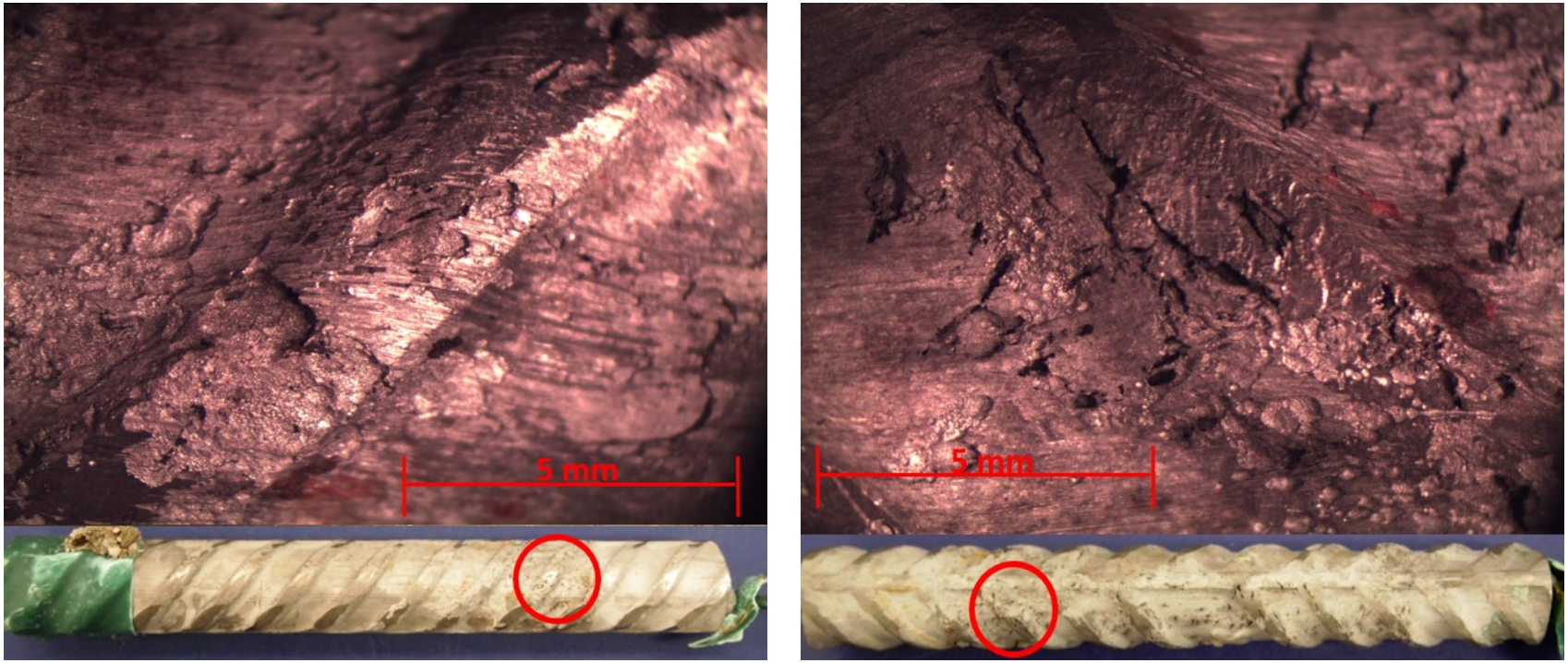

Figure D.6: RST Batch 6-400 Photomicrographs: a) pickled XM-28 AR 6.1 and b) pickled XM-28 AR 6.2

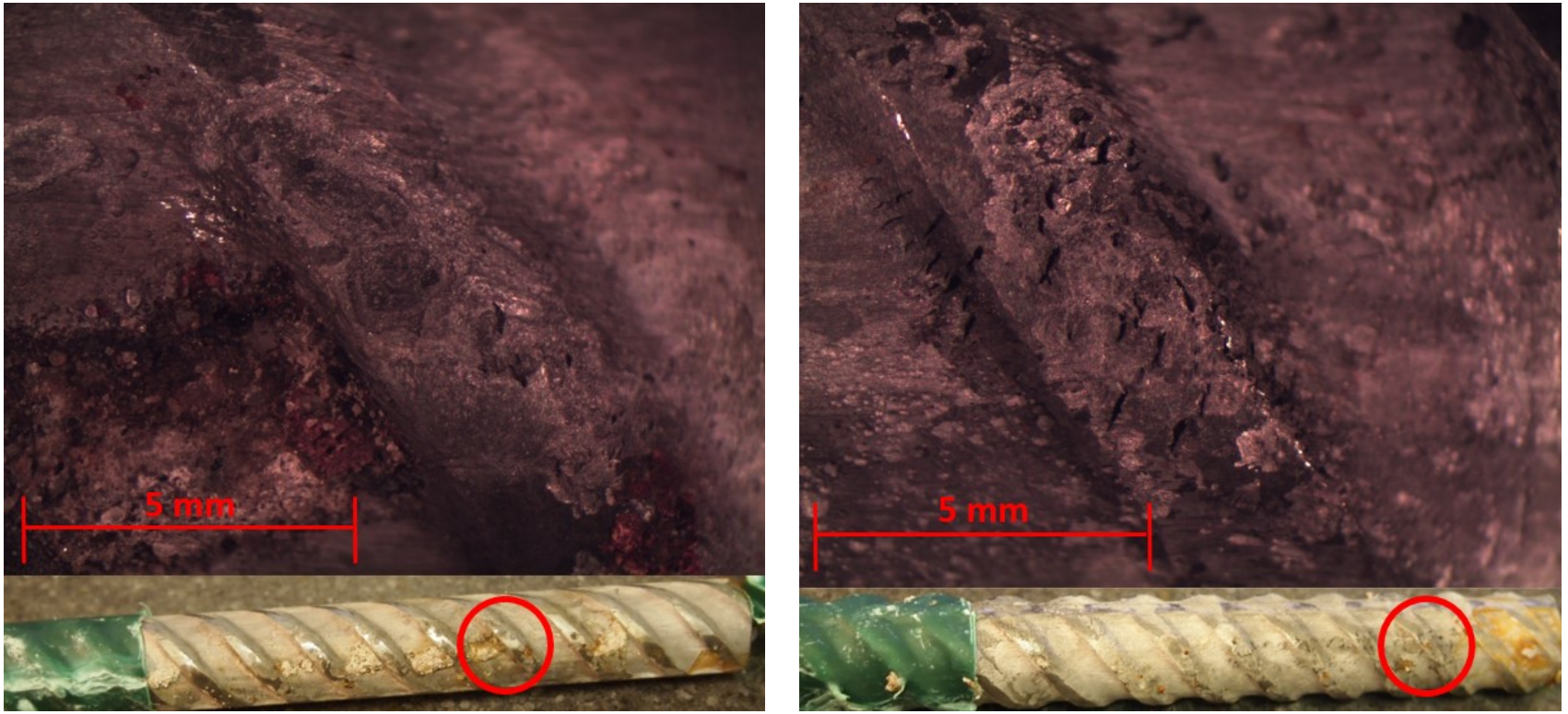

Figure D.7: RST Batch 6-400 Photomicrographs: a) pickled XM-28 AR 6.3 and b) pickled XM-28 AR 6.4. Staining from corrosion products observed underneath the lacquer on XM-28 AR 6.4

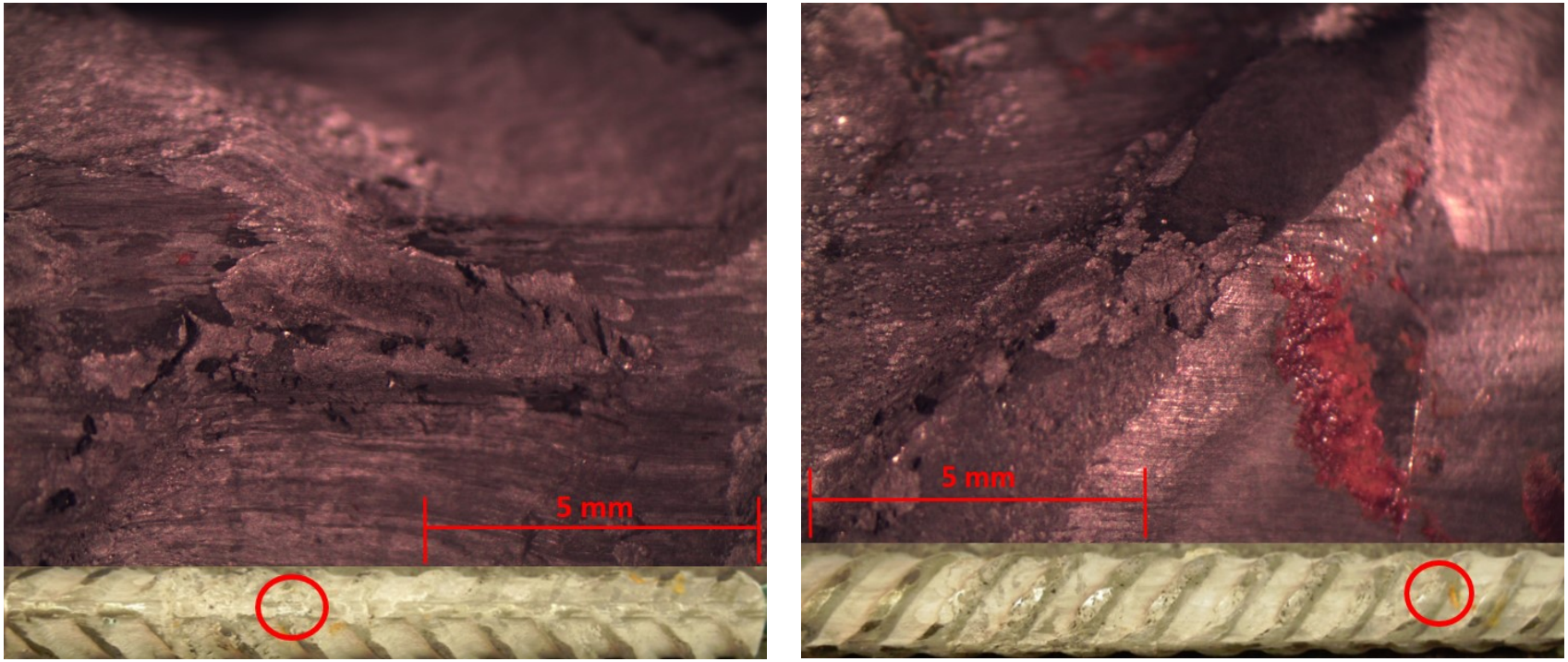

Figure D.8: RST Batch 6-400 Photomicrographs: pickled XM-28 AR 6.5

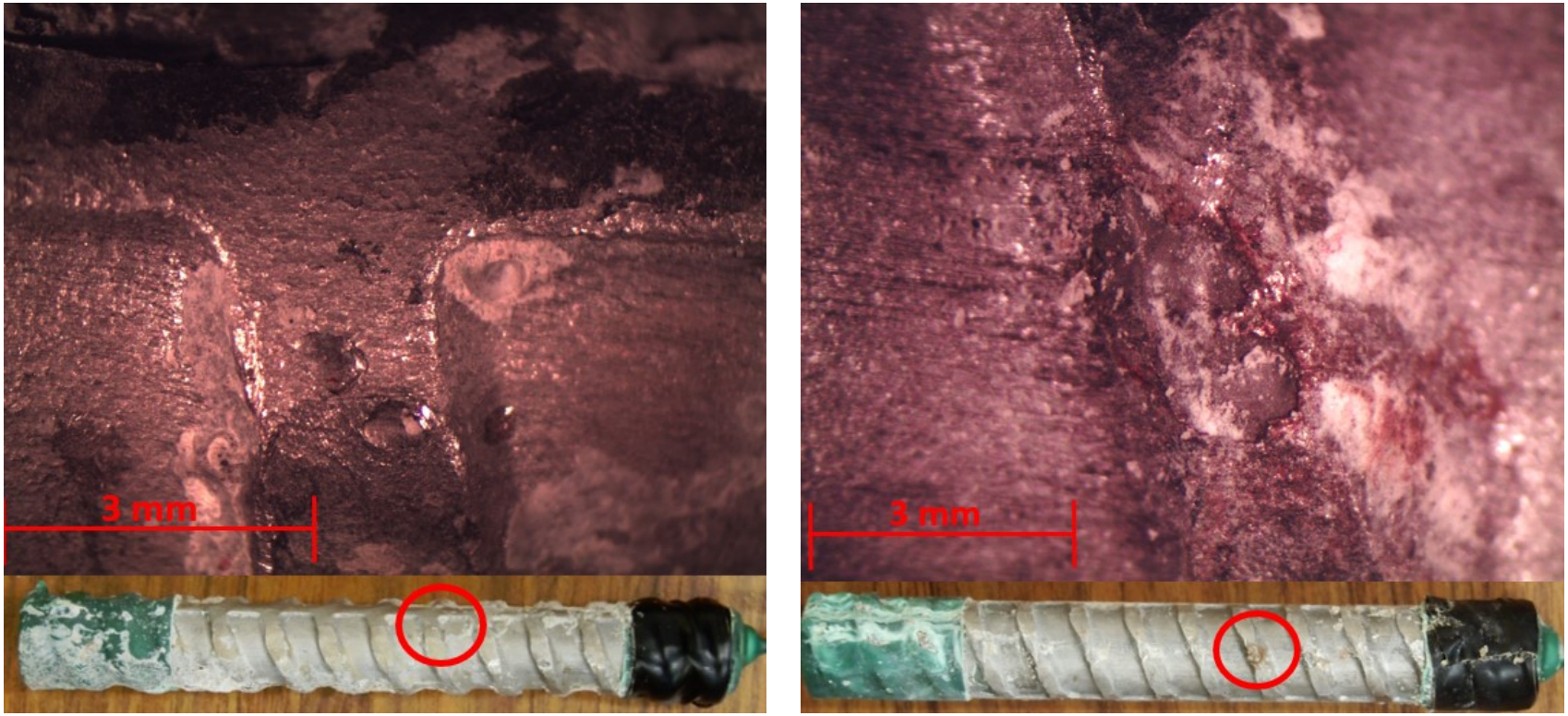

Figure D.9: RST Batch 6-400 Photomicrographs: a) pickled 2205 AR 5.4 and b) pickled 2205 AR 5.5

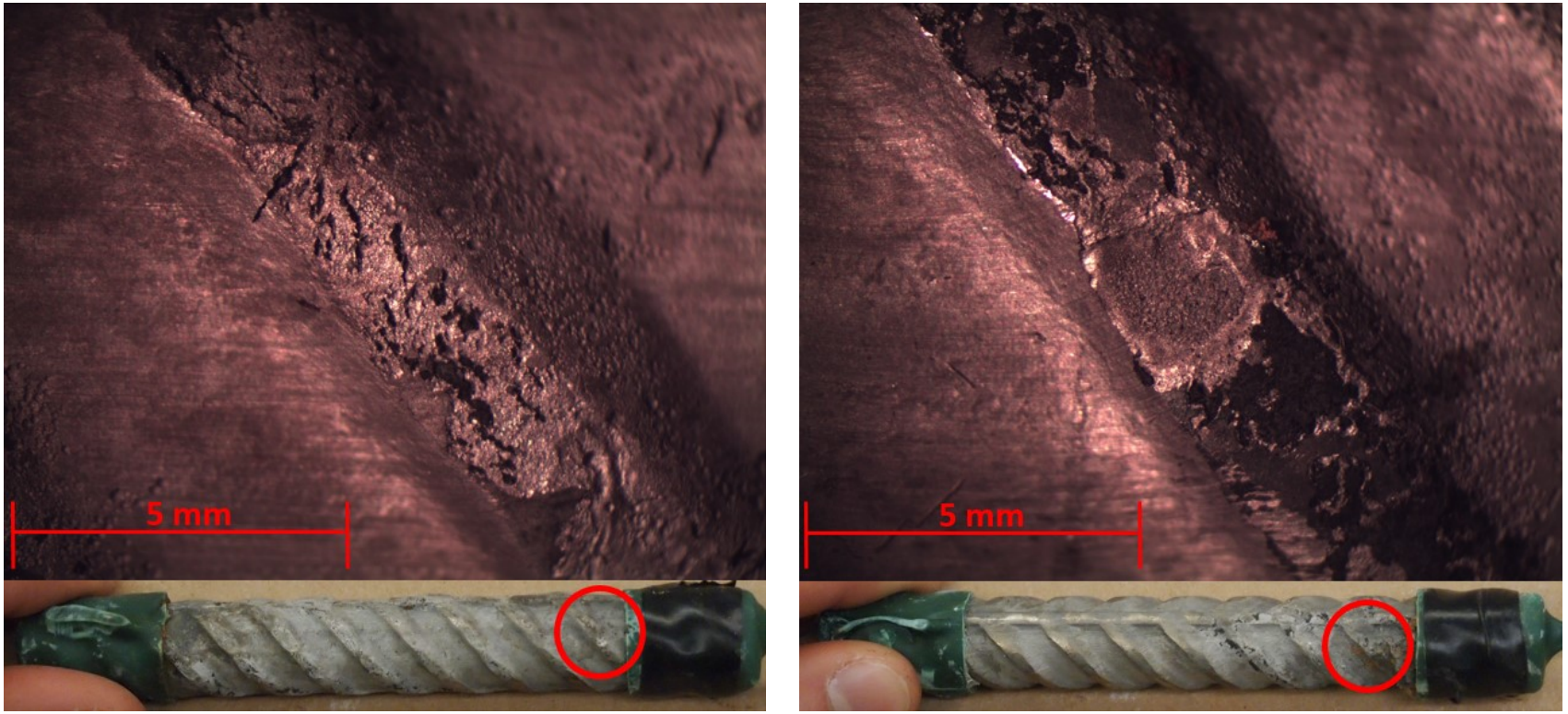

Figure D.10: RST Batch 7.5-200 Photomicrographs: a) pickled XM-28 AR 8.7 and b) pickled XM-28 AR 8.8

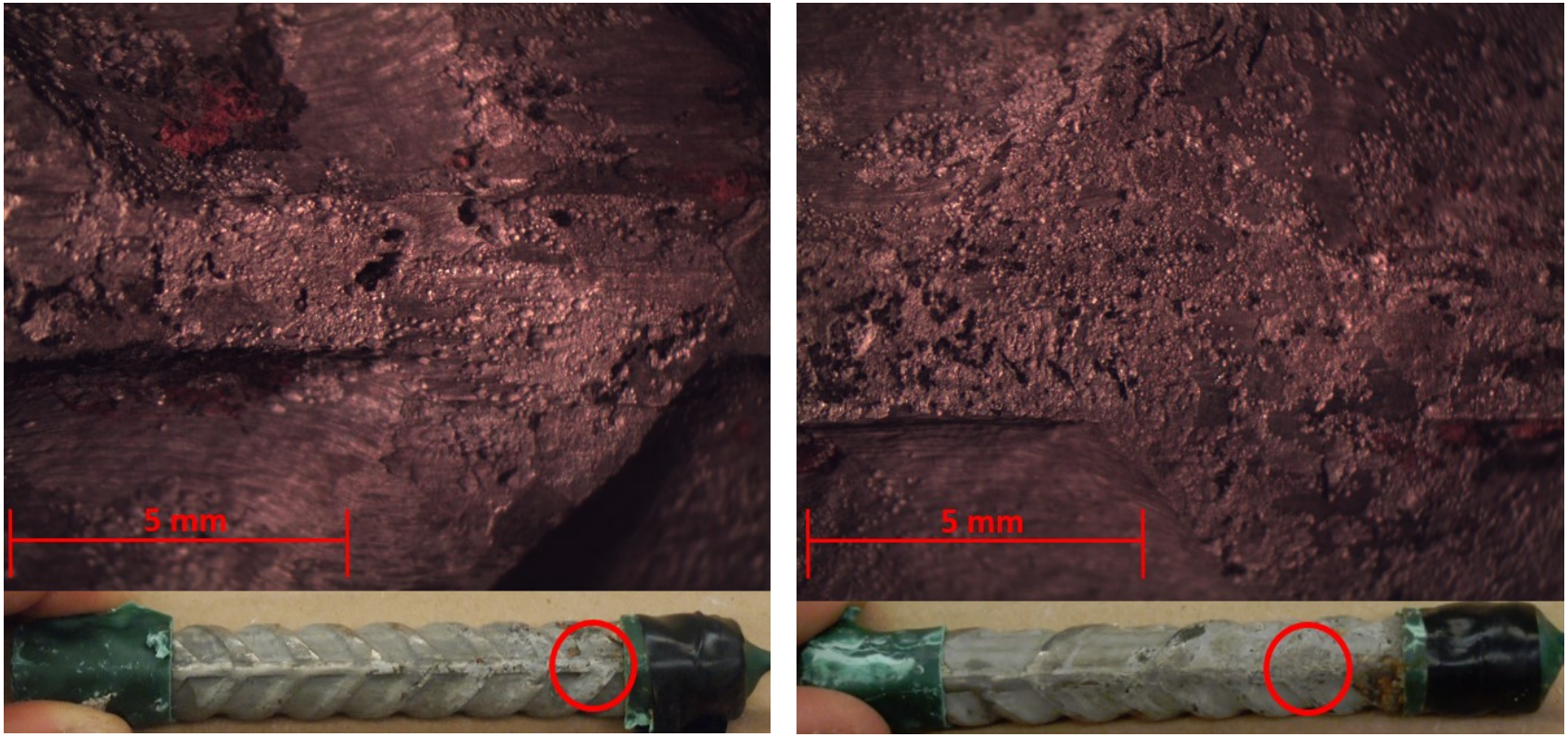

Figure D.11: RST Batch 7.5-200 Photomicrographs: a) pickled XM-28 AR 8.9 and b) pickled XM-28 AR 9.0

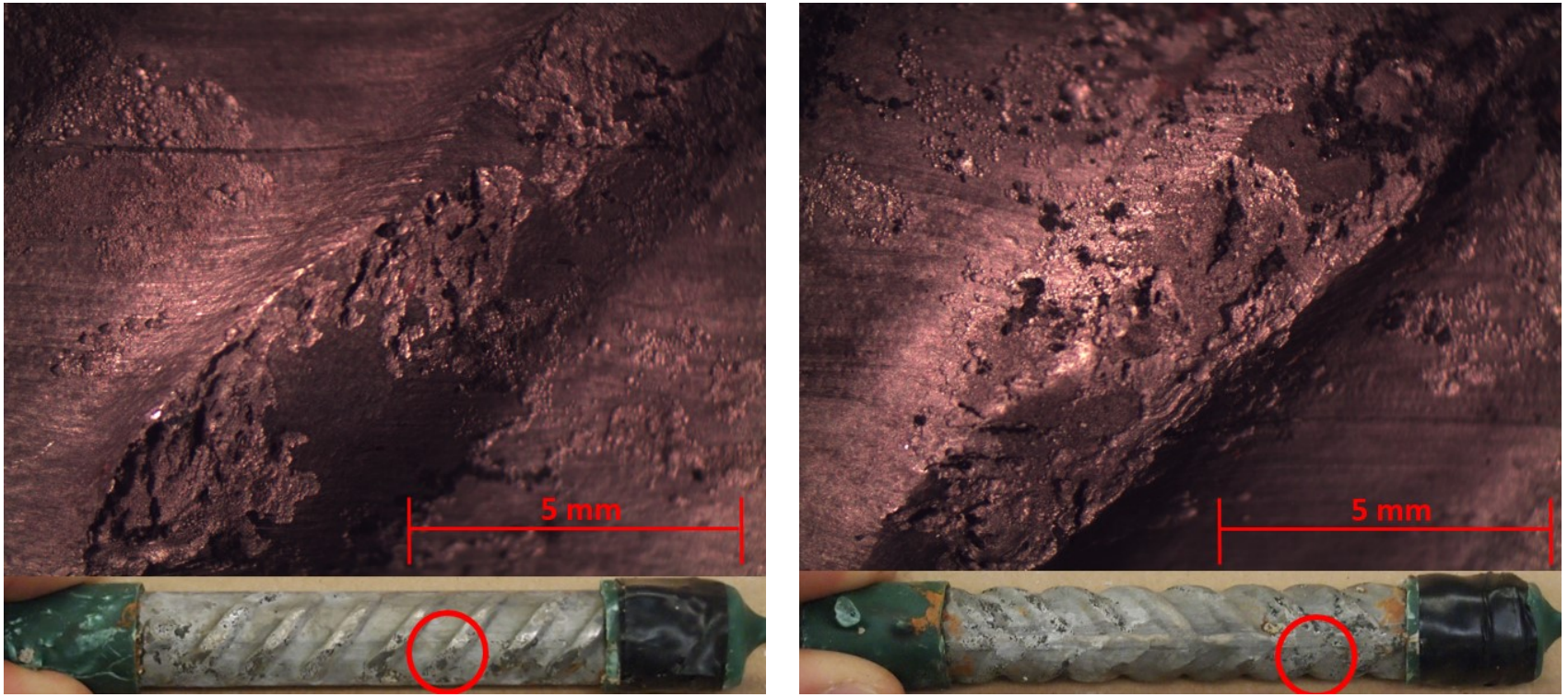

Figure D.12: RST Batch 7.5-200 Photomicrographs: a) pickled XM-28 AR 9.1 and b) pickled XM-28 AR 9.2

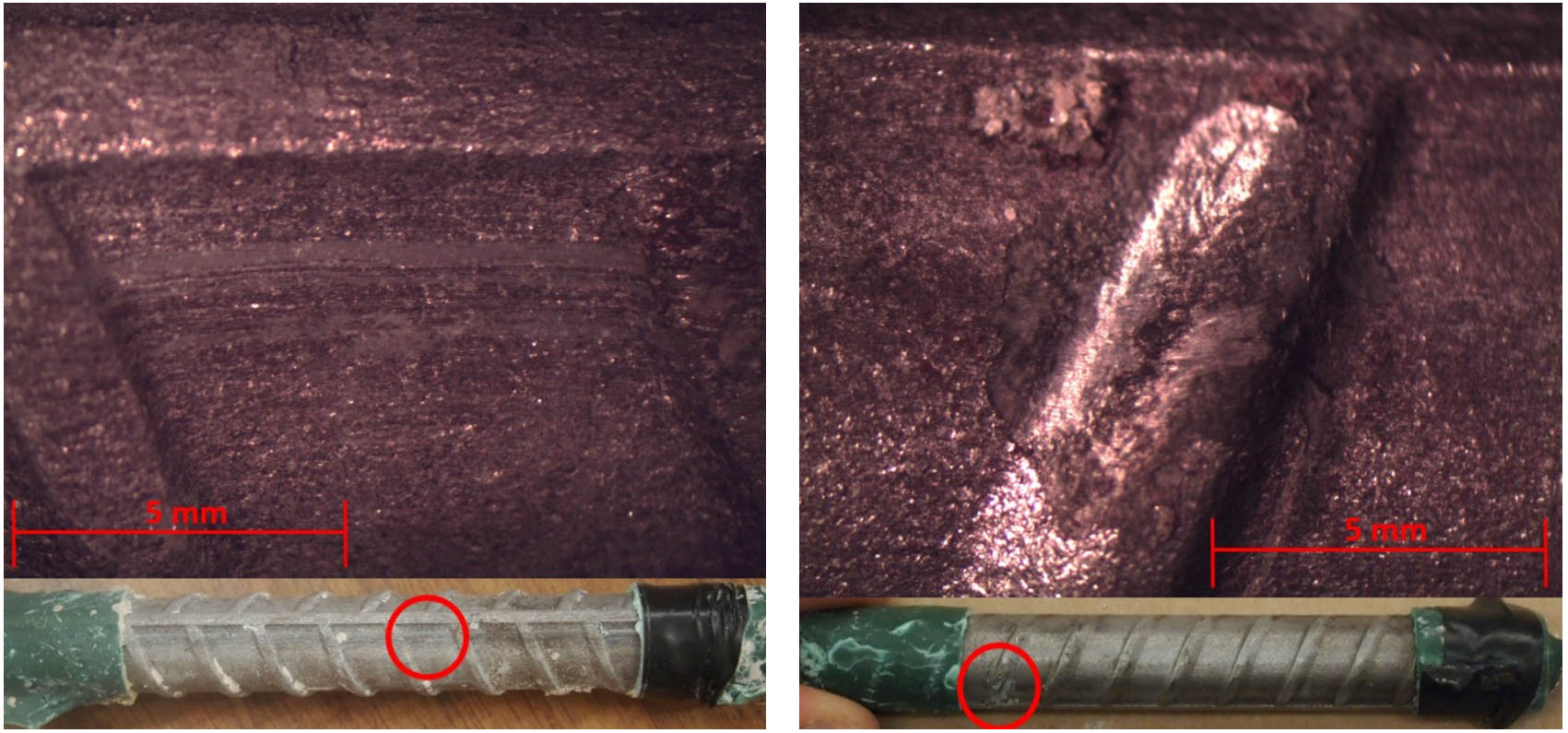

Figure D.13: RST Batch 7.5-200 Photomicrographs: a) pickled 2304 AR 7.7 and b) pickled 2304 AR 7.8

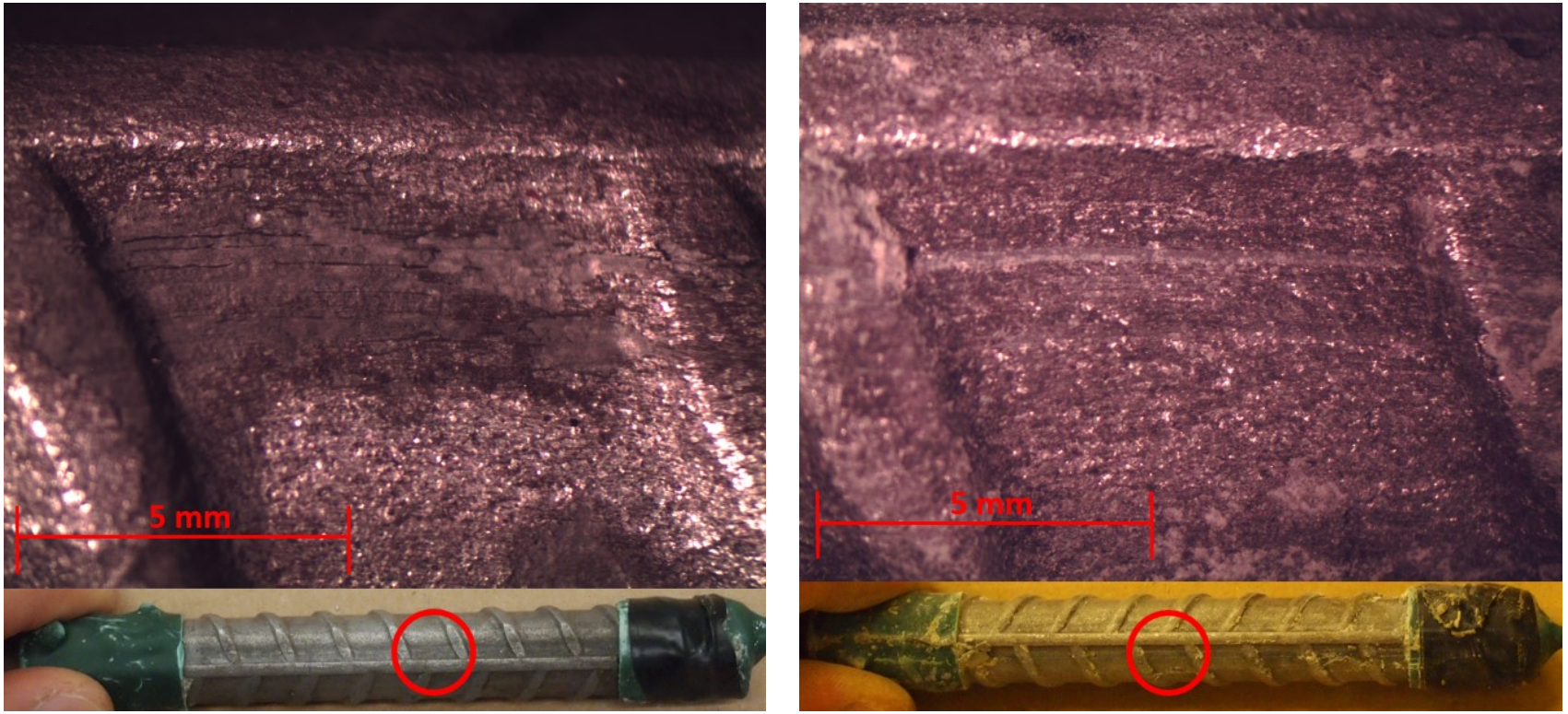

Figure D.14: RST Batch 7.5-200 Photomicrographs: a) pickled 2304 AR 7.9 and b) pickled 2304 AR 8.0

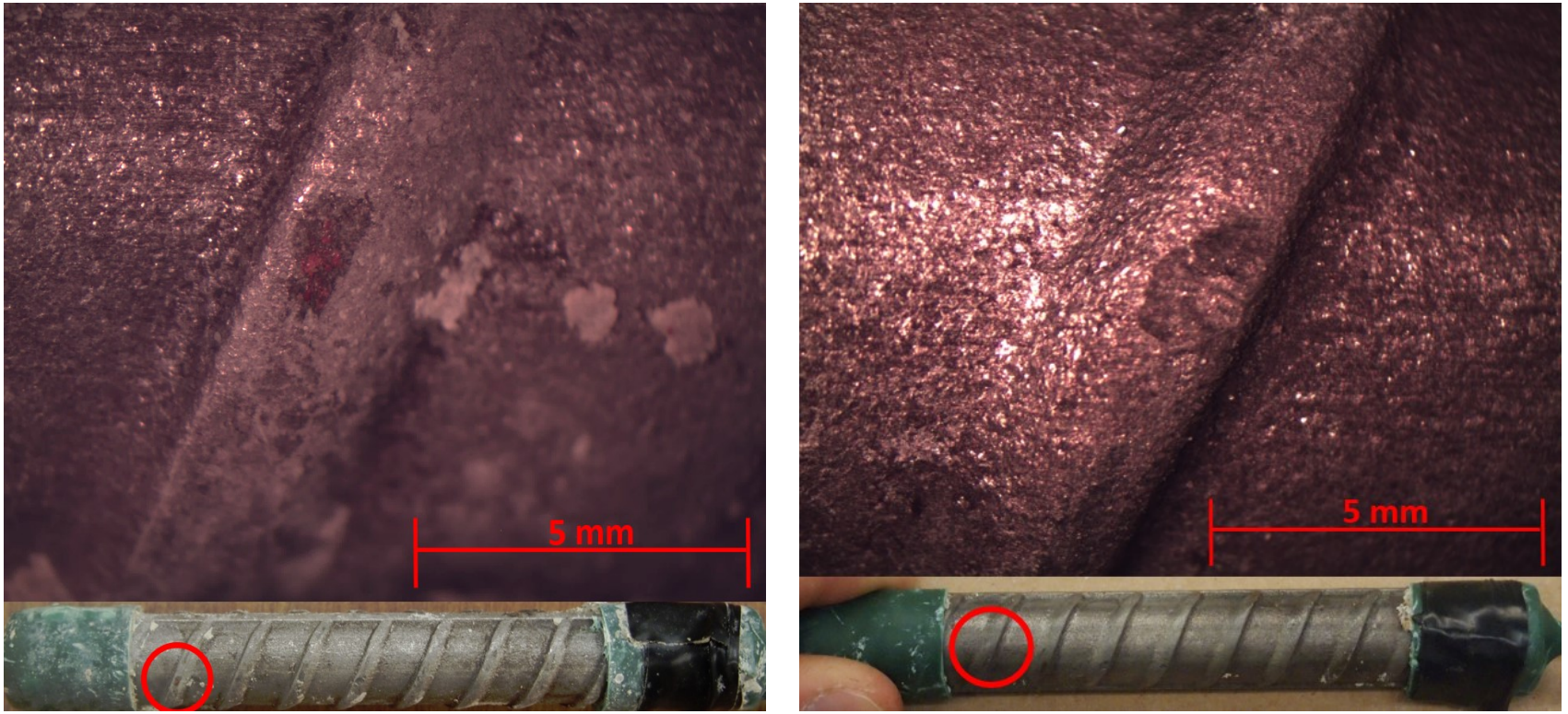

Figure D.15: RST Batch 7.5-200 Photomicrographs: a) corroded 2304 AR 8.1 and b) pickled 2304 AR 8.2.

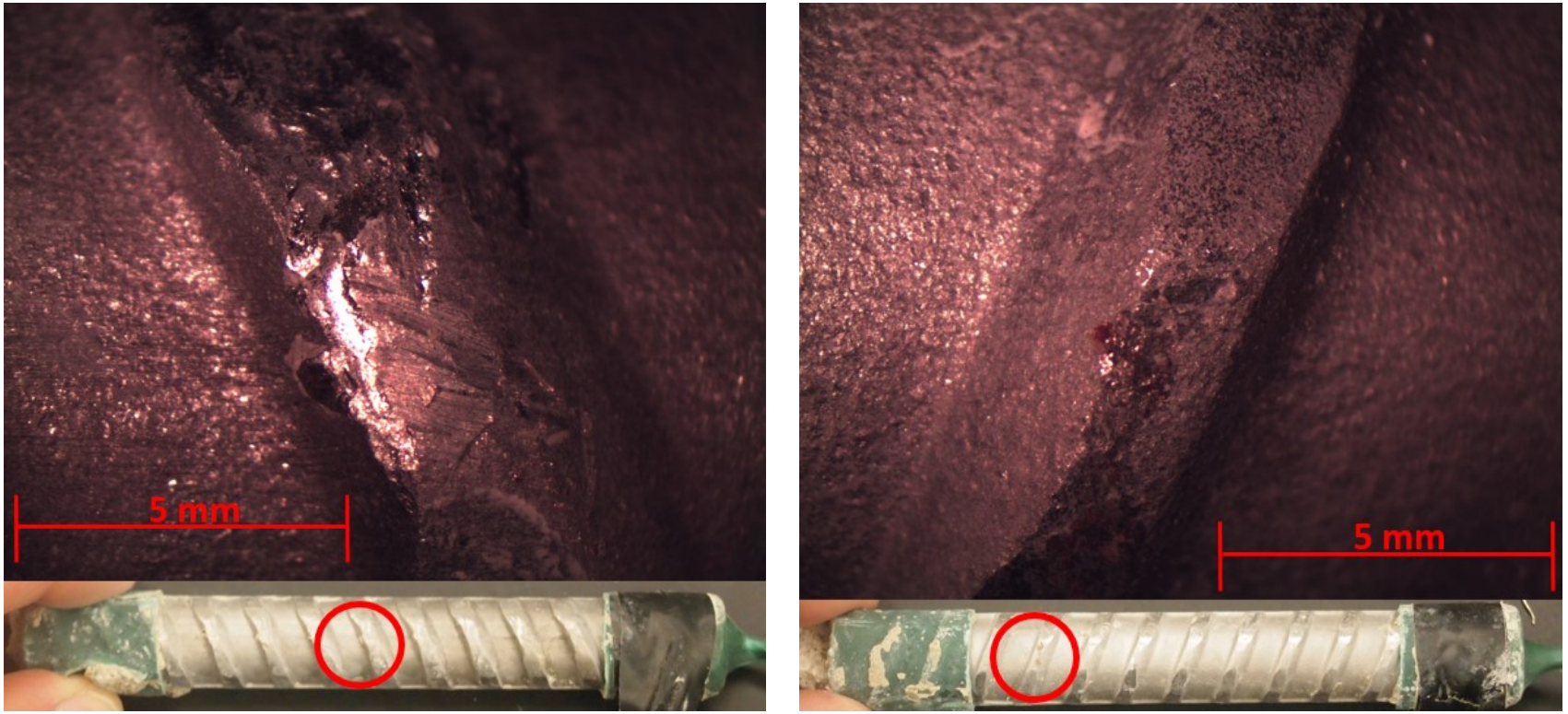

Figure D.16: RST Batch 7.5-200 Photomicrographs: a) pickled 2205 AR 7.7 and b) pickled 2205 AR 7.8

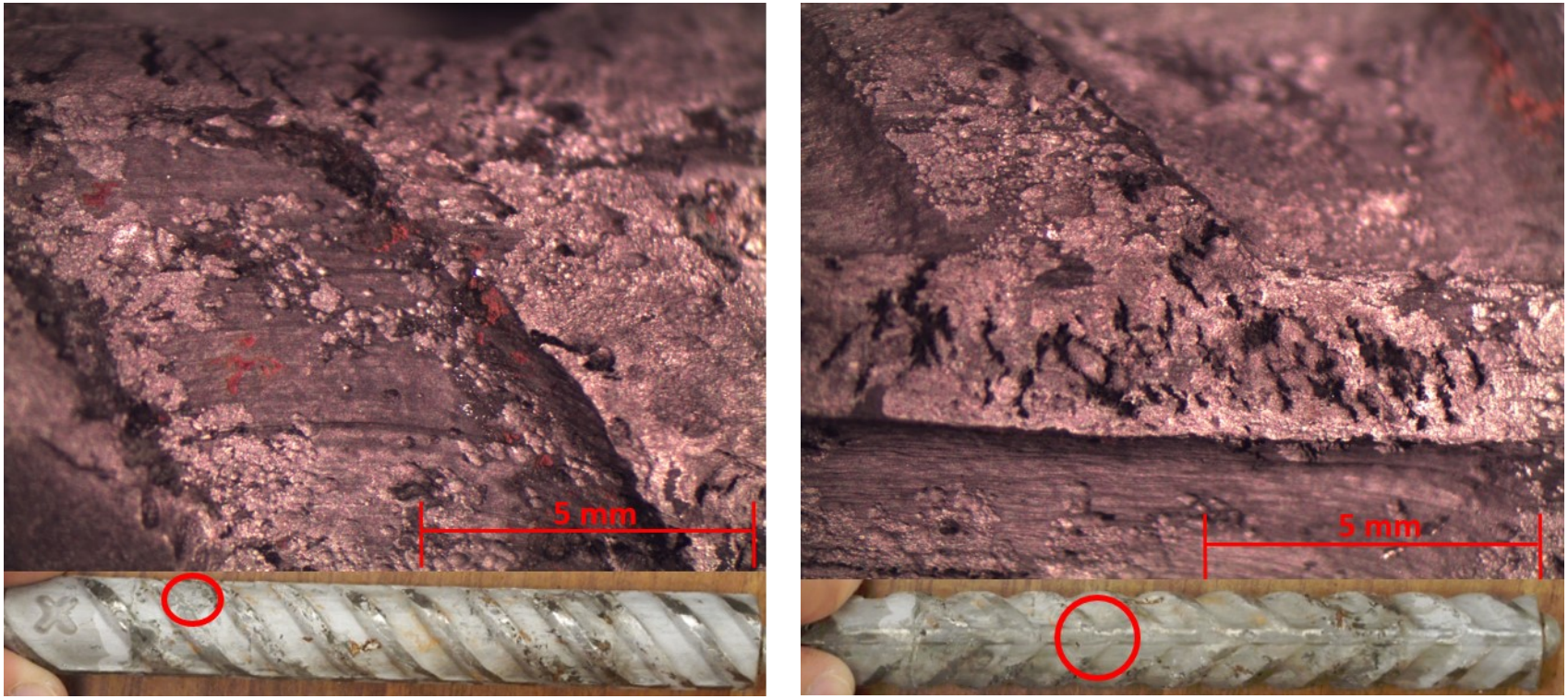

Figure D.17: RST Batch 7.5-300 Photomicrographs: a) pickled XM-28 AR 6.7 and b) pickled XM-28 AR 6.8

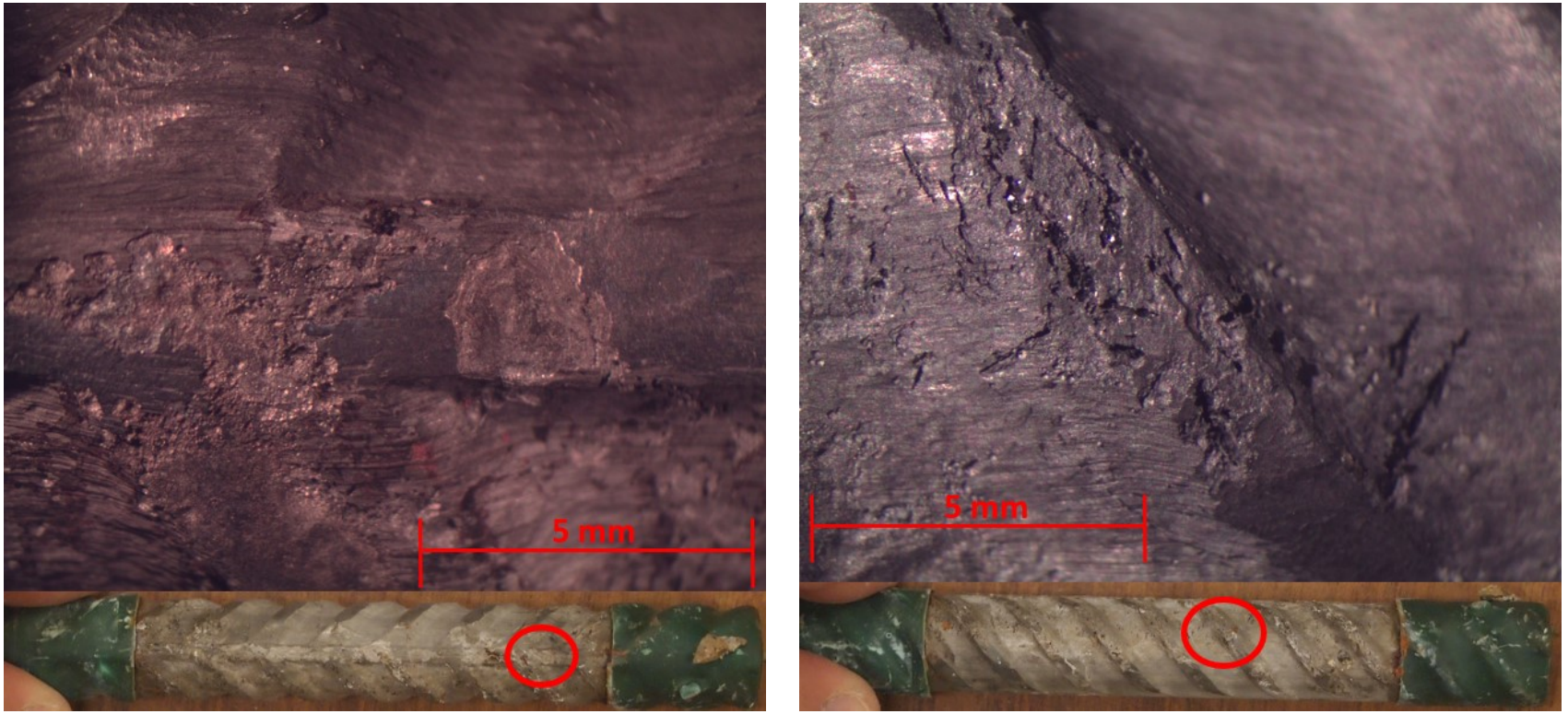

Figure D.18: RST Batch 7.5-300 Photomicrographs: a) pickled XM-28 AR 7.1 and b) pickled XM-28 AR 7.4

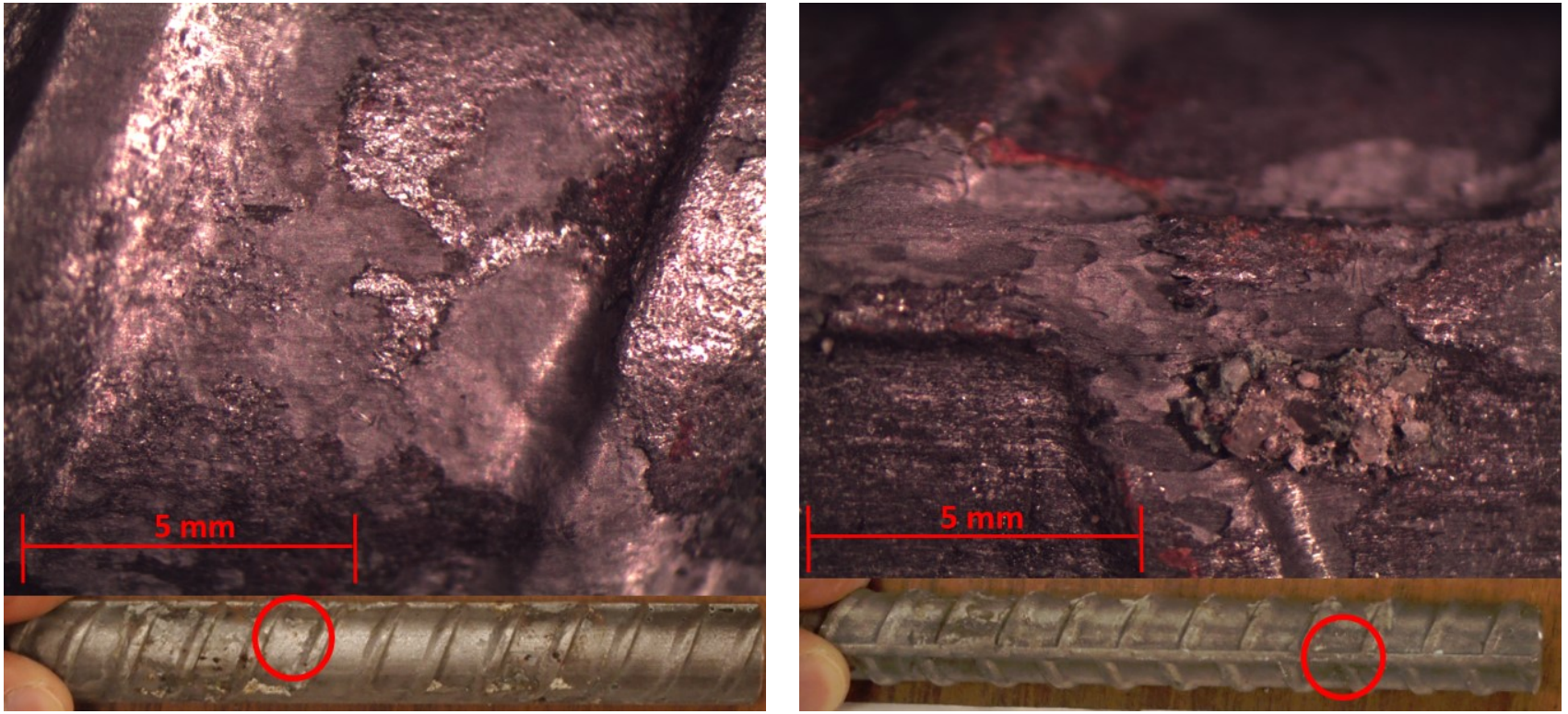

Figure D.19: RST Batch 7.5-300 Photomicrographs: a) pickled 2304 AR 5.7 and b) pickled 2304 AR 5.8

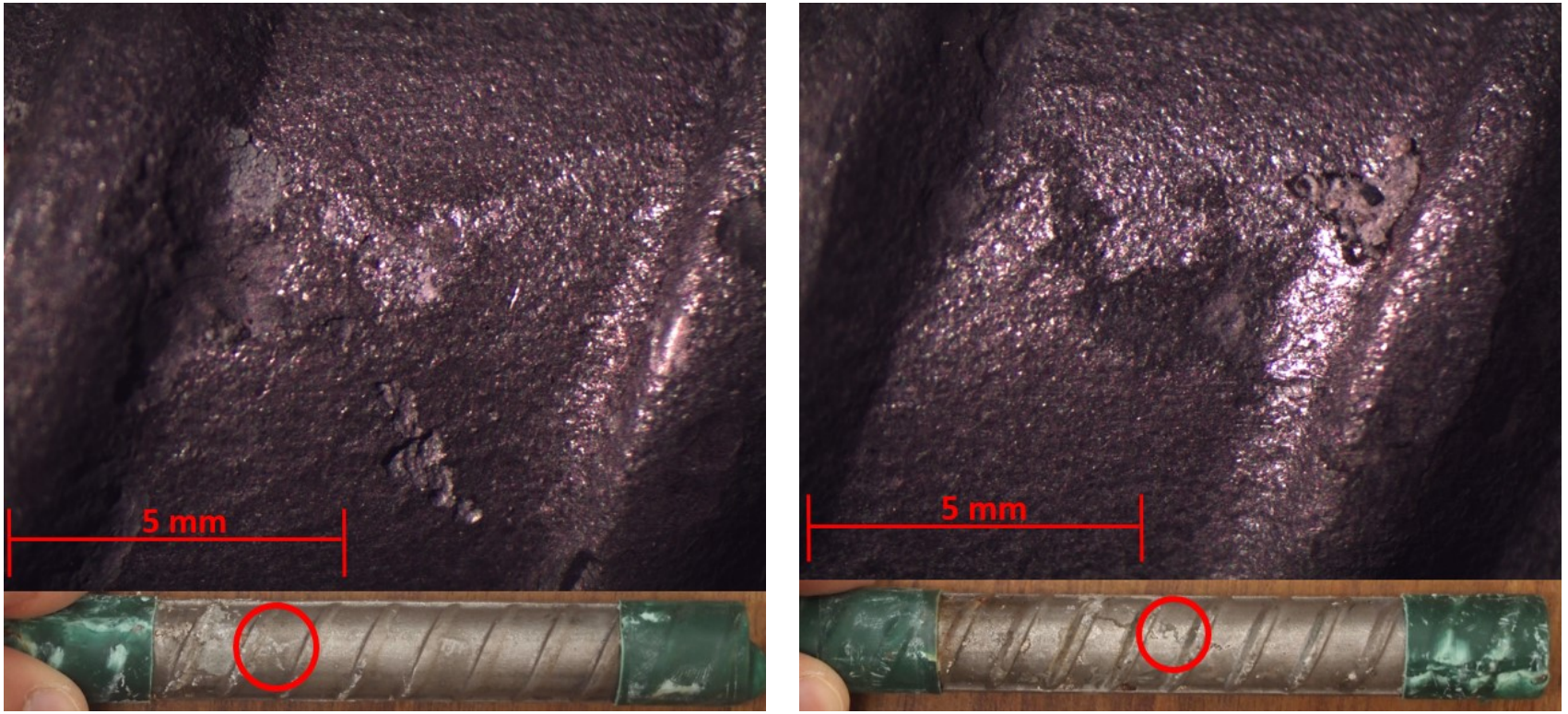

Figure D.20: RST Batch 7.5-300 Photomicrographs: a) pickled 2304 AR 6.3 and b) pickled 2304 AR 6.4

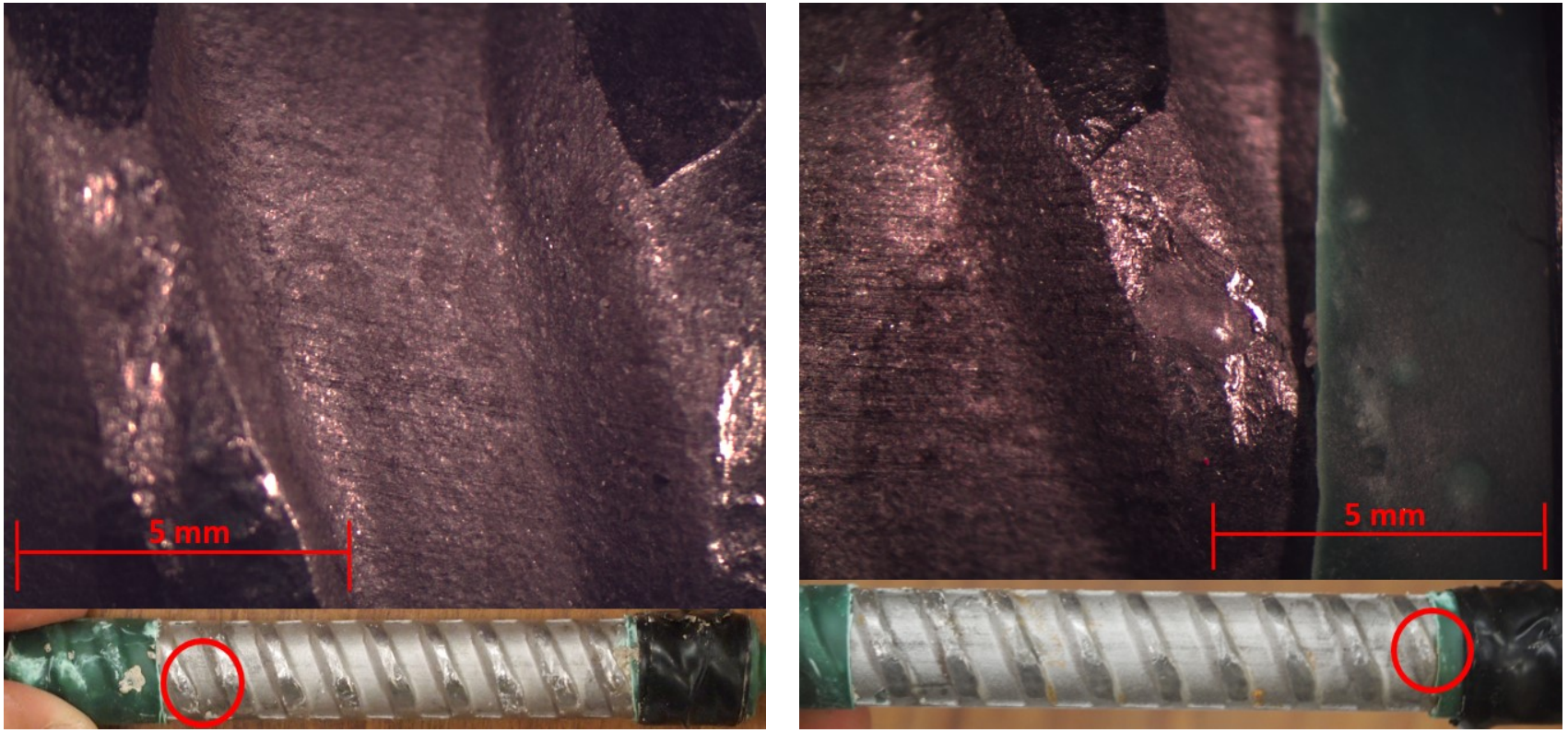

Figure D.21: RST Batch 7.5-300 Photomicrographs: a) pickled 2205 AR 5.7 and b) pickled 2205 AR 5.8

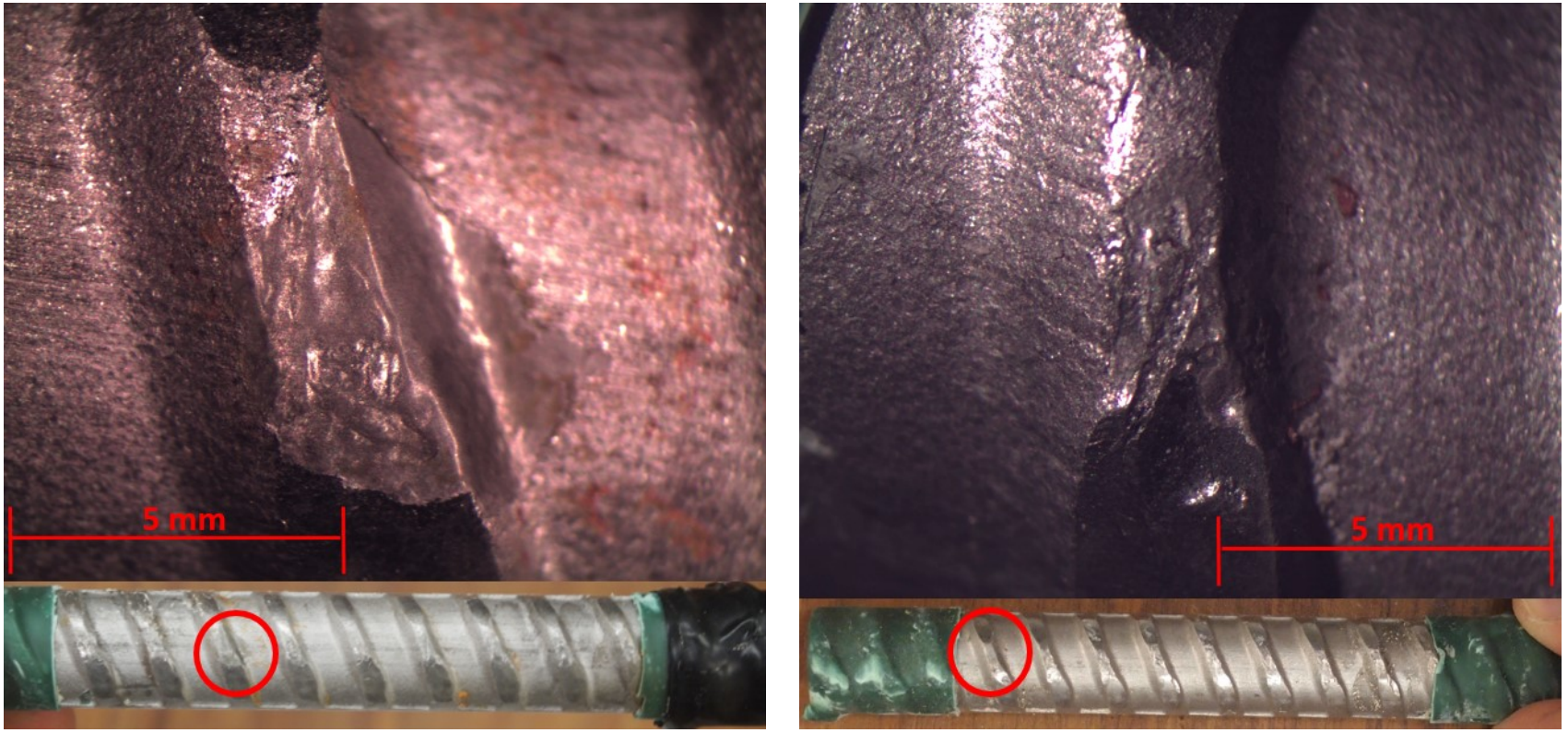

Figure D.22: RST Batch 7.5-300 Photomicrographs: a) pickled 2205 AR 5.8 and b) pickled 2205 AR 6.4

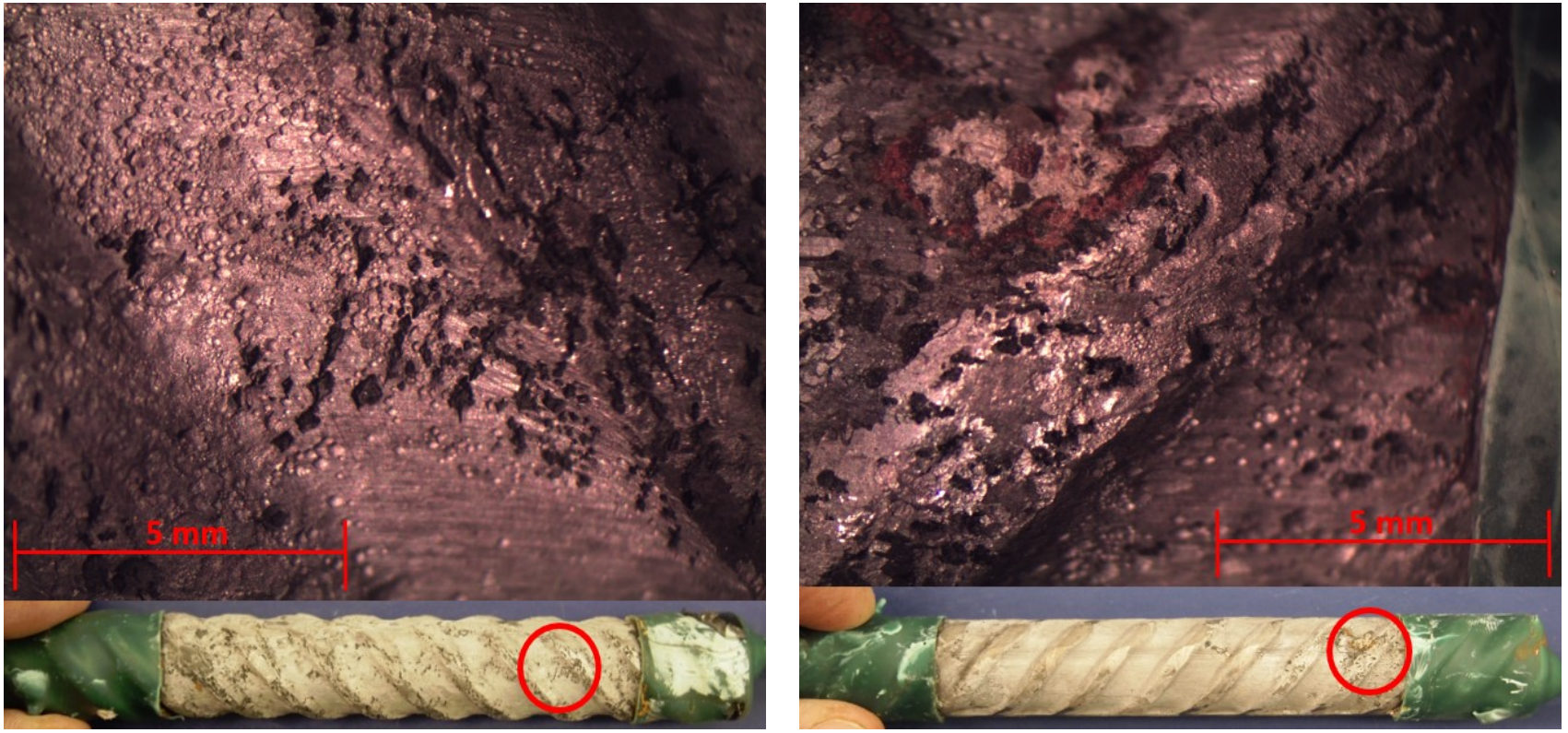

Figure D.23: RST Batch 7.5-400 Photomicrographs: a) pickled XM-28 AR 8.1 and b) pickled XM-28 AR 8.2

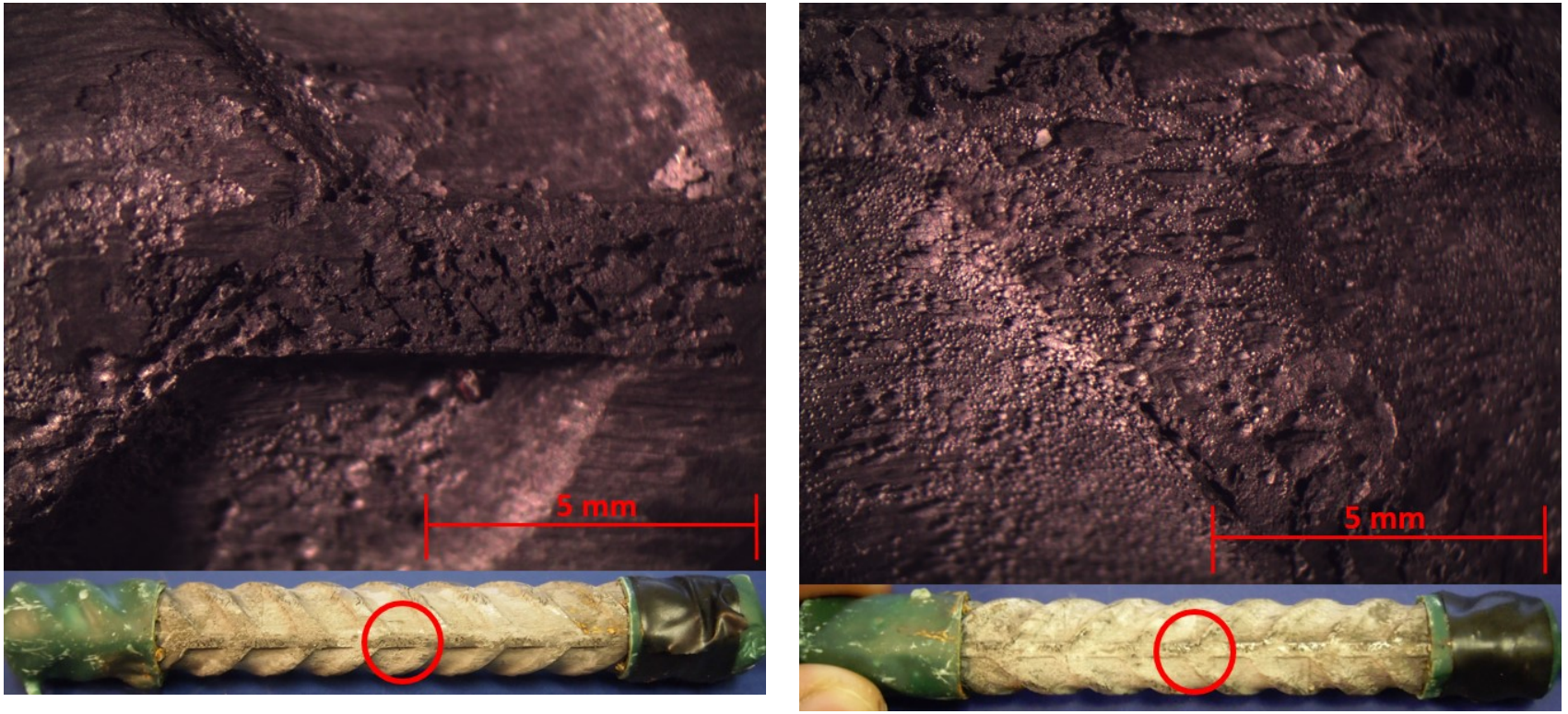

Figure D.24: RST Batch 7.5-400 Photomicrographs: a) pickled XM-28 AR 8.3 and b) pickled XM-28 AR 8.4

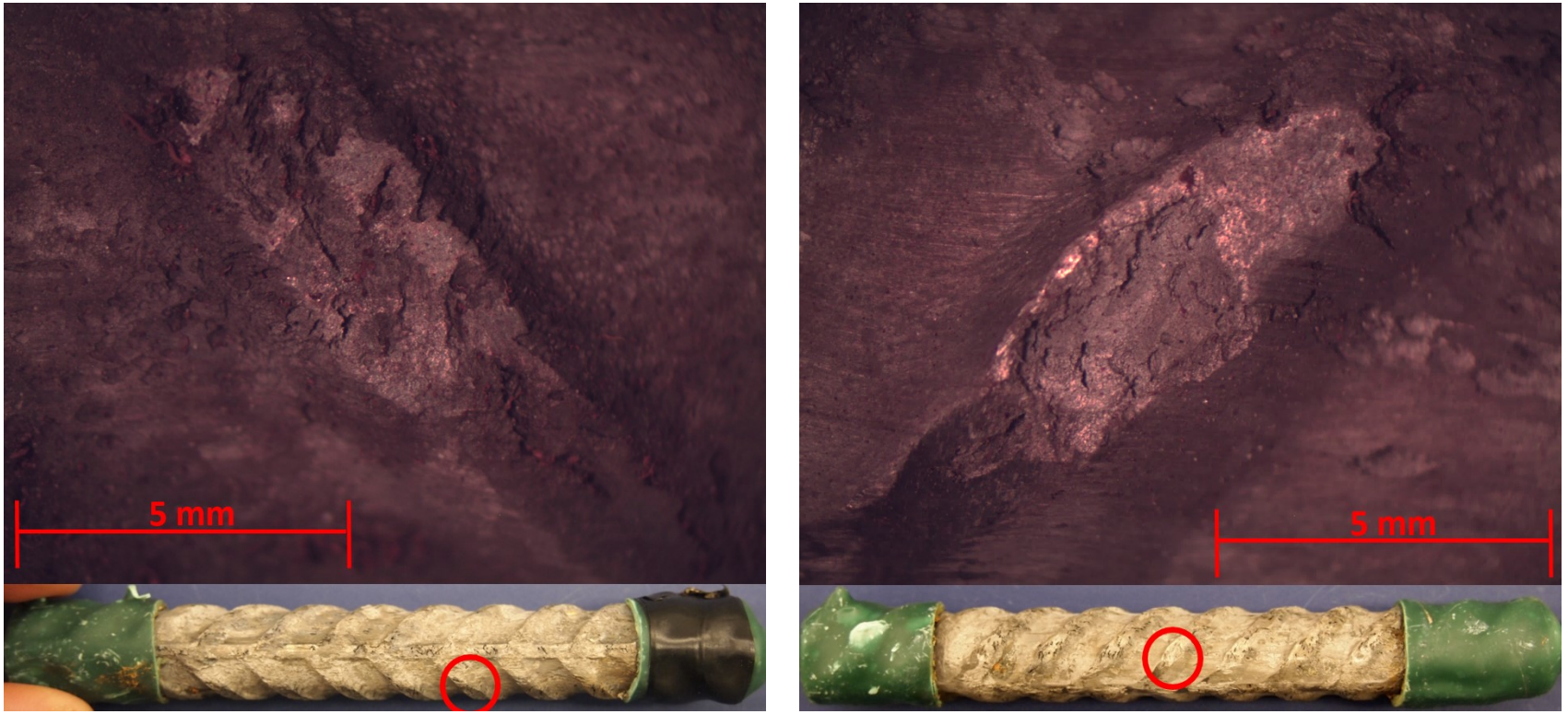

Figure D.25: RST Batch 7.5-400 Photomicrographs: a) pickled XM-28 AR 8.5 and b) pickled XM-28 AR 8.6

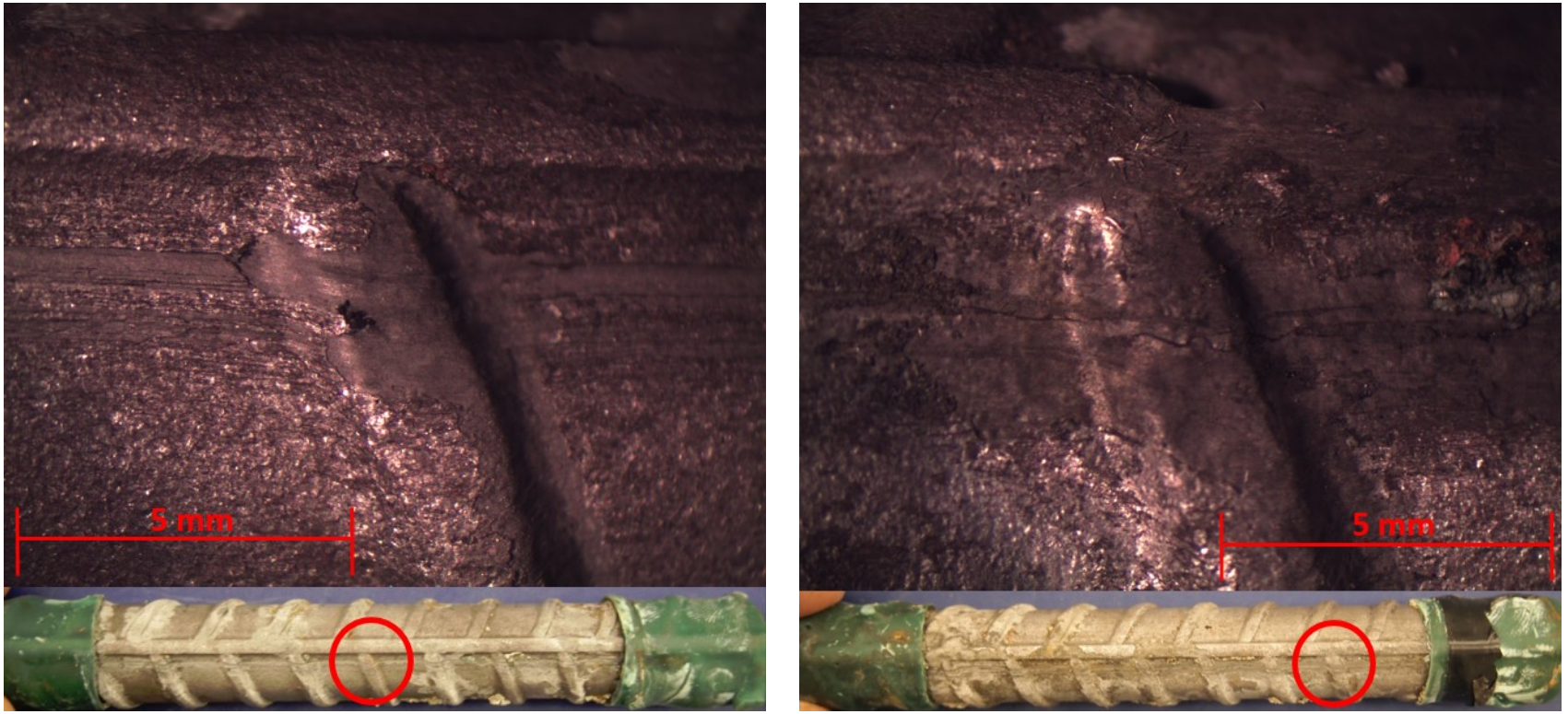

Figure D.26: RST Batch 7.5-400 Photomicrographs: a) pickled 2304 AR 7.1 and b) pickled 2304 AR 7.2

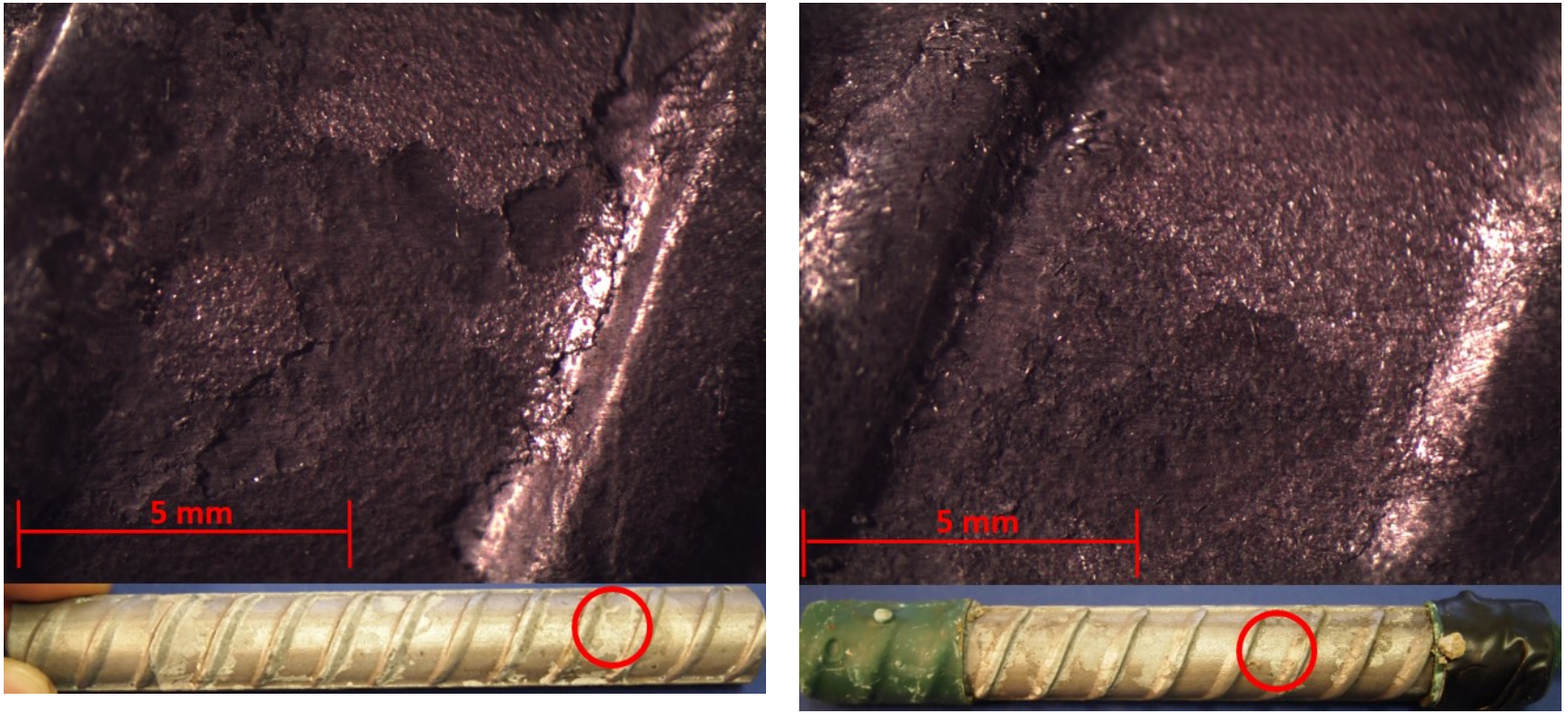

Figure D.27: RST Batch 7.5-400 Photomicrographs: a) pickled 2304 AR 7.3 and b) pickled 2304 AR 7.4

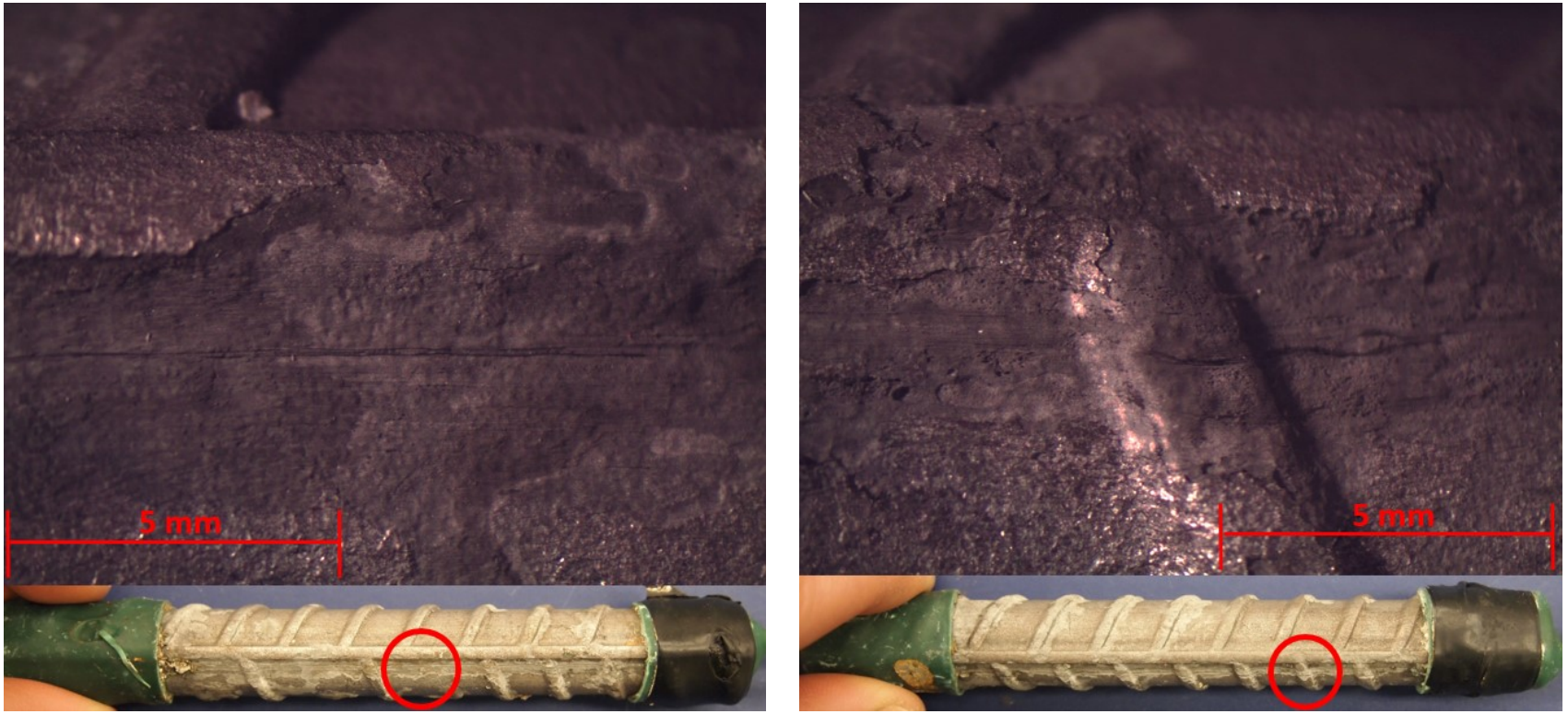

Figure D.28: RST Batch 7.5-400 Photomicrographs: a) pickled 2304 AR 7.5 and b) pickled 2304 AR 7.6

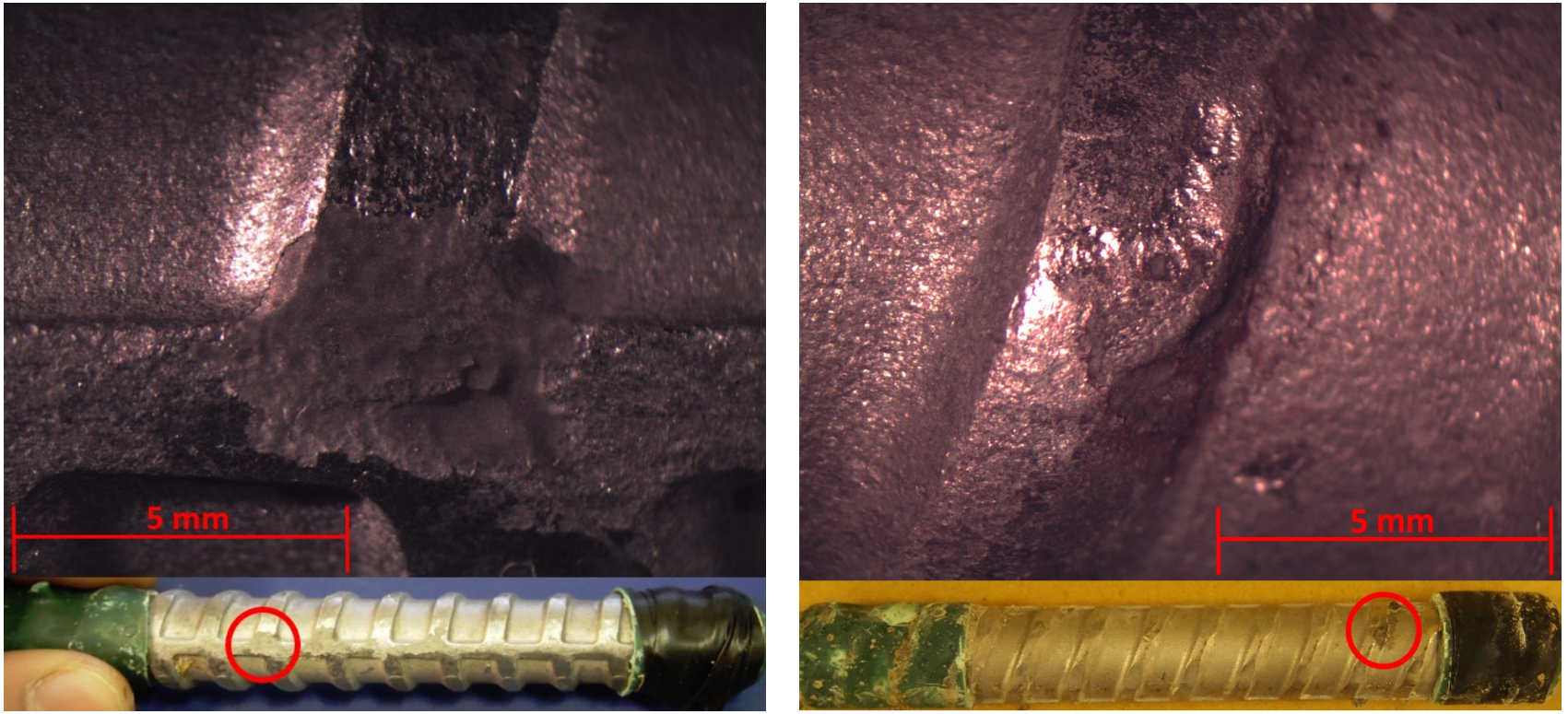

Figure D.29: RST Batch 7.5-400 Photomicrographs: a) pickled 2205 AR 7.3 and b) corroded 2205 AR 7.4

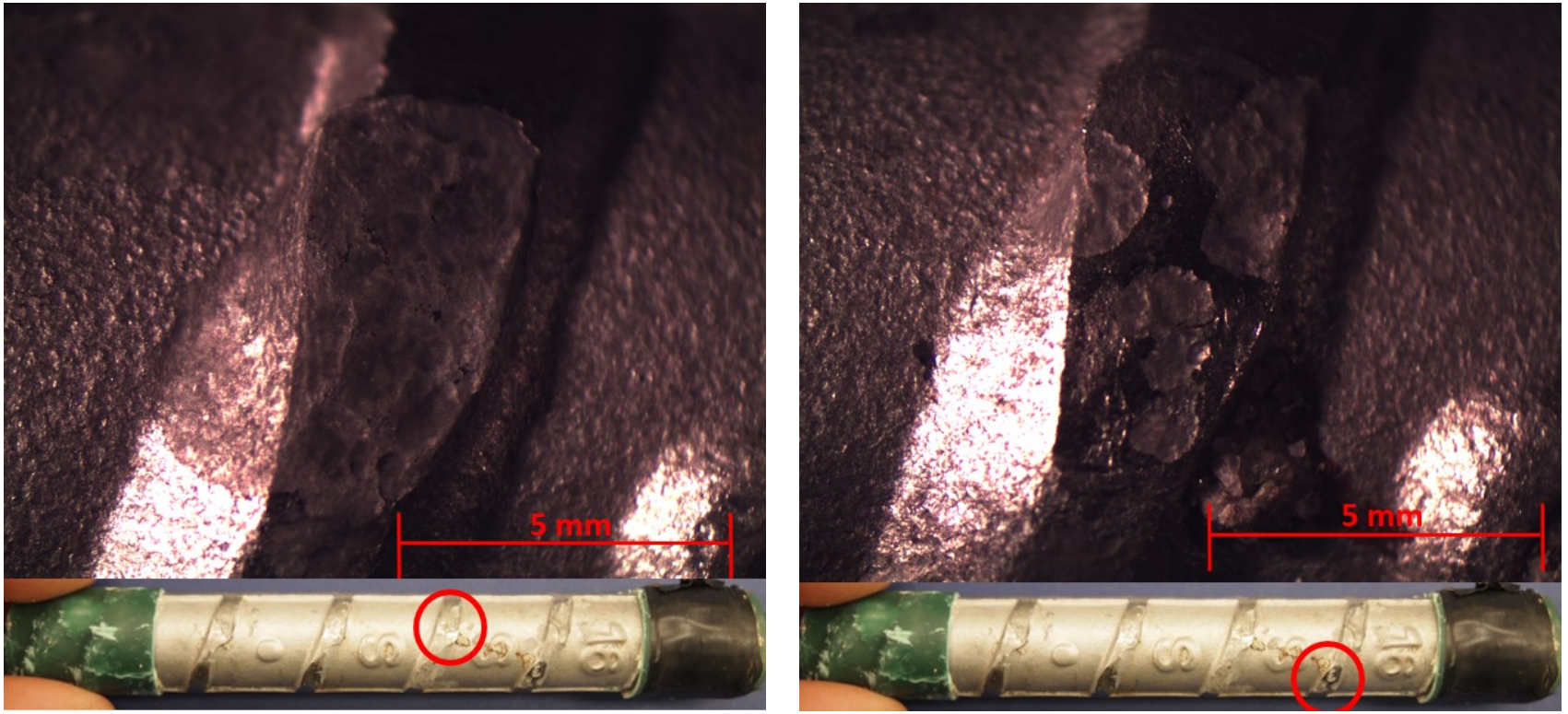

Figure D.30: RST Batch 7.5-400 Photomicrographs: pickled 2205 AR 7.6